PB83-153403

EFFECTS OF VARIATION IN LOAD HISTORY ON CYCLIC RESPONSE OF CONCRETE FLEXURAL MEMBERS

BY

TZE-HOW HWANG

and

C. F. SCRIBNER

A Report on a Research Project Sponsored by the
NATIONAL SCIENCE FOUNDATION
Research Grant No. CME - 8006711

University of Illinois at Urbana-Champaign
Urbana, Illinois
September 1982

50272-101

REPORT DOCUMENTATION PAGE	1. REPORT NO. UILU-ENG-82-2013	2.	3. Recipient's Accession No. PB83 153403
4. Title and Subtitle: Effects of Variation in Load History on Cyclic Response of Concrete Flexural Members			5. Report Date: September 1982 6.
7. Author(s): Tze-How Hwang and C. F. Scribner			8. Performing Organization Rept. No.
9. Performing Organization Name and Address: University of Illinois at Urbana-Champaign, Department of Civil Engineering, 208 N. Romine St., Urbana, IL 61801			10. Project/Task/Work Unit No. 11. Contract(C) or Grant(G) No. (C) (G) CME-8006711
12. Sponsoring Organization Name and Address: National Science Foundation, Washington, DC 20550			13. Type of Report & Period Covered 14.

15. Supplementary Notes

16. Abstract (Limit: 200 words)

Eleven reinforced concrete cantilever beam specimens were constructed and subjected to different load histories to study the effect of load history on the total energy dissipation capacity of flexural members under inelastic cyclic loading. Major variables included in this study were load history and maximum shear stress applied to the members. Four different load histories and three levels of maximum shear stress were used. Both variables were found to significantly affect the total amount of energy a specimen was able to dissipate prior to failure. The results of these tests indicated that, if member maximum displacement did not exceed 2 percent of its shear span length, severe deterioration of member shear strength would not take place within the number of cycles of load that a structural member could reasonably be expected to experience during a severe earthquake.

17. Document Analysis a. Descriptors

Cyclic Loading, Displacement History, Ductile Moment Frames, Dynamic Response, Earthquake Resistant Design, Energy Dissipation Capacity, Inelastic Response, Reinforced Concrete Stiffness Deterioration

b. Identifiers/Open-Ended Terms

c. COSATI Field/Group

18. Availability Statement	19. Security Class (This Report)	21. No. of Pages
Release Unlimited	Unclassified	231
	20. Security Class (This Page) Unclassified	22. Price

ACKNOWLEDGMENT

This report was prepared as a doctoral dissertation by Tze-How Hwang under the supervision of C. F. Scribner, Assistant Professor of Civil Engineering, and was submitted to the Graduate College of the University of Illinois at Urbana-Champaign in partial fulfillment of the requirements for the Ph.D. degree. Support for this work was provided by the National Science Foundation under grant CME-8006711. All opinions expressed in this report are solely those of the authors and do not necessarily represent the views of the National Science Foundation.

The authors would like to thank Professors Gamble, Pecknold and Schnobrich for their suggestions and assistance. The experimental work was conducted at the Nathan M. Newmark Civil Engineering Laboratory of the University of Illinois at Urbana-Champaign. Help from Mr. G. H. Lafenhagen, Mr. O. H. Ray and his staff for setting up instrumentation, data recording circuits, and for fabricating test specimens and hardware is gratefully acknowledged.

TABLE OF CONTENTS

Page

Page

LIST OF TABLES

LIST OF FIGURES

Page

Page

Page

Page

Page

Page

Page

Page

NOTATIONS

A_b bar area

A_v area of shear reinforcement within a distance S

A_s area of tension reinforcement

A'_s area of compression reinforcement

b width of beam

d distance from extreme compression fiber to centroid of tension reinforcement

d-d' distance between top and bottom reinforcement

e_b bottom steel elongation inside the enlarged end block

e_t top steel elongation inside the enlarged end block

E_c concrete modulus of elasticity obtained from cylinder tests

E_n energy dissipated during n-th cycle

f'_c specified compressive strength of concrete

f_h tensile stress developed by a standard hook

f_y yield strength of reinforcement

G_c concrete shear modulus = $\emptyset.4\ E_c$

H beam hinging zone length

I_E energy index

I'_E modified energy index

I'_w modified work index

K_n stiffness as defined in Fig.6.2

K_y stiffness as defined in Fig.6.2

ℓ' distance between beam hinging zone and loading point

ℓ beam shear span length

ℓ_e equivalent embedment length of a hook

n number of load cycles in which $P_n / p_y \geq \emptyset.75$

P_n beam strength as defined in Fig.6.2

P_y beam yield strength as defined in Fig.6.2

S spacing of stirrups

Sx-y group x specimen subjected to type y deflection schedule

u average bond stress

V applied shear force

V_c nominal shear strength provided by concrete

V_m maximum force applied to the beam during first quarter-cycle

V_s $A_v f_y (d / S)$

Δ_1 beam displacement caused by flexural deformation in the hinging zone

Δ_2 beam displacement caused by shear deformation in the hinging zone

Δ_3 flexural displacement of the beam between the hinging zone and loading point

Δ_4 shear displacement of the beam between the hinging zone and loading point

Δ_T total beam deflection at the loading point

Δ_{FE} beam displacement caused by fixed end rotation

Δ_n maximum positive beam displacement during n-th cycle (Fig.6.2)

Δ_y beam yield displacement (Fig.6.2)

θ_f flexural rotation of the hinging zone

θ_s shear rotation of the hinging zone

θ_{FE} fixed end rotation

ρ ratio of tension reinforcement

ρ_b balance reinforcement ratio

ρ_w A_v / b S

ξ constant for standard hook

γ elastic shear strain

$\Delta\sigma_s$ difference in steel stress between strain gages

$\sum_o$ bar perimeter

ΔX distance between strain gages

CHAPTER 1

INTRODUCTION

1.1 GENERAL

It is recognized that a reinforced concrete structure will generally experience localized inelastic deformations when it is subjected to strong ground motion. Because a structure's strength and its mode of failure can in most cases be inferred from the mode of failure of its individual elements, reinforced concrete structural members subjected to cyclic inelastic deformation have been investigated experimentally by numerous researchers. Over the last two decades, many simple structural members and subassemblages have been tested, and important information has been obtained.

The major difference between the behavior of monotonically loaded and cyclically loaded members, shear stiffness deterioration, has been discussed considerably. Most members would not suffer shear distress if loaded monotonically to failure. However, under repeated and reversed large deflections, shear distress may limit the ductility of these members. In order to have a reinforced concrete member withstand certain cyclic inelastic deformations, sufficient shear capacity and beam core confinement should be provided to insure the integrity and ductility of the beam hinging zone.

The behavior of a reinforced concrete member under cyclic inelastic deformation is complex and difficult to quantify. Total deformation includes the flexural deformation and deformations due to bond slip and shear, etc. Furthermore, the ramdomness of concrete cracking and shear capacity degradation add to the complexity of the problem. Several hysteresis models have been proposed to describe the load-deflection behavior of a reinforced concrete member in the inelastic range. The complexity of many argues against their use; the simplicity of others gives rise to questions concerning their accuracy in predicting actual structure response.

Besides predicting the hysteretic behavior of reinforced concrete members, estimation of the damage of a member is a subject of recent interest. It has been found that member monotonic ductility capacity can not adequately describe the capacity of the member to successfully endure inelastic cyclic loading. An alternative has been suggested in the form of empirical prediction of a member's total energy dissipation capacity. However, the total energy dissipation capacity of a member not only is a function of the basic properties of the materials and of the reinforcement details, but also may be a function of the number of loading excursions and peak deformations. Although many researchers have considered the behavior of reinforced concrete members subjected to cyclic inelastic deformation, they have all used unique load histories.

Currently there is no agreement as to which load history is most representative of seismic demand of a structural member. For this reason, this investigation was proposed to study the effect that load history may have on the total energy dissipation capacity of a member.

1.2 OBJECTIVES AND SCOPE

The primary objective of this investigation was to study experimentally the relationship between load history and total energy dissipation capacity of reinforced concrete flexural members. The secondary objective was to study the behavior of reinforced concrete flexural members subjected to various combinations of reversed inelastic loading in which maximum member displacements were 2% or 4% of shear span length.

A total of eleven cantilever beam specimens were tested. Major variables were load history and beam shear stress level. The load histories and range of the shear stress selected in this study are discussed in Chapter 2. The general test results and a description of each test specimen's behavior are presented in Chapter 3. A discussion of the change of load-carrying mechanism which was reflected in the nature of flexural and shear deformations in the beam hinging zone is given in Chapter 4. The anchorage behavior of the longitudinal reinforcement, based on the average bond stress, bond force and residual steel elongation during each cycle, is discussed in Chapter 5.

Finally, an empirical expression based on the present test results was used to consider the effect of load history on the total energy dissipation capacity of the members proposed. Test results from previous research efforts in this field are considered in light of the relationships indicated by these tests and a uniform method of evaluation of performance for reinforced concrete members is presented in Chapter 6.

1.3 REVIEW OF PREVIOUS RESEARCH

There has been considerable research on the behavior of reinforced concrete members under inelastic reversed loading since the early 1960's. Research which has lead to the present investigation is discussed briefly below.

Burns and Siess (14) were among the first researchers to consider inelastic behavior of reinforced concrete flexural members. Their test of 18 specimens, 3 of which were subjected to reversed loading, demonstrated the need for closely spaced ties to confine the core concrete, to insure member flexural ductility, and to prevent buckling of compression reinforcement. Those specimens tested to reversed loading were first subjected to load cycles in the elastic range, and were then loaded to large deflection reversals which caused failure of the specimens within 2 or 3 cycles of load application.

Brown and Jirsa (13) conducted tests of twelve reinforced concrete cantilever beams subjected to various

loadings. The main variable was loading history, which included (1) monotonic loading to failure, (2) repeated loading in one direction, and (3) reversed cyclic loading. The maximum displacement amplitudes used for reversed cyclic loading were in the order of 5 or 10 times the yield displacement. The test results indicated that the behavior of the specimens under reversed loading was influenced primarily by shear. Failure of the specimens was initiated by large shear deformations along nearly vertical planes which were not crossed by stirrups. The ability of the test specimens to maintain load and energy absorbing capacities was significantly improved by reducing stirrup spacings within regions of inelastic hinging.

Krawinkler and Popov (27) reported results from tests of nine reinforced concrete cantilever beams subjected to reversed loading. Three kinds of beams were tested; slender rectangular beams, a slender beam with monolithic slab, and short rectangular beams with high shear(maximum gross shear stress of approximately 6 $\sqrt{f'_c}$). A loading history consisting of cycles of step-wise increasing symmetric displacement was used. The test results showed that pinching of the load-deflection curves near zero load positions was caused mainly by low shear stiffness. They concluded that, in order to reduce shear stiffness degradation, adequate shear reinforcement should be provided. In addition, they speculated that slippage of the reinforcement in the zone of anchorage may have lead to

significant decrease in stiffness of the members during cyclic loading.

In order to improve the hysteretic behavior of flexural members with high shear stresses, special web reinforcement which contained diagonal bracing in the beam hinging zone was proposed by Bertero, Popov and Wang (1Ø). Their tests indicated that considerable improvements in delaying and reducing the degradation effects of the reversals of high shear was accomplished. The total energy dissipated by each member was used as one means of comparing the performance of the members considered in these tests. However, it was pointed out that the total energy dissipation measured for each specimen depended strongly on the loading program used, and comparison of energies dissipated by specimens was meaningful only when their loading programs were similar.

Scribner and Wight (36) attempted to delay shear strength decay by using intermediate longitudinal reinforcement in the beam hinging zone. One of the main variables included in their study was the maximum gross shear stress, which varied from 2 $\sqrt{f'_c}$ to 6 $\sqrt{f'_c}$. The test results indicated that maximum shear stress level was the main factor influencing the response of the test specimens. Questions as to the effect of different loading histories on specimen deterioration rate, and on specimen total energy dissipation capacity were raised, but could not be answered on the basis of their results.

A method to evaluate the performance of reinforced concrete members under reversed loading was first proposed by Gosain et al (19). They tried to compare results of tests in which different load or displacement histories had been used by formulating a nondimemsionalized member capacity called "work index". The work index was used as a substitute measure of the actual energy dissipation capacity of the members. However, because they did not consider effects of loading history on the work index significant scatter of the data remained in their work. Banon et al. (8) attempted to predict the damage within a reinforced concrete frame based on structural component energy dissipation test results. However, as in Gosain's study, possible effects of loading history were not considered in their work.

CHAPTER 2

OUTLINE OF EXPERIMENTAL WORK

2.1 INTRODUCTION

A brief description of the experimental work is given in this chapter. A more complete discussion of details is given in the appendices.

2.2 DESCRIPTION OF THE SPECIMENS

To simplify consideration of the problem, a specimen of cantilever type was chosen. The specimen consisted of an enlarged end block and the beam itself. The enlarged end block supported the beam, and provided anchorage for longitudinal reinforcement. The general configuration and overall dimensions of a typical specimen are shown in Fig. 2.1.

The ACI Building Code 318-77 and its Appendix A (1, 2) were used as a guide for designing all the specimens. A complete description of the specimen design is given in Appendix B.

Grade 60 deformed bars were used to fabricate reinforcement for all specimens, with the exception of the transverse reinforcement used in Group I and Group II specimens. For Group I and Group II specimens, grade 40 plain No. 2 bars were used as transverse reinforcement. Reinforcement details for all the specimens are given in Table 2.1. Type I cement was

used for all concrete. The concrete mix was designed to yield an average of 4000 psi compression strength at 28 days. Details of material properties and stress-strain curves for both concrete and steel are given in Appendix A.

2.3 VARIABLES

Variables considered in this investigation were load history and shear stress level imposed on the member. This section discusses how the values of the variables were chosen, and the range of the shear stress levels was studied.

2.3.1 LOAD HISTORY

The selection of a load history for use in testing structural components which most nearly approximates the forces which the component might experience during a severe earthquake has long been a subject of controversy. Because of economic and practical considerations, it is unlikely that reinforced concrete members can be studied as extensively in low cycle flexural fatigue as have steel components. Derecho et al. (16) investigated isolated structural walls, and proposed a representive loading program for use in static simulated earthquake loading tests. For the most part however, selection of a loading program to be used for studying the hysteretic behavior of reinforced concrete members has been somewhat arbitrary.

The load history of a member, sometimes equally correctly referred to as its displacement history, comprises the sum total of cycles of displacement and displacement amplitude during each cycle which the member experiences. For the case of reinforced concrete members subjected to cyclic inelastic flexure, the effects of load history on overall performance may be discovered by considering: (1) effects of amplitude per cycle of loading and (2) effects of changes in member performance resulting from changes in the sequence in which different displacement amplitudes are applied to the member.

For the last two decades, ductility factors have been used as a common measurement of the magnitude of displacement in a given load history. The use of ductility factors to describe displacement magnitudes is sometimes misleading or open to interpretation for a variety of reasons. Ductility can be defined as a function of the yield displacement, yield rotation, or yield curvature of a member at a particular section. The resulting values of "ductility" do not necessarily indicate equal amounts of displacement. In addition, the yield deformation of a member is difficult to determine for members containing longitudinal reinforcement whose yield point is poorly defined. Therefore, ductility does not explicitly indicate the absolute magnitude of displacement.

Either implicitly or explicitly, engineers have always designed structures in such a way that the maximum deformation

of the structure would not exceed some arbitrary maximum allowable deflection criterion for a given loading. An allowable deformation criterion may be expressed as a percentage of overall structure height, a percentage of member span length, or as an absolute maximum displacement.

In the recent Applied Technology Council recommendations for design to resist seismic forces (7), a lateral displacement of 2% of the story height has been recommended as the maximum allowable story drift for buildings subjected to earthquakes. It may be shown that story drift of a building may be directly related to the displacement of a structural component as a percentage of the components shear span length. The geometry of this relationship is shown in Fig.2.2. Percentages of a given length are terms that can be quantified and communicated easily. Therefore, the percentages of the shear span length were used to describe the displacement magnitude in a load history.

In previous research, load histories containing maximum displacements of between 5% and 10% of beam shear span length have been used in the testing of structural components. It is apparent that those load histories are much more severe than generally accepted displacement criteria would mandate. As a result, conclusions based on previous research could be too conservative. In order to determine the behavior of the reinforced concrete members under reasonable cyclic reversed

displacement and also have connection with the previous research, 2% and 4% of the shear span length uniform displacement, Type I and Type II load histories, as shown in Figs. 2.3(a) and (b) were used to study the effect of displacement magnitude on the specimen. The Type III and Type IV load histories, illustrated schematically in Fig. 2.3(c) and (d), were used to study the effect of displacement sequence on the members.

2.3.2 SHEAR STRESS LEVEL

It has been shown in previous research that members subjected to maximum gross shear stress levels less than $3\sqrt{f'_c}$ show primarily flexural response with little tendency to develop significant planes of shear slippage; members with maximum gross shear stress levels greater than $6\sqrt{f'_c}$ react primarily in shear, and were not able to endure enough cycles of repeated reversed loading to satisfy a consensus of load-carrying criteria(36).

Therefore, the members were designed such that the maximum gross shear stresses in the beams were in the range of $3\sqrt{f'_c}$ to $6\sqrt{f'_c}$. Group I specimens, designed to have a maximum gross shear stress of approximately $3\sqrt{f'_c}$, were referred to as low shear specimens; Group II specimens, designed to have a maximum gross shear stress of approximately $4.5\sqrt{f'_c}$., were referred to as moderate shear specimens; Group III specimens, designed to

have a maximum gross shear stress of approximately $6\sqrt{f'_c}$, were referred to as high shear specimens. The design shear stress and actual maximum gross shear stress developed in each specimen are given in Table 2.2.

Due to the nature of the variables used in this study, a mark of "Sx-y" was used to designate each specimen. The "x" variable indicated that the specimen was a Group x specimen; the "y" variable indicated that Type y load history was used in testing the specimen.

2.4 DATA ACQUISITION

Data from three sources were recorded during testing: (1) a load cell attached to the load ram, (2) four LVDTs over the hinging zone and one LVDT under the load application point, (3) thirteen electrical resistance strain gages attached to longitudinal and transverse reinforcement. Details of data acquisition equipment are given in Appendix C.

The load being applied to the specimen was measured by means of a load cell attached between the load ram and specimen. Deflection of the specimen at the load application point was measured by an independent LVDT. Load and displacement were continously recorded by an X-Y plotter during testing.

Four LVDTs were positioned over the beam plastic hinging zone, as shown in Fig. 2.4, to measure the shearing and

flexural deformation in this region. The plastic hinging zone was assumed to extend into the beam a distance from the face of the enlarged end block equal to overall beam depth.

Thirteen electrical resistance strain gages were bonded to reinforcement at various points in the specimen. The locations and designations of the strain gages, shown in Fig. 2.5, were the same for all specimens.

2.5 TEST SET UP AND TEST PROCEDURES

Each specimen was held fixed at its enlarged end block while the beam tip was slowly deflected by a hydraulic acutator. The load versus deflection curves recorded during testing were used to monitor the progress of the testing. Motion of the ram was stopped at various times to allow reading of strain gages and LVDTs. The rate of loading was slow enough to allow the loading to be considered static. Each test was terminated when the specimen had lost essentially all ability to resist displacement. Additional details of the test set up and test procedures are given in Appendix C.

CHAPTER 3

TEST RESULTS

3.1 INTRODUCTION

Typical examples of recorded data and a discussion of specimen behavior observed during testing are presented in this chapter. The recorded data included (1) applied shear force and load point displacement, (2) strains in the top and bottom longitudinal reinforcement and in selected stirrups in the hinging zone, and (3) shearing and flexural distortion of the beam as measured by four LVDTs positioned over the hinging zone.

Discussion of individual member behavior will include a description of visual observations made during testing.

3.2 RECORDED DATA

3.2.1 LOAD-DEFLECTION CURVES

The recorded beam tip load versus deflection curves for all specimens are shown in Figs.3.1(a) through 3.1(n). Because the rate of strength decay for specimens subjected to Type I load history is very low, it is not possible to show clearly all the load vs. deflection curves in one figure. Only selected load cycles are shown for these specimens, yet the selected load cycles still give enough indication of the hysteretic behavior of these specimens. As indicated in these figures, positive load and deflection have been assumed to correspond to load ram compression and to downward movement of the beam tip.

The load vs. deflection curves served as a guide for determining the points during loading at which time readings from LVDTs over the hinging zone and from strain gages on the reinforcement would be taken.

For all specimens, the load vs. deflection relationship during the first quarter cycle of displacement was unique and was never duplicated during subsequent cycles of loading. Specimen load vs. deflection behavior was generally linear up to the point at which a load producing yield of longitudinal tension steel was reached. As load was increased beyond this yield load, relatively larger deformation resulted from slight increases in load up to the point of maximum positive displacement.

The load vs. deflection curve between the point of maximum positive displacement during the first load cycle and the point of return to zero load had approximately the same average slope as had been seen between the point of initial zero load and the load at which longitudinal tension steel first yielded. As the applied load became negative, the slope of the load vs. deflection curve decreased gradually until it became approximately equal to the average slope which existed in the curve between the point of first tensile steel yield and the point of maximum positive displacement in the first quarter load cycle. There was no clearly defined point at which curve slope changed in response to yielding of longitudinal tension steel,

such as that which developed during the first quarter cycle of loading, during this loading.

After sufficient negative shear had been applied to produce the desired maximum negative beam tip deflection, load was again removed and the beam was allowed to return to its unloaded position. This position was different than the position which the beam had assumed following removal of positive shear because of inelastic deformations which had occurred in the beam as a result of negative shear. As can be seen in the load vs. deflection curve described by the fourth quarter-cycle of loading, the stiffness of the beam during unloading from negative shear was not as great as that which had existed during unloading from positive shear. As a result, deflection which remained in the beam following removal of negative load was not as large as that which had remained in the beam after removal of positive load, assuming both deflection to have been measured from the original unloaded beam position.

As positive loading was again applied to return the beam tip to its original unloaded position, the load vs. deflection relationship changed gradually. Abrupt changes in load vs. deflection curve slope occurred only at points of maximum positive and negative displacement as additional cycles of load were applied. As can be seen in Figs. 3.1(a) through 3.1(n), the slope of the load vs. deflection curves at points of zero load or small load decreased as the number of applied load

cycles increased, with the rate of which this slope decrease occurred being dependent on maximum displacement seen during loading and on the maximum shear stress experienced by the specimen.

3.2.2 STRAIN IN REINFORCEMENT

A total of 13 electrical resistance strain gages were attached to the reinforcement for each specimen. The locations of the strain gages are given in Fig.2.5. For all the gages, positive strain refers to tensile strain in the steel.

(a) STRAINS IN LONGITUDINAL REINFORCEMENT

It is possible to correlate ram load vs. deflection behavior with ram load vs. longitudinal steel strain behavior at any point at which ram load, specimen displacement, and steel strain were recorded.

The relationship between applied ram load and strains in top reinforcement at the face of the enlarged end block is shown in Fig.3.2 for Specimen S1-4. As shown in Fig.3.2, tensile steel strain increased almost linearly with increases in applied load up to the point at which yield strain in the steel was reached. Thereafter, small increases in ram load resulted in large increases in longitudinal strain. The point at which longitudinal tension steel first yielded was clearly indicated in the ram load vs. beam tip displacement curves previously

shown. The sharp break in slope of the load vs. deflection curve for Specimen S1-4, designated as point A in Fig.3.1(d), indicated that tension steel had probably yielded at that point. The strain measured in longitudinal steel at that time (point B, Fig.3.2) indicated that yield strain had indeed been reached in that steel.

As the applied load was removed, the slope of the load vs. strain relationship at that point was approximately equal to the slope which the relationship had had during the initial loading. Residual strain remained in the steel at zero ram load. No obvious yield point was observed as negative shear loading was applied. The steeper slope of the load vs. strain relationship near the point corresponding to maximum negative ram load resulted from the compression which was being carried by longitudinal steel when cracks were open being transferred to the concrete as the previously formed cracks closed.

The relationship of applied ram load to average strain in bottom longitudinal reinforcement at the face of the enlarged end block is shown in Fig.3.3 for Specimen S3-1. A small amount of compression was developed in this reinforcement during the first quarter cycle of loading. Negligible residual strain remained after first-cycle positive load was removed. As tensile ram load was applied, steel strain increased linearly with applied load until yield strain was reached. Thereafter, small increases in load ram tension caused large increases in

lower longitudinal steel strain. Following the occurrance of maximum tensile strain in this steel during the first load cycle, a residual tensile strain remained in the lower longitudinal steel for all loads during all subsequent cycles of loading.

The relationships between applied ram load and strain measured in the longitudinal steel in the beam at a distance of 10 in. from the face of the fixed support are shown in Fig.3.4(a) and (b). As is apparent from examination of these figures, the relationship of ram load to steel strain shown here are similar to those shown in Figs 3.3(a) and 3.3(b) and discussed previously. At corresponding load points strain readings in these gages were smaller than those in gages at the face of the enlarged block.

The relationships between the applied load and the steel strains in the anchorage block are shown in Figs.3.5(a) and (b) for both top and bottom reinforcement. As indicated in Fig. 3.5(a), strains at this location did not exceed the yield strain in the first load cycle. In successive cycles, the relationship between applied ram load and strain reading was quite stable. At the point of maximum negative load in each cycle, the load vs. strain relationship showed a larger slope than the slope in other parts of the curve. This behavior indicates that cracks previously formed along the member had closed and bonding between steel and concrete was effective. A qualitatively

similiar relationship between the applied load and the strain in the bottom reinforcement is shown in Fig. 3.5(b).

(B) STRAINS IN TRANSVERSE REINFORCEMENT

The relationship of load point displacement to strain in the transverse reinforcement in the hinging zone for Specimen S2-1 is shown in Figs.3.6(a)-(c). The crack pattern which developed during the first quarter cycle of load is also shown in these figures. It is possible to speculate that the magnitude of strain readings was dependent on the location and pattern of crack formation during the first quarter cycle of load. Initial increases in beam deflection resulted in relatively small increases in strain measured by gage 13 and no increase in strain measured by gages 11 and 12. Further increase in the beam deflection up to maximum displacement point in the first quarter cycle of load resulted in a larger strain increase in gage 13 and a small strain reading in gages 11 and 12. This behavior can be rationalized by considering the crack pattern which formed in the first quarter load cycle. The stirrups were placed at spacings of 2.5 in. starting 1 in. away from the face of the enlarged end block. As the beam-tip deflection increased, a vertical crack formed at the face of the fixed support. This crack did not cross any stirrup. Another crack formed at the opposite end of the hinging zone and first crossed the stirrup near the location of gage 13. The relationship between the load point deflection and strain

reading after the first load cycle indicates that the crack pattern and crack width remained more or less the same for many cycles. Most of the measured strains in transverse reinforcement did not exceed the yield strain in specimens tested in this program.

3.2.3 READINGS FROM LVDTs OVER THE HINGING ZONE

The position of the LVDTs over the hinging zone is shown in Fig.2.4. Deformations measured by these LVDTs were used to calculate shearing and flexural deformations in the hinging zone. The algorithms used to determine these deformation and a discussion of the implication of these deformation are given in Chapter 4.

3.3 OBSERVATIONS OF SPECIMEN BEHAVIOR

3.3.1 CRACK PATTERN

Cracks in the concrete were considered to be an important indicator of damage level within a specimen. Cracking patterns indicated the type and extent of damage present in any specimen at any point in loading and mode of failure. For all the specimens tested in this program, cracks developed during the first two cycles of loading and remained basically the same until the end of each test. Each test was terminated when the specimen had lost its ability to resist displacement. Prior to termination of each test the following sequence of events had occurred in the beam hinging zone: crack widths had increased as

a result of abrasion during inelastic response, concrete cover had spalled off at various location, and longitudinal and transverse reinforcement had been exposed.

A common crack pattern is illustrated in Fig.3.7. As the applied load and deflection exceeded the cracking load during the first quarter cycle of loading, vertical cracks formed near the face of the fixed support and in the hinging zone. Inclined cracks also developed between the end of the hinging zone and the load application point. As the deflection was increased beyond the yield deflection, cracks lengthened, and cracks in the hinging zone inclined toward the lower beam region near the enlarged block. Crushing of bottom concrete near the enlarged end block occurred in all specimens loaded to a deflection of 4% of their shear span length in the first quarter cycle; crushing of concrete was minor for specimens loaded to a deflection of 2% of their shear span length. Release of downward load from the maximum displacement of first quarter cycle did not cause any change in the crack pattern. A residual downward deflection remained at zero load. As the loading was reversed, the same sequence of events occurred, with the exception that vertical cracks did not originate at the bottom face of the specimen, and crushing of the concrete at the top of the beam near the enlarged end block did not occur in the first load cycle. Generally speaking, the number of the cracks in the hinging zone depended on the magnitude of the displacement imposed in the

beam during the first two cycles, with more cracks observed for specimens that were first deflected to 4% of beam shear span length deflection.

After the second loading cycle, crack pattern consisted of a large number of intersecting vertical and inclined cracks, and a big chunk of concrete block was surrounded by these intersecting cracks.

Although crack patterns were similar in the early stages of testing for all specimens, the final crack patterns were not the same. Variations in the crack patterns during the final stage of testing of each specimen appear to have been related to the magnitude of the shear stress imposed in the specimen and to the shear span length. High shear stress also appeared to have given rise to larger dowel force developed by longitudinal reinforcement and caused severe spltting of the concrete along the longitudinal reinforcement. Stirrup spacing was the same in all specimens, although stirrups were bent from No. 2 bars for specimens subjected to low and moderate shear stresses, and from No. 3 bars for specimens subjected to high shear stresses.

The appearance of one specimen from each group of the three groups of specimens which made up the total test series at the conclusion of the testing is shown in Figs 3.8(a)-(c). As illustrated in these figures, spalling concrete in the hinging zone and splitting of the concrete cover along the longitudinal

reinforcement were more severe and extended further along the beam in Group II specimens than in Group I specimens. In Group III specimens, the shear span length was so short, only twice the hinging zone length, that extension of cracks into the beam was limited by the confinement provided by the loading fixture, and spalling of concrete occurred only in the hinging zone near the enlarged block.

3.3.2 FAILURE MODES

In order to determine the total cyclic energy dissipation capacity of each specimen, a specific displacement history was applied until the specimen could not develop a force equal to fifty percent of the load required to cause first yield of tension reinforcement at the maximum deflection for its assigned load history.

All but one of the specimens exhibited a gradual decrease of strength at the same maximum deflection until the the specimen was deemed to have failed. Specimen S2-3 failed suddenly at the maximum positive deflection of its eighth displacement cycle as a result of severe bond slip caused by spalling of concrete cover along the top reinforcement.

During the first load cycle, all of the specimens were able to develop their flexural yield strength and to undergo inelastic deflections with no sudden decrease in load carrying capacity. In almost all cases, final failure resulted from

cracking and spalling of the concrete in the hinging zone, which gave rise to stiffness and strength decay. No buckling or failure in anchorage of the longitudinal reinforcement was observed.

A failure criterion which defines the minimum required strength a member should have is dificult to determine. The fact that many specimens were subjected to displacement histories in which maximum displacement was not equal for all cycles of load made it impossible to arbitrarily consider the specimen to have been failed if it failed to attain a specified load at maximum displacement during each load cycle. In addition, a general failure criterion based on physical appearance of the specimen was found to be unreliable. Many specimens showed considerable strength and stiffness even after longitudinal reinforcement had been exposed as a result of spalling of cover concrete. However, if failure of the specimen was defined to have occurred when (1) the specimen had experienced a significant or sudden decrease in load carrying capacity or (2)the specimen was unable to resist a force equal to 75% of the force which was required to cause first yield of tensile steel at the maximum deflection of its given load history, then the total number of cycles of load reversals that a specimen had withstood prior to failure can be determined. The number of cycles of loading withstood by each specimen based on these criteria are given in Table 3.3.

3.4 DESCRIPTION OF INDIVIDUAL SPECIMEN BEHAVIOR

The calculated and measured yield moments experienced during the first cycle of loading are given in Table 3.1 for all specimens. A comparison of measured maximum shear and allowable shear stress calculated according to ACI 318-77 is presented in Table 3.2. Parameters which were chosen as testing variables and which had a major effect on specimen behavior are listed in Table 3.3. For convenience, beam tip displacements of 4% and 2% of beam shear span length have been designated as simply 4% and 2% displacements. The maximum gross shear stress measured in the first quarter load cycle as a multiple of $\sqrt{f'_c}$, and the designation for the assigned load history for each specimen are given to aid the discussion.

Specimen S1-1 (Shear Stress= 3.3, Type I loading schedule)

The load-deflection curves for this specimen are plotted in two separate figures for clarity. Because the rate of strength decrease at maximum positive displacement is very low, it is not practical to show all the load-deflection curves in one figure. Selected load cycles 1-5, 10, 31, 61, 100, 101, 105 and 106 are plotted and shown in Fig.3.1(a). The two curves shown dotted in this plot indicate two instances in which malfunction of the MTS ram control module caused larger than planned deflections, once each at the maximum positive deflections of load cycles 100 and 105. In Fig.3.1(b) the first

load cycle has been plotted along with load cycles 121-128 so that the deterioration of stiffness and strength of the specimen can be easily seen.

The specimen was subjected to Type I loading for the first 120 cycles of displacement. At that time, the strength of the specimen at the displacement of 2% of its shear span length had decreased to approximately 73% of its original yield strength. It was decided at that time that for practical application purposes, this specimen would survive any type of loading history as long as the maximum deflection was required to be less than 2% of its shear span length. In order to determine how much reserve cyclic strength remained in the specimen, the maximum positive and negative deflections were increased to 4% of shear span length. As shown in Fig.3.1(b), this specimen was able to develop its original yield strength at approximately 3% displacement after 121 cycles of displacement to 2% shear span length. This specimen was subjected to five more load cycles at the 4% displacement limit before the strength dropped below 75% of its original yield strength.

The crack pattern of this specimen developed in the first load cycle and stablized in the second load cycle. Maximum crack width remained essentially unchanged until large deflections were imposed after 120 cycles of load. Deterioration of stiffness and strength resulted primarily from loss of interlock of the concrete along cracks during the Type I

loading schedule. Strain along the top longitudinal reinforcement during the fiftith load cycle, shown in Fig.3.10, indicated that bond had deteriorated in the enlarged end block, and that anchorage of the top longitudinal reinforcement was being provided almost solely by the standard 90 degree hooks. Increases in the maximum deflection limits resulted in increased opening of cracks, and twisting of the beam in a clockwise (as viewed from the beam free end) direction. Also, spalling of the concrete in the hinging zone occurred when the larger maximum displacements were imposed. The appearance of this specimen at the conclusion of testing is shown in Fig.3.9.

Specimen S1-2 (Shear Stress = 3.6, Type II loading schedule)

This specimen was able to withstand thirteen inelastic load cycles before the strength of the specimen at 4% displacement dropped to 78% of its original yield strength. The degradation of strength at maximum displacement increased after the thirteenth load cycle, as shown in Fig.3.1(c). The crack pattern which had developed during the first cycle of load is shown in Fig.3.11. As shown in this figure, inclined cracks formed in the hinging zone, isolating a large block of concrete which remained intact until the end of testing, shown in Fig.3.12. Vertical cracks also developed on both sides of the enlarged end block during the first two cycles of load, and remained unchanged for the remainer of the testing. Strain readings in the longitudinal reinforcement at the beginning of

the 90-degree hook, shown in Fig.3.13, indicated that satisfactory anchorage was provided for longitudinal reinforcement by the enlarged block and by the development reinforcement length. Spalling of concrete in the beam hinging zone started during the twelfth load cycle, and both transverse and longitudinal reinforcement were exposed at that time.

Specimen S1-4 (Shear stress = 3.5, Type IV loading schedule)

The reinforcing steel used in this specimen showed a slightly lower yield stress than that used in Specimens S1-2 and S1-3. As a result, the yield load for this specimen was slightly lower than the yield loads of specimens S1-2 and S1-3 had been. However, shear stress as a multiple of $\sqrt{f'_c}$ remained approximately equal to that which had been present in Specimen S1-2 because of the lower strength of the concrete used in this specimen.

This specimen withstood only seven load cycles at 4% maximum displacement and six load cycles at 2% maximum displacement before the strength of the specimen at 4% positive displacement dropped below 75% of its original yield strength. The relationship of load vs. strain in the longitudinal reinforcement at the face of the enlarged block, shown in Fig.3.2, did not change greatly as the applied ram load changed after six cycles of load. This indicated that the bond between concrete and steel had deteriorated along the top reinforcement

during the first six load cycles. Anchorage of the longitudinal reinforcement was provided almost entirely by the standard 90-degree hooks in the enlarged block. Wide cracks existed along both sides of the hinging zone at the maximum positive deflection in the tenth load cycle, as shown in Fig.3.14. No spalling of concrete was observed until the twelfth load cycle. After the concrete in the hinging zone had spalled off, the specimen showed a large strength degradation in the subsequent cycles as indicated in the load vs. deflection relationship shown in Fig.3.1(d).

Specimen S2-1 (Shear stress = 5.1, Type I loading schedule)

Displacement during the seventh cycle of load of this specimen was inadvertently allowed to exceed 2% of beam shear span length. As a result, strength at 2% displacement dropped significantly in the eighth load cycle. Nevertheless, the specimen was able to maintain its strength with only gradual degradation at the 2% displacement limit in subsequent cycles. As shown in Fig.3.1(e) the strength degradation at 2% displacement was very slow after the eighth load cycle, and only load cycles 50, 100, 200 and 230 had been plotted. The total number of cycles of load endured by this specimen prior to the tentatively defined failure criterion was approximately half of that endured by Specimen S1-1. This indicated that higher shear stress level caused a reduction of total number of cycles before failure.

The specimen had withstood 230 cycles of load before its strength at the positive 2% displacement dropped to 47% of its original yield strength. In order to determine the remaining cyclic strength of this specimen, the maximum positive and negative displacements were increased to 4% of beam shear span length. Unlike the behavior of Specimen S1-1, this specimen developed 70% of its original yield strength at 2.7% displacement and then the strength remained uniform until 4% displacement had been reached. The test was terminated after this load cycle. The load-deflection curve recorded during this cycle of displacement is shown in Fig.3.1(f).

Nearly all cracks in the hinging zone were formed during the first cycle of load. Although a few more cracks developed in the next few cycles,the crack pattern remained virtually unchanged throughout testing. Cracks which had formed at the conclusion of one and ten load cycles are illustrated in Figs 3.15 and 3.16. As shown in Fig.3.15, the angles between the longitudinal axis and the inclined cracks were smaller in this specimen than those of the Group I specimens.

Only minor crushing of concrete on the lower beam surface near the enlarged end block occurred at the maximum displacement in the first quarter cycle. After 100 cycles of load had been applied, concrete on both sides of the hinging zone had cracked badly, and transverse reinforcement was visible through the cracks. Concrete in the hinging zone did not begin to spall off

until 200th load cycles.

Specimen S2-2 (shear stress = 5.2, Type II loading schedule)

During the first quarter cycle of loading, concrete crushing on the beam bottom surface near the fixed support, as shown in Fig.3.17, was visible as the deflection exceeded 2% displacement and became severe as the deflection reached the maximum.

Basically, the load vs. deflection relationship for this specimen was identical to that of Specimen S1-2. Stiffness decreased more rapidly in this specimen than in Specimen S1-2. Although crack patterns developed in this specimen in the same way as did the crack patterns in Specimen S2-1, more cracks were observed in the hinging zone in this specimen. During the fourth cycle of load, the hinging zone bulged severely and concrete started spalling off exposing transverse and longitudinal reinforcement. This beam twisted approximately 4.2 degrees clockwise (as viewed from the beam free end) about its longitudinal axis at the maximum positive displacement of the seventh cycle. The total number of cycles of load endured by this specimen prior to a decrease to 75% of original yield strength at the maximum displacement was one third that of Specimen S1-2. This indicated that the effects of shear stress levels were more severe when specimens were loaded to 4% displacements than when specimens were loaded to 2% displacements.

Specimen S2-3 (Shear stress = 6.Ø, Type III loading schedule)

Because higher yield strength reinforcement was used in this specimen than in other specimens in this group, higher yield and maximum loads were observed in the first cycle of loading of this specimen than had been seen in the other specimens. As a result, the maximum shear stress in this specimen was higher than in the other specimens in this group.

Concrete did not crush on upper or lower faces beam in the hinging zone during the first two cycles of displacement. This specimen was able to withstand inelastic loading at 4% displacement for three cycles and at 2% displacement for four cycles before its strength dropped below 75% of its original yield strength. The first two cycles of load at 2% displacement did not cause a reduction of the shear carrying capacity in the beam. As a result, the specimen was able to develop its yield strength at 3% positive displacement during the third cycle of loading. The top concrete cover split off along the top reinforcement as the beam was deflected to the maximum positive displacement during the eighth load cycle. As indicated in the load vs. deflection curve (Fig.3.1(h)),the specimen showed a uniform strength at the positive maximum deflection of the eighth load cycle, and the strength dropped dramatically in subsequent cycles having the same maximum displacement. The appearance of the specimen at the maximum negative displacement of the 11th load cycle is shown in Fig.3.19. Severe cracks

extended along both the top and bottom longitudinal reinforcement from the face of the enlarged end block to the point of load application.

As illustrated in Fig.3.18 the strain in the fourth tie from the enlarged end block exceeded the yield strain during the third load cycle. The strains recorded in the other two stirrups, the second and third from the enlarged end block, were stable and remained less than the yield strain throughout the testing.

Specimen S2-4 (Shear stress = 5.6, Type IV loading schedule)

This specimen showed severe strength decay after the first two 4% displacement load cycles had been imposed, and the strength at the 4% displacement dropped below 75% of original yield strength in the sixth load cycle. Similiar to Specimen S2-2, the basic crack pattern was formed during the first load cycle. The second load cycle caused extension and widening of the cracks formed during the first load cycle. As shown in Fig.3.2Ø, the crushing of bottom concrete near the enlarged end block was more severe in this specimen than that which had taken place in Specimen S2-2. Concrete started spalling off and stirrups were exposed during the fourth load cycle. The appearance of the specimen at maximum positive displacement during the sixth load cycle is shown in Fig.3.21. Severe cracks extending out of the hinging zone and debris of the concrete spalled from the hinging zone are evident in Fig.3.21.

Strains in the third and fourth ties from the face of the enlarged end block exceeded yield strain as beam displacement reached the maximum positive displacement during the second load cycle. The strain recorded in the second stirrup from the face of the enlarged end block never exceeded the tie steel yield strain throurhout the testing. The strains recorded in the top and bottom longitudinal reinforcement near the hooks showed a stable behavior which indicated that anchorage provided by the hooks was effective throughout the testing.

Specimen S3-1 (Shear stress = 7.1, Type I loading schedule)

Although the maximum shear stress developed in this specimen was very high, the strength decay was slow during application of the Type I load history. The specimen was able to withstand fifty cycles of load before its strength at the maximum positive displacement was reduced to 75% of its original yield strength. The specimen was cyclically loaded until the strength at maximum positive displacement dropped below 50% of its original yield strength, at which time maximum positive and negative displacements were increased to 4% of beam shear span to determine remaining cyclic strength.

The specimen was able to develop only 76% of its original yield strength at a positive 4% displacement during the 117th load cycle. Although this specimen was subjected to three more cycles of 4% displacement, it had lost essentially all ability

to resist displacement after the 117th cycle. Selected load vs. deflection curves for load cycles 1-4, 7, 10, 20, 30, 50, 70 and 100 are shown in Fig.3.1(j). Load cycles 116-120 together with load cycles 1 and 30 are shown in Fig.3.1(k). Deterioration of the strength of the specimen is graphically illustrated in this figure.

In comparing the load deflection curves of this specimen with those of Specimens S1-1 and S2-1, it is possible to speculate that shear stress level seems to be more important in reducing total number of cycles before failure in the range of $3\sqrt{f'_c}$ to $5\sqrt{f'_c}$ than in the range of $5\sqrt{f'_c}$ to $7\sqrt{f'_c}$. Total load cycle preceeding the point of tentative failure 110 cycles for Specimen S1-1 with a maximum shear stress of $3.3\sqrt{f'_c}$; 60 cycles for Specimen S2-1 with a maximum shear stress of $5.1\sqrt{f'_c}$; 50 cycles for Specimen S3-1 with a maximum shear stress of $7.1\sqrt{f'_c}$. Only very minor crushing of concrete occurred on the bottom face of the beam near the enlarged end block during the first load cycle. As shown in Fig.3.22 more cracks were formed in the hinging zone in this specimen than had been formed in Specimen S2-1 after ten cycles of load. Severe spalling occurred near the enlarged block during the fiftith load cycle, as shown in Fig.3.23, and both transverse and longitudinal steel were exposed. The strength of the specimen dropped below 75% of its original yield strength after this cycle.

Specimen S3-2 (Shear stress = 7.3, Type II loading schedule)

During the first quarter load cycle, crushing of the bottom face of the specimen near the enlarged end block began at a deflection of 1.5% of beam shear span length; spalling began at a deflection of 2.5% of beam shear span length. Only minor crushing occurred on the top surface near the fixed support after load reversal. After completion of the 2nd load cycle, the hinging zone swelled laterally and longitudinal cracks appeared on the bottom face of the specimen. Concrete on the bottom of hinging zone spalled off during the fourth load cycle.

The strength of the specimen at the maximum positive displacement decreased at a rate of approximately five kips per cycle until the fifth load cycle. As shown in Fig.3.24, at maximum negative displacement during the second cycle, concrete in the hinging zone had cracked badly. The integrity of the hinging zone was lost during the fourth cycle of load, as shown in Fig.3.25. Although the maximum shear stress developed in this specimen was 2.1 $\sqrt{f'_c}$ higher than that on Specimen S2-2, this specimen had withstood the same number of cycles as Specimen S2-2 did, four cycles, before the strength at 4% displacement decreased to 75% of the original yield strength.

Specimen S3-3 (Shear stress = 7.Ø, Type III loading schedule)

The specimen was able to develop its design moment capacity at a displacement of 2.6% of beam shear span length

during the third cycle of load. This indicated that the shear carrying capacity of the specimen had not been impaired during the first two cycles of load. The strain recorded in the fourth stirrup from the face of the enlarged end block (Fig.3.27) indicated that the application of 4% displacement during the third cycle of load caused a large strain increase in the stirrup, and the relationship between the applied load and strain showed a large decrease in slope after this cycle. Unlike the situation which had existed in some Group II specimens, the stirrup strains in this specimen never reached the yield strain.

Cracks in the specimen which formed in the first load cycle (Fig.3.26) were more widely spaced than those observed in Specimen S3-1. Longitudinal cracks were noted along the sides of the beam in the region of top reinforcement at approximated the yield load. Crushing of concrete was found at the beam bottom face near the enlarged block after the first cycle of load.

The major difference between the load vs. deflection curves of this specimen and Specimen S2-3 was that this specimen showed a gradual strength decay at 4% displacement until the end of the testing.

Specimen S3-4 (Shear stress = 7.4, Type IV loading schedule)

The sequence of deterioration of this specimen followed

that seen during the testing of Specimen S3-2 for the first two cycles of load. However, crack openings were smaller in this specimen than in Specimen S2-2, as shown in Fig.3.28. Because the hinging zone of this specimen was not so badly cracked as that of Specimen S3-2 after the first two load cycles, the strength of this specimen at 2% displacement was higher than that in Specimen S3-2. During the fourth load cycle, concrete started spalling off and longitudinal and transverse reinforcement were exposed, as shown in Fig.3.29. Applied ram load vs. stirrup strain in the second tie from the enlarged block face was typical of the other load vs. stirrup strain relationships for all stirrups whose strain was measured and is shown in Fig.3.30. As shown in Fig.3.30, after the first two cycles of load, the relationship between the applied ram load and strain in the stirrup was quite stable and linear. Measured strain of all stirrups in the hinging zone never exceeded the steel yield strain.

CHAPTER 4

FLEXURAL AND SHEAR DISPLACEMENT IN THE HINGING ZONE

4.1 INTRODUCTION

For a transversely loaded reinforced concrete beam, total beam deflection consists primarily of flexural and shear deformation. Under service loading conditions, cracks in the concrete are small and calculation of total beam deflection can be simplified by neglecting the deflection resulting from shear. If the beam is loaded beyond the elastic range, however, or loaded cyclically to maximum displacements as large as several times yield displacement, a large amount of beam deflection results from shear deformation and from severe cracking.

For the cantilever beam specimens tested in this program, cracking and spalling of the concrete were concentrated mainly in the hinging zone, a region of the beam defined to be between the face of the enlarged end block and a section located a distance equal to overall beam depth from the face of the enlarged end block. As discussed in Chapter 3, the behavior of this region was pivotal in determining the overall behavior of the tested specimens. Four LVDTs were positioned over the hinging zone, as shown schematically in Fig.2.4, to record the distortion of this region. Deformations measured by these LVDTs were used to calculate shear and flexural displacements in this region. A discussion of the change in flexural and shear

displacement and the associated failure mechanism is presented in this chapter. Also, a qualitative study of the effects of load history and shear stress level on member behavior is presented in this chapter.

4.2 FLEXURAL AND SHEAR DISPLACEMENT

A cantilever beam having only flexural deformation is shown in Fig.4.1. As shown in this figure, the elongation of the top fibers and shortening of the bottom fibers causes a rotation of an arbitrarily defined hinging zone end section. From geometry, the angle through which the hinging zone end section rotates is twice as large as the angle between the original longitudinal axis of the beam and the line connecting the mid points of the sections at the face of the enlarged end block and at the end of the hinging zone. The angle θ_f between these two lines is defined to be flexural rotation, and the displacement at the hinging zone end section, H X TAN(θ_f), is called flexural displacement in the hinging zone.

In a cantilever beam having only shear deformation in the hinging zone, as illustrated in Fig.4.2, enlongation of the top and bottom fibers is equal and there is no relative rotation of hinging zone end sections. But there is a angle between the two neutral axes before and after shear deformation. This angle θ_s is defined to be shear rotation, and the corresponding displacement at the hinging zone end section, H X TAN(θ_s), may

be defined to be hinging zone shear displacement. It must be noted that if the total displacement at the hinging zone end section is calculated by H X TAN($\theta_f + \theta_s$), it will not be the same as that resulting from the calculation H X (TAN(θ_f) + TAN(θ_s)). For the specimens tested, the result as given by the first calculation was less than Ø.Ø1% larger than that given by the second calculation at the maximum displacement of a given load cycle. Therefore, H X (TAN(θ_f) + TAN(θ_s)) was used to calculate the total displacement of the hinging zone.

4.3 COMPARISON OF CALCULATED AND MEASURED DEFLECTIONS

Assuming shear and flexural displacement of the hinging zone to have been defined as discussed in the previous section and assuming linear elastic behavior of the beam between its hinging zone and point of load application, the beam deflection at several loading points was calculated. The calculated and measured deflections of the beam at the loading point were compared to verify the recorded deflection data.

The total beam deflection at the loading point can be expressed as follows:

$$\Delta_T = \Delta_1 + \Delta_2 + \Delta_3 + \Delta_4$$

where

Δ_1 =beam displacement caused by flexural displacement of the hinging zone

Δ_2 =beam displacement caused by shear displacement in the hinging zone

Δ_3 =flexural displacement of the beam between the hinging zone and loading point

Δ_4 =shear displacement of the beam between the hinging zone and loading point

The quantity Δ_1 included not only flexural deflection within the hinging zone, but also deflection at the beam loading point resulting from rotation of an assumed rigid beam extending from the hinging zone end section to the loading point. This latter quantity was calculated as ℓ' X SIN(Θ), where ℓ' was the distance between the hinging zone and loading point, and Θ was the angle between hinging zone end sections of a given deformation.

The quantity Δ_3 was calculated by using the moment-area theorem, assuming a cracked section and linear distribution of curvature between the hinging zone and the loading point.

The quantity Δ_4 was calculated using elastic analysis as

$$\Delta_4 = \gamma \ell' = \frac{V \ell'}{b \, d \, G_c}$$

where

γ =elastic shear strain

ℓ' =distance between beam hinging zone and loading point

G_c =concrete shear modulus = $\emptyset.4 \, E_c$

E_c =concrete modulus of elasticity obtained from cylinder tests

The calculated deflection components and measured total deflections of one specimen from each group of specimens during the first quarter-cycle of load is given in Table 4.1. All these specimens were loaded to a displacement of 4% shear span length in the first load cycle. As given in this table, calculated deflections and measured deflections agree closely. The relationship between the various components of deflection and the total deflection is shown in Figs 4.3(a)-(c). As shown in these figures, the total beam deflection resulted primarily from deformations of the hinging zone. The following sections discuss the changes in the shear and flexural behavior in the hinging zone which took place as the tests proceeded.

4.4 GENERAL BEHAVIOR CHARACTERISTICS

4.4.1 ONE-DIRECTION LOADING

The relationships between calculated beam hinging zone shear displacement, hinging zone flexural displacement and the applied ram load for specimens S1-4, S2-2 and S3-2 during the first quarter cycle of load is shown in Figs 4.4(a)-(c). Several general observations can be made for the relationships shown in these figures.

First, before flexural cracks were formed, the relationships of applied load to shear displacement and of applied load to flexural displacement were linear. This indicated that the hinging zone behaved elastically in both

flexure and shear. Because the applied shear force was resisted primarily by the uncracked concrete, the shear displacement was negligible due to high shear stiffness, and the hinging zone showed primarily flexural displacement.

Second, as the flexural cracking load was exceeded, vertical cracks formed at the top of the hinging zone. These cracks resulted in small amounts of loss of flexural and shear stiffness in the hinging zone. The flexural stiffness decreased due to a reduction of moment of inertia of the sections as the applied load continued to increase. The shear stiffness decreased because part of the shear force previously carried by the uncracked concrete then now carried by dowel action, aggregate interlock and friction across the vertical cracks. As the applied load continuously increased, inclined cracks formed and further decreased the shear stiffness. As shown in these figures, the loss of both flexural and shear stiffness continued gradually up to the load at which longitudinal tension steel first yielded.

Third, as the applied load produced a moment exceeding the yield moment at the face of the specimen's enlarged end block, the relationships between flexural displacement and shear displacement, and the applied load became abruptly nonlinear. Small increases in applied load then caused large increases in both flexural and shear displacements in the hinging zone. It is apparent that after the longitudinal steel yielded at the

face of the enlarged end block, small increases of applied load would result in large increases of strain in the steel and, consequently, large flexural displacement in the hinging zone. However, the large increases in the shear displacement which occurred as the yield load was exceeded may have been due to a change of shear-resisting mechanism(42). It has been found that as the applied load increases beyond the yield load, most of the shear being carried by the compressed concrete, friction forces and dowel forces is transferred over to the stirrups. In addition, yielding of the longitudinal reinforcement resulted in large increases of the crack widths which would lead to large vertical slippage between crack surfaces and, consequently, large increases of shear displacement in the hinging zone.

4.4.2 LOADING REVERSAL

(a) SHEARING BEHAVIOR OF THE HINGING ZONE

A typical relationship between applied load and shear displacement in the hinging zone for Specimen S1-4 is shown in Fig.4.5. When load had been decreased from the maximum positive load in the first cycle to zero load, a residual shear displacement remained as a result of inelastic deformation which had occurred in the hinging zone during the first quarter-cycle of load. After the loading was reversed in direction, the same events described in the previous section were repeated. As shown in Fig.4.5, the slope of the load vs. shear displacement relationship after loading reversal was flatter than the slope

during initial loading in the first quarter load cycle. This occurred primarily because concrete in the hinging zone had been cracked and overall shear stiffness had been reduced during the first quarter cycle of load.

After the beam had gone through several load reversals, an obvious "pinch" in curves was shown near the zero load portion of the load vs. shear displacement relationship when the applied load was reversed in direction. An assumed shear-carrying mechanism of a specimen having inclined cracks is shown in Fig.4.6. As illustrated in this figure, the total shear transferred across an inclined crack consisted of contributions from the uncracked compressed concrete, forces in stirrups crossed by inclined cracks, aggregate interlock or friction force along cracks, and dowel forces from the longitudinal reinforcement. The components of the shear-carrying mechanism did not change as the loading changed, but the magnitude of the shear carried by each shear-carrying element changed as the crack widths and material behavior changed.

After the beam had gone through one cycle of load reversals, vertical and inclined cracks had been developed in the hinging zone. Along vertical cracks, shear was transferred by aggregate interlock, friction and dowel action. Along inclined cracks which crossed stirrups, shear was carried by stirrups as well as by aggregate interlock, friction and dowel

action. The shear carried by uncracked concrete was small because all sections in the hinging zone had been cracked. As the applied load was reduced from the maximum positive(and negative) loads, a large amount of shear displacement remained at points of zero load. At those times, cracks remained open in the upper (lower) part of the hinging zone (Fig.4.7(a)). When the load was reversed in direction, the shear was resisted mainly by dowel action until cracks closed to allow aggregate interlock, friction between cracks, and stirrups to begin carrying load (Fig.4.7(b) & Fig.4.7(c)). During these periods, shear resistance was extremely low until cracks had been closed, and then shear stiffness increased as load was increased. As the number of load reversals which the beam had experienced increased, the shear-carrying capacity of aggregate interlock, friction, and dowel action of the longitudinal reinforcement became less effective as (1) crack widths and abrasion of concrete surfaces along cracks increased, and (2) concrete cover spalled off in the hinging zone. Also, additional minor cracks developed in the concrete, causing deterioration of the bond between stirrups and concrete. A decrease of the shear stiffness in the hinging zone and an increase in the shear displacement at the same level of applied load resulted in consecutive cycles.

(b) FLEXURAL BEHAVIOR OF THE HINGING ZONE

The relationship between applied load and flexural

displacement in the hinging zone for Specimen S1-4 is shown in Fig.4.8. The relationship of the load vs. flexural displacement was more stable than that of load vs. shear displacement. Although there was slight "pinching" of the curve as loading was reversed in direction, the degree and severity of the "pinched" region was small compared to that shown in the relationship of load vs. shear displacement for this specimen in Fig.4.5.

As mentioned in the previous section, vertical and inclined cracks had developed at the top and bottom of the hinging zone after the first cycle of load. The moment produced by the applied loading was resisted primarily by the top and bottom longitudinal reinforcement before cracks closed. After cracks closed due to local compression and shearing deformation, part of the compressive force was transferred from the compressed reinforcement to the compressed concrete. The transition of the compression forces from steel to concrete during the process of crack closing did not cause increases in flexural stiffness.

It has been shown from strain gage data that the standard 90 degree hooks located inside the enlarged end block provided anchorage effectively for longitudinal reinforcement throughout testing for all specimens. A moment-resisting mechanism shown in Fig.4.9 was assumed to explain the behavior observed in the load vs. flexural displacement relationship. As the deterioration of bond along the straight development length

inside the enlarged end block increased, the length of unbonded longitudinal reinforcement increased and the displacement required to develop the strength of the member also increased. Consequently, at the same maximum displacements, the strength of the member decreased with increasing number of cycles.

4.5 EFFECTS OF SHEAR STRESS LEVEL

The relationships between applied load and shear displacement in the hinging zone for specimens S1-4, S2-4 and S3-4 during the first quarter cycle are shown in Fig.4.1Ø for comparison. The maximum displacement reached in these three specimens was 4% shear span length. The main differences between these specimens were the shear span length and the maximum shear force reached at the 4% shear span length displacement.

Under monotonic loading, the shear stiffness was the same for all specimens as the load was initially applied. Because the shear span length of Specimen S3-4 was much shorter than that of specimens S2-4 and S1-4, the moment at the face of the enlarged end block was higher in Specimens S1-4 and S2-4 than in S3-4 for comparable amounts of applied load. As a result, flexural cracks would form at the lowest ram load in Specimen S1-4, at a larger ram load in Specimen S2-4 and at the highest ram load in Specimen S3-4. The flexural cracks formed in the hinging zone reduced somewhat the shear stiffness in this

region. Therefore, the shear stiffnesses of the hinging zones of Specimens S1-4 and S2-4 were lower than that of Specimen S3-4 after their respective flexural cracking loads had been exceeded. However, once the yield load had been exceeded, the shear stiffnesses of all specimens were approximately the same until the maximum load was reached. Because the maximum shear forces were not the same in all specimens, the maximum shear displacements reached in each specimen were not the same at beam displacements of 4% shear span length. The change of shear stiffness accompanying the exceeding of yield loads can be easily seen in Fig.4.11 in which the applied load has been normalized with respect to the yield load.

After the completion of a full inelastic load reversal, the crack "opening and closing" behavior (Fig.4.7) significantly affected in the shear-resisting mechanism in the hinging zone. Under Type I loading history, the maximum force reached in each cycle decreased with an increasing number of cycles. However, the maximum shear force experienced by the Group III specimen in each cycle was still much larger than those experienced by Group I and Group II specimens. The shear displacement in the hinging zone at the maximum positive displacement of each cycle for specimens subjected to Type I loading history shown in Figs 4.12 to 4.14. The same general trends were shown in all these figures, and the effects of different maximum shear forces reached in each group of specimens with number of cycles may be seen by comparing the relationships shown in these figures.

As shown in Fig.4.12, the shear displacement in the hinging zone of Specimen S1-1 increased with the increasing number of cycles during the first few cycles and then remained almost constant in following cycles. This indicated that the deterioration of shear stiffness slowed down after the first few cycles.

A similar trend was observed in Fig.4.13 for Specimen S2-1. However, the shear displacements of Specimen S2-1 were much larger than those of Specimen S1-1 in corresponding cycles, and the rate of increase of shear displacement was higher in Specimen S2-1 than in Specimen S1-1 during increasing numbers of cycles. Specimen S2-1 was inadvertently loaded to a maximum positive displacement of 2.47% of shear span length during the 7th load cycle. The shear displacement in the following cycles at 2% shear span length displacement did not show much increase. However, the strength of the specimen dropped significantly in the following cycles at that displacement. It was shown in Chapter 5 that this strength drop resulted primarily from bond deterioration in the enlarged end block of the specimen.

The rate of increase of shear displacement with increasing number of cycles for Specimen S3-1, shown in Fig.4.14, was the most pronounced one among these three specimens. The maximum gross shear stress experienced by Specimens S1-1, S2-1 and S3-1 were 3.3, 5.1 and 7.1 $\sqrt{f'_c}$ respectively, while the maximum shear displacement in the hinging zone of these specimen during

30th load cycle were approximately 16, 32 and 58 percent of the beam displacement at the loading point.

Increases of shear displacement in the hinging zone resulted in less straining of the longitudinal steel at prescribed maximum displacements and eventually reduced the strength a specimen could develop at the same maximum displacement. As a result, Specimen S3-1 withstood the least total number of cycles of displacement of these three specimens before the strength at the maximum positive displacement dropped below 75% of its original yield strength.

When specimens were subjected to displacement reversals with maximum displacements of 4% of shear span length, severe cracks in the concrete extended out of the hinging zone. As a result, methods used to measure the shear and flexural displacements in the hinging zone were inaccurate. Therefore, a comparison of deflection components based on these data is not appropriate and has not been shown here.

4.6 EFFECTS OF LOAD HISTORY

Because the cracking of concrete of Group III specimens took place mainly within the hinging zone, and because specimens of different shear stress levels subjected to the same type of loading history exhibited similar relationships between applied load and displacements in the hinging zone, Group III specimens will be used to illustrate a general discussion of the effects

of load history on member behavior. Relationships between applied load and flexural displacement in the hinging zone as well as relationships between applied load and shear displacement in the hinging zone for Group III specimens are shown in Figs.4.15 to 4.18.

(1) Type I loading: As shown in Fig.4.15, during the first load cycle, both relationships were unique and never reproduced again. After the first load cycle, flexural behavior in the hinging zone was extremely stable, and no severe "pinch" of the curves was observed. However, the relationship between applied load and shear displacement in the hinging zone exhibited a gradual increase of shear displacement at the same level of applied load with increasing number of cycles. A severe "pinch" of curves was shown whenever the applied load was reversed in direction. The gradual increases of shear displacement with increasing numbers of cycles resulted from degradation of concrete and from reduction of shear stiffness in the hinging zone. This "pinching" of curves also resulted from the crack "opening and closing" behavior shown in Fig.4.7.

(2) Type II loading: Relationships between applied load and displacements in the hinging zone for Specimen S3-2 are shown in Fig.4.16. Under uniform reversed displacements of 4% shear span length, both flexural and shear stiffnesses in the hinging degraded quickly with increasing number of cycles. As was the case for Specimen S3-1, severe "pinching" was observed in the relationship of applied load to shear displacement only.

After only four cycles of load, the hinging zone lost almost all ability to resist applied shear force.

(3) Type III loading: As shown in Fig.4.17, the flexural and shearing behavior in the hinging zone of Specimen S3-3 exhibited similar overall relationships with the applied load during the first two cycls as have been shown in Fig.4.15 for Specimen S3-1. Once the maximum positive and negative displacements were increased to 4% shear span length during the third cycle, both flexural and shearing stiffnesses were reduced greatly during the following cycles. Another application of load cycle at 4% shear span length displacement limit resulted in another large reduction in shear stiffness while the flexural stiffness did not show as obvious a reduction as had been seen during the third load cycle. The degradation of both flexural and shear stiffnesses during the 5th and 6th load cycles at 2% shear span length limits was negligible compared to that which had been caused by load cycles at 4% shear span length limits.

(4) Type IV loading: During the first two load cycles, the relationships shown in Fig.4.18 for Specimen S3-4 are quite similar to those shown in Fig.4.16 for Specimen S3-2. After the first two cycles, Specimen S3-4 was subjected to two cycles of maximum displacements of 2% shear span length. These two cycles did not show many differences between each other, and did not seem to affect the hinging zone behavior during the fifth cycle. Load cycles which contained maximum displacements of 4% shear span length contributed most of the degradation of stiffness of the member.

CHAPTER 5

BOND AND ANCHORAGE BEHAVIOR

5.1 INTRODUCTION

Previous investigations have shown that the nature of bond between concrete and a deformed reinforcing bar is dependant on bearing of the bar lugs on concrete, the strength of concrete between lugs, and to some extent the chemical adhesion and friction between the two materials(3,30). Regardless of the components of the bond resisting mechanism, average bond stress has often been used as an index to evaluate anchorage performance. This chapter will discuss the performance of anchorage of longitudinal bars during the first quarter cycle of loading based on the calculated average bond stress between gages attached to the longitudinal reinforcement within the enlarged end block and the zone of plastic beam hinging. Elongation of the longitudinal reinforcement in the enlarged end block will be calculated and the results will be used to illustrate the effects of load history on the behavior of bond within the members.

5.2 BOND STRESS

The magnitude of average bond stress developed along longitudinal reinforcement between strain gages and the manner in which these stresses changed as the applied beam tip deflection was increased can be calculated by considering the

strain gage readings at various points along longitudinal reinforcement in conjunction with known stress-strain behavior of longitudinal bars(Fig.2.5). The strain and corresponding stress variations along the top longitudinal reinforcement of specimens S1-4, S2-2 and S3-2 are shown in Figs 5.1-5.3. Two distinct behaviors were observed in these figures: (1) before the yield load was reached, increases of the strains along the bar were relative small, but the corresponding increases of stresses were large; (2) after the yield load was exceeded, small increases of the applied load resulted dramatic increases of the strains at the face of the enlarged end block, however, the corresponding increases of stress was small. This indicated that there were palpable changes in the bond mechanism as the applied load increased. The average bond stress was then calculated to show the changes of the bond resistance between gages. To calculate the average bond stress, u, the following expression was used

$$u = \frac{A_b \, \Delta\sigma_s}{\Sigma_o \, \Delta X}$$

where

A_b = bar area

$\Delta\sigma_s$ = difference in steel stress between gages

Σ_o = bar perimeter

ΔX = distance between gages

As shown in Fig.5.4, the longitudinal reinforcement was segmented into four regions by the strain gages and the tangent

of the 90-degree hook. The calculated average bond stresses in regions II, III and IV during the first quarter cycle of load for specimens S1-4, S2-2 and S3-2 have been plotted vs. the load point deflection and these relationships are shown in Figs 5.5-5.7. Although there were variations of the average bond stresses in a given region between different specimens, similar general trends can be observed for all specimens in these figures. The changes of the average bond stress in each region due to increases in the applied deflection reflect changes in the bond resisting mechanism.

The following general observations can be made for the relationships shown in Fig.5.6. First, the average bond stresses in Region II and III increased as the applied deflection increased. The rate of increase of average bond stress was higher in Region III than in Region II, indicating that during the initial loading stage, Region III was more effective in providing anchorage to the longitudinal steel than was Region II. Second, after the average bond stress in Region III reached a maximum the average bond stress in this region declined as the applied deflection was increased continuously. However, the average bond stress in Region II kept increasing with increasing applied deflection. This indicated that the bond resistance was deteriorating in Region III, and that Region II was becoming more effective in providing anchorage than was Region III. Third, as the deflection increased well beyond the

yield deflection, large straining of the longitudinal reinforcement in Region III produced wedge action in the surrounding concrete, producing increases in the average bond stress as the applied deflection was increased. However, the continuously decreasing average bond stress in Region II indicated that deterioration of bond was gradually extending further into the enlarged end block along the reinforcing bars.

The relationship of average bond stress in region IV to the applied deflection showed behavior similar to that shown in region III. However, the average bond stresses in region IV were generally smaller than those in region III, partly because of the small moment gradient existing in this region, and partly because of the flexural-shear cracks which formed in this region.

Because the top longitudinal reinforcement of both Group II and Group III specimens was fabricated from No. 7 bars from the same heat, the maximum average bond stresses first reached in Region II and Region III were calculated and are given in Table 5.1 for comparison. The maximum average bond stresses developed in Region II were more than twice as much as the maximum average bond stresses developed in Region III for all the specimens compared in Table 5.1. This indicated that the anchorage development length further away from the face of the enlarged end block was more effective than that closer to the face of the enlarged end block in providing anchorage to the

longitudinal reinforcement. The maximum average bond stress was lower in Group III specimens than in Group II specimens. This may have been due to the differences in the maximum gross shear force in the beam. Higher shear force caused higher dowel force, which tended to produce more local disruption of the bond near the face of the enlarged end block.

To determine the proportion of the anchorage force provided by the standard 90-degree hook, by Region I, and by the straight development length in Regions II and III, the anchorage force in each region was calculated by a method similar to that used to determine bond stress. The relationships between the anchorage force in each region and the applied tensile force during the first quarter cycle of load are shown in Figs 5.8-5.10 for specimens S1-4, S2-2 and S3-2. The nature of general behavior of anchorage forces shown in these figures indicates that the anchorage force provided by the standard 90-degree hook, Region I, increased as the applied tensile force increased. At the maximum displacement, the percentage of total anchorage provided by the hooks was 54.8% in specimen S1-4, 77.2% in specimen S2-2, and 82% in specimen S3-2 respectively. Therefore, Region I's were the most important sources of anchorage for the longitudinal steel in all cases.

5.3 ELONGATION OF LONGITUDINAL REINFORCEMENT

After a specimen had been subjected to inelastic reversed

loading, the reinforcing bars had been subjected to cycles of inelastic strain. The calculation of the average bond stress between gages based on the strain readings in the bar and on the monotonic stress-strain relationship of the steel would be misleading. In an attempt to quantify bond deterioration resulting from cyclic loading, elongation of the longitudinal reinforcement inside the enlarged end block was calculated and used as an alternative indicator of bond deterioration.

To calculate the elongation of the longitudinal steel, a linear variation of strain along the bar was assumed as illustrated in Fig.5.11. Because of the large strains which developed in the longitudinal reinforcement at the face of the enlarged end block, strain gages were broken in some specimens after a few cycles of loading. As a result, the elongation of the longitudinal reinforcement could be calculated only for a limited number of the specimens and for a limited number of cycles.

The relationship between the elongation of the top longitudinal reinforcement in the enlarged end block and the steel strain at the face of the enlarged end block is shown in Fig.5.12 for Group II and Group III specimens. The elongation of the anchored steel increased approximately linearly with the steel strain up to the yield strain, and then the rate of increase in elongation decreased after the yield strain was exceeded. The rate of increase in steel elongation increased

again after the strain hardening strain was reached. The changes of the rate of increase in steel elongation resulted from the sequence of the bond deterioration along the steel discussed in the previous section.

The elongation of the top reinforcement inside the enlarged end block for specimen S3-4 is plotted vs. applied load and load point deflection for the first cycle of load in Figs.5.13(a) and 5.13(b) respectively. As shown in Fig.5.13(a), the steel first yielded at the face of the enlarged end block between points A and B, and reached the strain hardening strain between points C and D. During unloading of the beam, the steel recovered elastic strain retained a residual elongation at zero load. When loading direction was reversed an almost linear relationship existed between the applied deflection and shortening of the steel from E to F as shown in Fig.5.13(b). Further increase in negative loading caused small shortening of the top reinforcement because the flexural cracks previously formed in the top portion of the beam were then closed. Decreasing the negative beam load resulted in some recovery of the steel deformation between points G and H. The general relationships shown in Fig.5.13 are very much similar to the relationship between the applied ram load and the steel strain at the face of the enlarged block. This indicated that the steel strain at the face of the end block accounted for the majority of the elongation of the steel in the block.

The elongation of the top reinforcement inside the enlarged end block for all load cycles are plotted with respect to the applied load and load point deflection for Specimen S3-4 in Figs 5.14(a) and (b) respectively. The relationships between the steel elongation and the applied load and deflection showed quite stable behavior after the first load cycle.

The same assumptions and calculation procedure used to find the elongation of the top reinforcement can be employed to find the shortening of the bottom reinforcement. The relationship between the calculated shortening of the bottom steel and the measured compressive steel strain at the face of the enlarged end block during the first quarter-cycle of load is shown in Fig.5.15 for Group II and III specimens. The relationship was nearly linear up to a compressive strain of approximate Ø.ØØ15, and then the rate of increase in shortening decreased as the compressive strain continued to increase. However, the shortening of the bottom longitudinal reinforcement was quite small compared to the elongation of the top longitudinal reinforcement, and therefore compression reinforcement bond deterioration was not significant under monotonic loading.

The relationship between the calculated shortening of the bottom longitudinal reinforcement in the enlarged end block and the applied load is shown in Fig.5.16 for Specimen S3-1. The general character of the relationship shown in Fig.5.16 is quite

similiar to that of the relationship between the applied load and the steel strain at the face of the enlarged end block. After completion of the first load cycle, bottom steel exhibited a residual elongation and retained net positive elongation for all loads during all subsequent cycles of load.

The residual elongation of the top longitudinal reinforcement at the zero load point (Fig.5.17) of each cycle was plotted vs. the number of load cycles, as shown in Figs 5.18 to 5.20, to determine the effect of load history on the bond deterioration of reinforcement anchorage. The strain gages used in Specimen S2-2, S2-3, S2-4 and S3-2 at the face of the enlarged end block broke after the first cycle of load. As a result, elongation of the top reinforcment of these specimens could not be calculated and are not shown in these figures.

As shown in Fig.5.18, during the first 3 to 5 cycles of load, residual steel elongations increased with increasing number of cycles and then remained almost constant in the following cycles. The increases of residual steel elongation during the first few cycles resulted primarily from bond deterioration along the bar. Under loading to uniform 2% shear span maximum displacement limits, the longitudinal steel elongation did not increase significantly after the first few load cycles had been completed and shear deformation in the hinging zone dominated the response of the beam with increasing number of cycles.

Specimen S2-1 was inadvertently loaded beyond the planned maximum positive displacement limit during the seventh load cycle. As a result, the residual steel elongation increased from Ø.Ø318 to Ø.Ø394 inches, and the elongation remained approximately constant after conclusion of the following cycles. This indicated that bond deterioration of the anchored reinforcement was more closely related to the maximum displacement than to the number of cycles the beam had experienced, and that the damage of bond was irreversible.

The main difference between Specimens S2-1 and S3-1 were the maximum gross shear stresses and the size of the transverse reinforcement in the members. Had Specimen S2-1 not been excessively deflected during the seventh load cycle, the residual steel elongation within Specimen S2-1 following all cycles but the first cycle would still have been much larger than those in Specimen S3-1. The difference of residual steel elongation may be speculated to have resulted from the differences between shear deformations in the hinging zones of the two specimens during cyclic loading which resulted in less straining of the longitudinal reinforcement and , consequently, smaller residual steel elongation remaining after cyclic loading in Specimen S3-1.

Although the gross shear stress in Specimen S1-1 was much lower than in Specimens S2-1 and S3-1, Specimen S1-1 was fabricated with No. 6 bars while No. 7 bars were used in the

other group of specimens. As a result, direct comparison can not be made between the two. However, satisfactory anchorage was provided to the longitudinal reinforcement as indicated by small residual elongation with cycling for No. 6 bar shown in Fig.5.18.

Residual steel elongations at zero loads for specimens of Groups I and III are shown in Figs 5.19 and 5.20 respectively. An irregular change of calculated residual steel elongation was observed in Specimen S1-4 and S3-4. This may have been caused by the assumption of linear strain distribution between gages. Changes of the maximum displacements in the loading history from 2% to 4% shear span length significantly affected bond deterioration and, as a result, the residual steel elongation seen in Specimen S3-3. Note that within each group of specimens having a common maximum gross shear stress, load histories which contained displacements to 4% of shear span length caused much larger amounts of residual steel strain than did histories which contained displacements of 2% of shear span length.

5.4 FIXED END ROTATION

Due to differential elongations of the top and bottom longitudinal reinforcement inside the enlarged end block, an angular rotation could be assumed to be concentrated at the face of the enlarged end block. This rotation may be referred to as "fixed end rotation", and is calculated as following

$$\theta_{FE} = \frac{e_t - e_b}{d - d'}$$

where

e_t = top steel elongation

e_b = bottom steel elongation

d-d' = distance between top and bottom steel

The beam displacement at the load application point due to fixed end rotation can be determined as $\Delta_{FE} = l \times SIN(\theta_{FE})$ where l is the shear span length. In Chapter 4, θ_{FE} and Δ_{FE} were included as flexural rotation in the hinging zone and flexural displacement at the loading point. Percentage of Δ_{FE} with respect to the flexural displacement at the loading point and total beam displacement is given in Table 5.2 for all spceimens at the maximum positive displacement of the first cycle. As shown in Table 5.2, Δ_{FE} actually was a major source of the total displacement.

Calculation of θ_{FE} required good strain readings from all strain gages inside the enlarged end block. For most of the specimens tested in this investigation, at least one strain gage broke during the first load cycle. Therefore, exact comparisons of the calculated fixed end rotation between specimens were not possible because of lack of data. However, useful information can be drawn from the relationships between applied load and fixed end rotation shown in Figs 5.21 and 5.22 for Specimen S3-1 and S3-3, two specimens for which at least partial data was available.

As shown in these figures, a slight "pinch" of the curves

resulting from Bauschinger effects was observed as applied load was reversed in direction. But the degree of the "pinch" was minor compared to what had been shown in Figs 4.15(b) and 4.17(b) in the relationship between applied load and shear displacement in the hinging zone. The general configuration of Figs 5.21 and 5.22 is similar to that of the relationship between applied load and flexural displacement in the hinging shown in Figs 4.15(a) and 4.17(a).

Two conclusion can be made as follows regarding behavior of anchorage of reinforcement: (1) anchorage of the longitudinal reinforcement was satisfactorily provided by the 90-degree hooks regardless of the bond deterioration which had occurred along the straight development length, (2) the low stiffness behavior visible near zero load points in load-deflection curves was contributed mainly by the shear stiffness decay in the beam hinging zone rather than by bond deterioration in the anchorage zone.

CHAPTER 6

ENERGY DISSIPATION CAPACITY

6.1 INTRODUCTION

Due to practical and economic considerations, the possibility of structure inelastic deformation during the course of a severe earthquake must be anticipated during the designing of a reinforced concrete structure which is to be situated in a zone of seismic activity. If the structure is to survive, the individual structural components must be ductile and possess a reserve of energy dissipation capacity. Present design philosophy implicitly assumes that the larger the energy dissipation capacity a member has, the better the performance of the member and structure will be. To this end, code provisions specifically attempt to prevent non-ductile failure modes such as (1) sudden shear failure of members, (2) buckling of the main longitudinal reinforcement, and (3) loss of bond (bond slip) and of anchorage. These failure modes and their prevention have been the subjects of numerous research projects during the past decade. However, because of a lack of agreement as to what constituted a displacement history that was representative of what an actual structural member might be forced to endure during a severe earthquake, the loading history used in each project was somewhat arbitrary. A common criterion which could be used to evaluate and compare the test results from different sources to determine effects of a given parameter and the

overall ability of a given specimen to perform its structural function did not exist.

Gosain et al.(19) addressed this problem, and attempted to make a comparison of test results from different sources by formulating a measure of nondimensionalized component capacity which they termed "work index". However, the possible influence of loading history on the "work index" was not considered, and considerable scatter of the data remained in this work.

In addition to the evaluation and prediction of total energy dissipation capacity of a member, estimation of the damage of a member based on the amount of energy dissipated before failure is a subject deserving consideration. It is reasonable to say that the more energy a member dissipates, the more damage the member will sustain, and the less energy dissipation capacity will remain in the member. Banon et al. (8) attempted to predict the damage within a reinforced concrete frame based on structural component energy dissipation test results. However, as in Gosain's study, possible effects of the loading history on the energy dissipation capacity of frame members were still not considered in their work.

In order to consider the possible influence of loading history on the energy dissipation capacity of reinforced concrete members subjected to inelastic loading reversals, an "energy index" is proposed in this chapter. The formulation of

this index of member energy dissipation capacity is based on the results of the present test series and considers displacement history, stiffness degradation, and maximum gross shear stress experienced by each member. Because the present test series used only a narrow range of displacement histories for this empirical formulation, test results from other sources were also considered to verify the applicability of this energy index data treatment to specimens subjected to a wide range of displacement histories.

6.2 WORK INDEX

In an attempt to make comparisons of member cyclic inelastic capacity between test results from different sources, a "work index" was proposed by Gosain et al. (19) as a nondimensional measure of energy dissipation capacity of reinforced concrete members subjected to inelastic loading reversals. Instead of attempting to represent the actual area within member load-deflection curves, the work index approach used an empirical relationship based on displacement ductility (Δ_n / Δ_y), the ratio of maximum load in a given cycle to the section's monotonic flexural yield load (P_n / P_y), the level of axial load carried by the section, and the member's shear span to depth ratio (a/d) to predict member capacity. Because simplifications are made in calculating the work index, some obvious problems arise in the computation of work index. As pointed out by Gosain, the same value of work index would be

calculated for a specimen loaded 4 times to a displacement ductility of 5 as for one loaded twice to a displacement ductility of 1Ø. Neverthless, he admitted the likelihood that the loading to a displacement of 1Ø times yield displacement would damage the member more severely. This prognosis has been verified by the test results of this investigation: specimens subjected to a loading history containing 4% shear span length displacements lost their ability to resist deformation in much fewer cycles than did those subjected to a load history containing only 2% shear span length displacements, and further, the "work indices" for two similar specimens so loaded were significantly different.

In Fig.6.1, the test results obtained in this investigation are presented in a form identical to that used by Gosain et al, (see Gosain et al. Fig. 1Ø). As shown in this figure, the work indices calculated for specimens considered here are far from the statistical mean work index for all specimens considered by Gosain. Furthermore, the work indices of specimens subjected to Type I loading history were always much larger than those of specimens subjected other than Type I loading history. Therefore, a better representation of the energy dissipation capacity of a member which can take the difference of loading history into account is needed when comparison is to be made between test results from different sources.

6.3 ENERGY INDEX

The energy dissipated by a member subjected to inelastic loading reversals may be determined by measuring the area under the member's load-deflection curves. Because complete load-deflection curves were recorded for the specimens tested in this investigation, the energy dissipated during each load cycle by each specimen could be measured easily. The total energy dissipated by each member was calculated by summing the energy dissipated in each cycle for all cycles prior to the cycle in which the applied load at the maximum positive displacement of the assigned load history dropped below 75% of the load at which first yielding of the longitudinal reinforcement occurred.

The total energy dissipated by each specimen is tabulated in Table 6.1. As indicated in this table, specimens subjected to Type I loading were able to dissipate much more energy than were specimens subjected to loading histories other than the Type I load history. In order to consider the difference of total energy dissipation between specimens resulting from differences of loading historys, an "energy index" is proposed and is defined as follows:

$$I_E = \sum_{1}^{n} E_n \frac{K_n}{K_y} \left(\frac{\Delta_n}{\Delta_y}\right)^2$$

where

E_n = energy dissipated during nth cycle

K_y, K_n = stiffnesses as defined in Fig.6.2

Δ_n, Δ_y = displacements as defined in Fig.6.2

n= number of cycles in which $P_n / P_y \geq 0.75$

The "energy index" as calculated by this procedure for each of the specimen in this test series is given in Table 6.1. As shown in this table, differences between values for specimens within the same group are much smaller than are the differences between values of actual total energy dissipation for those same specimens. This indicates that this treatment of energy dissipation data, in conjunction with the known displacement history for the specimens in this investigation, has had the effect of compensating for differing displacement histories.

As has been previously discussed, the displacement histories used in formulating the "energy index" approach varied within narrow limits of maximum displacement magnitude and variation of maximum displacement magnitude with respect to load cycle number. An important test of the proposed method of load history normalization was to determine whether or not it could be realistically applied to the results of tests in which maximum displacement amplitudes varied widely. Because calculation of energy index requires a knowledge of actual energy dissipation for each cycle of loading, only the results of tests which reported these data were used. Results of studies performed by Lee et al. (28) and by Scribner and Wight (36) were selected to serve as tests of the method. The

calculated energy index values for these tests are given in Table 6.2 and are plotted in normalized form against maximum first cycle shear stress experienced by each specimen in Fig. 6.3. If the degree to which the relationship approaches linearity is taken as a verification of the acceptability of the data treatment, then that verification is evidenced by the small scatter of data present in Fig. 6.3.

6.4 FACTORS AFFECTING ENERGY INDEX

Using energy index as a measure of the energy dissipation capacity of members subjected to reversed inelastic loading, a study of factors which influence the energy index is given in this section by considering test results from different sources. To compare the energy index of specimens which differed in size and flexural stiffness, the energy index of each specimen was normalized by dividing by the yield load and by the yield displacement of each specimen. The test results and relevant parameters considered in this study are listed in Table 6.2. Because a large range of energy index values was present for the specimens considered, the energy index has been plotted on a logarithmic scale when comparisons have been made between specimens.

One of the most important factors which has been considered to affect the performance of a member subjected to loading reversals is the maximum shear stress level. Indeed the

linearity of this relationship has been used in this report and in previous investigations as a measure of data reduction method acceptability. In comparison with Fig.6.1 (by Gosain), the scatter of data is considerably reduced by use of the "energy index" reduction. In general, higher values of normalized energy index resulted from lower shear stress levels. A regression line based on the least squares method is also shown in the figure to represent the general trend. The sample correlation coefficient is -Ø.748, indicating reasonably good linearity of the relationship.

The influence of the ratio of transverse reinforcement on the normalized energy index is shown in Fig.6.4. It is apparent that no defineable relationship exists between normalized energy index and the transverse reinforcement ratio. To investigate the influence of the transverse reinforcement further, the ratio of the shear capacity of the transverse reinforcement to the maximum applied shear V_s / V_m is plotted against the index in Fig.6.5. The shear capacity of the transverse reinforcement V_s was calculated as $A_v f_y (d/s)$. Although some scatter of the data exists, the general trend shown in this figure indicates that the normalized energy index increases as the ratio V_s / V_m increases.

Shear span to depth ratio (a/d) has also been considered to be a significant factor in influencing the ability of a member to withstand reversed loading. For any given member, an

increase of the a/d ratio results in a decrease of the maximum shear stress and, consequently, a potential increase in the energy dissipation capacity for the member. The relationship between the normalized energy index and shear span to depth ratio, shown in Fig.6.6, does indicate a general trend of increasing normalized energy index with increasing shear span to depth ratio.

It is required by Appendix A of the ACI code that the maximum tension reinforcement ratio of a section shall not exceed 50% of the balanced reinforcement ratio if the section is to be designed to withstand earthquake loading. The relationship of tension reinforcement ratio to normalized energy index can be observed in Fig.6.7. The linear regression line shown in Fig.6.7 has a correlation coefficient of -0.772, which indicates that a relationship exists between the normalized energy index and the ratio of ρ / ρ_b . The general trend evident here is that an increase in energy dissipation capacity accompanys lower percentages of tension reinforcement.

In an attempt to reduce further the scatter of the data, the shear span to effective depth ratio (a/d) may be used to modify the energy index as:

$$I_E' = I_E \ (1- d/a \ )$$

The relationship between modified normalized energy index and the measured shear stress is shown in Fig.6.8. The data

still shows a scatter similar to that shown in Fig.6.3. However, the absolute value of the correlation coefficient of the data increases from Ø.748 to Ø.792 as a result of the modification. This indicates that the linearity of the relationship between the normalized energy index and shear stress has been somewhat improved.

The relationship between modified normalized energy index and the ratio ρ / ρ_b is shown in Fig.6.9. The correlation coefficient of the regression for this relationship is improved from -Ø.772 to -Ø.784 as a result of the modification.

6.5 SUMMARY

It has been shown in the previous sections that loading history significantly affects the total energy dissipation capacity of a member subjected to loading reversals. An "energy index" evaluation has been proposed to take into account the effects of loading history, and has been used as a measure of normalizing energy dissipation capacity of members subjected to various magnitudes of inelastic loading reversals. Factors which influence the energy index have been found to be the shear stress level, shear span to effective depth ratio, the shear capacity of the transverse reinforcement, and the ratio of the percentage of the tension reinforcement to the balanced reinforcement ratio.

CHAPTER 7

SUMMARY AND CONCLUSION

7.1 OBJECT AND SCOPE

The primary objective of this investigation was to study experimentally the effect of load history on the total energy dissipation capacity of reinforced concrete flexural members. A secondary objective was to study the hysteretic behavior of reinforced concrete flexural members under inelastic reversed loading whose displacement amplitudes were in the range of 2% or 4% of the member's shear span length. To achieve the objectives, eleven reinforced concrete cantilever specimens were constructed and tested under various conditions of inelastic loading reversal. Variables included in this study were loading history and maximum shear stress level.

7.2 SUMMARY

7.2.1 OUTLINE OF EXPERIMENTAL WORK

To make the specimen as simple as possible, a specimen of cantilever type was chosen. The specimen consisted of an enlarged end block and the cantilever beam itself. The enlarged end block provided anchorage for the beam longitudinal reinforcement and supported the beam. The ACI Building Code (318-77) and its Appendix A were used as a guide for designing all the specimens.

Loading history was considered to be the most important variable in this study. The displacement amplitude of each loading history was measured in terms of percentages of the beam shear span length. Loading histories which contained uniform 2% or 4% shear span length displacement amplitudes were used to study the effect of displacement magnitude on the specimen response; Loading histories which contained both 2% and 4% shear span length displacement amplitudes were used to study the effect of displacement sequence on the member behavior. The other variable considered was the maximum shear stress level. Specimens were divided into three groups on the basis of the maximum shear stress level. The maximum shear stresses applied to the specimens ranged from 3.3 $\sqrt{f'_c}$ to 7.4 $\sqrt{f'_c}$.

During testing, each specimen was held fixed at its enlarged end block while the beam tip was slowly deflected by a hydraulic actuator. Data recorded included (1) load-deflection curves, (2) strains in the top and bottom longitudinal reinforcement and in selected stirrups in the beam hinging zone, and (3) shearing and flexural distortion of the beam hinging zone as measured by four LVDTs in this region. In order to determine the total energy dissipation capacity of each specimen, the specimen was tested until the strength of the specimen at the maximum displacement of its assigned load history dropped below fifty percent of its original yield strength.

7.2.2 OBSERVED SPECIMEN BEHAVIOR

All specimens were able to develop their flexural yield strength and to undergo cyclic inelastic deflections with no sudden decrease in load carrying capacity. In almost all cases, final failure resulted from cracking and spalling of the concrete in the hinging zone, which gave rise to stiffness and strength decay. No buckling or failure in anchorage of the longitudinal reinforcement was observed.

All specimens subjected to Type I loading history (Fig. 2.3(a)) exhibited extremely stable load-deflection behavior after the first few cycles regardless of the maximum shear stress level or the shear span to effective depth ratios. However, specimens subjected to lower shear stress were able to sustain more load cycles prior to failure than were specimens with high shear stress. Specimens subjected to Type II loading (Fig.2.3(b)) showed strength and stiffness degradation with increasing numbers of cycles. The load-deflection curves of these specimens were never stablized. High shear stress aggravated the decay of both stiffness and strength of the specimen. Specimens subjected to Type III or Type IV loading history (Fig.2.3(a) & (b)) showed behavior similar to that shown by specimens subjected to Type II loading history. Load cycles which contained maximum displacement amplitudes of 2% shear span length did very little damage to the specimen as compared to what was done by load cycles which contained displacement

amplitude of 4% shear span length. Specimens that were first subjected to 2% shear span length displacement load cycles retained the ability to develop a moment larger than the original yield moment when the specimens were loaded to a 4% shear span length displacement during the third load cycle.

7.2.3 FLEXURAL AND SHEAR DEFORMATION OF THE HINGING ZONE

During monotonic loading, the flexural and shear displacement of the hinging zone provided a good indication of changes of shear-resisting mechanism. First, before flexural cracks were formed, the applied shear was resisted primarily by the uncracked concrete. Because of the high shear stiffness of the uncracked concrete, shear displacement within the beam hinging zone was almost negligible and the hinging zone showed primarily flexural displacement. Second, as the flexural cracking load was exceeded, vertical and diagonal cracks formed in the hinging zone and inclined as the load was continuously increased. These cracks resulted in a change of shear-resisting mechanism: part of the shear force previously carried by the uncracked concrete then was carried by dowel action, aggregate interlock, stirrups, and friction across the cracks. Third, as the applied load produced a moment exceeding the yield moment at the face of the specimen's enlarged end block, small increases in the applied load caused large increases of the longitudinal reinforcement strain which resulted in large increases of the crack widths and, consequently, large increases in shear and

flexural displacements.

When the applied load was reversed in direction, the crack "opening and closing" behavior affected in shear-resisting mechanisms. This behavior resulted in severe "pinching" in the applied load vs. hinging zone shear displacement relationship near the zero load beam position and in the "pinching" of load vs. deflection curves of the specimen at the same locations.

As the number of load reversals the beam had experienced increased, the shear-resisting capacity of aggregate interlock, friction and dowel action of the longitudinal reinforcement became less effective as (1) crack widths and abrasion of concrete surfaces along cracks increased, and (2) concrete cover spalled off in the hinging zone. Also, additional minor cracks developed in the concrete, causing deterioration of the bond between stirrups and concrete. The shear stiffness decreased and the shear displacement in the hinging zone increased with increasing number of cycles at the same maximum beam displacement. Increases of shear displacement in the hinging zone allowed beam tip displacement to take place with decreasing amounts of total strain in longitudinal reinforcement. As avresult, the resisting force a specimen could develop at a given displacement diminished during cyclic load application.

7.2.4 BOND AND ANCHORAGE BEHAVIOR

The deterioration of bond along the top longitudinal

reinforcement in the enlarged end block during the first monotonic loading was discussed on the basis of average bond stresses and bond forces. The test results indicated that bond deterioration first started at the face of the enlarged end block, and then gradually extended into the enlarged end block along the longitudinal reinforcement. The straight portion of the longitudinal reinforcement at a distance from the face of the enlarged end block was able to develop higher average bond stress than was the portion closer to the face of the enlarged end block. The maximum average bond stress was lower in Group III specimens than in Group II specimens. This may have been due to the differences in the maximum shear forces in the beams. Higher shear force caused higher dowel force, which tended to produce more local disruption of the bond near the face of the enlarged end block.

During loading reversals, the residual steel elongation resulting from each cycle of load was used as an alternative measure of the bond deterioration along longitudinal reinforcement in the enlarged end block. During the first few cycles, the total residual steel elongations increased with increasing number of cycles and then remained almost constant in the following cycles. After the first few load cycles had been completed, shear deformation in the hinging zone increasingly dominated the response of the beam with increasing numbers of cycles, and the rate of deterioration of bond became relatively

slower than had been the case during the first few cycles. The bond deterioration along reinforcement anchorage seemed to be more closly related to the beam maximum displacement than to the number of cycles the beam had experienced at a given displacement limit. Also, the bond deterioration over a certain length of longitudinal reinforcement was found to contribute little to the "pinching" of the load-deflection relationship near zero load points as long as the anchorage of the longitudinal reinforcement was satisfactorily provided beyond the location of bond deterioration.

7.2.5 ENERGY DISSIPATION CAPACITY

As indicated by test results, identical specimens subjected to different magnitudes of inelastic loading reversals showed different energy dissipation capacity. To take the effect of loading history on the total energy dissipation capacity of the specimen into account, an "energy index" was proposed and was used as a measure of normalized total energy dissipation capacity of reinforced concrete flexural members. Test results of other researchers were used to verify the applicability of the proposed "energy index" to members tested under a wide range of displacement histories. Factors which influenced the energy index were found to be (1) the maximum shear stress level, (2) shear span to effective depth ratio, (3) the shear capacity of the transverse reinforcement, and (4) the ratio of the percentage of the tension reinforcement to the

balanced reinforcement ratio.

7.3 CONCLUSION

Based on the results of tests discussed here and in conjunction with research done by others, the following conclusions can be drawn:

1. The strength and stiffness degradation of reinforced concrete members during repeated reversed inelastic loading were closely related to the magnitude of the maximum displacement in each cycle and the maximum shear stress level experienced by the member.

2. The total energy dissipation capacity of a reinforced concrete member depended strongly on the displacement history the member is to experience. Estimation of the damage or comparison of the performance of reinforced concrete member subjected to inelastic reversed loading based on energy the member had dissipated needed to consider the displacement history the member had experienced.

3. Under maximum member displacement to 2% of the member's shear span length, the failure of the member was not likely to occur during the number of cycles of loading which might conservatively be expected to accompany a major earthquake.

4. As long as the maximum member displacement was kept in the range of 2% of the member's shear span length in cyclic reversed loading, the strength degradation of high shear flexural member designed in accordance with ACI Code (318-77) would not be excessive.

5. An increase in gross shear stress in a flexural member caused a reduction in the total number of cycles to failure for any given load history.

6. The degradation of bond resistance between reinforcement and concrete in the anchorage zone was more closely related to the beam maximum displacement than to the number of cycles the member has experienced at a given displacement amplitude.

TABLES

Table 2.1
Reinforcement Details

Speimen	Shear Span (IN)	A_s	A'_s	A_v
Group I	39	3- # 6	3- # 5	2 @2.5"
Group II	34	3- # 7	3- # 6	2 @2.5"
Group III	25	3- # 7	3- # 6	3 @2.5"

Table 2.2
Design Shear Stress, and Testing Schedule

Specimen	Design * Shear Stress	Measured * Shear Stress	Load History
S1-1	3.Ø	3.3	I
S1-2	3.Ø	3.6	II
S1-4	3.Ø	3.5	IV
S2-1	4.5	5.1	I
S2-2	4.5	5.2	II
S2-3	4.5	6.Ø	III
S2-4	4.5	5.6	IV
S3-1	6.Ø	7.1	I
S3-2	6.Ø	7.3	II
S3-3	6.Ø	7.Ø	III
S3-4	6.Ø	7.4	IV

* Shear Stress is Counted As a Multiple of $\sqrt{f'_c}$

Table 3.1
Calculated and Measured Yield Moments

Specimen	Measured (k-in)	Calculated (k-in)	Measured / Calculated
S1-1	729	671	1.09
S1-2	724	674	1.07
S1-4	672	578	1.16
S2-1	881	777	1.13
S2-2	836	780	1.07
S2-3	881	924	0.95
S2-4	879	795	1.11
S3-1	888	804	1.10
S3-2	894	827	1.08
S3-3	860	804	1.07
S3-4	900	818	1.10

Table 3.2
Shear Strength of Specimens

Specimen	Max * Shear (Kips)	Max Shear Stress (psi)	f'_c (psi)	Max Shear Stress	Allowable V_c (psi)	Allowable V_s (psi)
S1-1	20.21	255	5900	3.3	154	267
S1-2	21.83	270	5880	3.6	153	267
S1-4	19.17	242	4980	3.5	141	291
S2-1	28.10	366	5100	5.1	143	267
S2-2	29.43	383	5390	5.2	147	267
S2-3	31.53	406	4710	6.0	137	291
S2-4	29.95	390	4780	5.6	138	267
S3-1	38.40	495	4910	7.1	140	561
S3-2	39.65	506	4970	7.3	141	564**
S3-3	38.04	495	4980	7.0	141	565**
S3-4	40.97	528	5060	7.4	142	569**

* Maximum Shear Measured at Maximum Positive Displacement in the First Cycle.

**ACI Code Limits Allowable Stirrup Stress to a Value of $8\sqrt{f'_c}$, Actual V_s = 830 psi.

Table 3.3
Selected Testing Parameters and Test Results

Specimen	Load History	Maximum Shear *	Cycle before Failure **	Shear Span / effective Depth	2% Shear Span / Yield Def.
S1-1	I	3.3	11Ø	3.9	2.Ø
S1-2	II	3.6	13	3.9	2.Ø
S1-4	IV	3.5	13	3.9	2.Ø
S2-1	I	5.1	6Ø	3.5	1.8
S2-2	II	5.2	4	3.5	1.8
S2-3	III	6.Ø	7	3.5	1.6
S2-4	IV	5.6	5	3.5	1.8
S3-1	I	7.1	5Ø	2.6	2.1
S3-2	II	7.3	4	2.6	2.1
S3-3	III	7.Ø	8	2.6	2.1
S3-4	IV	7.4	6	2.6	2.1

* Maximum Gross Shear Stress Measured at Maximum Positive Displacement in the First Load Cycle; as a Multiple of $\sqrt{f'_c}$

**Failure is Tentative Defined to be the Cycle When the Strength at the maximum Positive Displacement of the Given Deflection Schedule Dropped Below 3/4 of the Original Yield Strength

Table 4.1(a)
Calculated Deflection Components for First Quarter-Cycle of Load - Specimen S1-4

Applied Load (kip)	Measured Displacement (in)	Δ_1 (in)	Δ_2 (in)	Δ_3 (in)	Δ_4 (in)	Total Calculated Displacement (in)
0	0	0	0	0	0	0
4.86	0.05	0.0374	0.0029	0.0198	0.0010	0.061
9.83	0.16	0.1004	0.0132	0.0401	0.0021	0.156
14.75	0.28	0.1814	0.0233	0.0602	0.0031	0.257
17.09	0.40	0.2645	0.0354	0.0698	0.0036	0.373
17.40	0.59	0.4319	0.0626	0.0711	0.0037	0.569
17.95	0.78	0.6078	0.0887	0.0733	0.0038	0.774
18.35	1.04	0.8394	0.1233	0.0749	0.0039	1.042
18.54	1.30	1.0785	0.1521	0.0757	0.0039	1.310
18.92	1.57	1.3065	0.1837	0.0770	0.0040	1.571

Table 4.1(b)
Calculated Deflection Components for First Quarter-Cycle of Load - Specimen S2-2

Applied Load (kip)	Measured Displacement (in)	Δ_1 (in)	Δ_2 (in)	Δ_3 (in)	Δ_4 (in)	Total Calculated Displacement (in)
0	0	0	0	0	0	0
7.11	0.05	0.0535	0.0032	0.0120	0.0012	0.070
13.64	0.14	0.1206	0.0130	0.0230	0.0023	0.159
20.55	0.25	0.1929	0.0276	0.0346	0.0035	0.259
24.42	0.36	0.2713	0.0479	0.0411	0.0042	0.364
26.09	0.54	0.4130	0.0797	0.0439	0.0045	0.541
27.44	0.81	0.6513	0.1281	0.0462	0.0047	0.830
28.48	1.08	0.8754	0.1795	0.0480	0.0049	1.108
29.08	1.36	1.1103	0.2400	0.0490	0.0050	1.405

Table 4.1(c)
Calculated Deflection Components for First Quarter-Cycle of Load - Specimen S3-2

Applied Load (kip)	Measured Displacement (in)	Δ_1 (in)	Δ_2 (in)	Δ_3 (in)	Δ_4 (in)	Total Calculated Displacement (in)
0	0	0	0	0	0	0
7.75	0.02	0.0194	0.0008	0.0025	0.0008	0.023
15.60	0.07	0.0496	0.0111	0.0050	0.0016	0.067
23.80	0.13	0.0855	0.0255	0.0076	0.0024	0.121
29.21	0.18	0.1166	0.0372	0.0093	0.0030	0.166
34.03	0.25	0.1590	0.0541	0.0109	0.0035	0.227
36.17	0.37	0.2556	0.0846	0.0115	0.0037	0.355
37.45	0.50	0.3558	0.1122	0.0119	0.0039	0.484
38.03	0.63	0.4540	0.1355	0.0121	0.0039	0.606
38.56	0.73	0.5507	0.1592	0.0123	0.0040	0.726
38.87	0.88	0.6437	0.1803	0.0124	0.0040	0.840
39.17	1.00	0.7378	0.2010	0.0125	0.0040	0.955

Table 5.1
Comparison of Maximum Average Bond Stress
First Reached in Region II and Region III
During the First Quarter-Cycle of Load

Specimen	Maximum Average Bond Stress			
	Region II		Region III	
	u (psi)	$\frac{u}{\sqrt{f'_c}}$	u (psi)	$\frac{u}{\sqrt{f'_c}}$
S2-1	1189	16.65	443	6.20
S2-2	950	12.94	418	5.69
S2-3	1164	16.96	477	6.95
S2-4	910	13.16	430	6.39
mean	1053	14.93	442	6.31
S3-1	658	9.39	392	5.59
S3-2	1112	15.77	329	4.67
S3-3	924	13.09	392	5.55
S3-4	1037	14.58	430	6.04
mean	933	13.21	386	5.46

Table 5.2
Comparison of the Beam Total Displacement and Beam Displacement due to Fixed End Rotation, and due to Flexural Deformation

Specimen	Δ_{FE} (in)	Δ_1 (in)	Δ_T (in)	$\frac{\Delta_{FE}}{\Delta_1}$	$\frac{\Delta_{FE}}{\Delta_T}$
S1-1	0.284	0.665	0.78	0.43	0.36
S1-2	0.498	1.249	1.50	0.40	0.33
S1-4	0.480	1.307	1.57	0.37	0.31
S2-1	0.240	0.524	0.68	0.46	0.35
S2-2	0.548	1.110	1.36	0.49	0.40
S2-3	0.245	0.480	0.68	0.51	0.36
S2-4	0.358	1.140	1.36	0.31	0.26
S3-1	0.194	0.375	0.50	0.52	0.39
S3-2	0.437	0.738	1.00	0.59	0.44
S3-3	0.181	0.342	0.50	0.53	0.36
S3-4	0.477	0.793	1.00	0.60	0.48

Δ_T = Beam Total Displacement at Loading Point

Δ_1 = Beam Flexural Displacement at Loading Point

Table 6.1
Energy Dissipation Capacity

Specimen	Load History	Total Energy Dissipation (in-kip)	Total Energy Index, I_E (in-kip)	Modified * Work Index I'_w
S1-1	I	590	972	169
S1-2	II	343	1306	40
S1-4	IV	248	879	31
S2-1	I	360	578	88
S2-2	II	160	620	11
S2-3	III	171	542	16
S2-4	IV	151	557	13
S3-1	I	320	631	78
S3-2	II	155	683	11
S3-3	III	196	760	17
S3-4	IV	178	750	14

* Modified Work Index = $I'_w = (P_n/P_y) \times (\frac{\Delta_n}{\Delta_y})(1-d_c/a)$
see Gosain et al(19).

Table 6.2

Test Results from Three Sources

Specimen	b (in)	d (in)	f'_c (ksi)	ρ_w	$\frac{a}{d}$	$\frac{\rho}{\rho_b}$	$\frac{V_m}{\sqrt{f'_c}}$	$\frac{V_s}{V_m}$	P_y (kip)	Δ_y (in)	I_E (in-kip)
Hwang & Scribner											
S1-1	8.0	9.9	5.90	0.005	3.9	0.41	3.3	1.07	18.9	0.41	972
S1-2	8.0	10.1	5.88	0.005	3.9	0.40	3.6	0.97	18.6	0.41	1306
S1-4	8.0	9.9	4.98	0.005	3.9	0.41	3.5	1.20	17.2	0.40	879
S2-1	8.0	9.6	5.10	0.005	3.5	0.49	5.1	0.73	25.9	0.38	568
S2-2	8.0	9.6	5.39	0.005	3.5	0.48	5.2	0.70	24.6	0.37	620
S2-3	8.0	9.7	4.71	0.005	3.5	0.55	6.0	0.71	25.9	0.44	542
S2-4	8.0	9.6	4.78	0.005	3.5	0.50	5.6	0.68	25.9	0.37	557
S3-1	8.0	9.7	4.91	0.011	2.6	0.50	7.1	1.68	35.8	0.25	631
S3-2	8.0	9.8	4.97	0.011	2.6	0.50	7.3	1.64	34.4	0.25	683
S3-3	8.0	9.6	4.98	0.011	2.6	0.51	7.0	1.68	35.5	0.25	760
S3-4	8.0	9.7	5.06	0.011	2.6	0.50	7.4	1.57	36.1	0.25	750
Scribner & Wight											
1	8.0	8.6	4.97	0.006	4.8	0.24	2.1	1.85	8.9	0.39	2656
2	8.0	8.6	4.97	0.006	4.8	0.23	2.2	1.68	8.9	0.47	2486
3	8.0	10.1	4.97	0.005	4.1	0.29	3.1	1.01	14.4	0.54	945
4	8.0	10.1	4.97	0.005	4.1	0.28	3.5	0.89	16.4	0.66	1770
5	8.0	8.6	3.98	0.006	3.6	0.30	3.4	1.29	11.6	0.43	1282
6	8.0	8.6	3.98	0.006	3.6	0.29	3.4	1.23	12.0	0.37	1827
7	8.0	10.1	3.98	0.011	4.1	0.36	3.6	3.72	15.3	0.70	1450
8	8.0	10.1	3.98	0.005	4.1	0.35	3.8	0.89	17.0	0.80	1171
9	10.	12.1	4.94	0.007	5.0	0.55	4.9	1.14	34.2	1.10	5291
10	10.	12.1	4.94	0.007	5.0	0.53	5.1	1.12	35.8	1.07	6047
11	10.	12.1	4.94	0.007	4.0	0.55	6.2	0.92	41.0	0.72	3060
12	10.	12.1	4.94	0.007	4.0	0.53	6.9	0.81	46.0	0.90	2663
Lee et al.											
1	8.0	8.0	3.70	0.006	5.8	0.29	2.1	1.98	6.8	0.54	531
2	8.0	8.0	3.70	0.006	5.8	0.29	1.9	2.17	6.4	0.56	1281
3	8.0	8.0	3.70	0.003	5.8	0.29	1.7	1.22	6.0	0.53	340
4	8.0	8.0	3.70	0.003	5.8	0.29	1.8	1.04	6.6	0.53	1120
5	8.0	8.0	4.20	0.003	5.2	0.32	2.2	1.70	7.9	0.52	1544
6	8.0	8.0	4.20	0.006	5.2	0.32	2.2	0.88	7.5	0.50	1358
7	8.0	8.0	4.20	0.003	5.2	0.31	2.1	0.90	7.5	0.47	1072
8	8.0	8.0	4.20	0.003	5.2	0.29	2.1	0.93	7.4	0.46	866

FIGURES

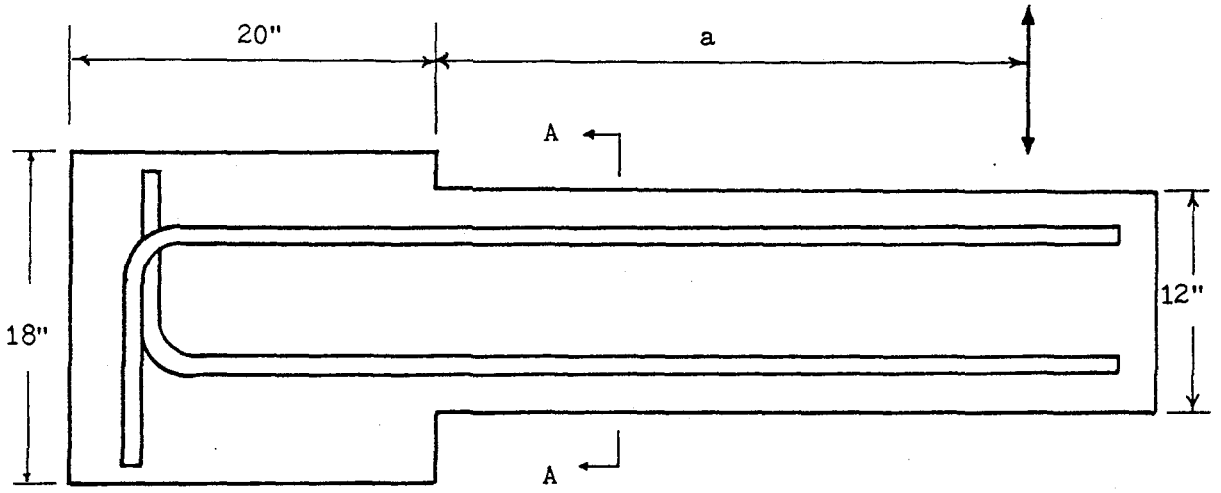

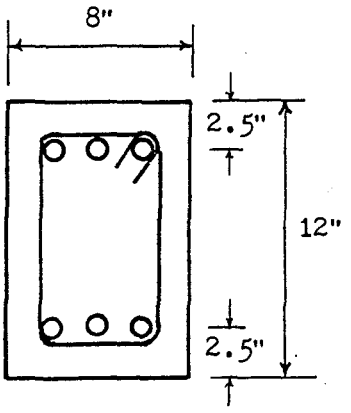

Section A-A

Fig. 2.1 Specimen Configuration and Dimension

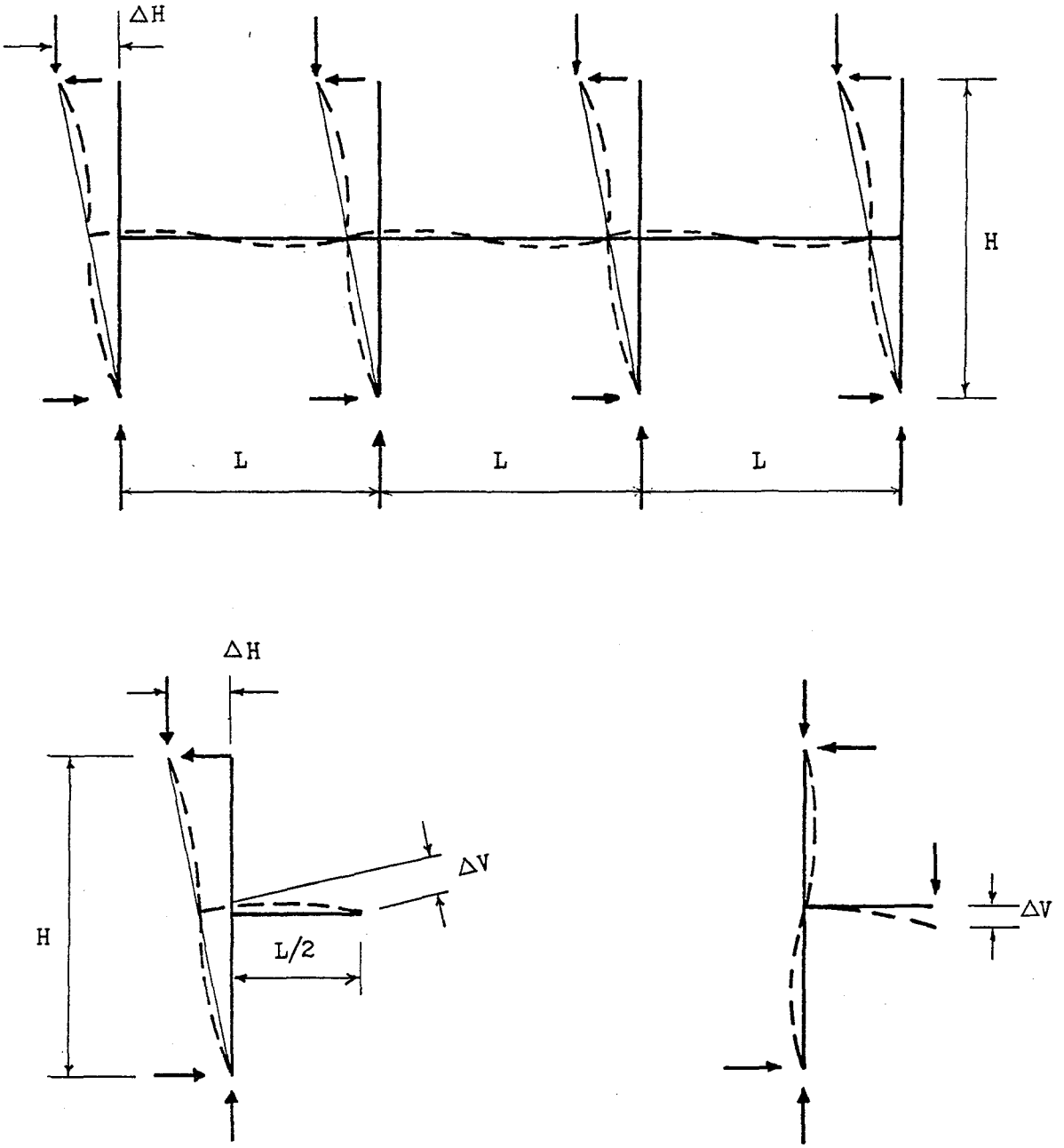

Fig. 2.2 Relationship Between Story Drift and Structural Member Displacement

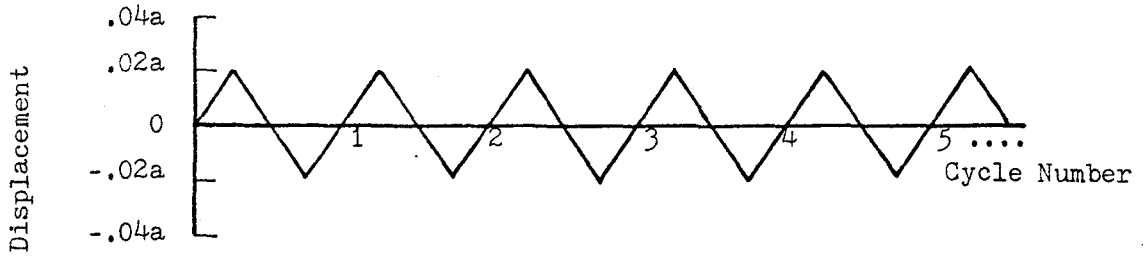

(a) Deflection Schedule I

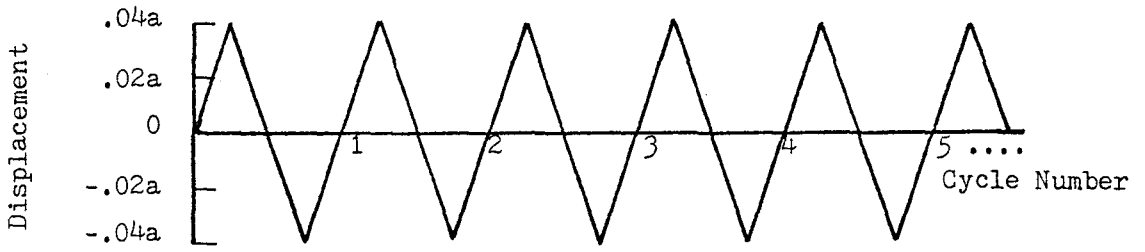

(b) Deflection Schedule II

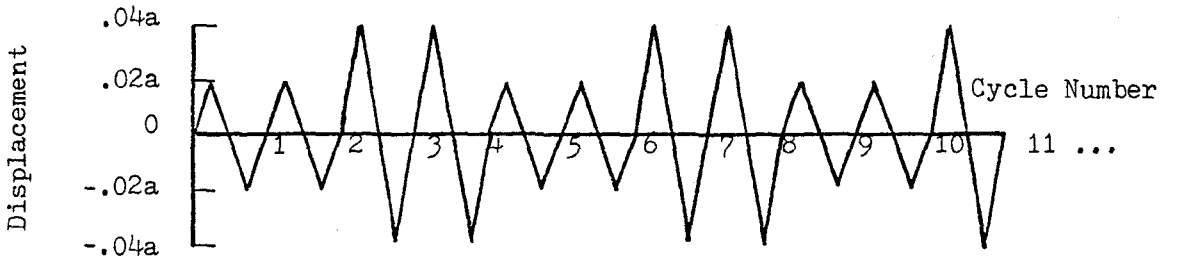

(c) Deflection Schedule III

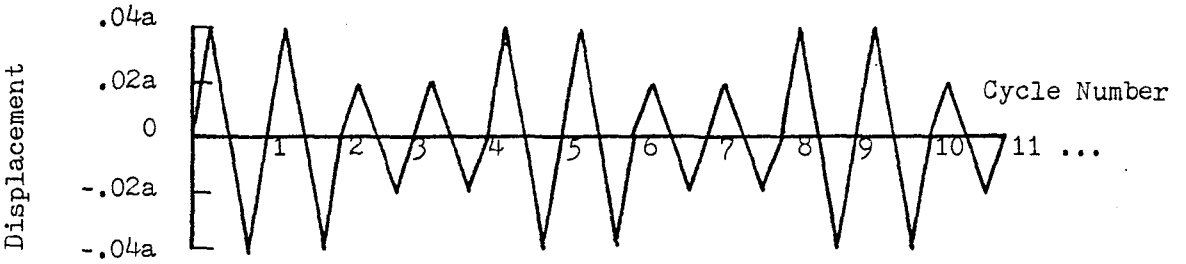

(d) Deflection Schedule IV

* a is the shear Span Length for Each Specimen

Fig. 2.3 Deflection Schedule

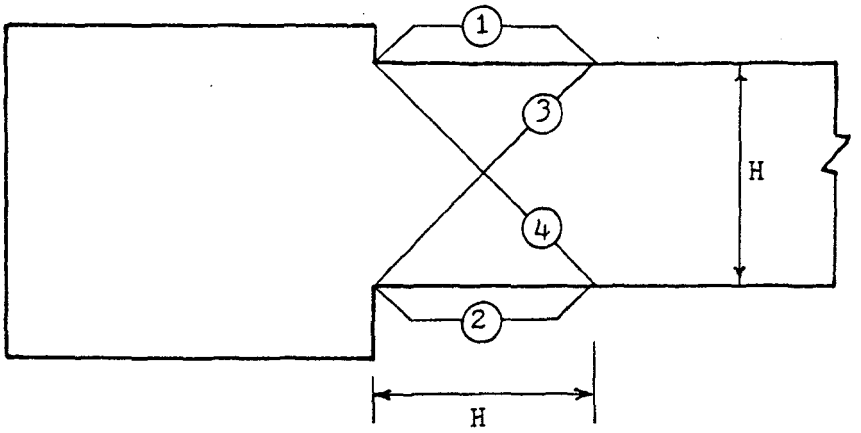

Fig. 2.4 LVDTs Positioned Over Beam Hinging Zone

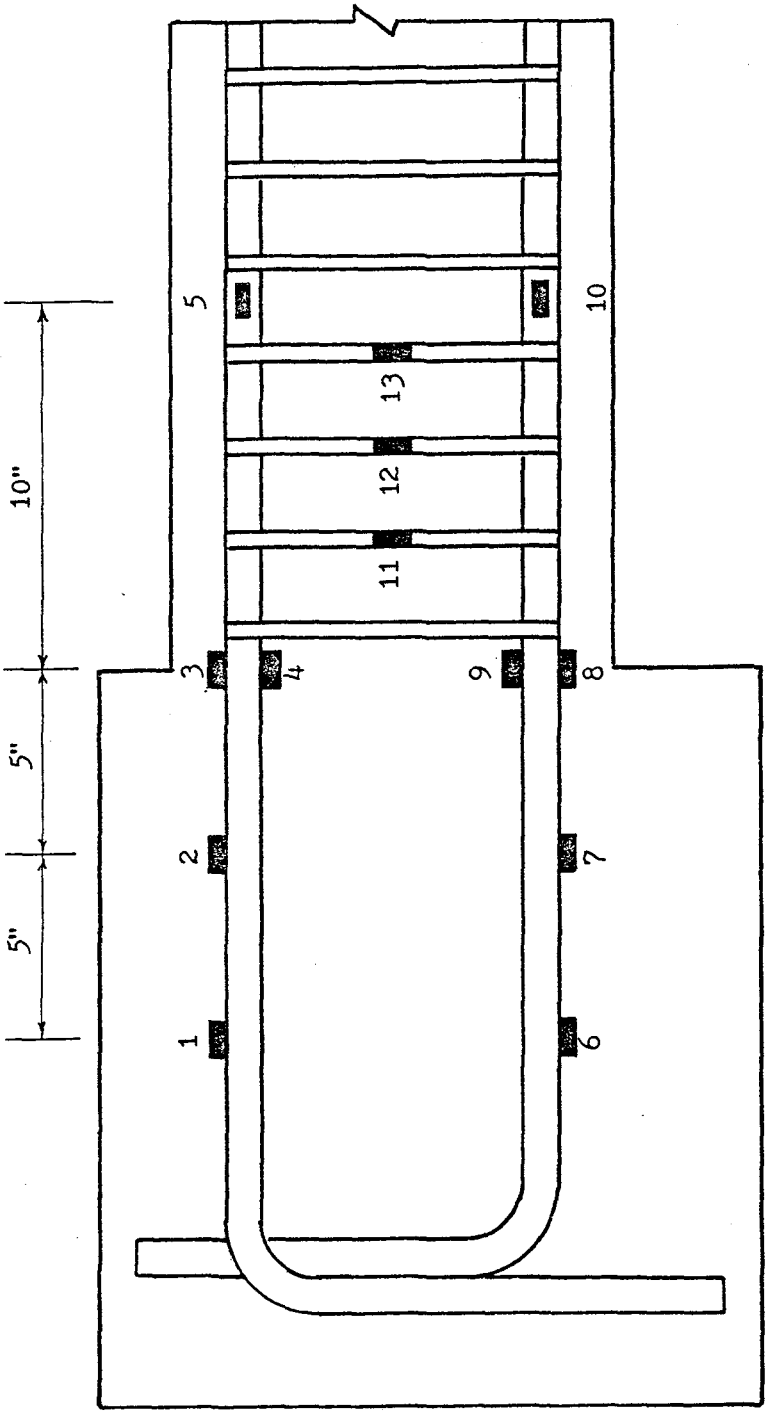

Fig. 2.5 Strain Gage Locations

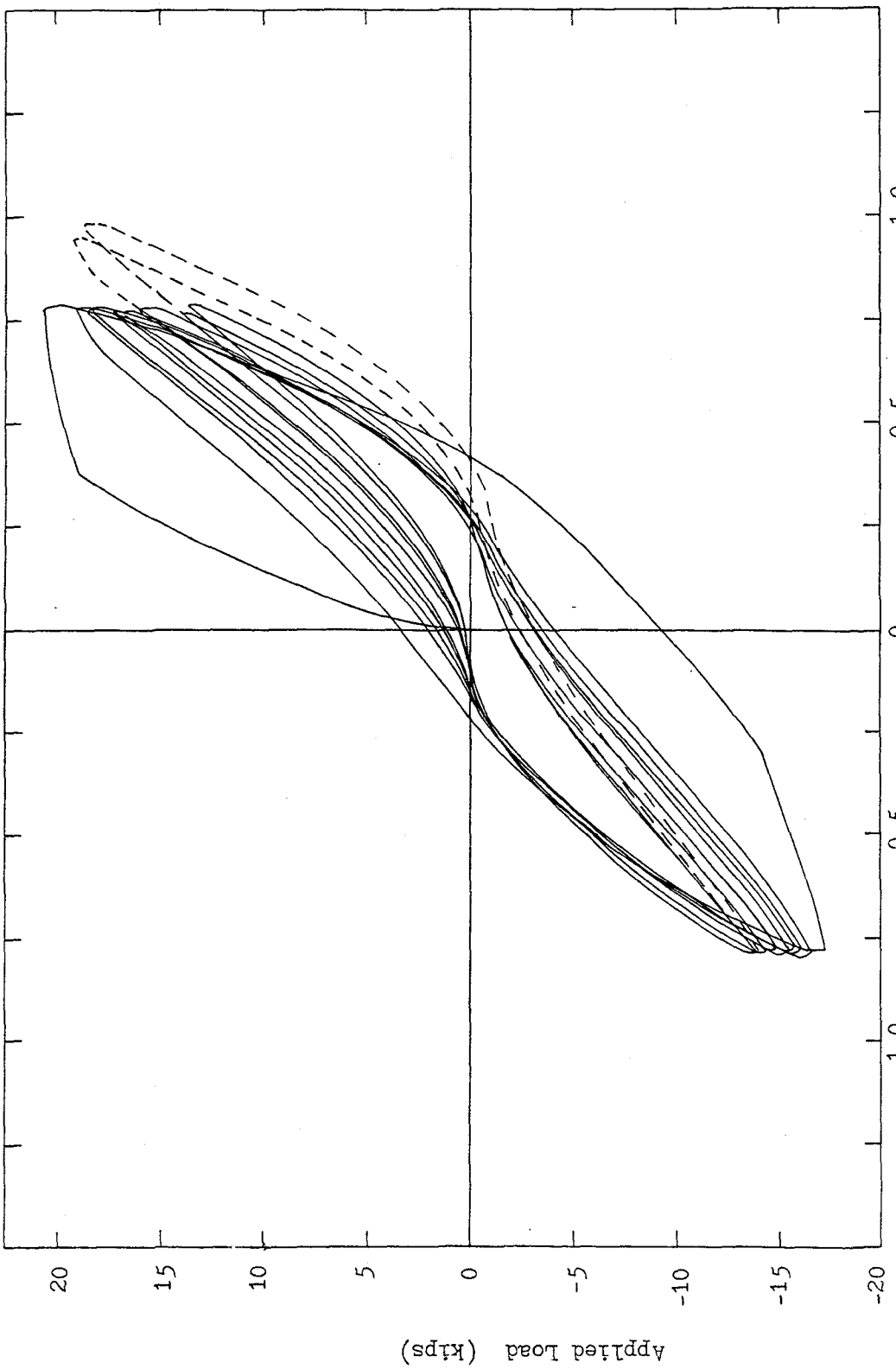

Fig. 3.1(a) Load-Deflection Relationship, Specimen S1-1

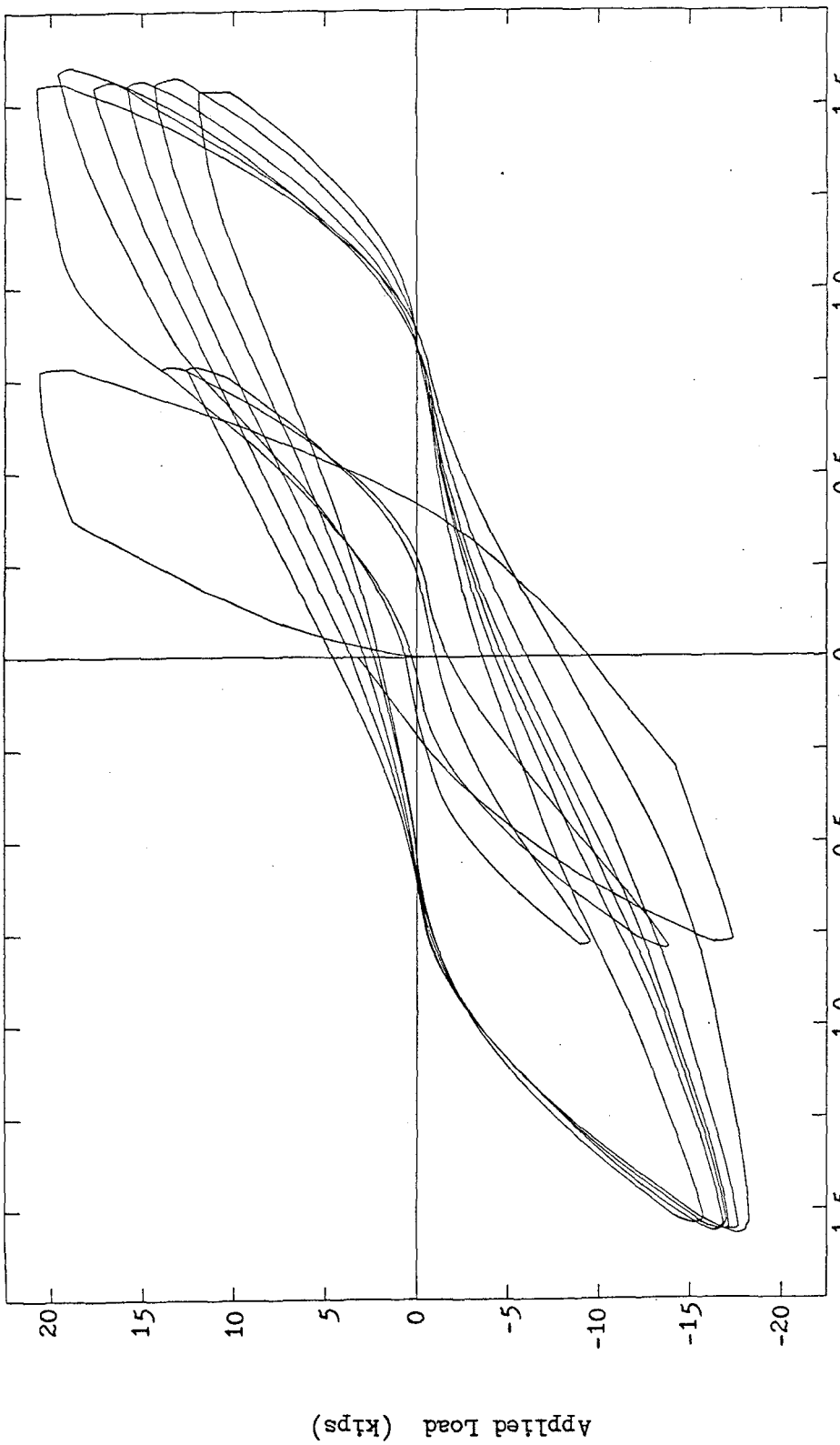

Fig. 3.1(b) Load-Deflection Relationship, Specimen S1-1

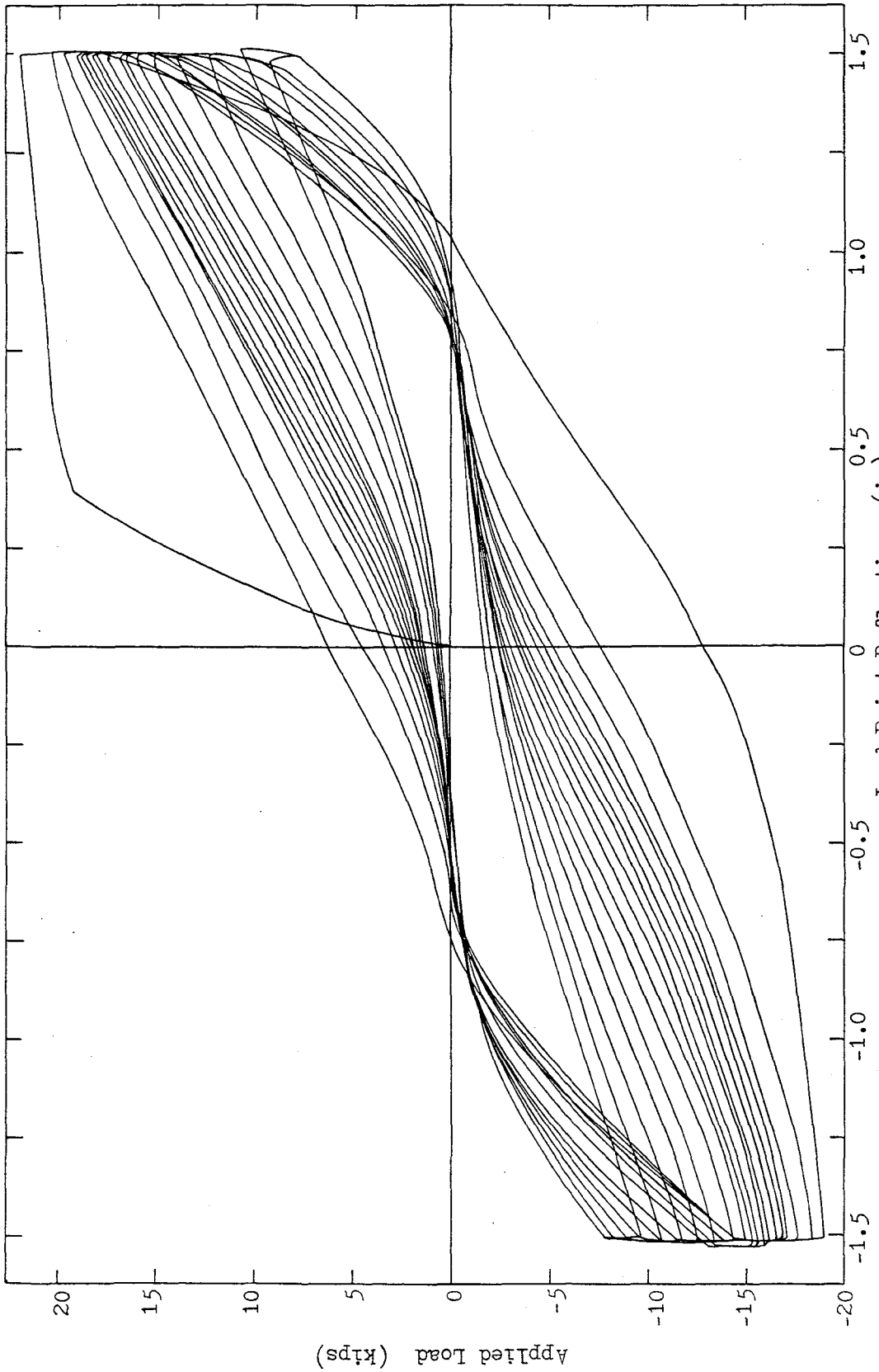

Fig. 3.1(c) Load-Deflection Relationship, Specimen S1-2

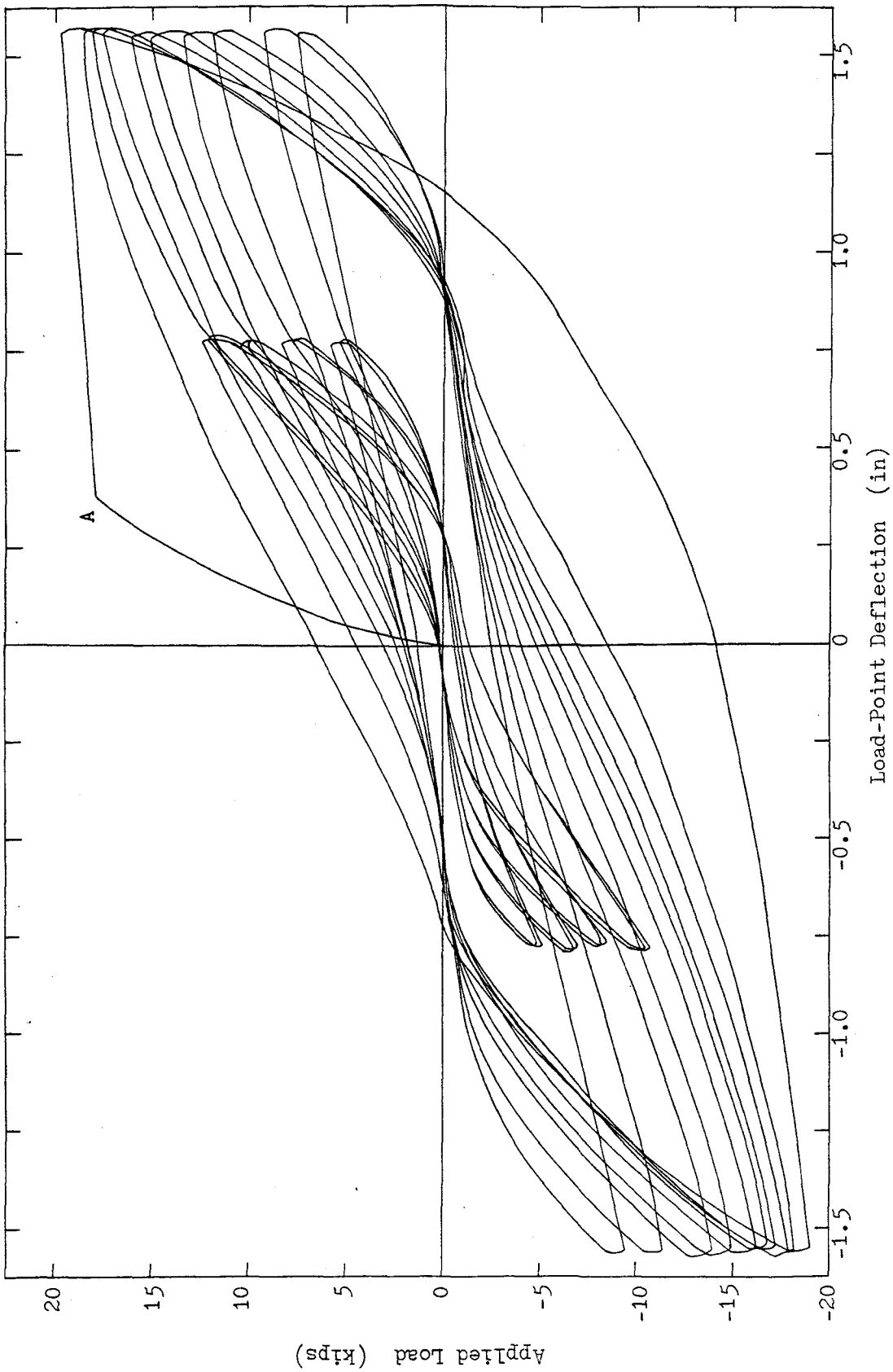

Fig. 3.1(d) Load-Deflection Relationship, Specimen S1-4

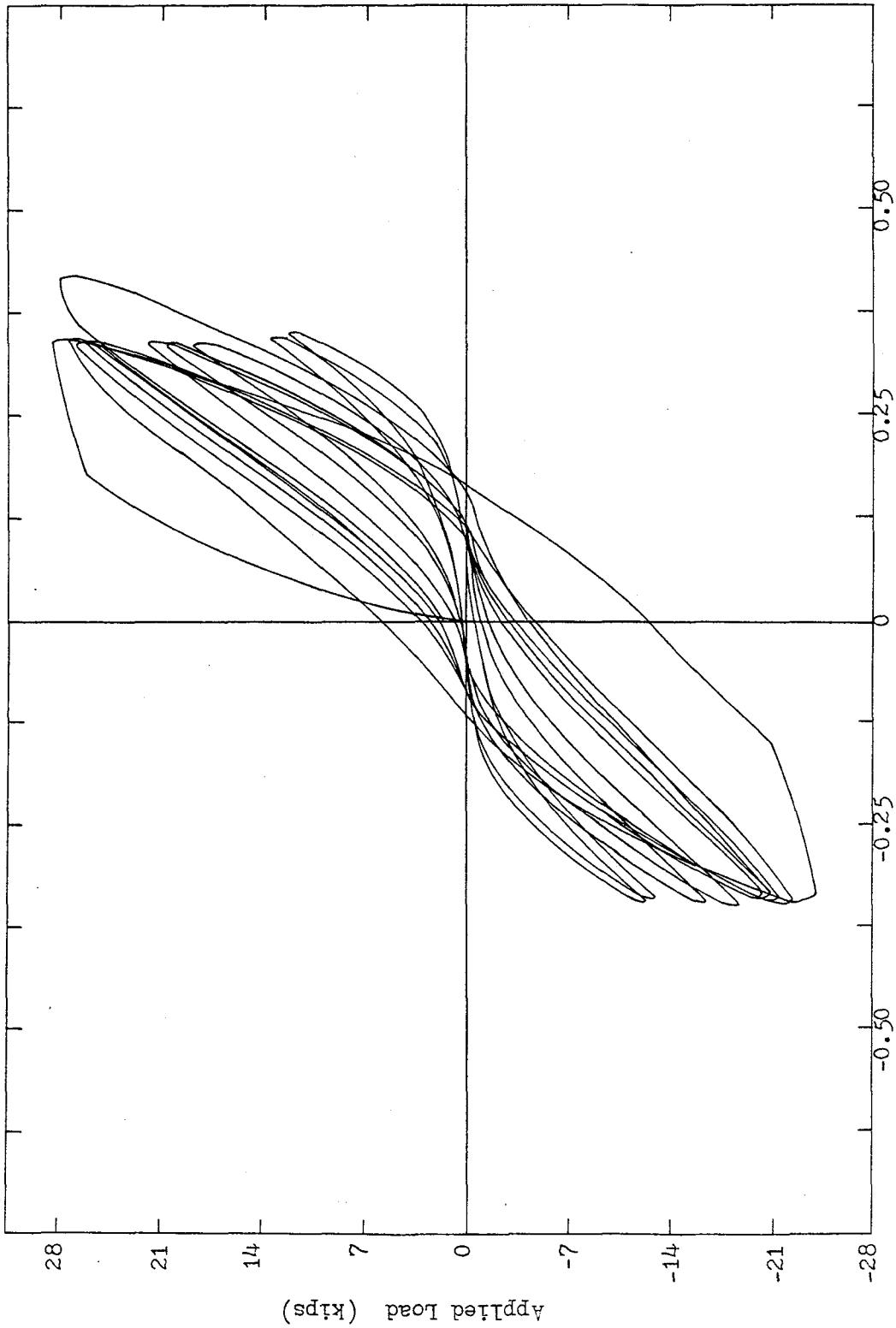

Fig. 3.1(e) Load-Deflection Relationship, Specimen S2-1

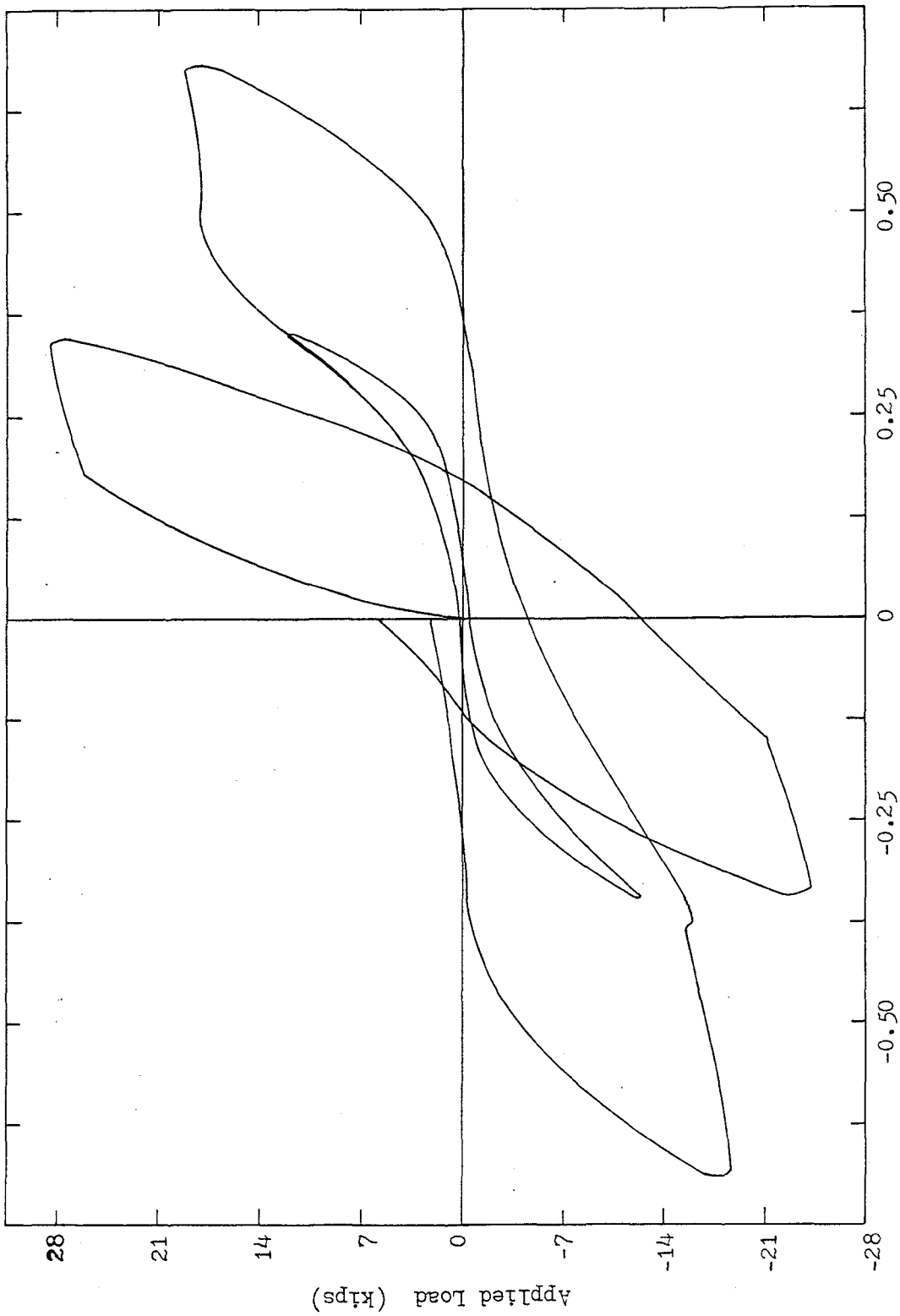

Fig. 3.1(f) Load-Deflection Relationship, Specimen S2-1

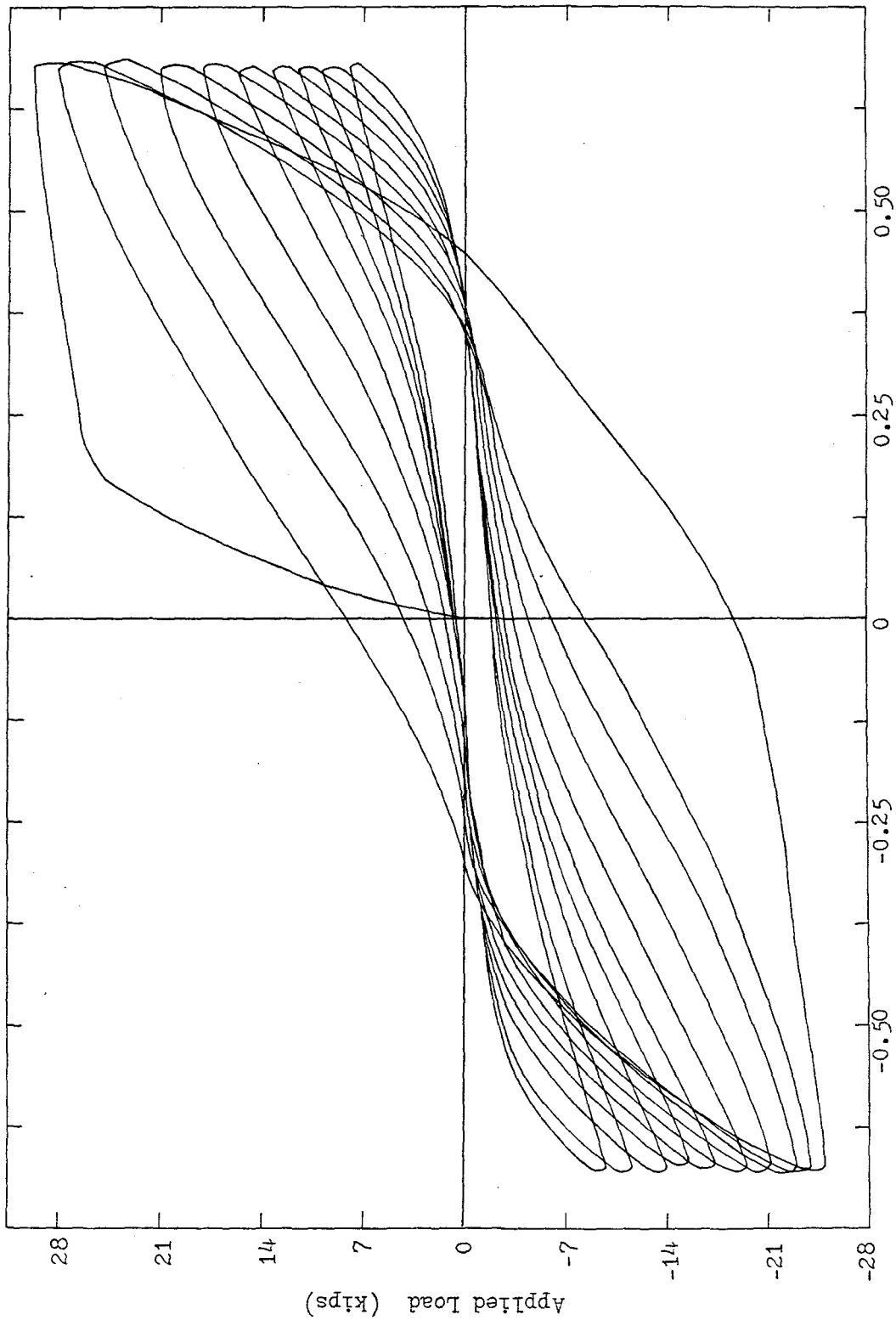

Fig. 3.1(g) Load-Deflection Relationship, Specimen S2-2

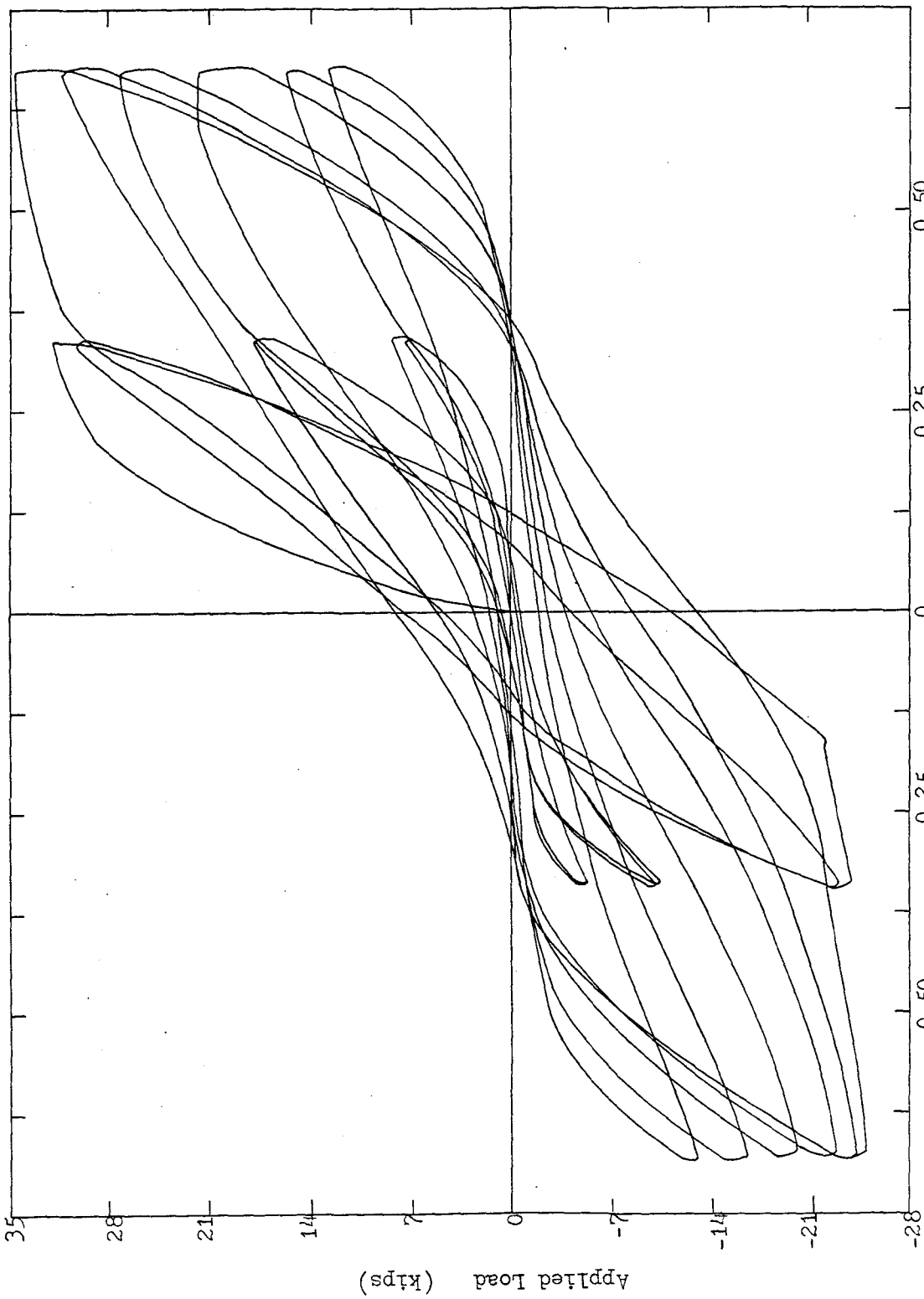

Fig. 3.1(h) Load-Deflection Relationship, Specimen S2-3

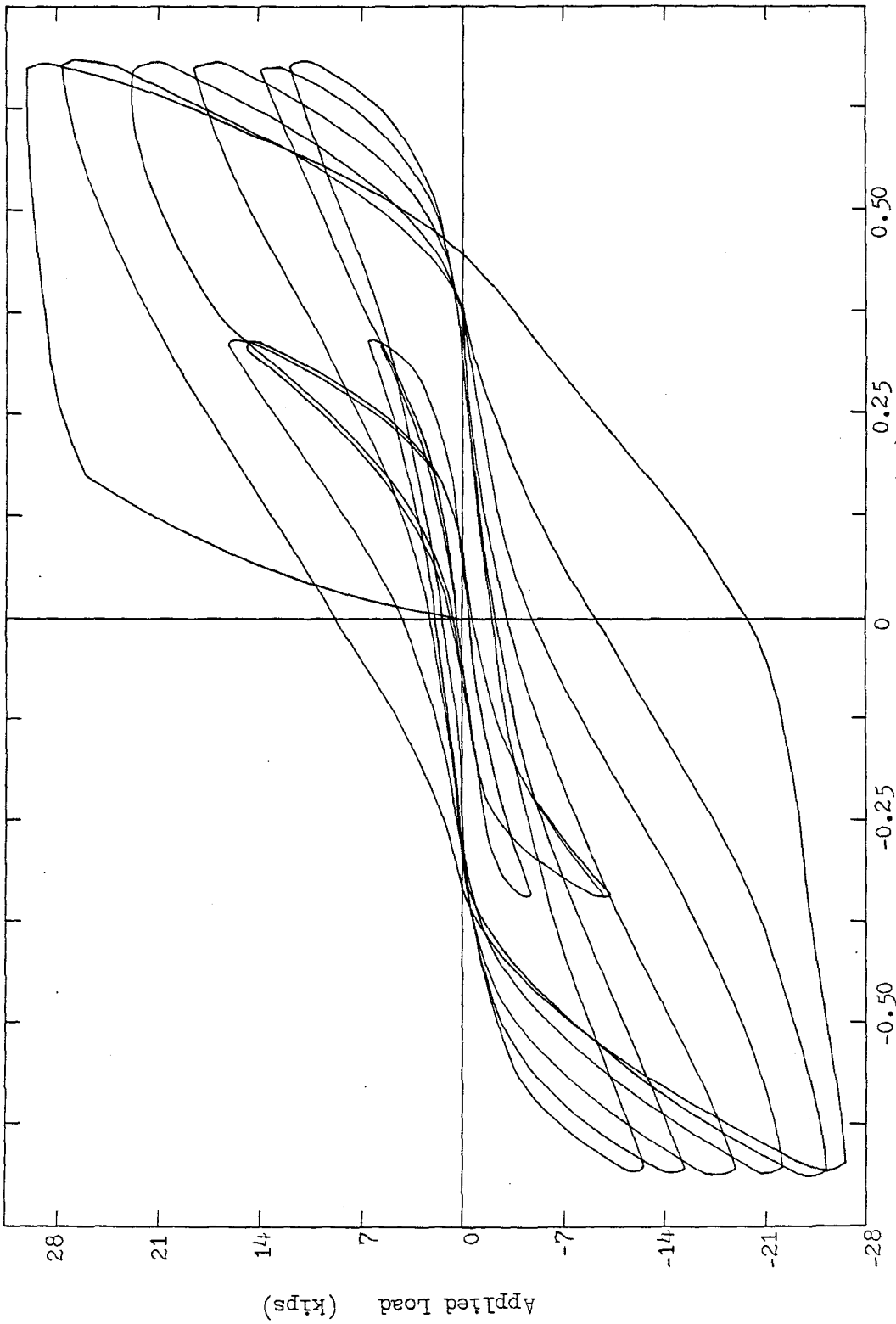

Fig. 3.1(i) Load-Deflection Relationship, Specimen S2-4

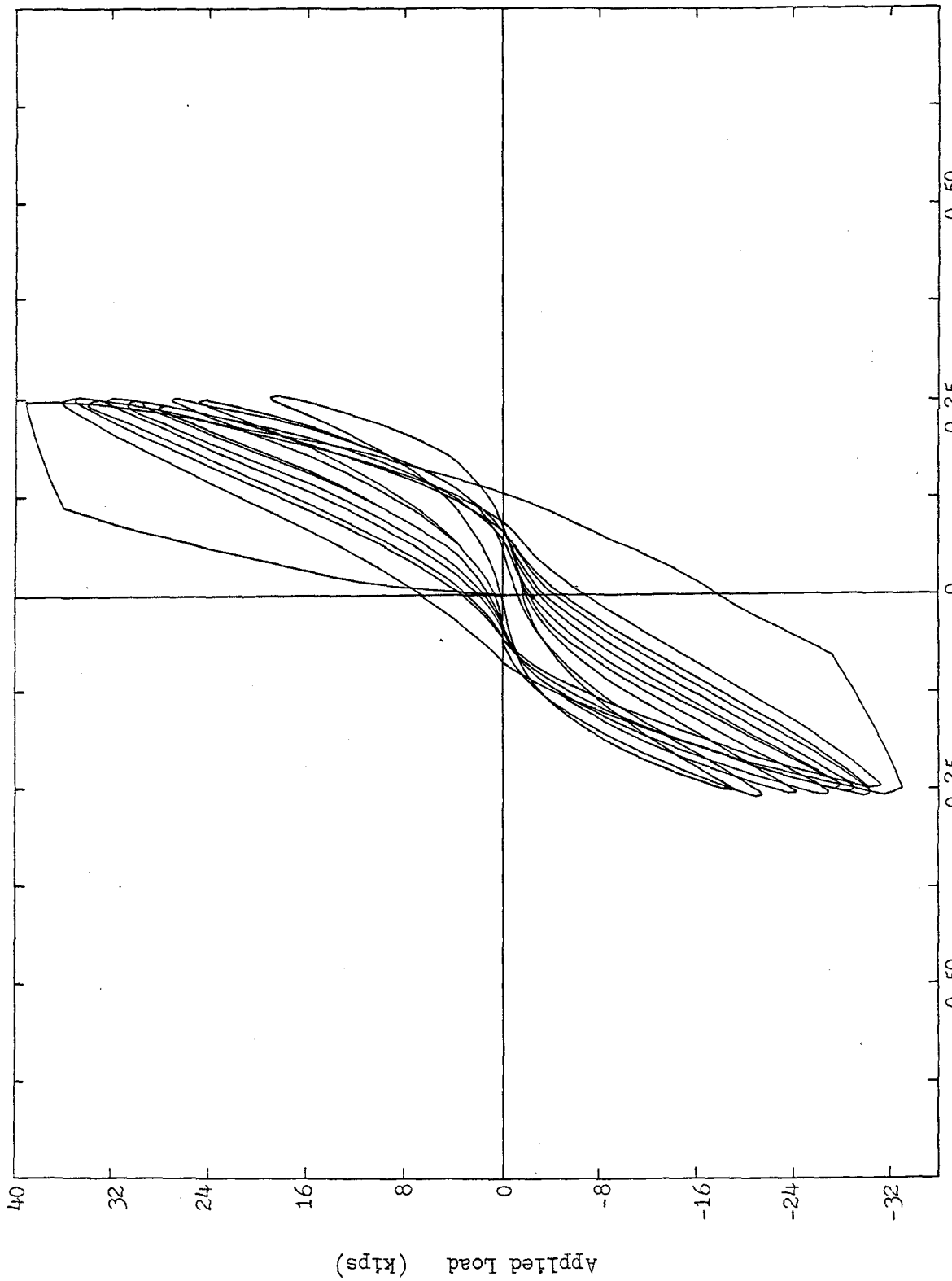

Fig. 3.1(j) Load-Deflection Relationship, Specimen S3-1

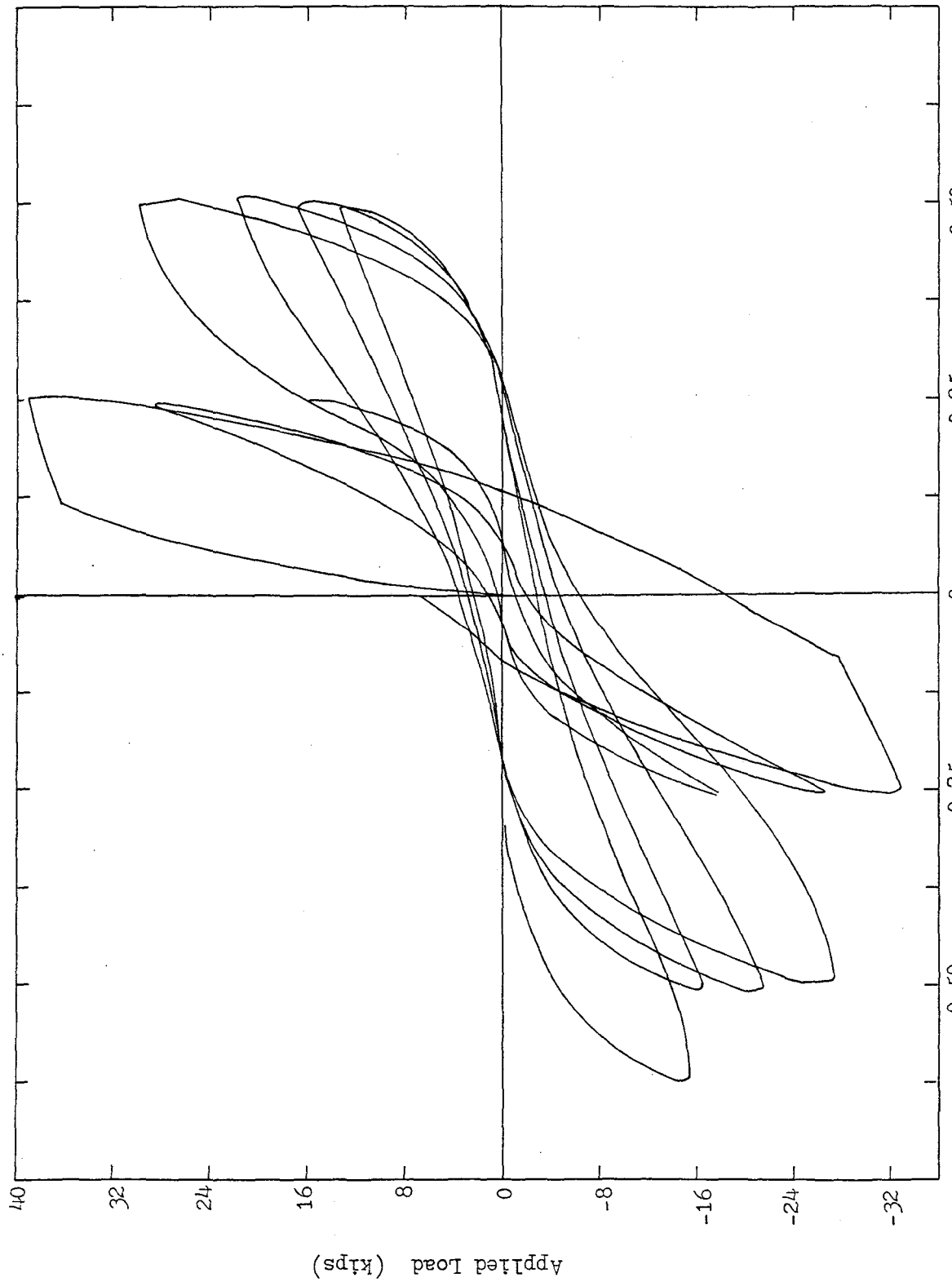

Fig. 3.1(k) Load-Deflection Relationship, Specimen S3-1

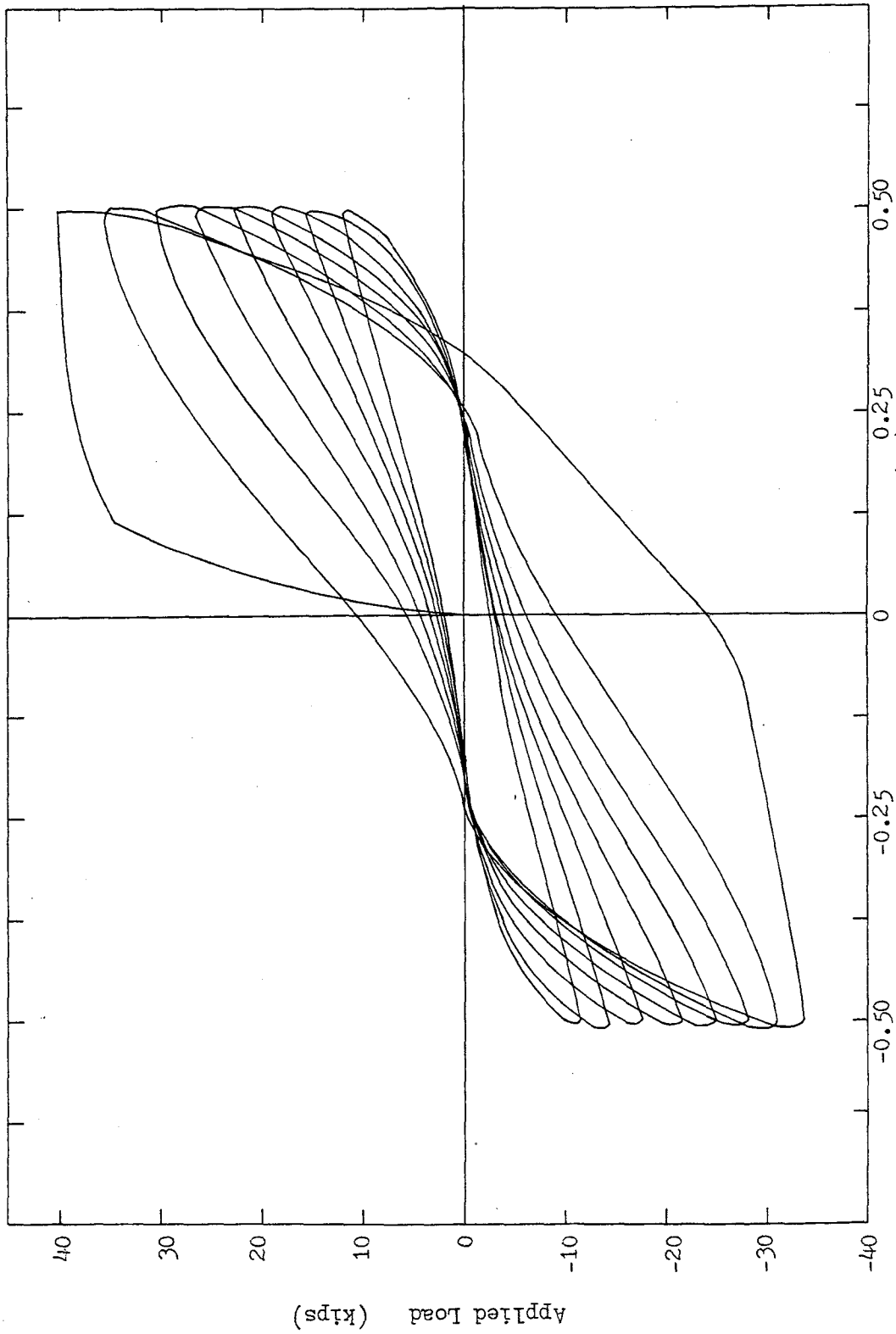

Fig. 3.1(1) Load-Deflection Relationship, Specimen S3-2

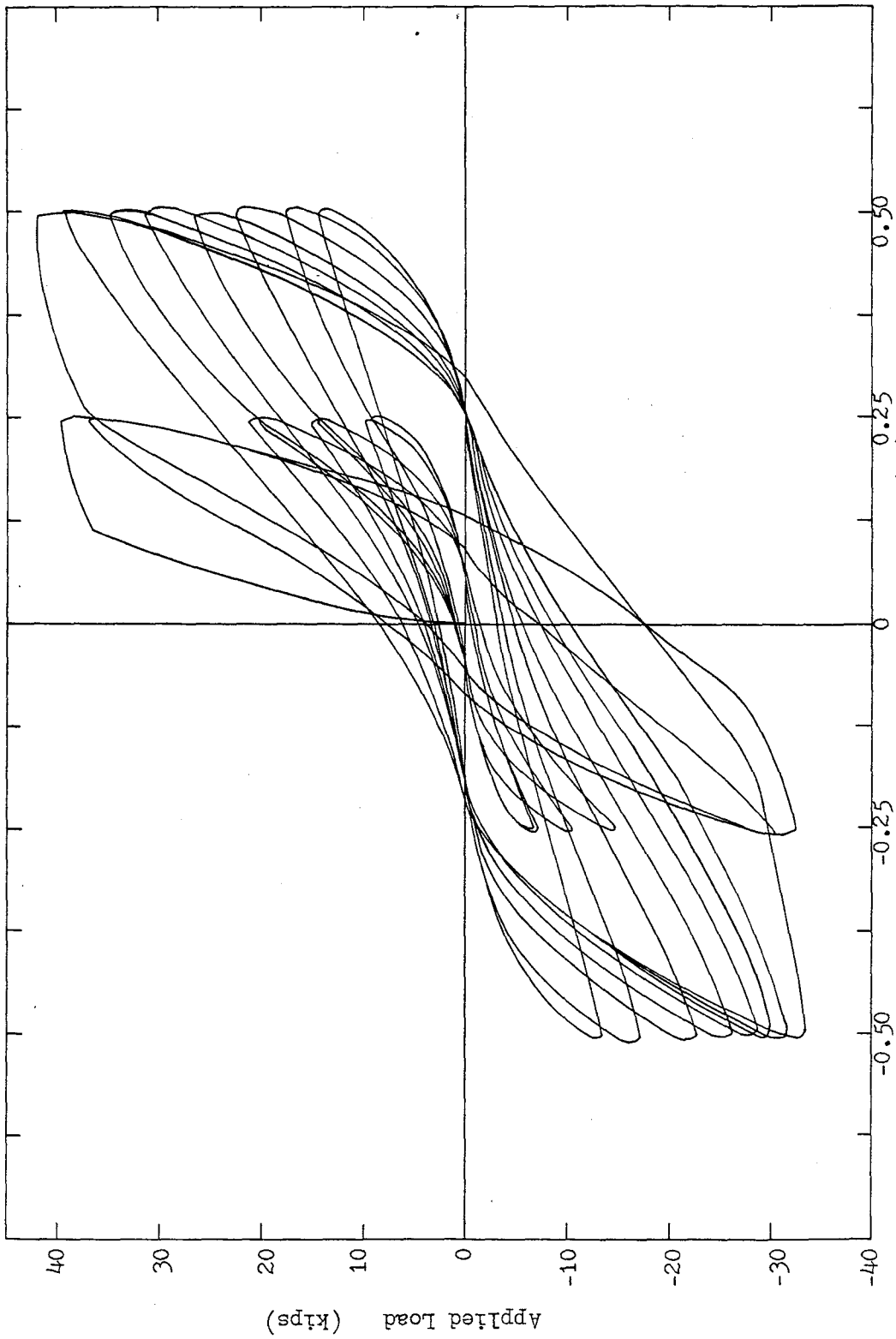

Fig. 3.1(m) Load-Deflection Relationship, Specimen S3-3

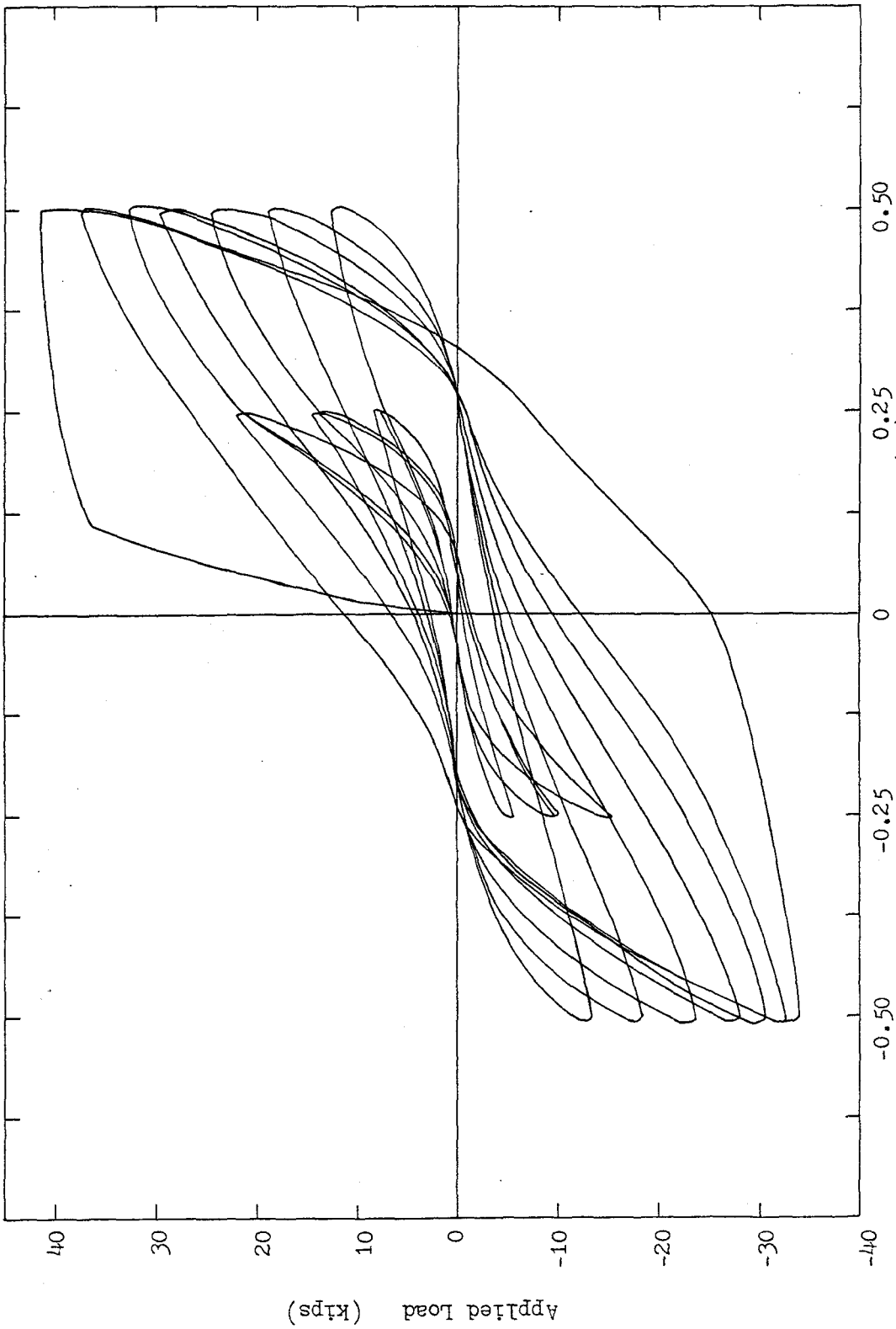

Fig. 3.1(n) Load-Deflection Relationship, Specimen S3-4

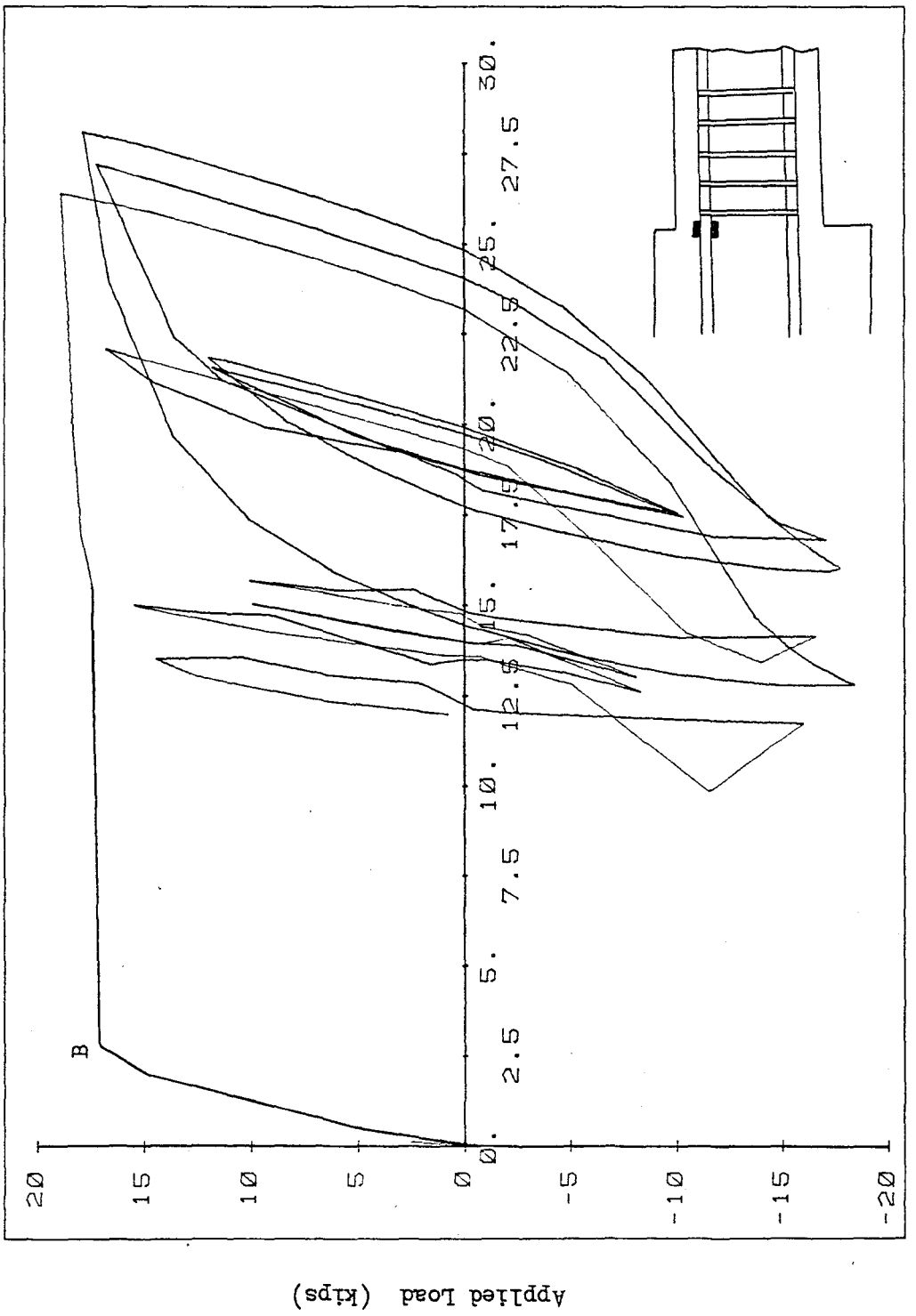

Fig. 3.2 Applied Load vs. Strain at the Face of the Enlarged End Block in Top Longitudinal Reinforcement, Specimen S1-4

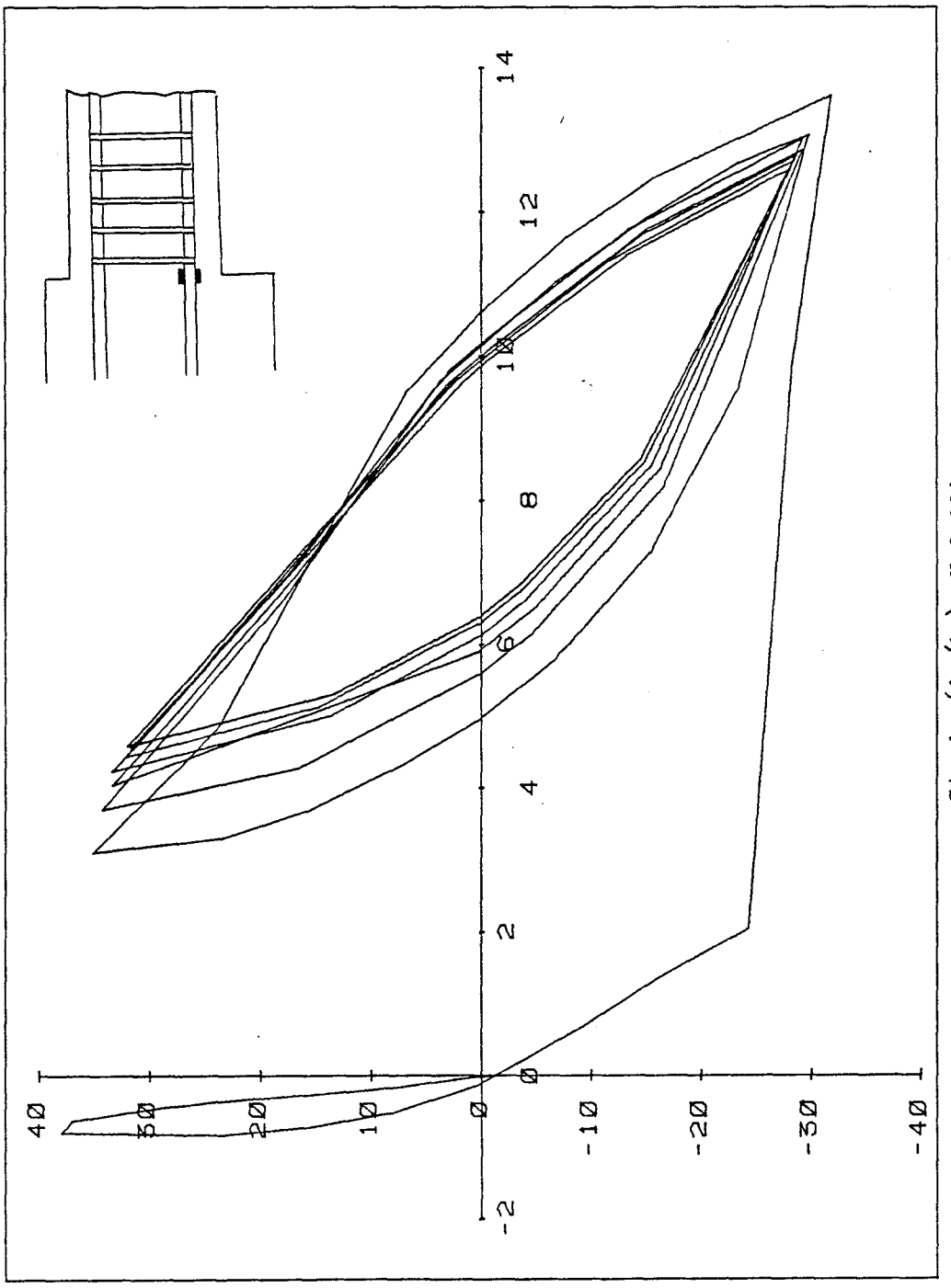

Fig. 3.3 Applied Load vs. Strain at the Face of the Enlarged End Block in Bottom Longitudinal Reinforcement, Specimen S3-1

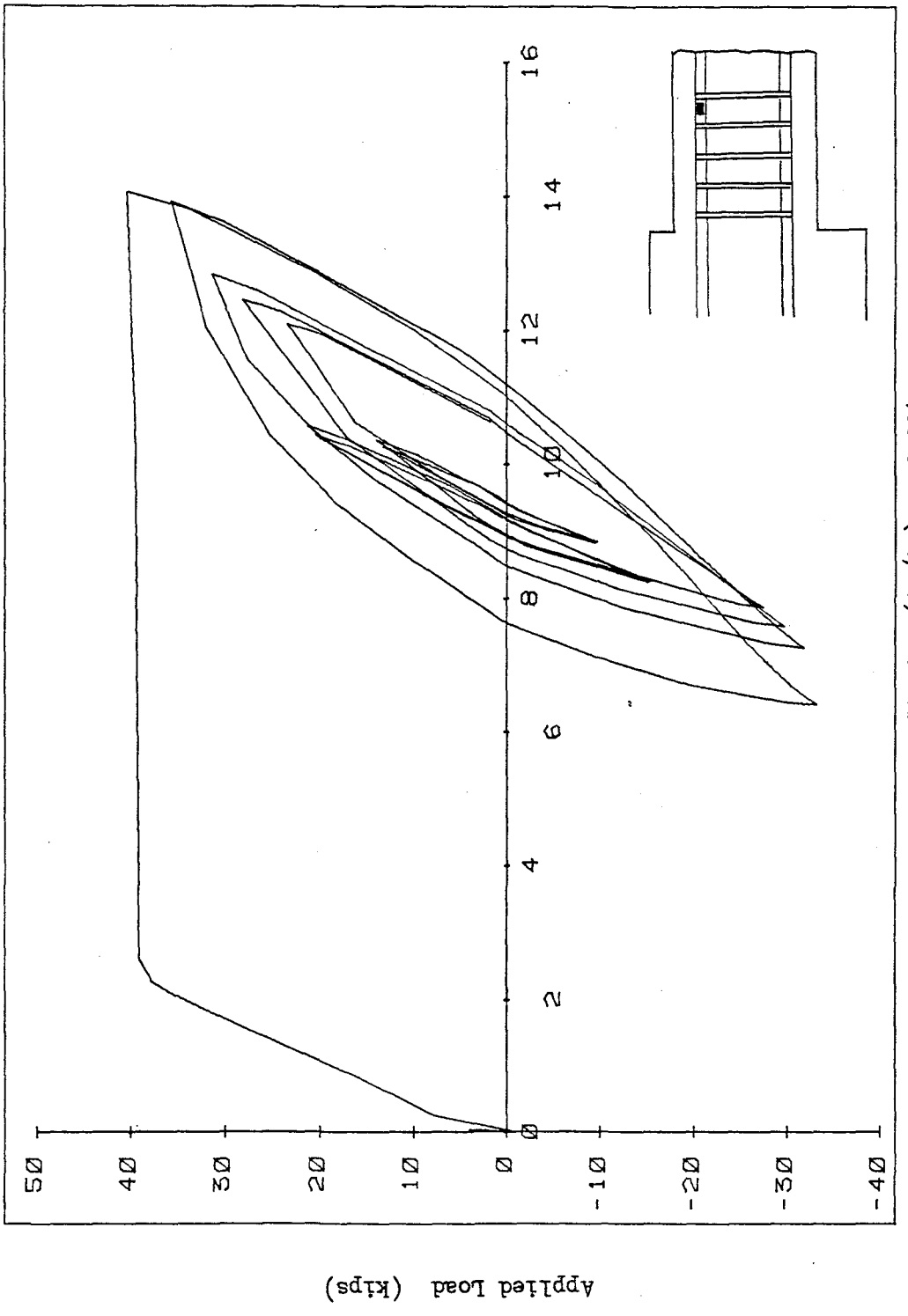

Fig. 3.4(a) Applied Load vs. Strain in Top Longitudinal Reinforcement in Hinging Zone, Specimen S3-4

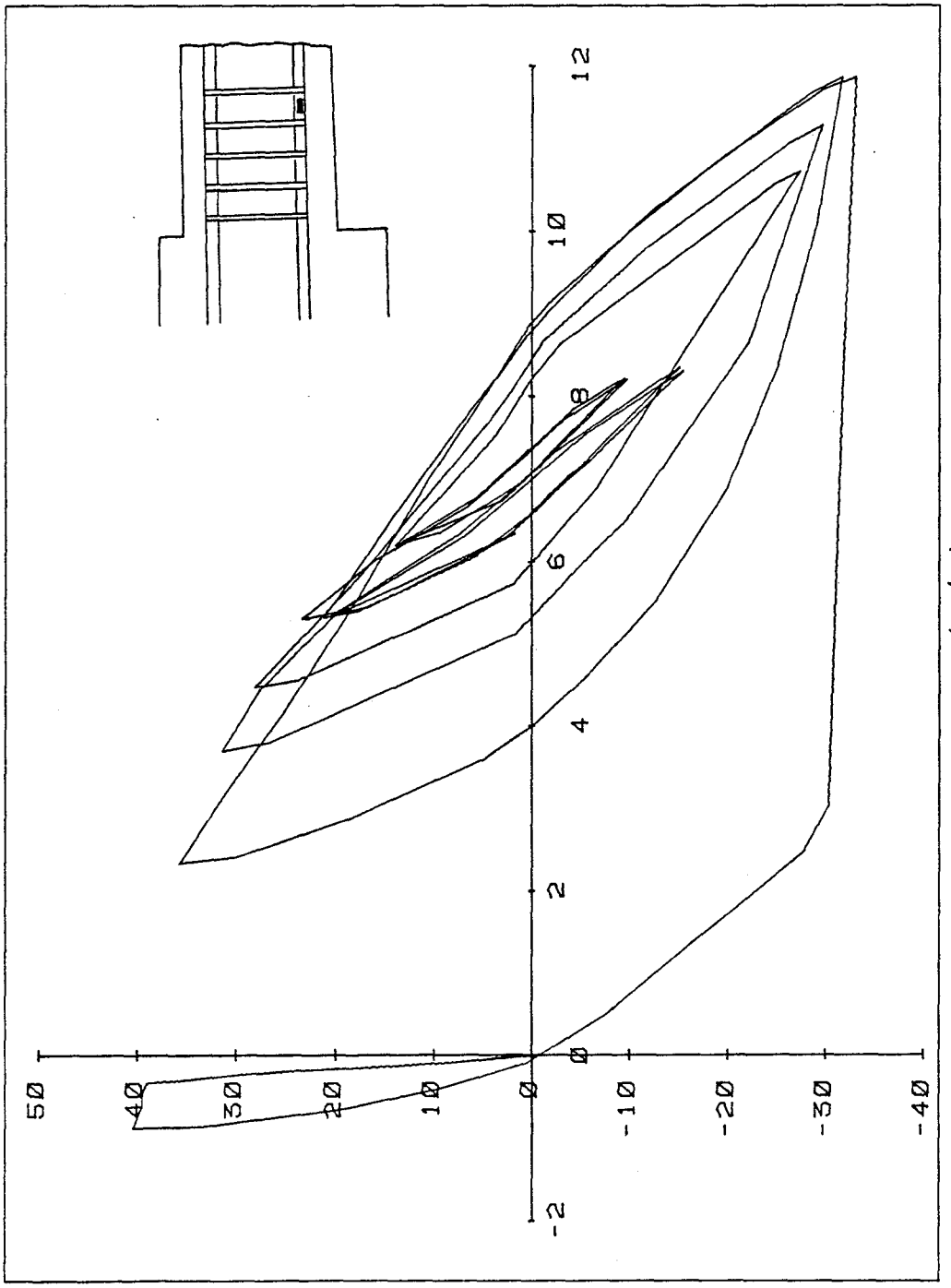

Fig. 3.4(b) Applied Load vs. Strain in Bottom Longitudinal Reinforcement in Hinging Zone, Specimen S3-4

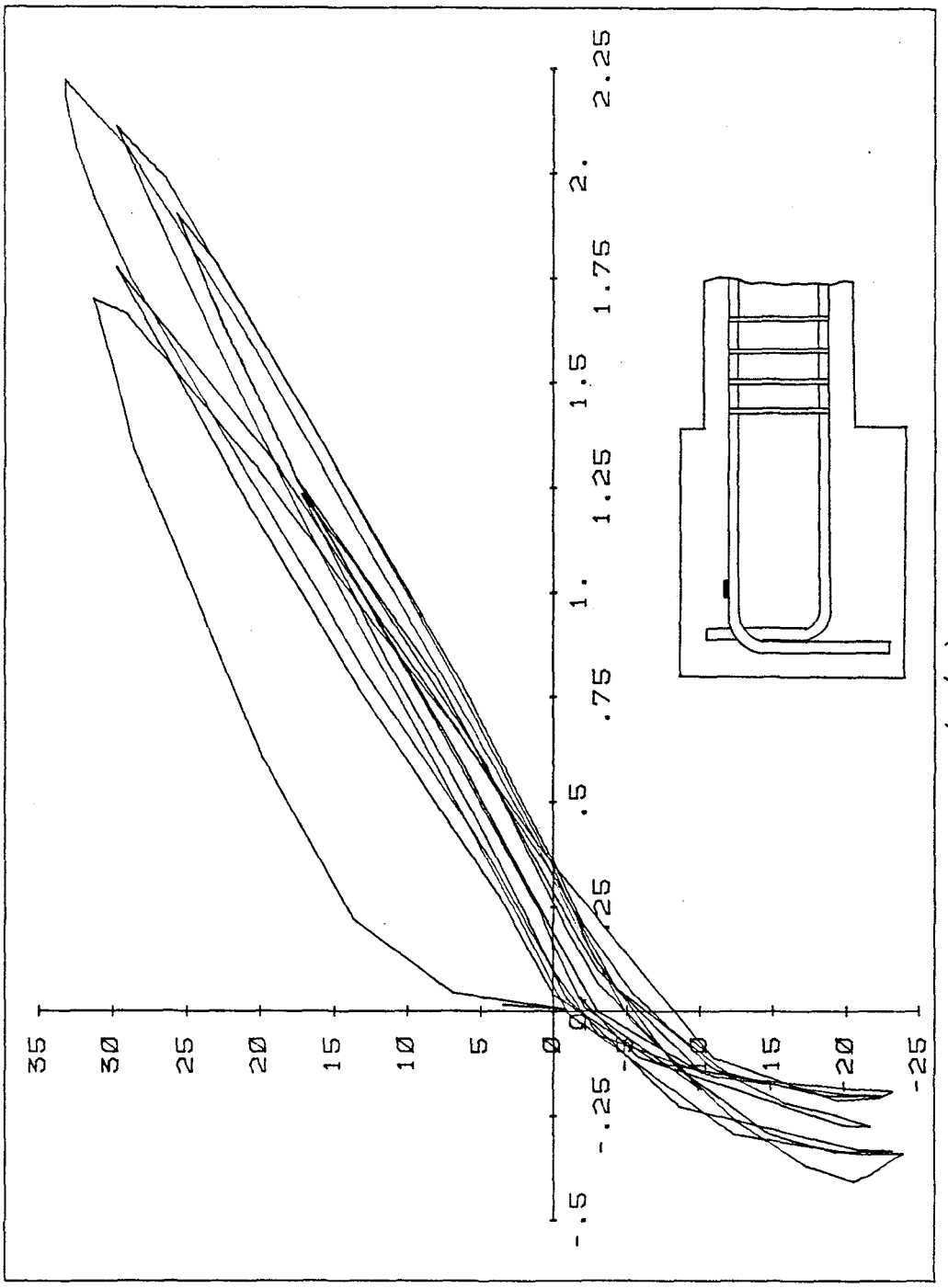

Fig. 3.5(a) Applied Load vs. Strain at the Beginning of the Hook in Top Longitudinal Reinforcement, Specimen S2-3

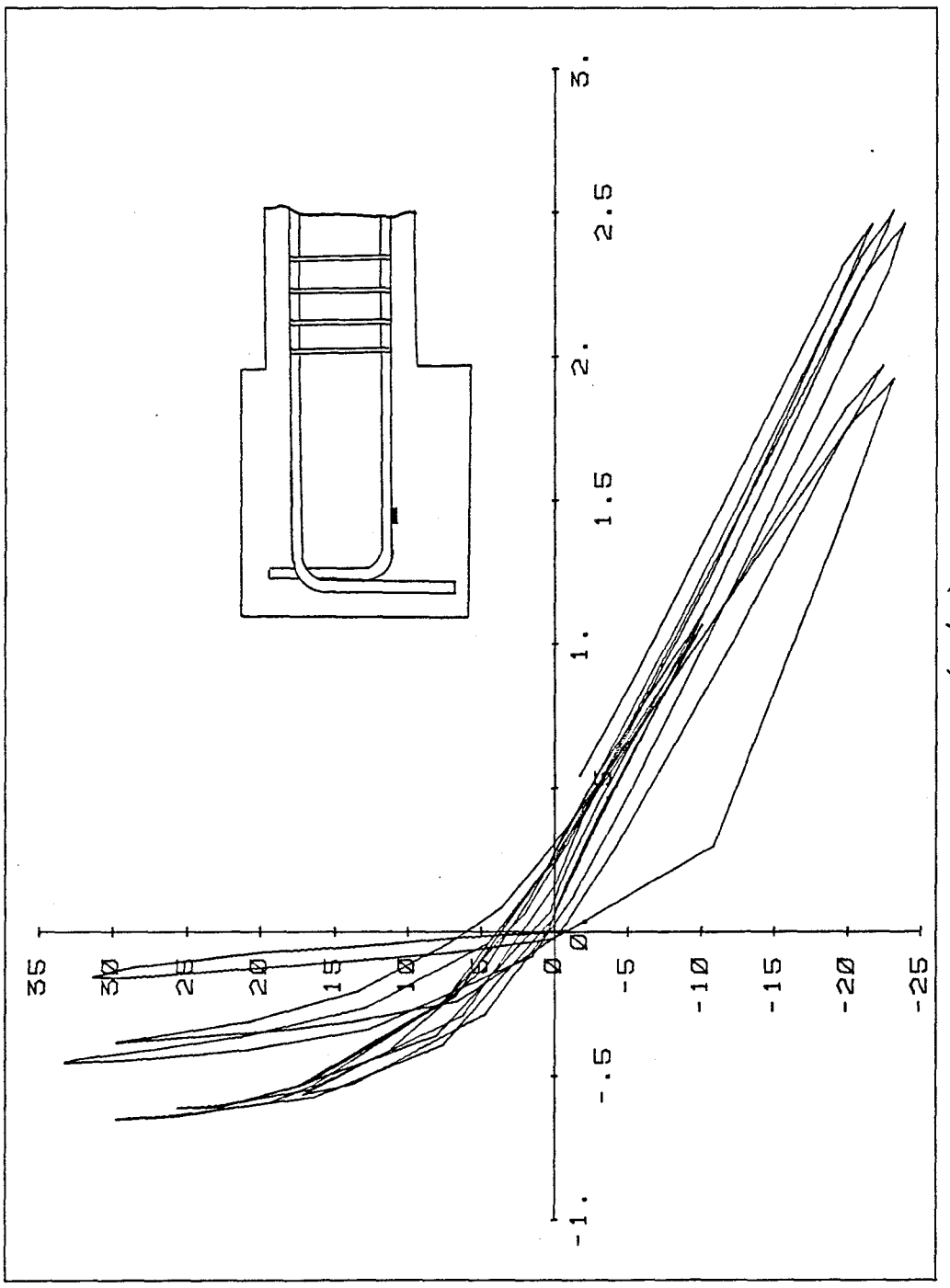

Fig. 3.5(b) Applied Load vs. Strain at the Beginning of the Hook in Bottom Longitudinal Reinforcement, Specimen S2-3

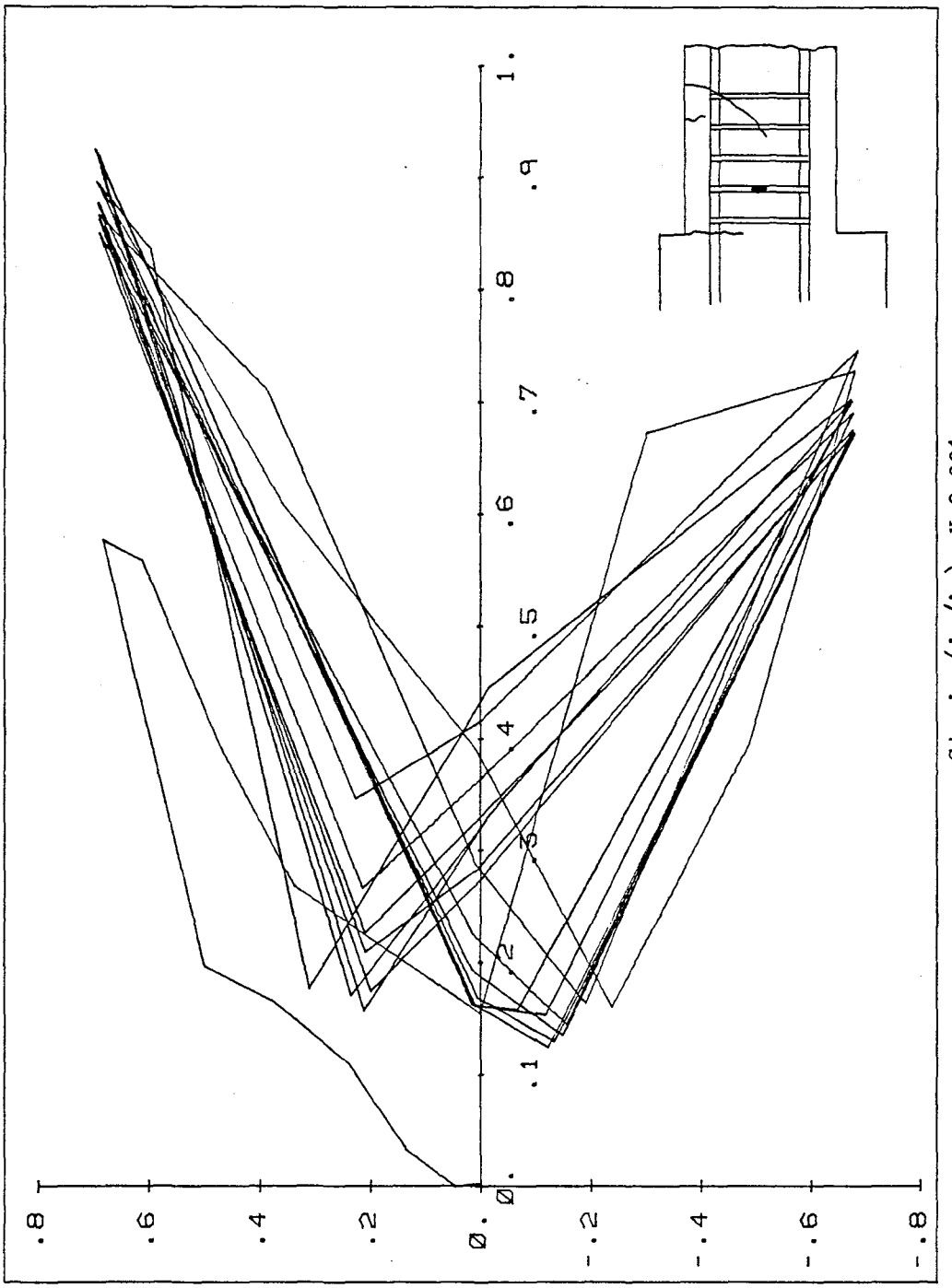

Fig. 3.6(a) Load-Point Deflection vs. Stirrup Strain, Specimen S2-1

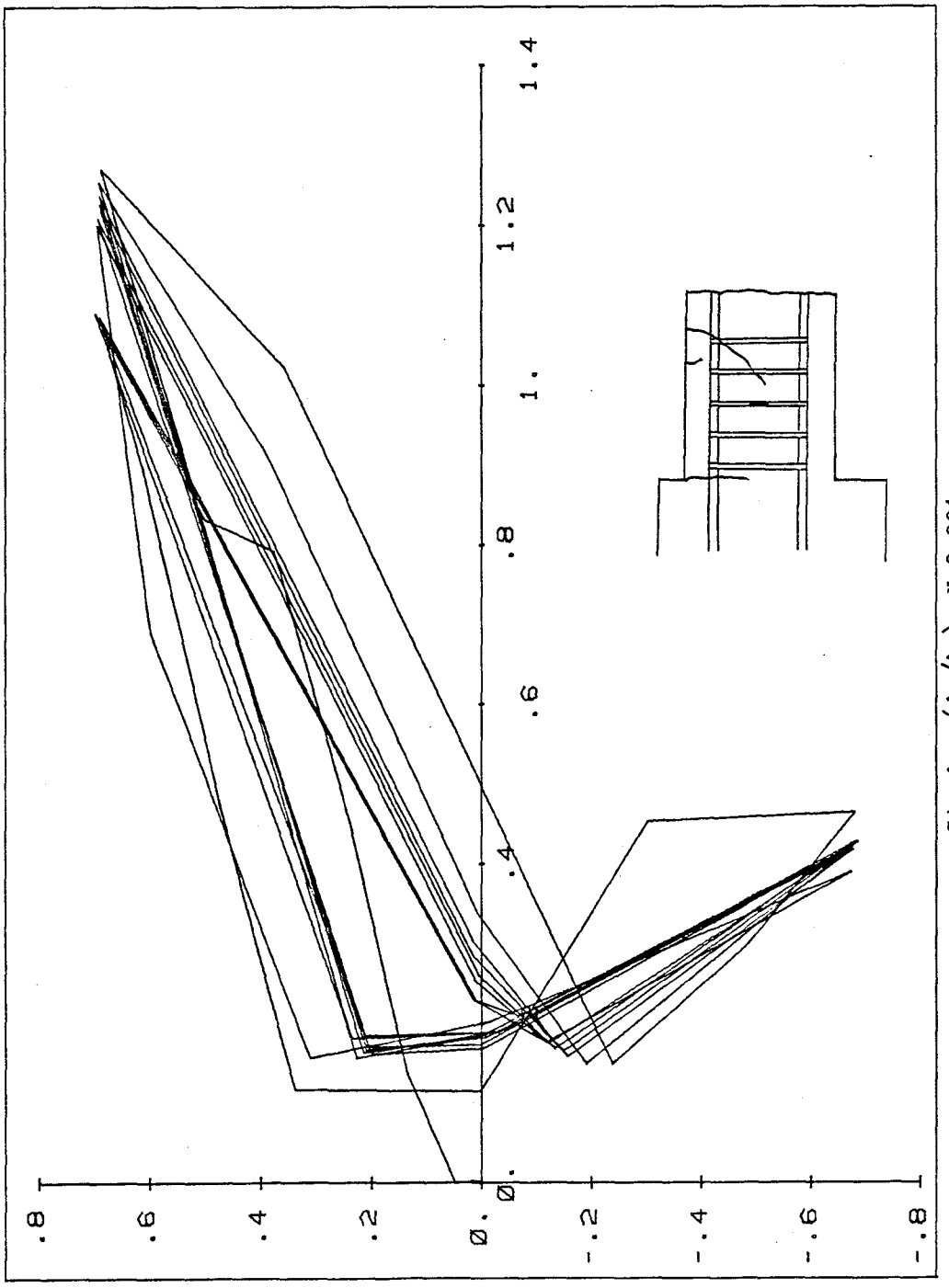

Fig. 3.6(b) Load-Point Deflection vs. Stirrup Strain, Specimen S2-1

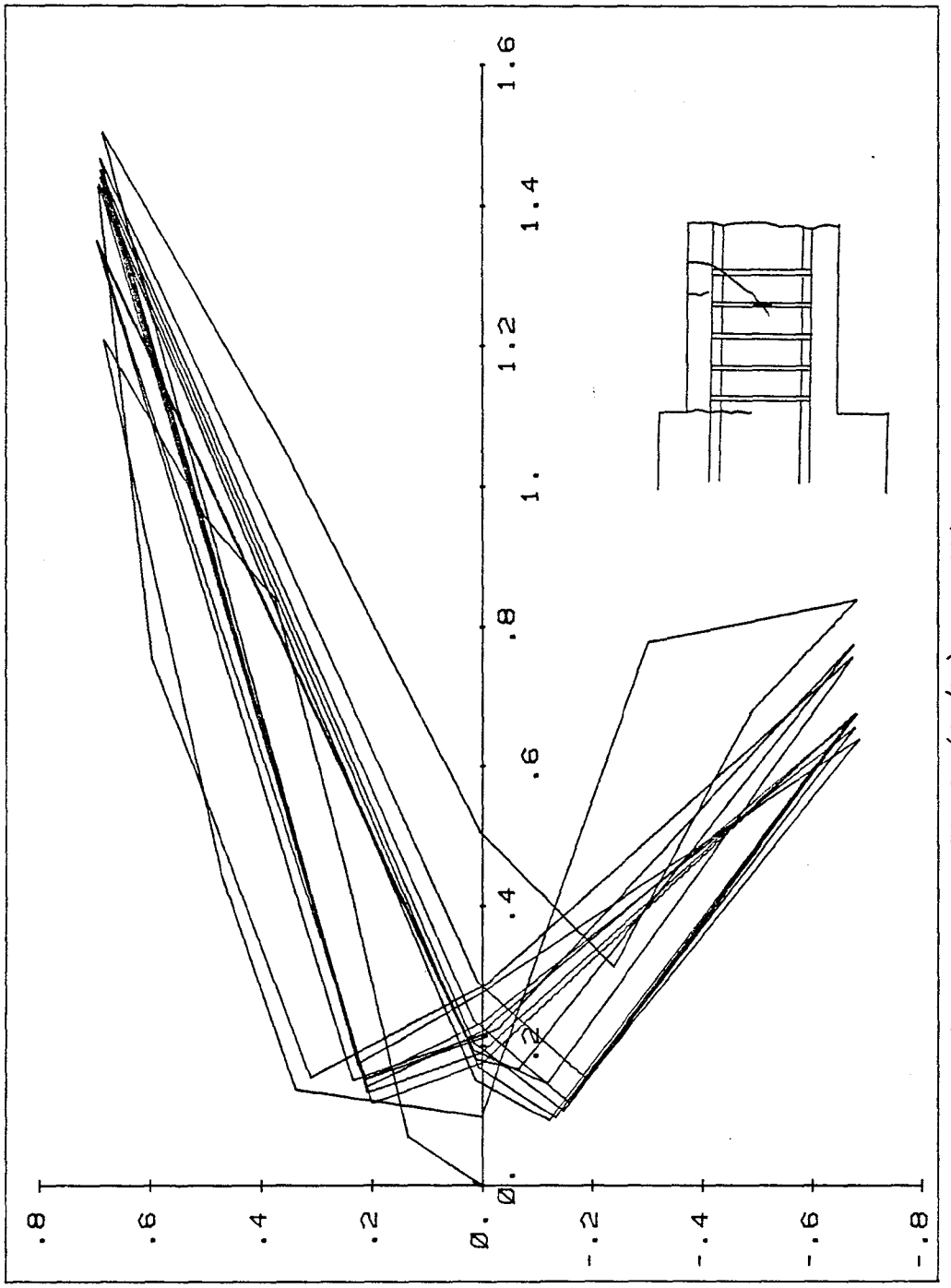

Fig. 3.6(c) Load-Point Deflection vs. Stirrup Strain, Specimen S2-1

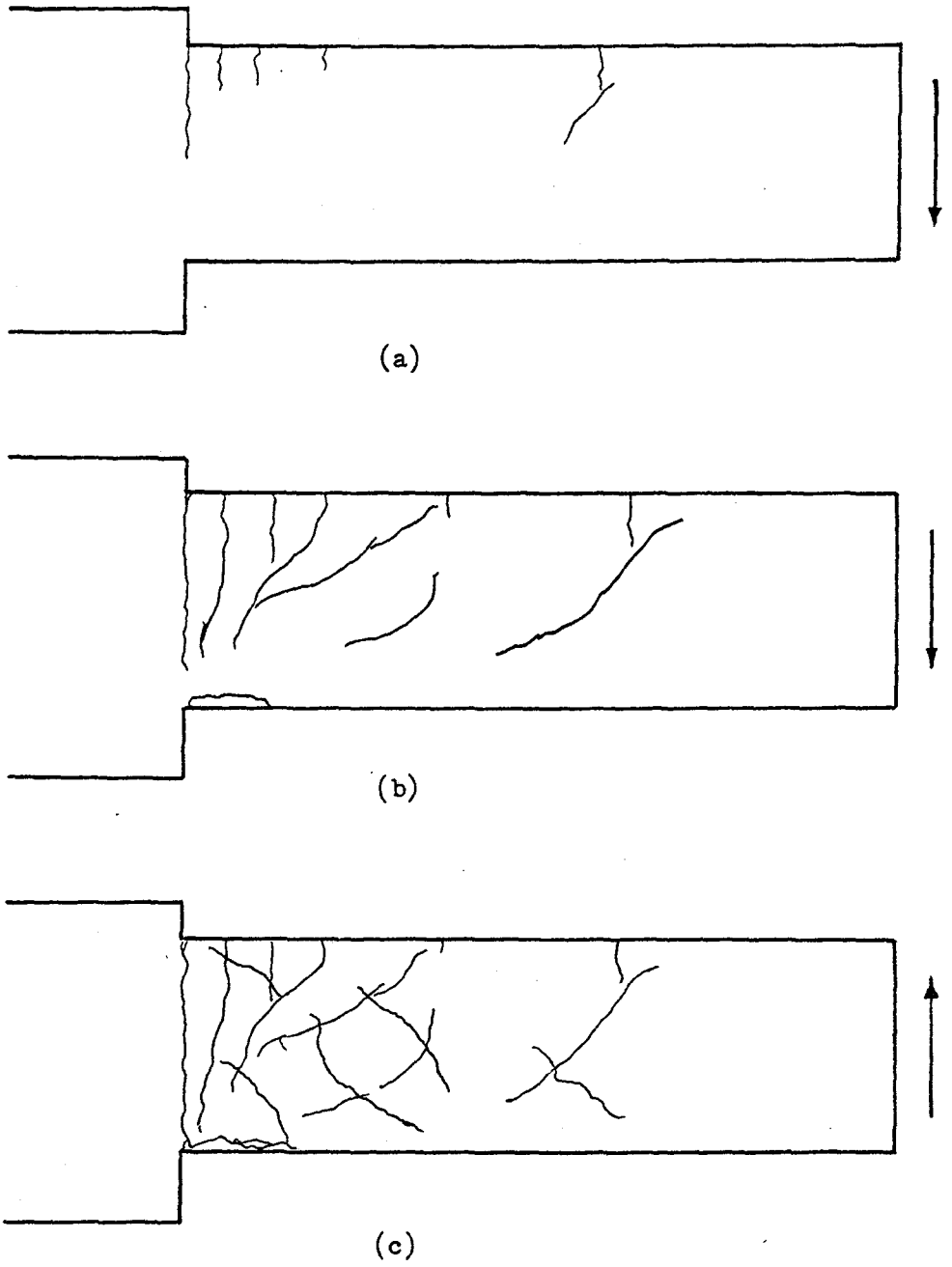

Fig. 3.7 Formation of Cracks During the First Cycle

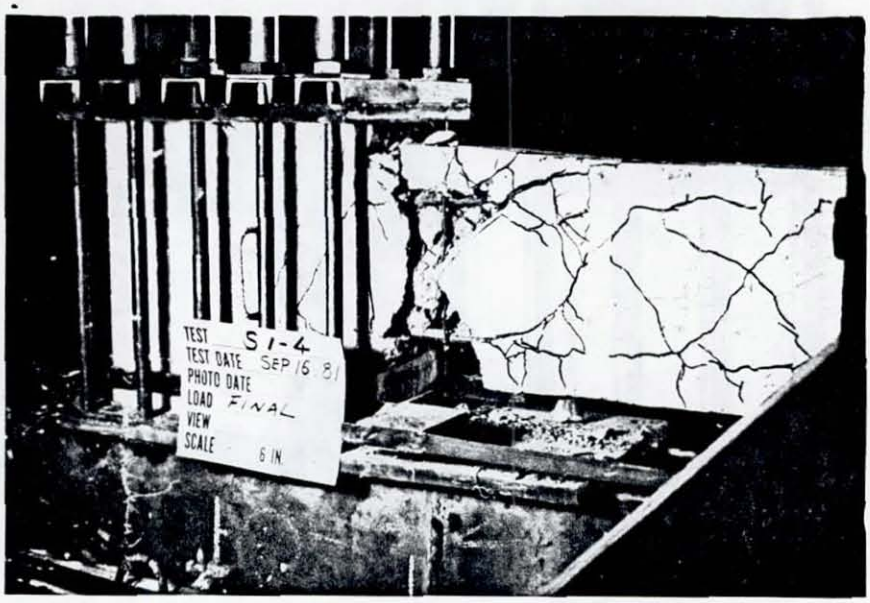

Fig. 3.8(a) Typical Crack Pattern of Group I Specimens at Conclusion of Test

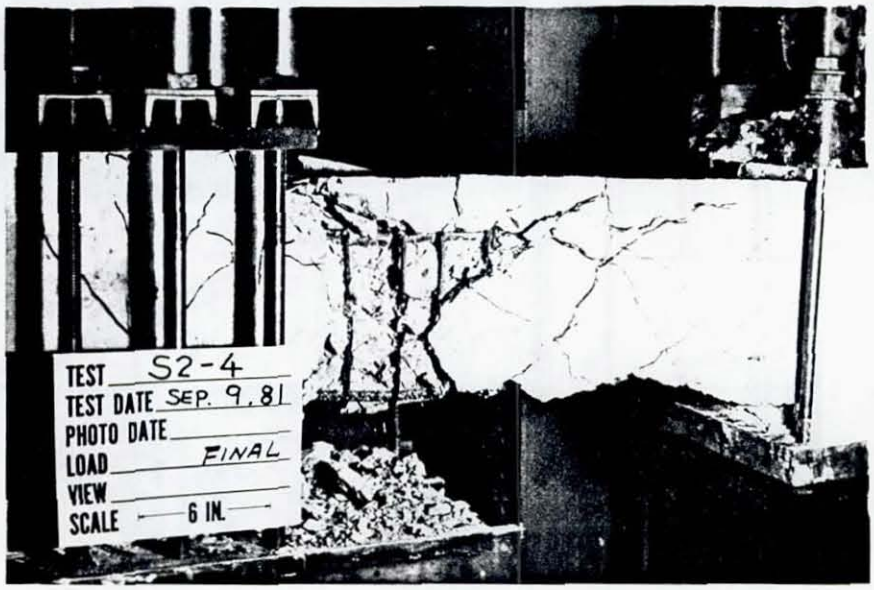

Fig. 3.8(b) Typical Crack Pattern of Group II Specimens at Conclusion of Test

Fig. 3.8(c) Typical Crack Pattern of Group III Specimens at Conclusion of Test

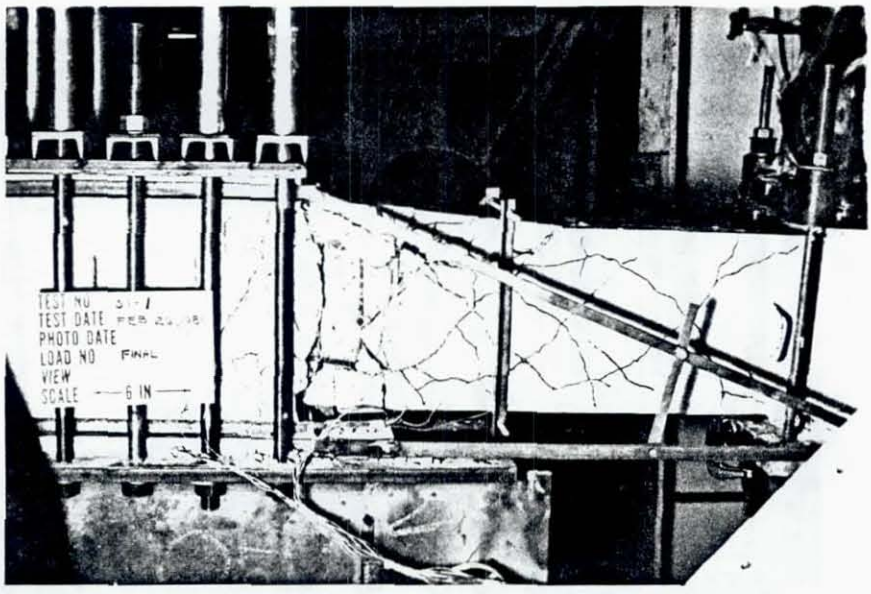

Fig. 3.9 Specimen S1-1 at Conclusion of Test

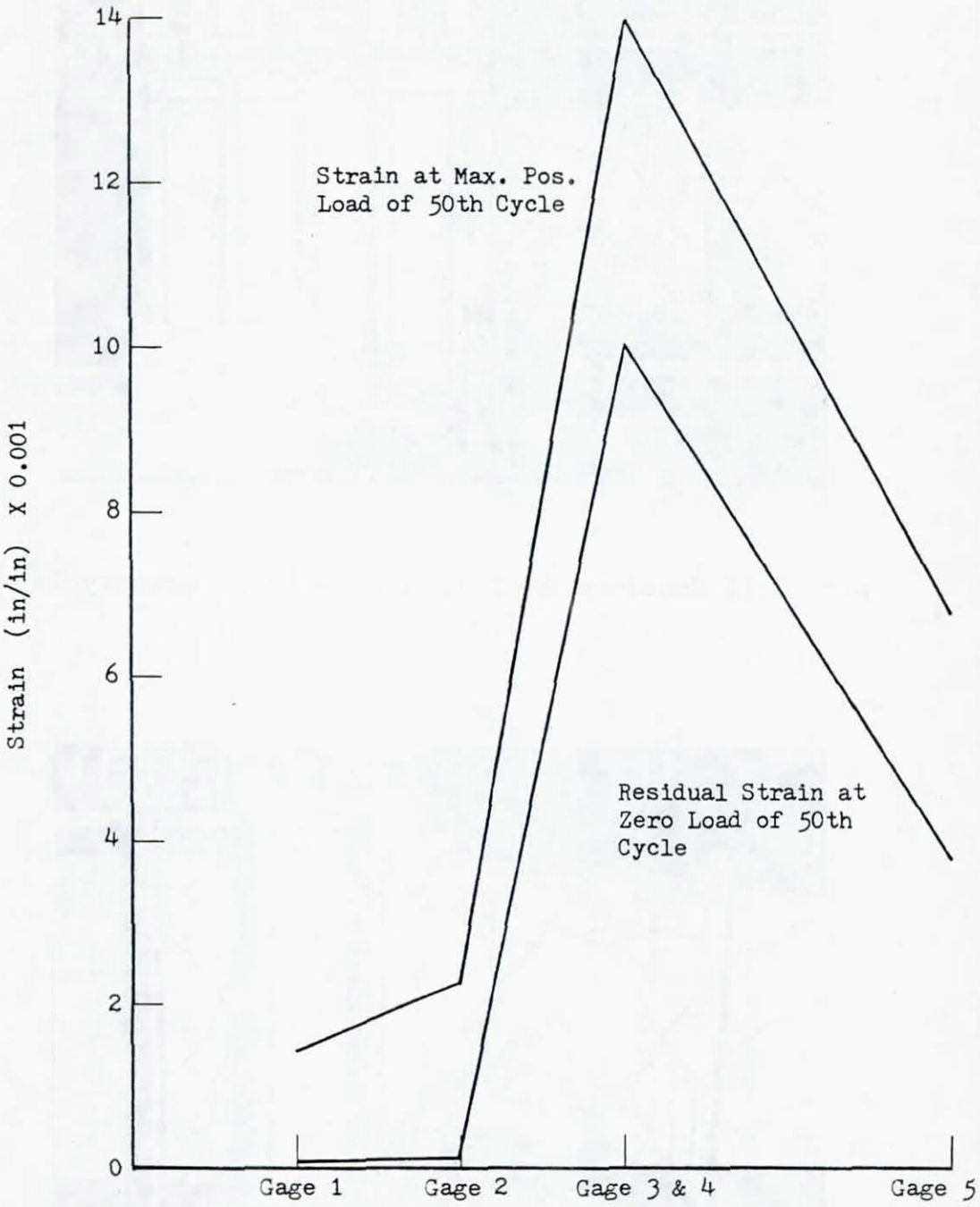

Fig. 3.10 Strains Along the Top Longitudinal Reinforcement in the Enlarged End Block after 50 Cycles of Load, Specimen S1-1

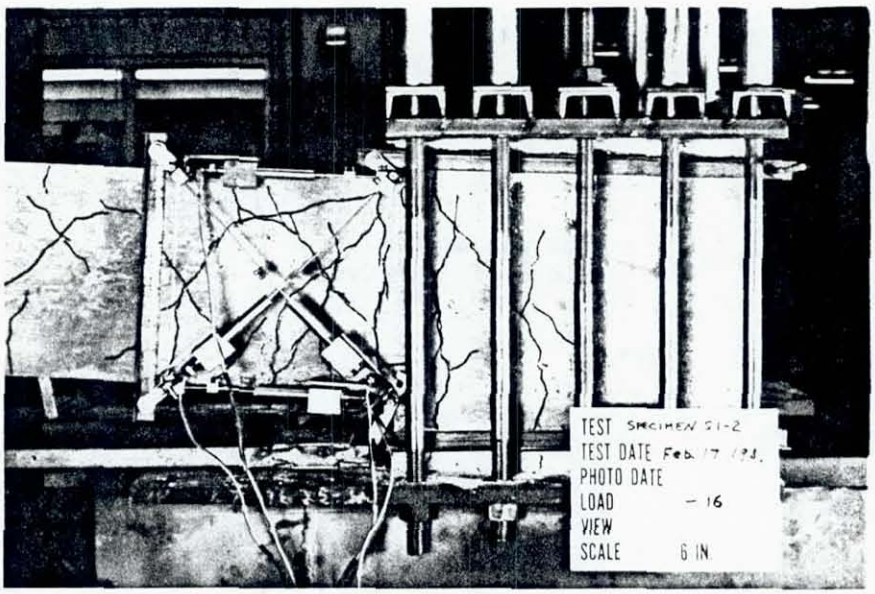

Fig. 3.11 Specimen S1-2 During the First Load Cycle

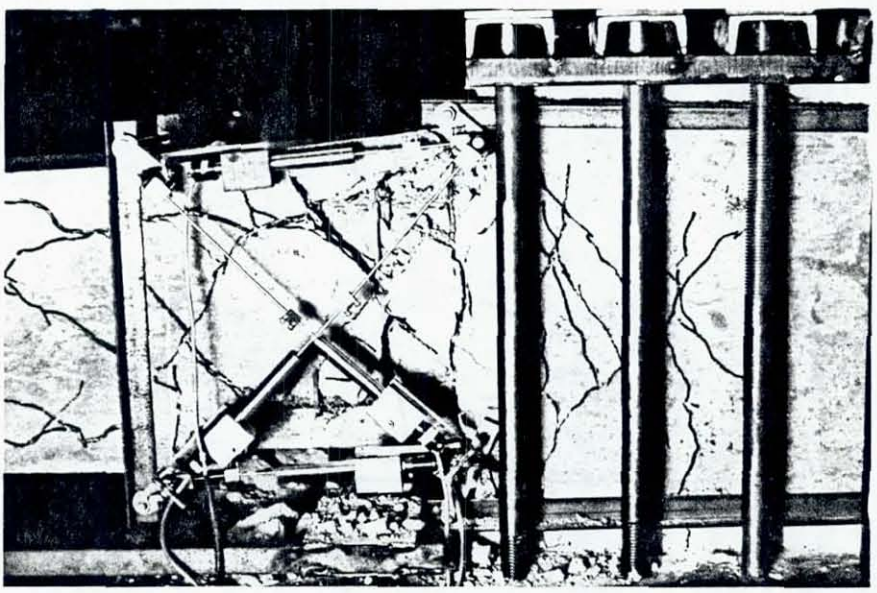

Fig. 3.12 Specimen S1-2 at Conclusion of Test

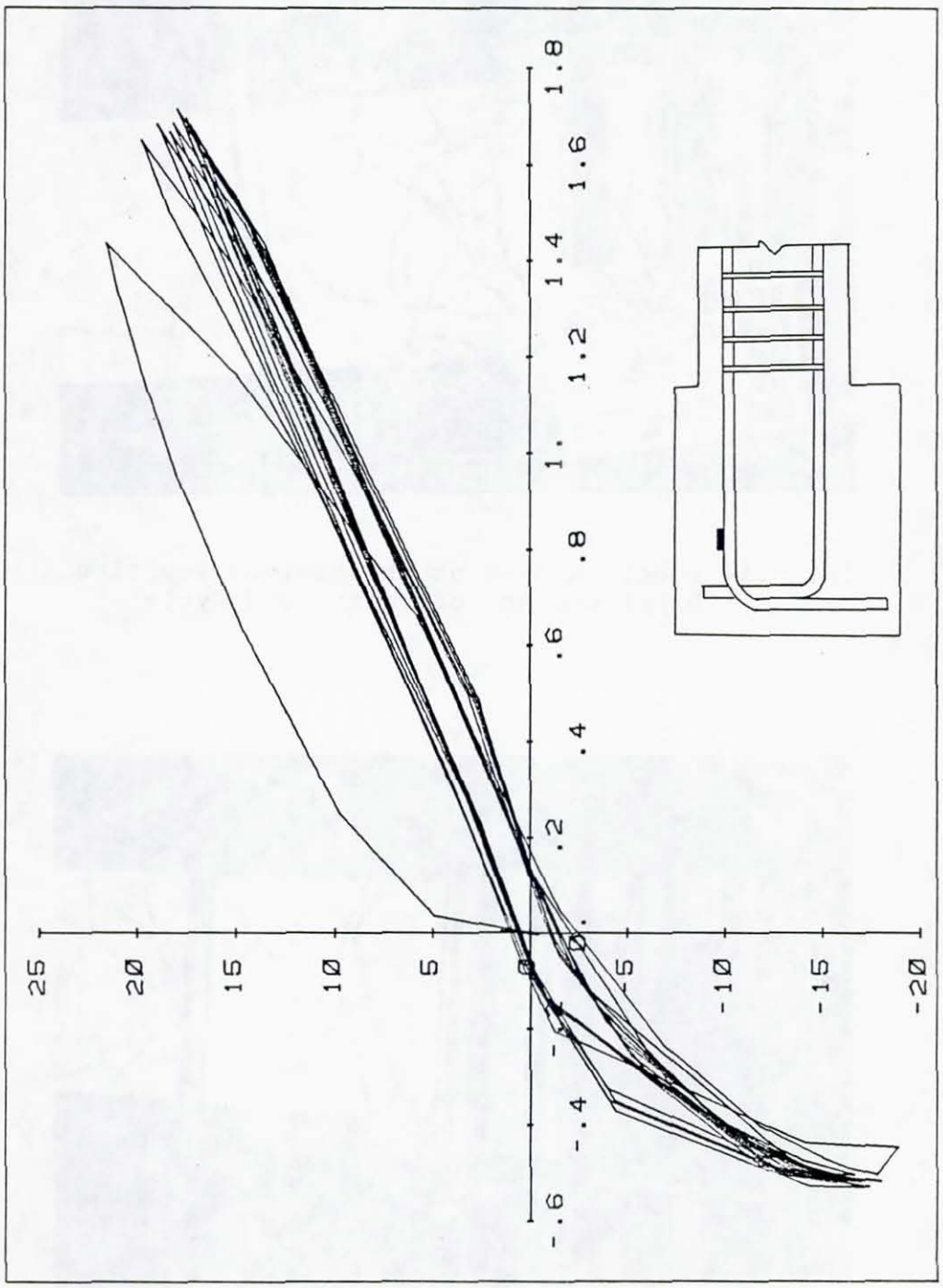

Fig. 3.13 Applied Load vs. Strain at the Beginning of the Hook in Top Longitudinal Reinforcement, Specimen S1-2

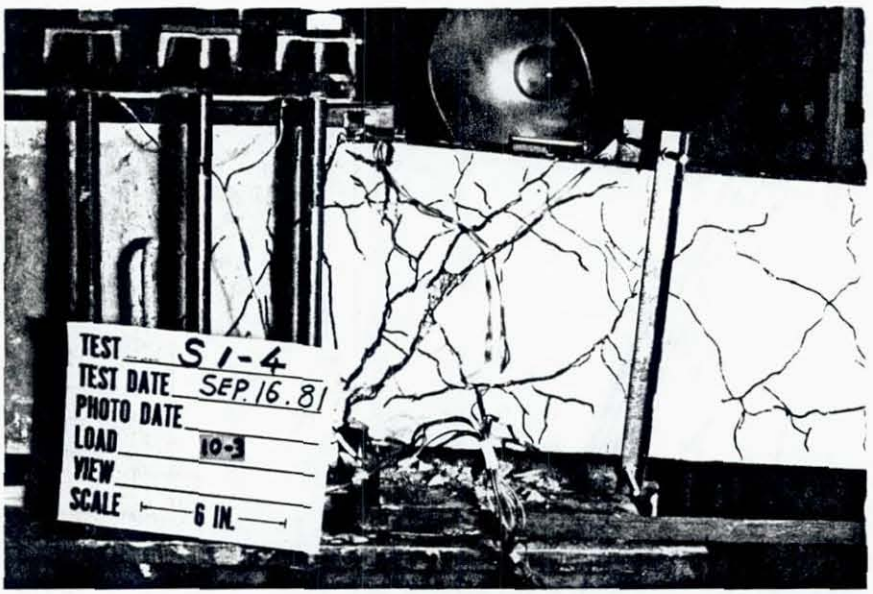

Fig. 3.14 Specimen S1-4 at the Maximum Positive Displacement of Tenth Load Cycle

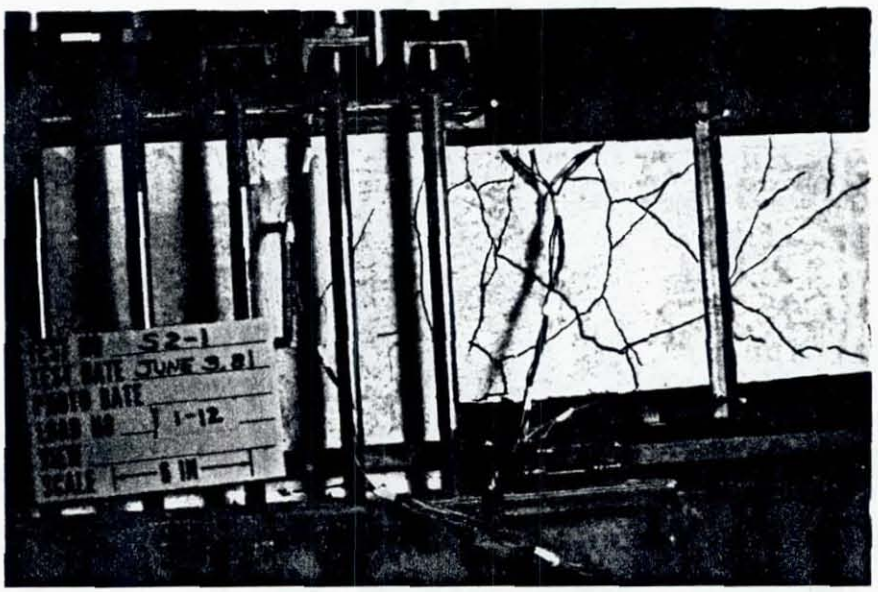

Fig. 3.15 Specimen S2-1 at the Conclusion of First Load Cycle

Fig. 3.16 Specimen S2-1 at the Conclusion of Tenth Load Cycle

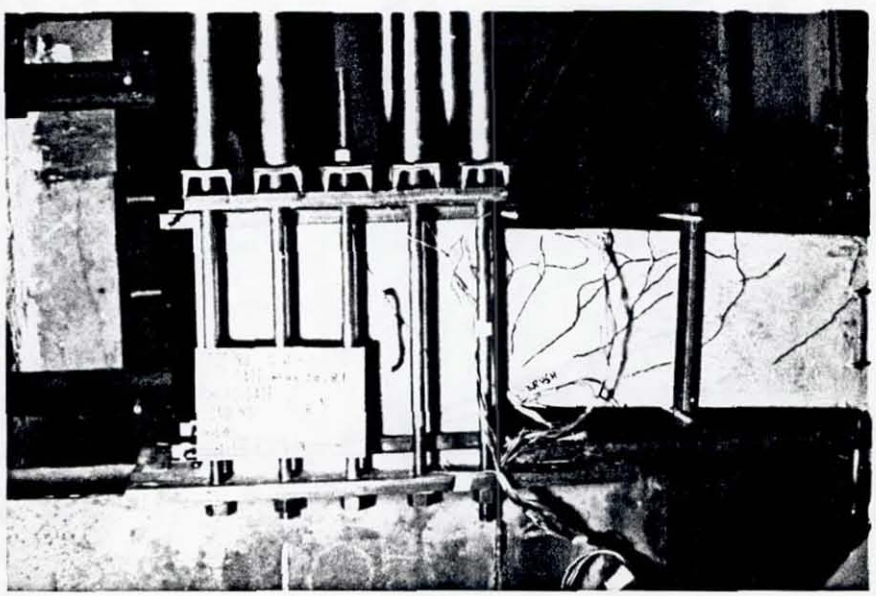

Fig. 3.17 Specimen S2-2 at the Maximum Positive Displacement of First Load Cycle

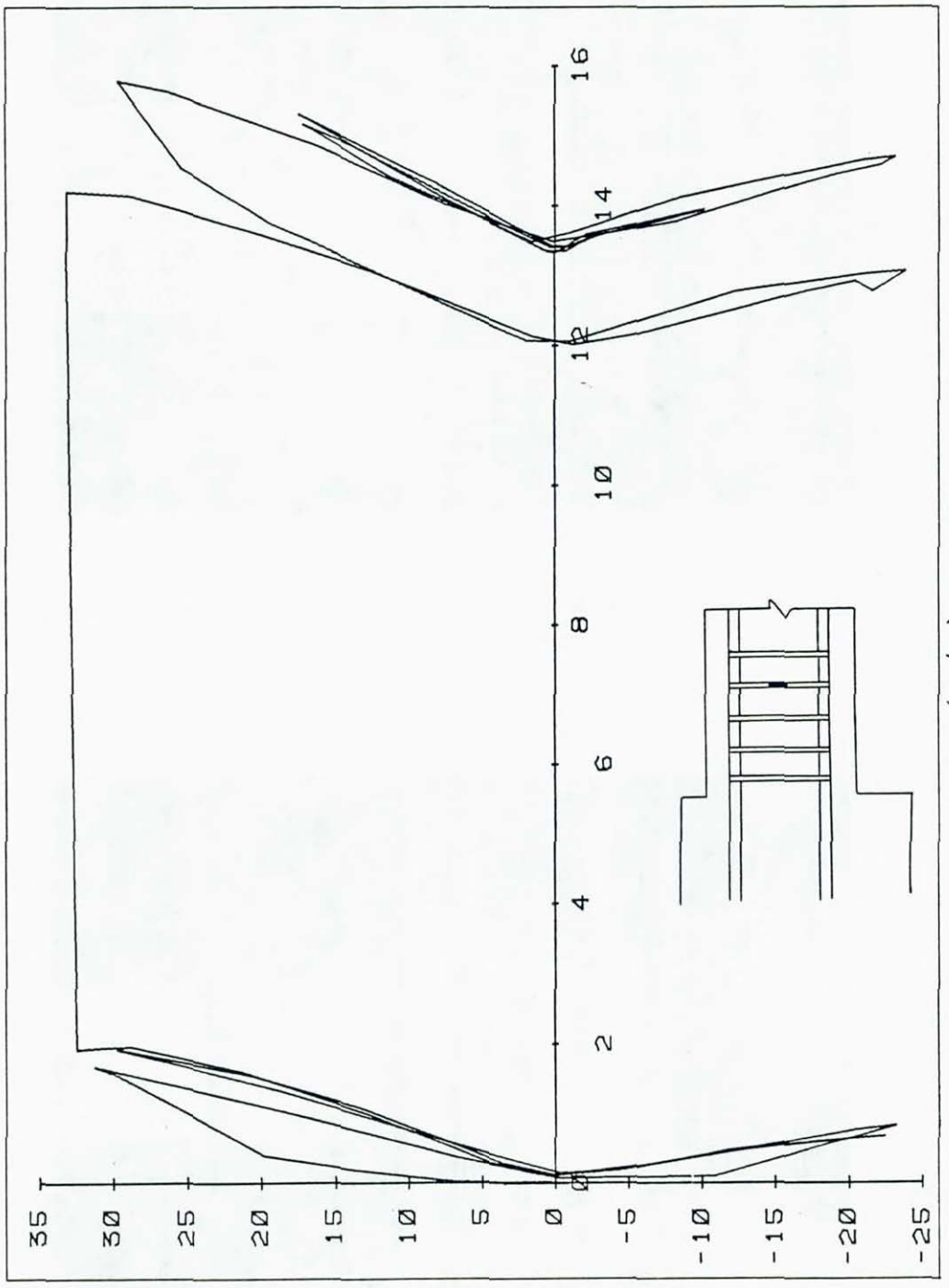

Fig. 3.18 Applied Load vs. Stirrup Strain, Specimen S2-3

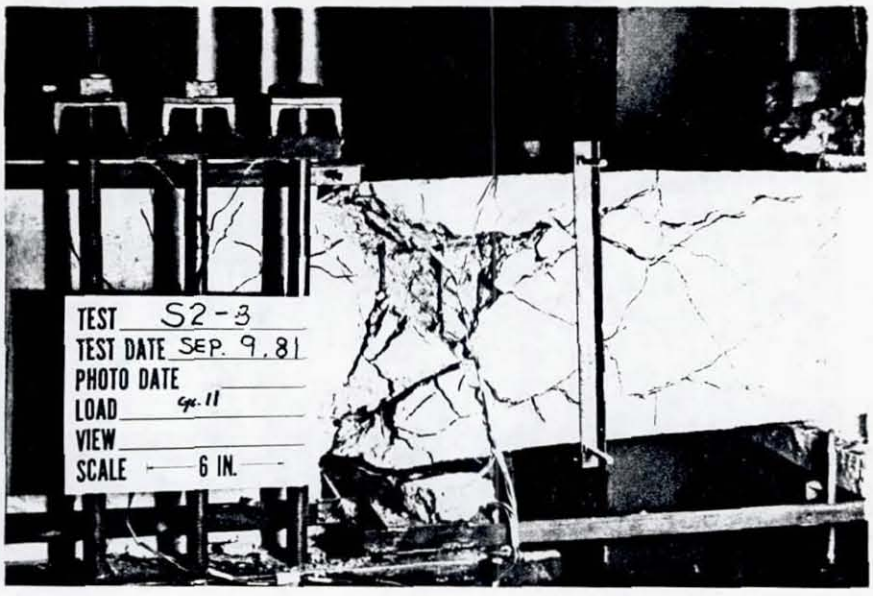

Fig. 3.19 Specimen S2-3 at Maximum Negative Displacement of 11th Load Cycle

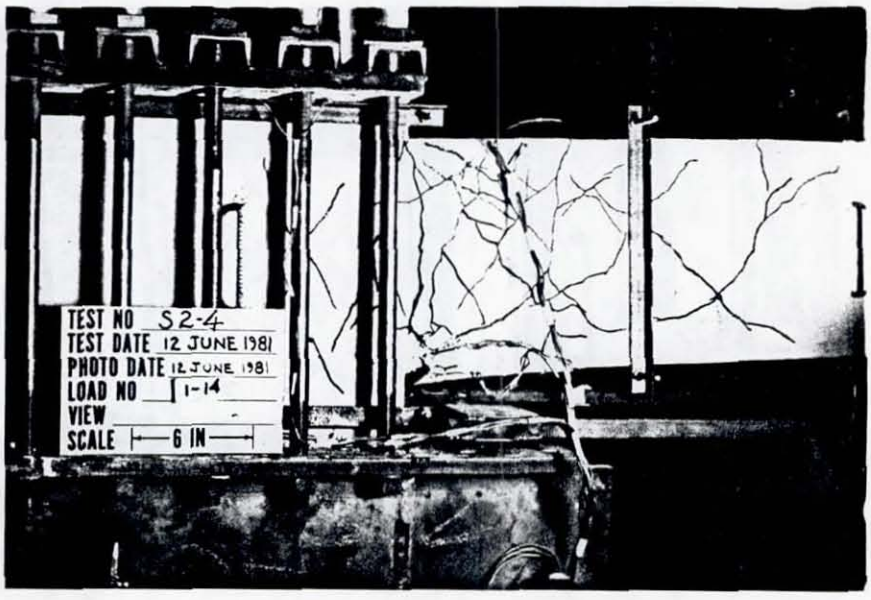

Fig. 3.20 Specimen S2-4 at Conclusion of First Load Cycle

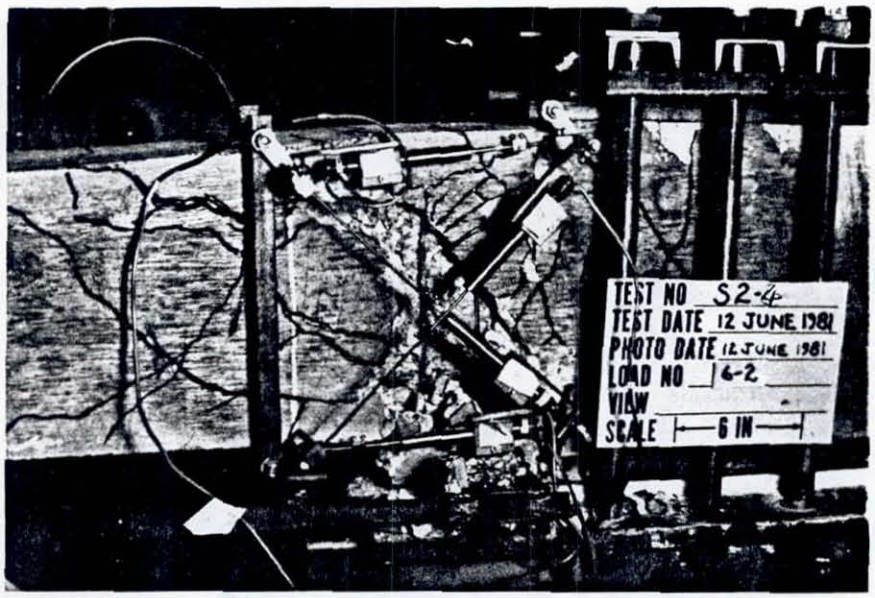

Fig. 3.21 Specimen S2-4 at Maximum Positive Displacement of Sixth Load Cycle

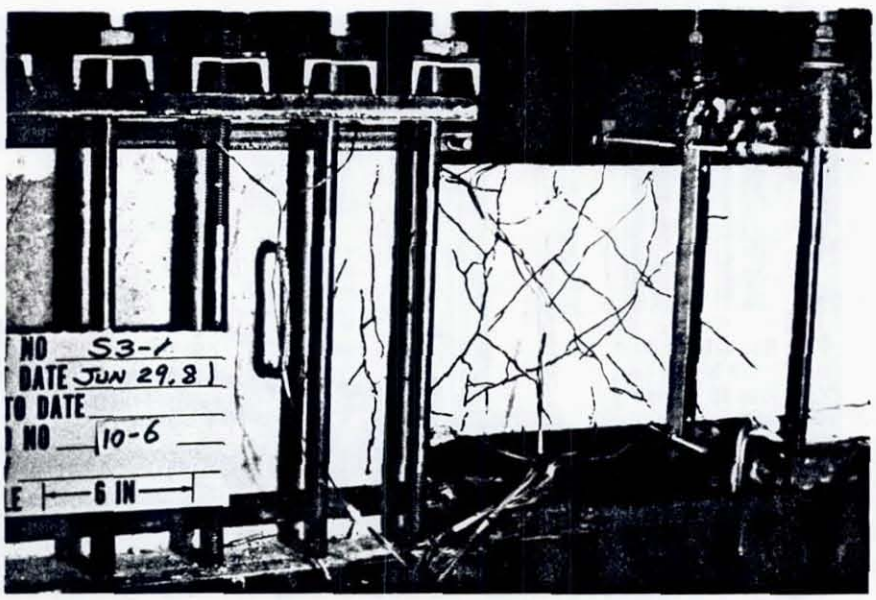

Fig. 3.22 Specimen S3-1 at the Conclusion of Tenth Load Cycle

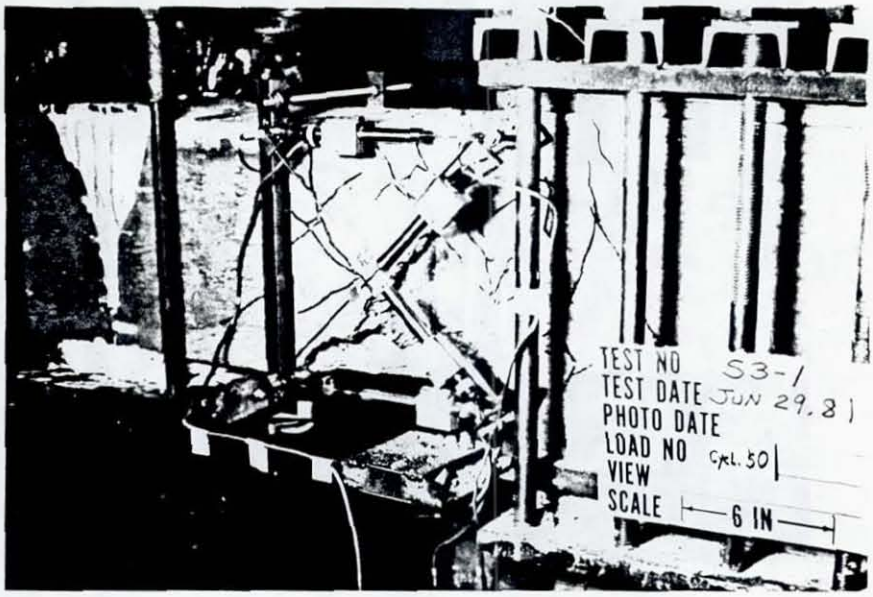

Fig. 3.23 Specimen S3-1 at the Conclusion of 50th Load Cycle

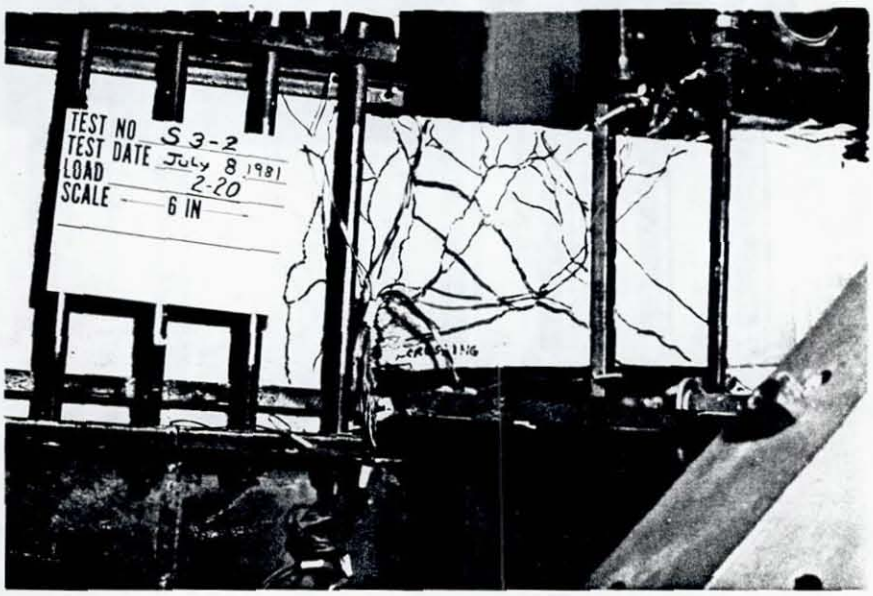

Fig. 3.24 Specimen S3-2 at the Maximum Negative Displacement of Second Load Cycle

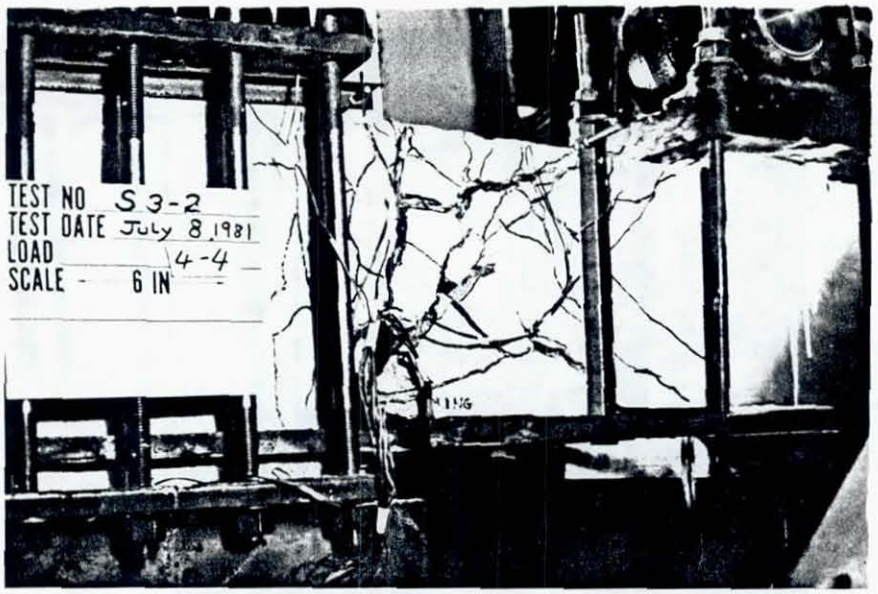

Fig. 3.25 Specimen S3-2 During the Fourth Load Cycle

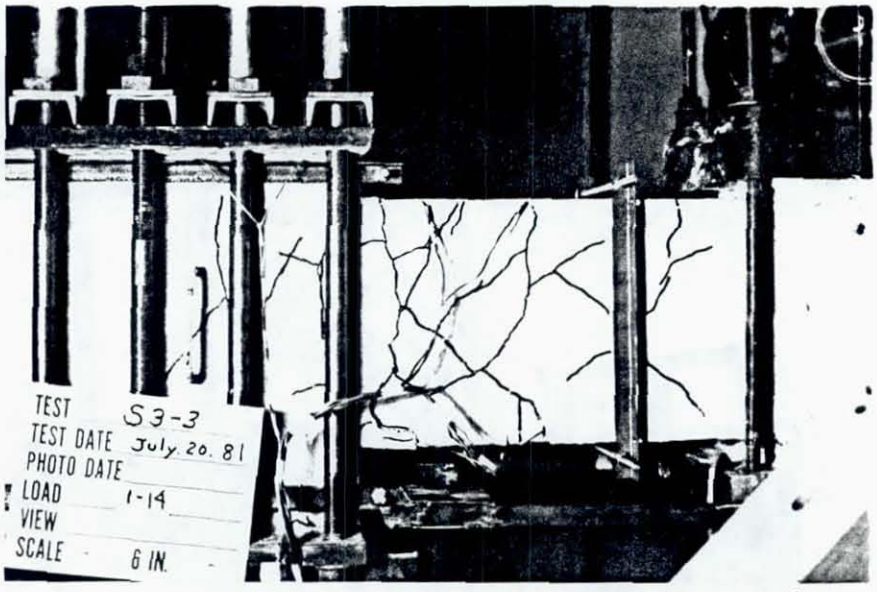

Fig. 3.26 Specimen S3-3 at the Maximum Negative Displacement of First Load Cycle

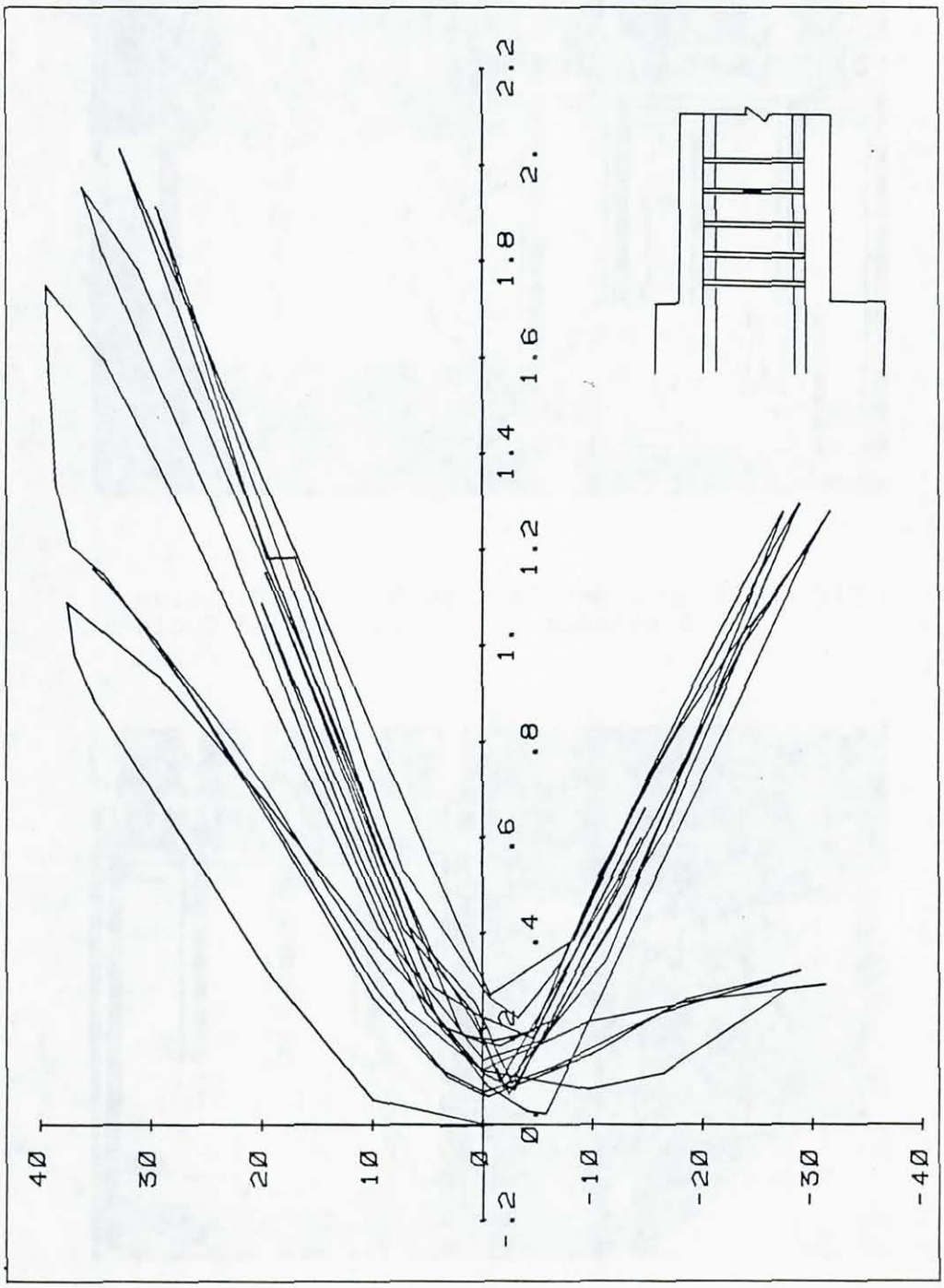

Fig. 3.27 Applied Load vs. Stirrup Strain, Specimen S3-3

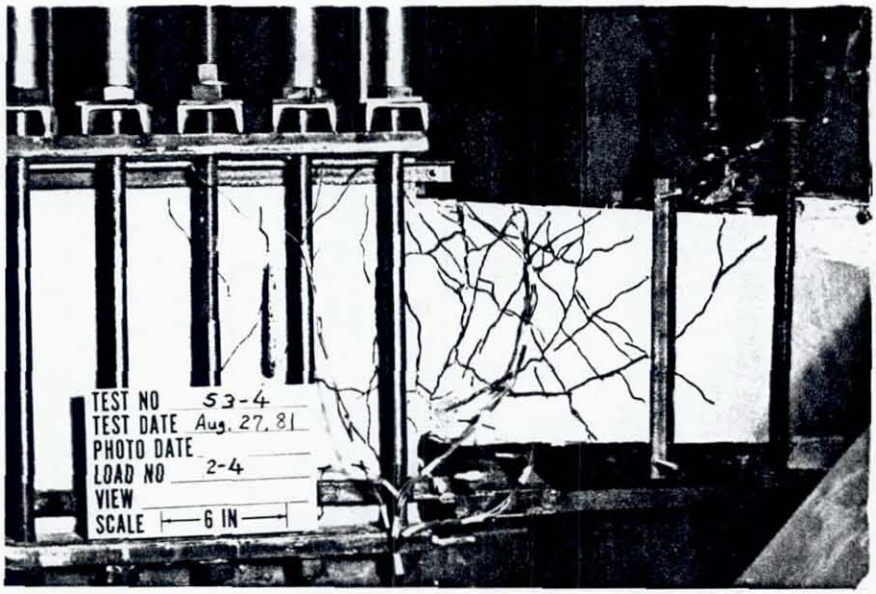

Fig. 3.28 Specimen S3-4 at Maximum Positive Displacement of Second Load Cycle

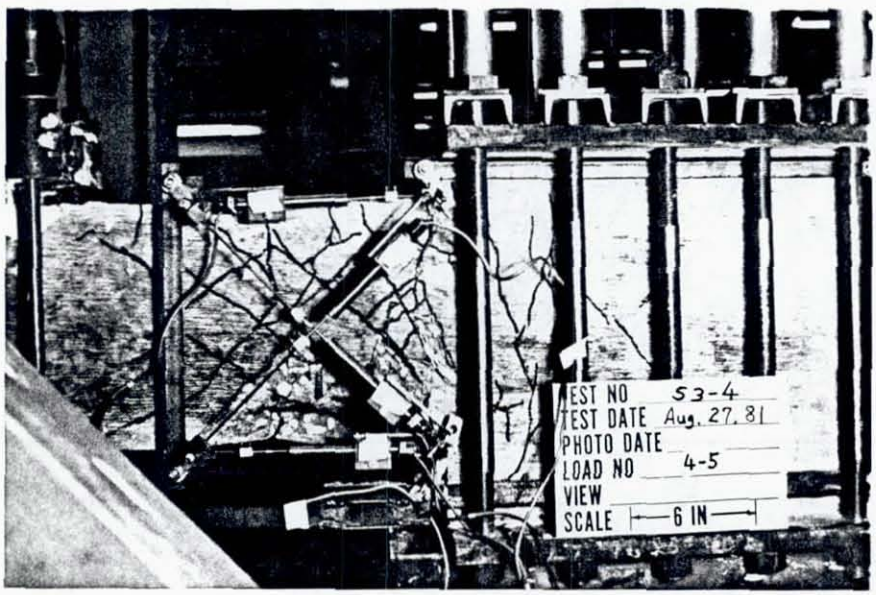

Fig. 3.29 Specimen S3-4 During Fourth Load Cycle

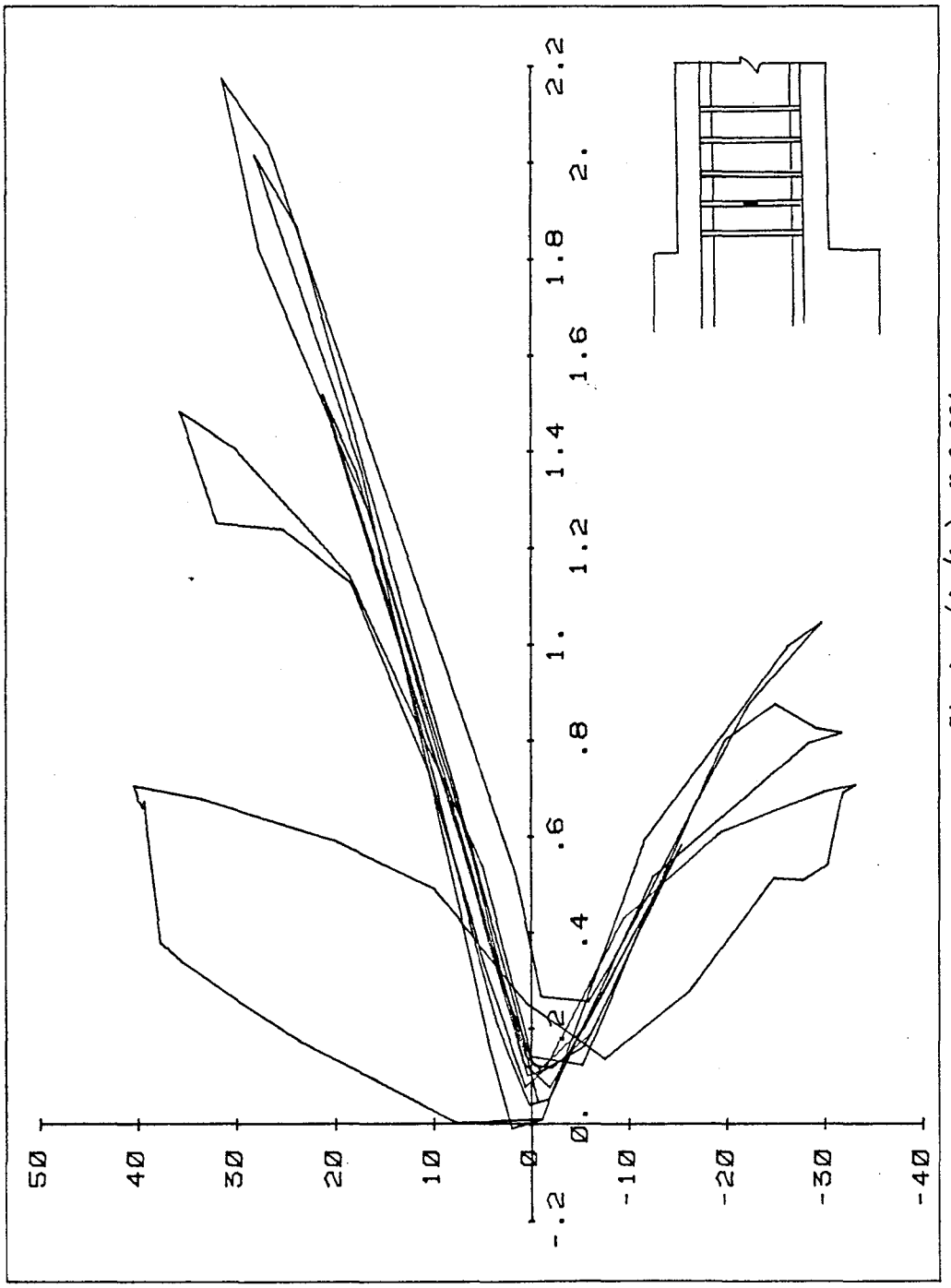

Fig. 3.30 Applied Load vs. Stirrup Strain, Specimen S3-4

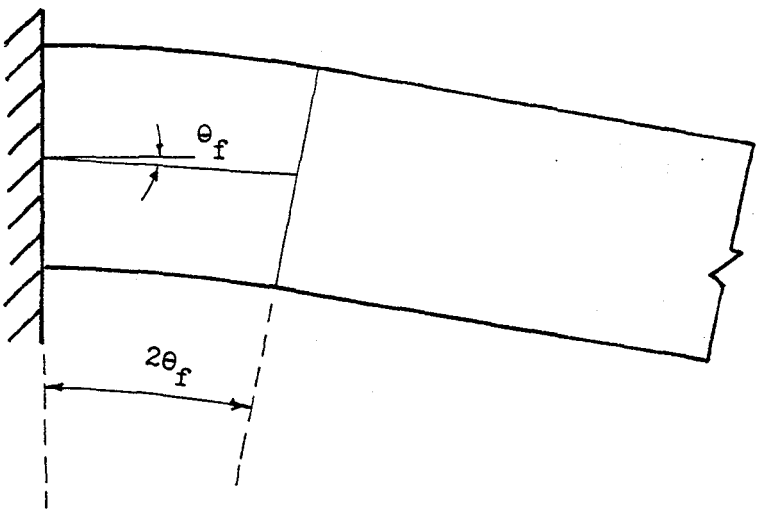

Fig. 4.1 Pure Flexural Displacement in the Hinging Zone

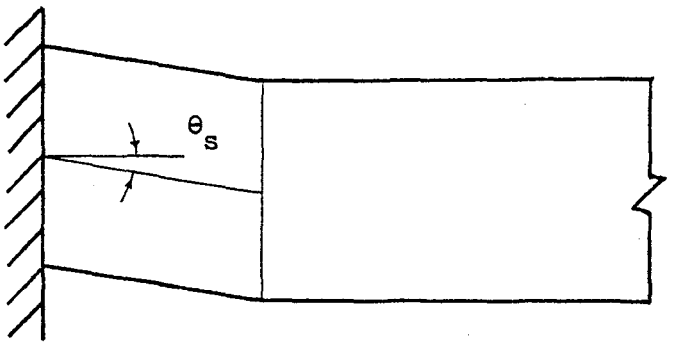

Fig. 4.2 Pure Shear Displacement of the Hinging Zone

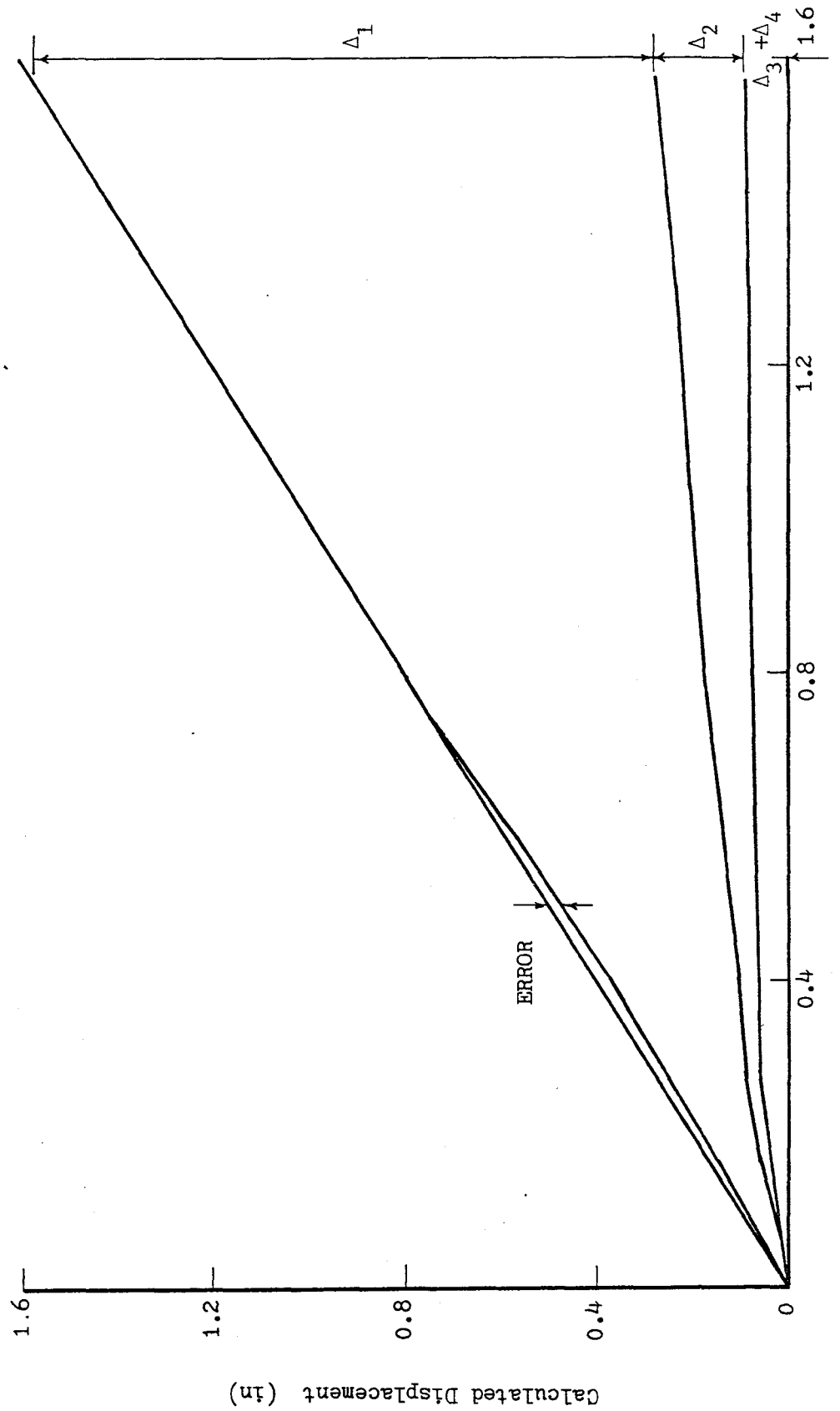

Fig. 4.3(a) Components of Deflection During First Quarter-Cycle of Load, Specimen S1-4

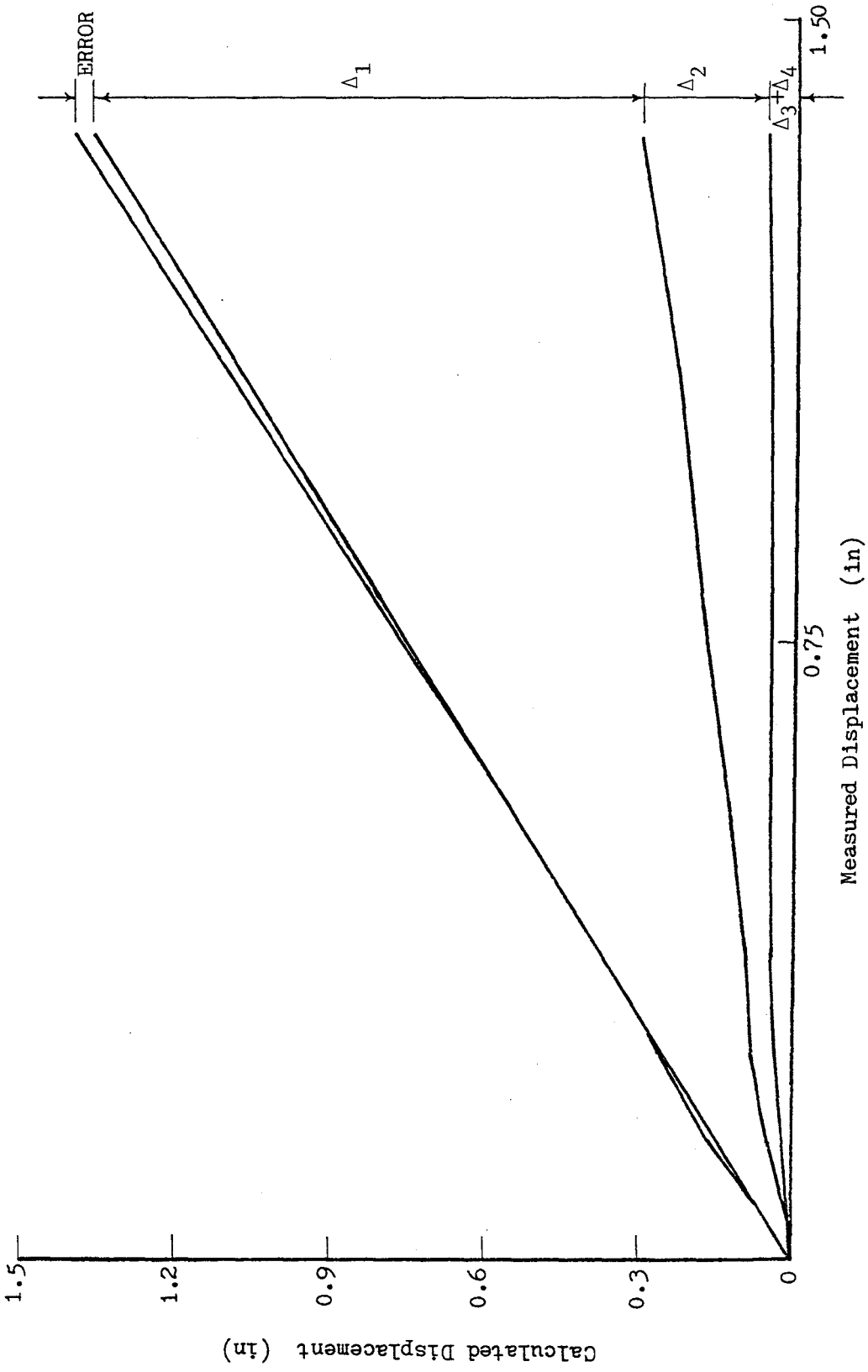

Fig. 4.3(b) Components of Deflection During First Quarter-Cycle of Load, Specimen S2-2

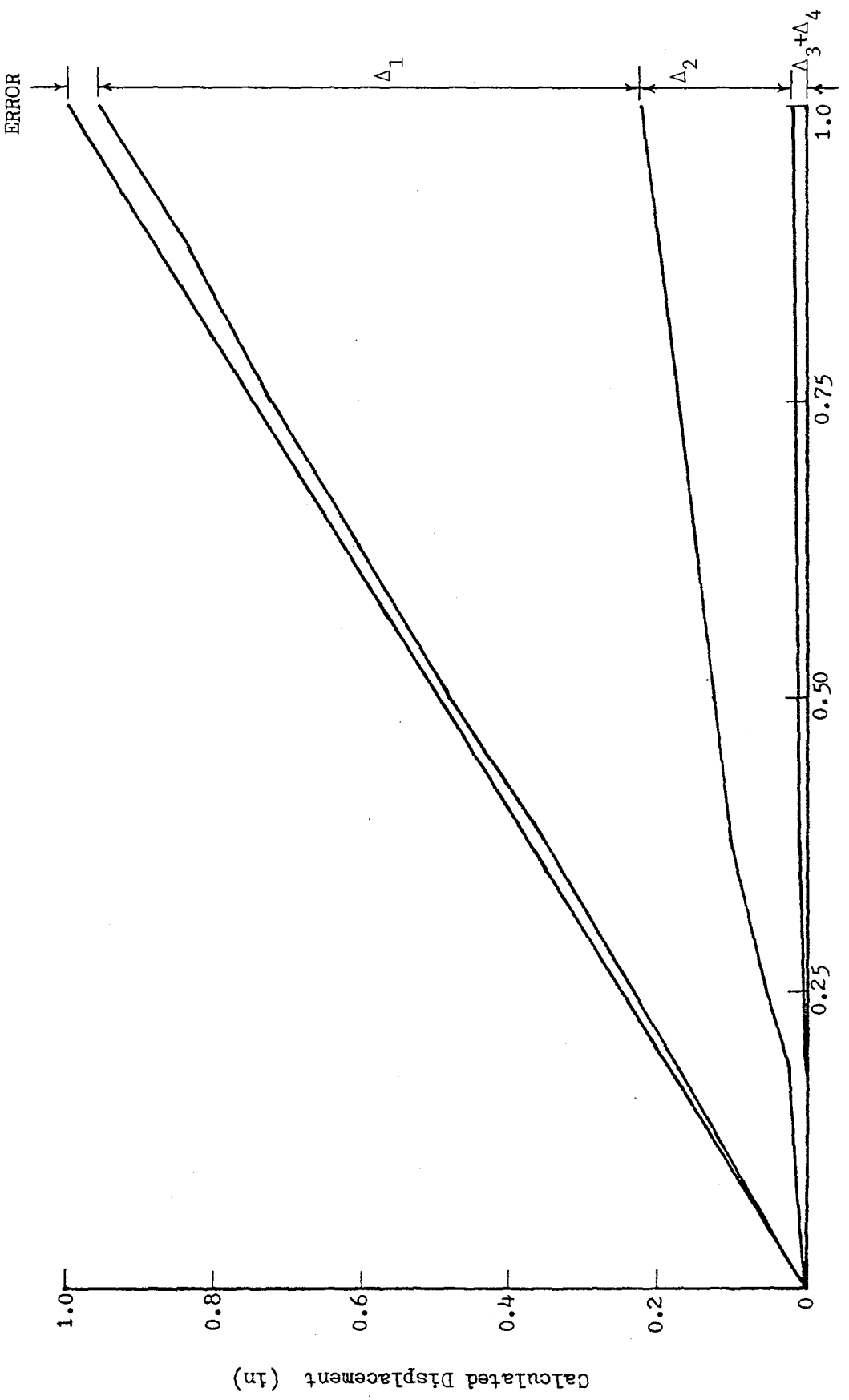

Fig. 4.3(c) Components of Deflection During First Quarter-Cycle of Load, Specimen S3-2

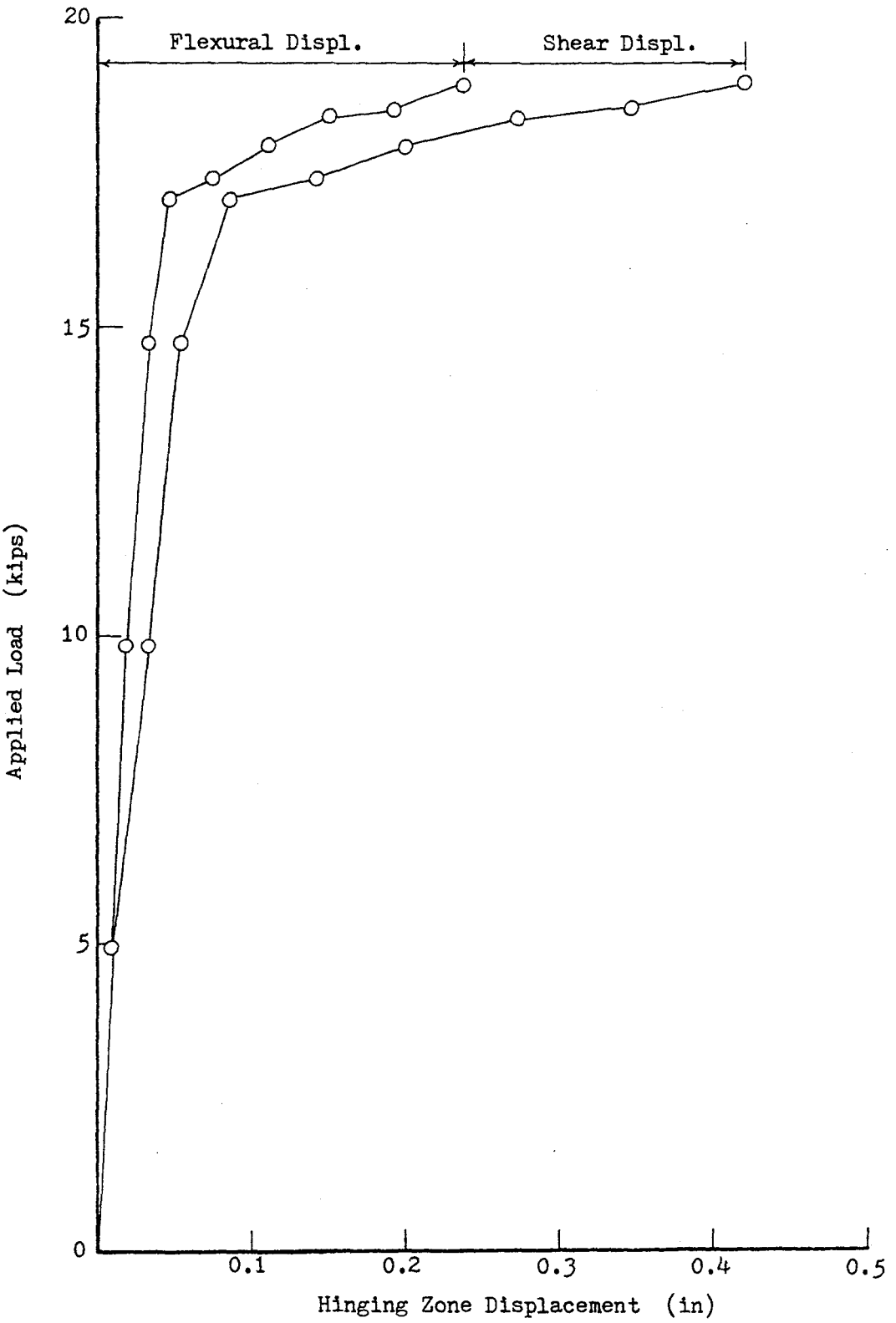

Fig. 4.4(a) Flexural and Shear Displacement in the Hinging Zone, Specimen S1-4

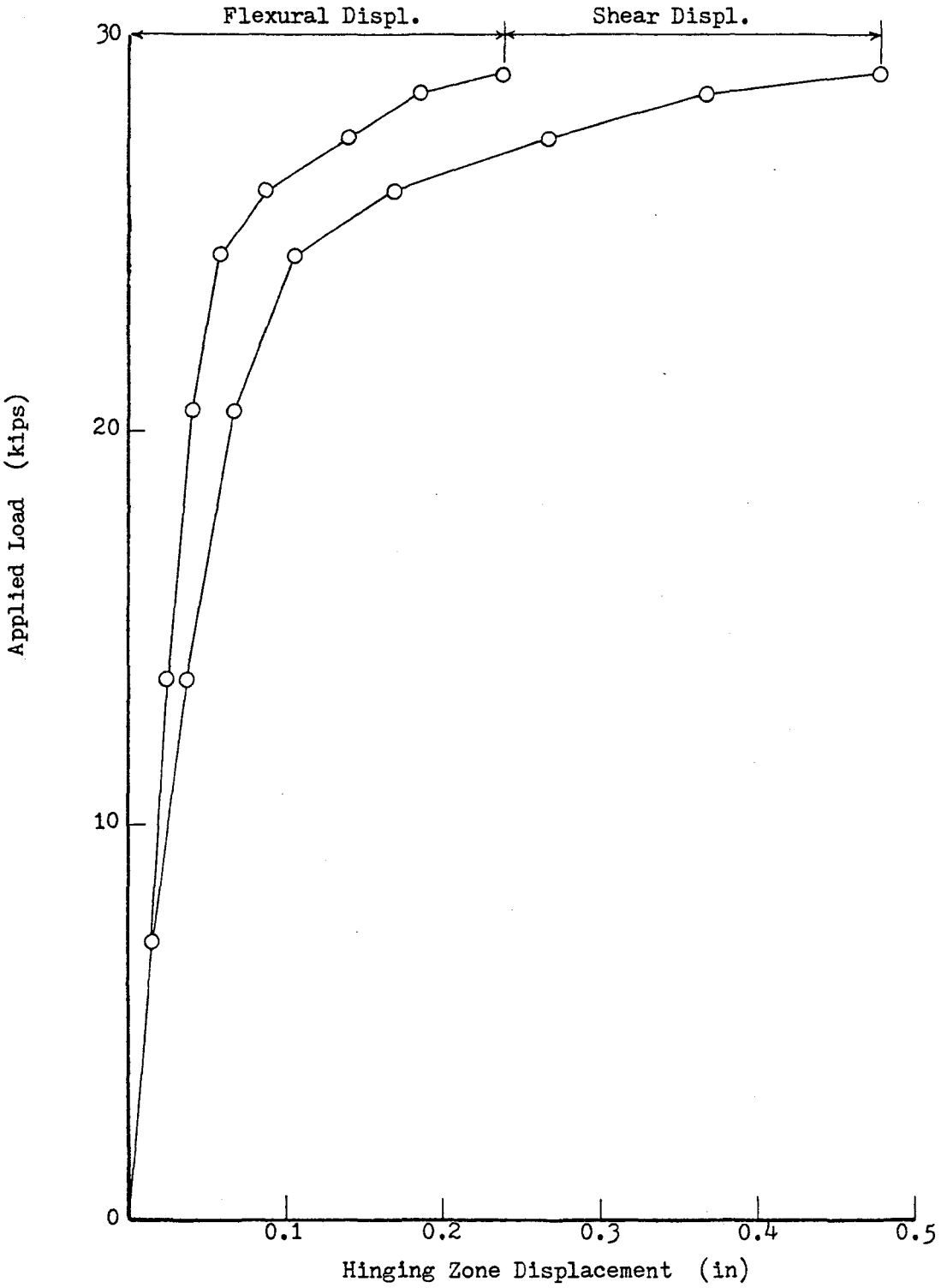

Fig. 4.4(b) Flexural and Shear Displacement in the Hinging Zone, Specimen S2-2

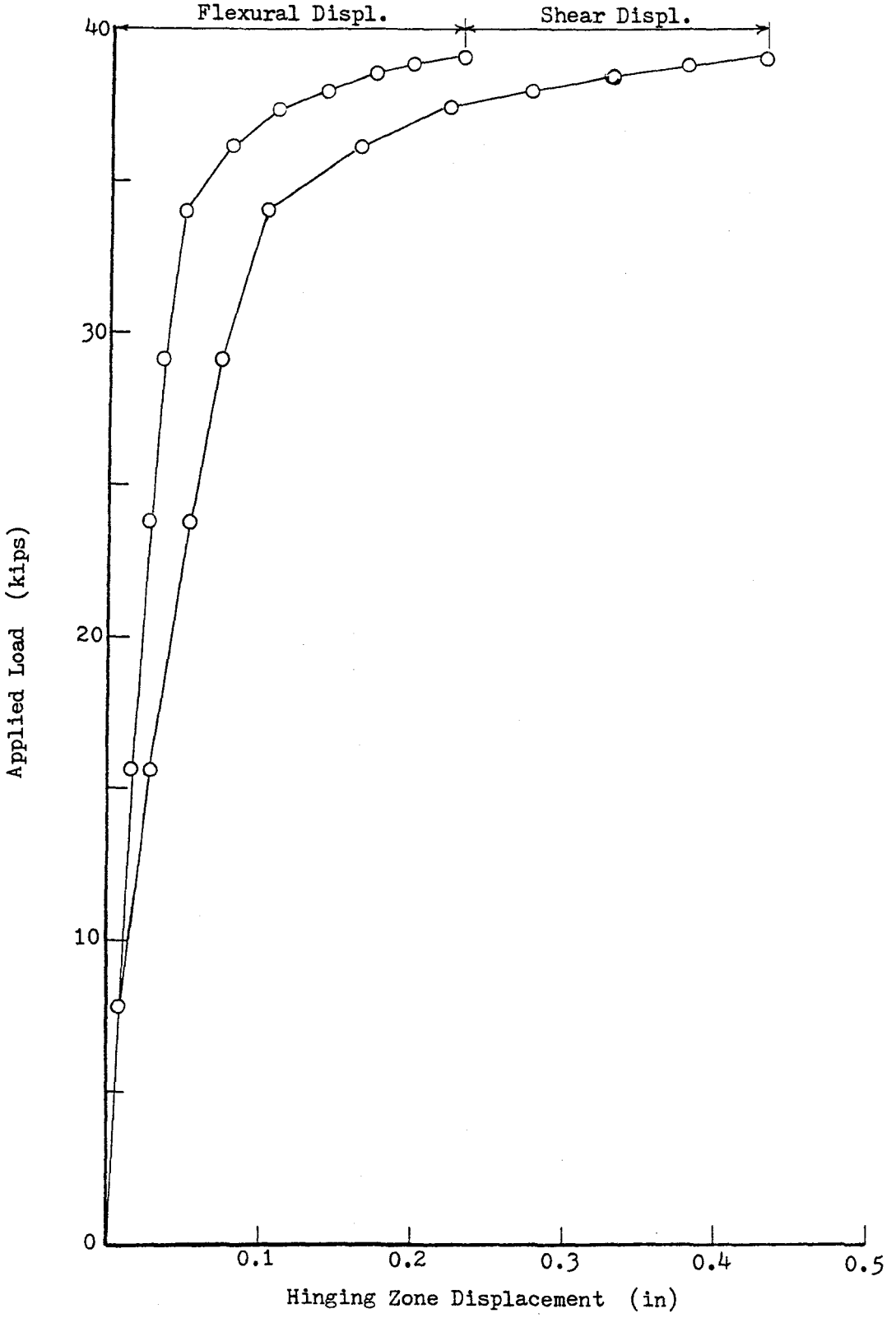

Fig. 4.4(c) Flexural and Shear Displacement in the Hinging Zone, Specimen S3-2

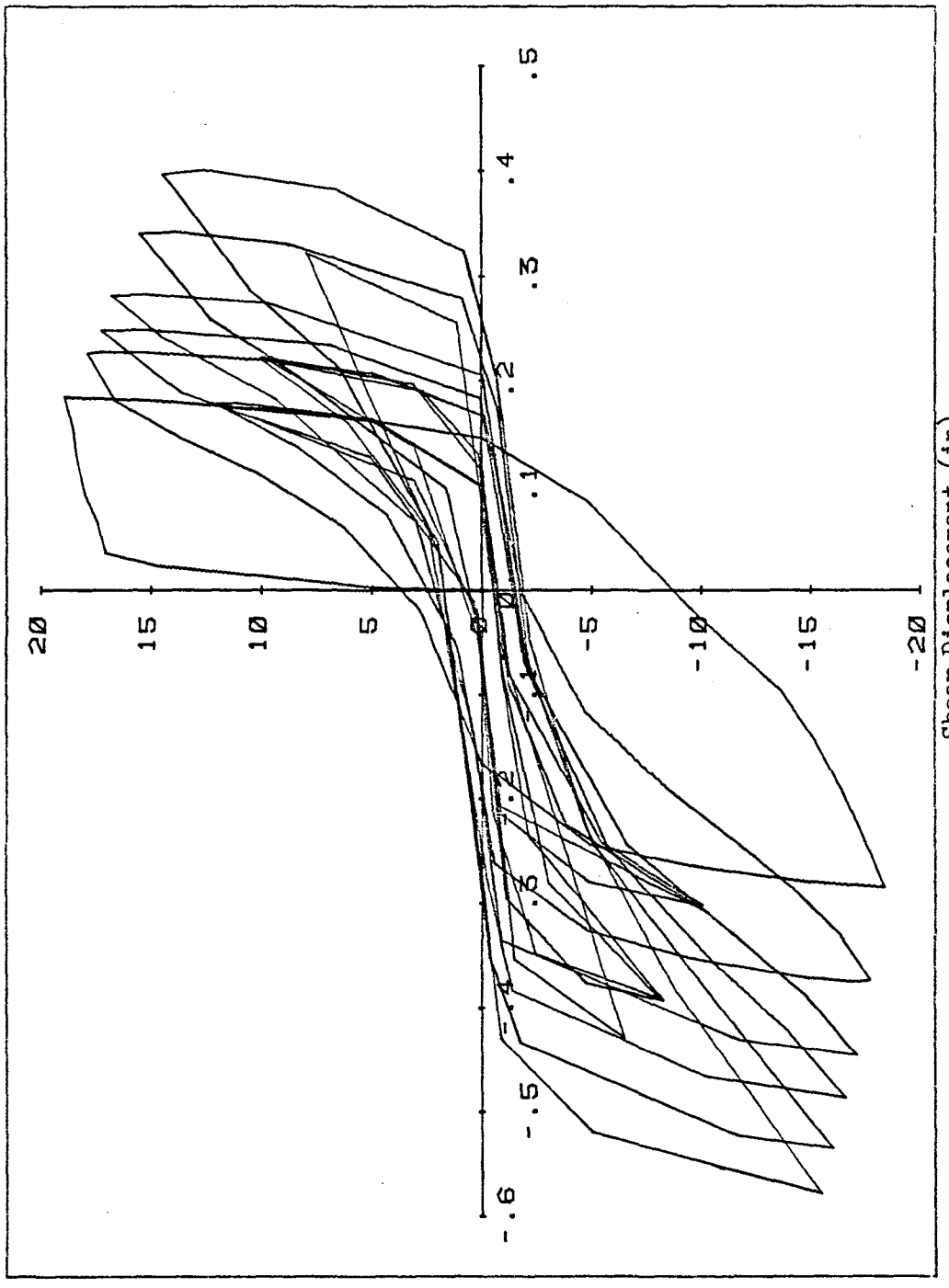

Fig. 4.5 Relationship Between Applied Load and Shear Displacement in the Hinging Zone, Specimen S1-4

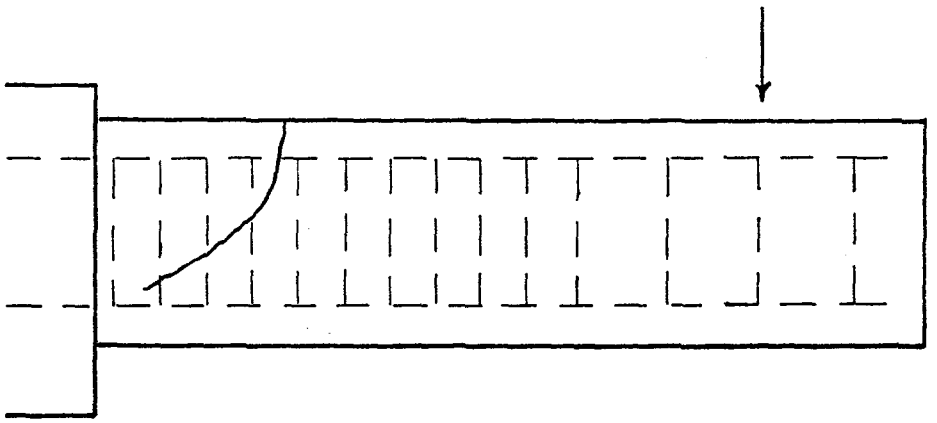

(a) Idealized Flexural-Shear Crack

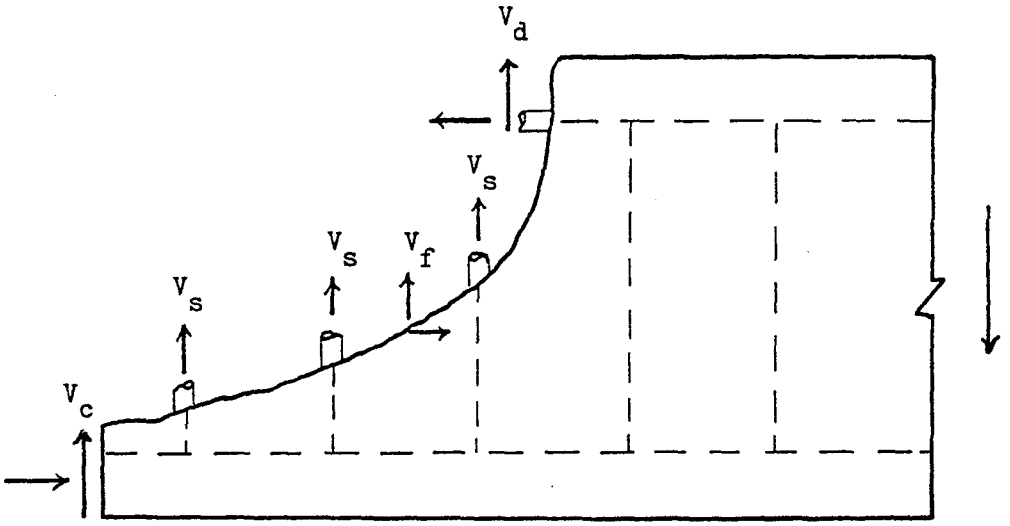

(b) Shear-Carrying Mechanism

Fig. 4.6 Shear-Carrying Mechanism of Test Specimen

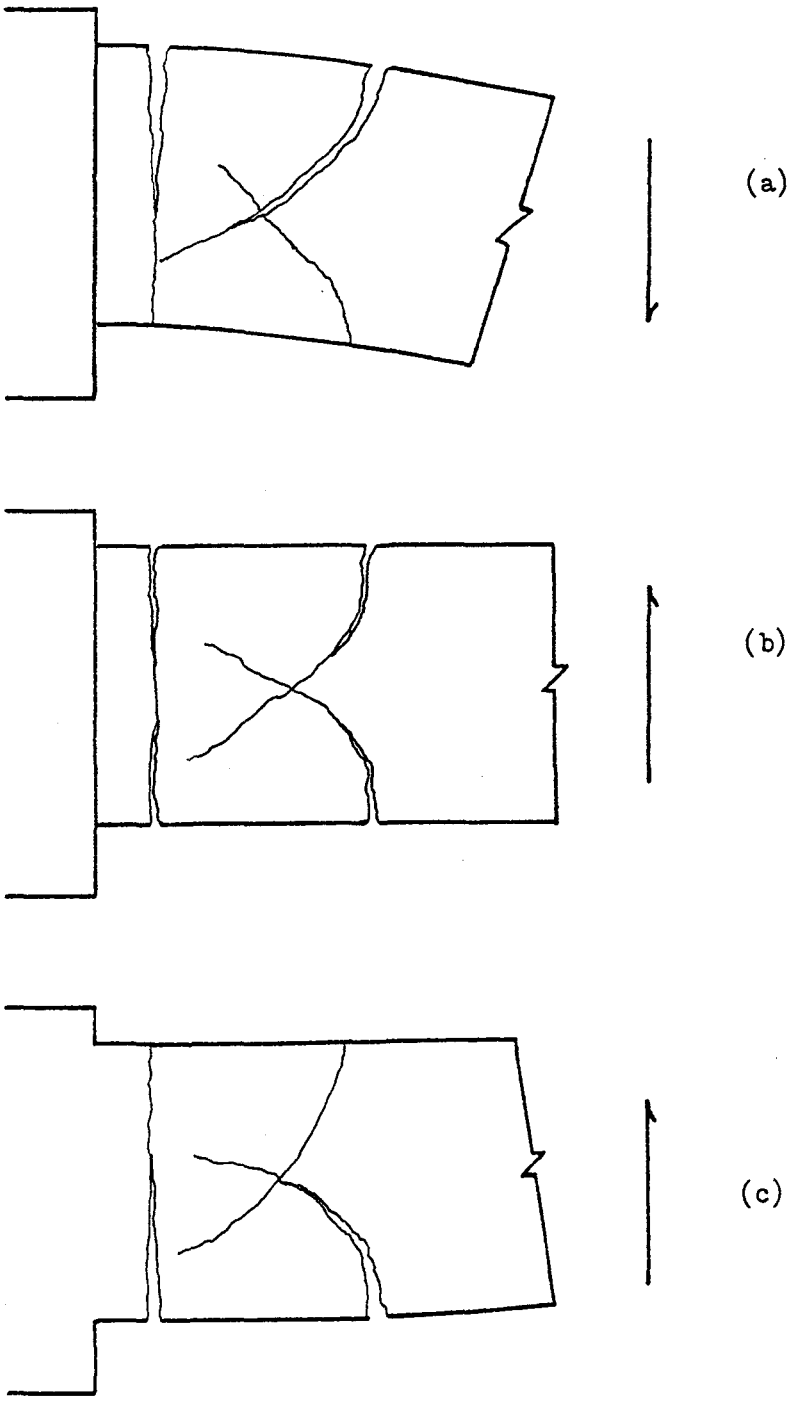

Fig. 4.7 Assumed Hinging Zone Behavior Under Loading Reversal

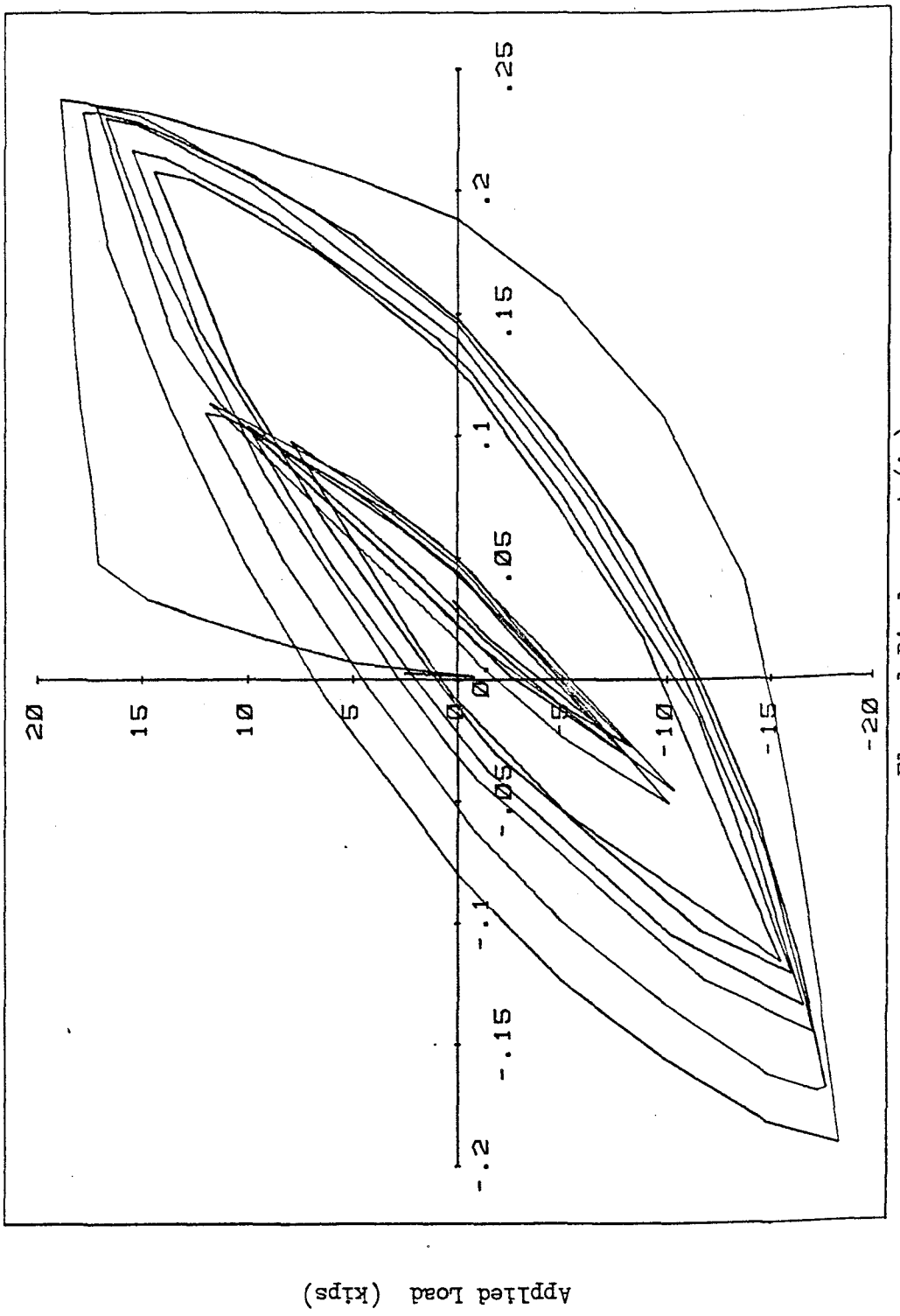

Fig. 4.8 Relationship Between Applied Load and Flexural Displacement of the Hinging Zone, Specimen S1-4

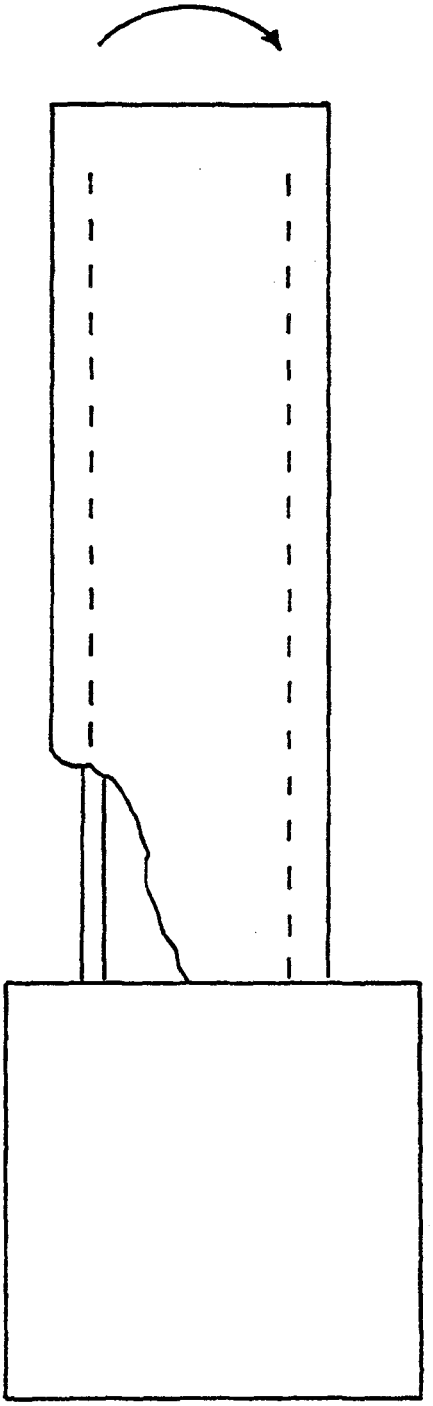

Fig. 4.9 Assumed Flexure-Resisting Mechanism

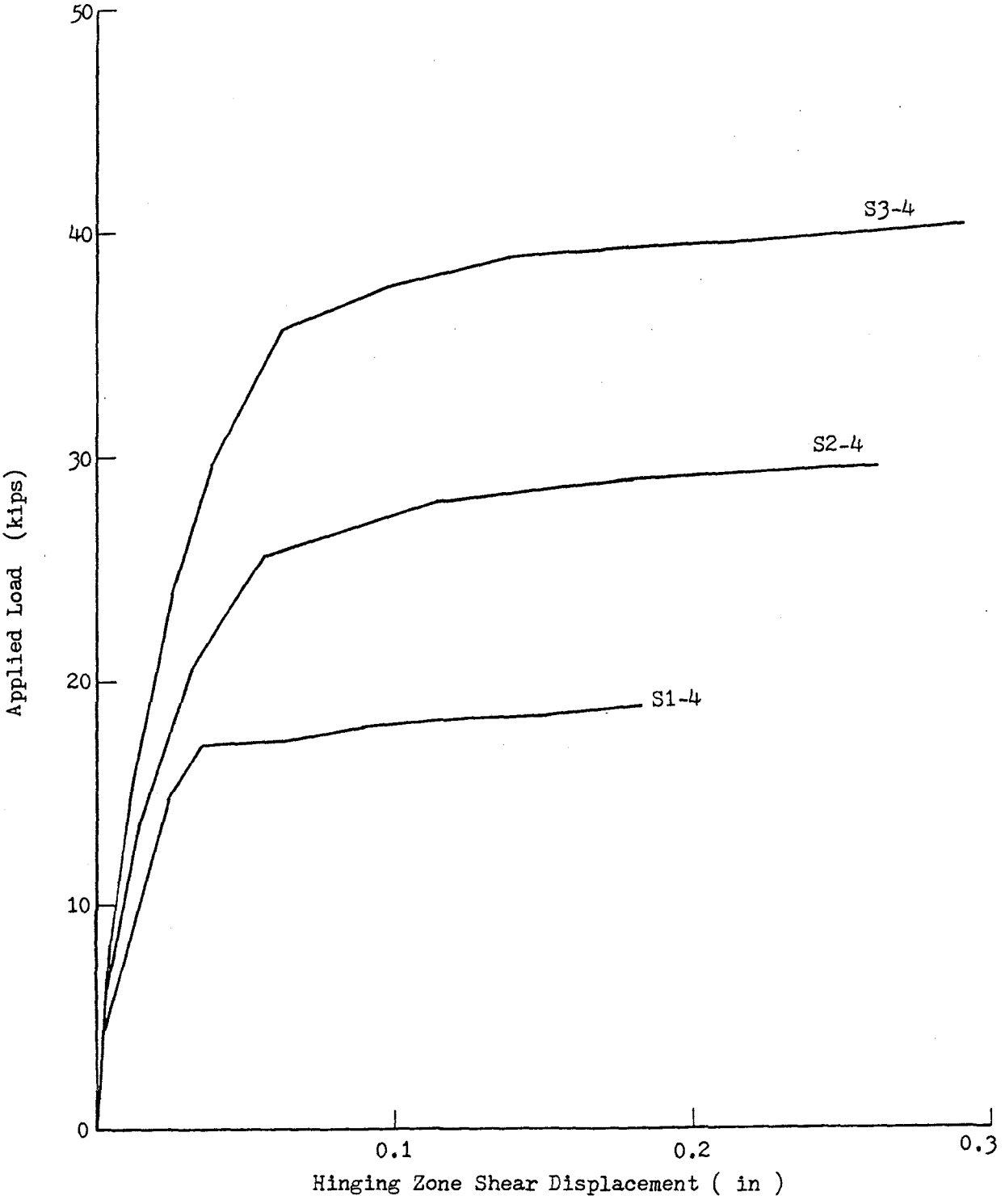

Fig. 4.10 Applied Load vs. Shear Displacement of the Hinging Zone, Specimen S1-4, S2-4, S3-4

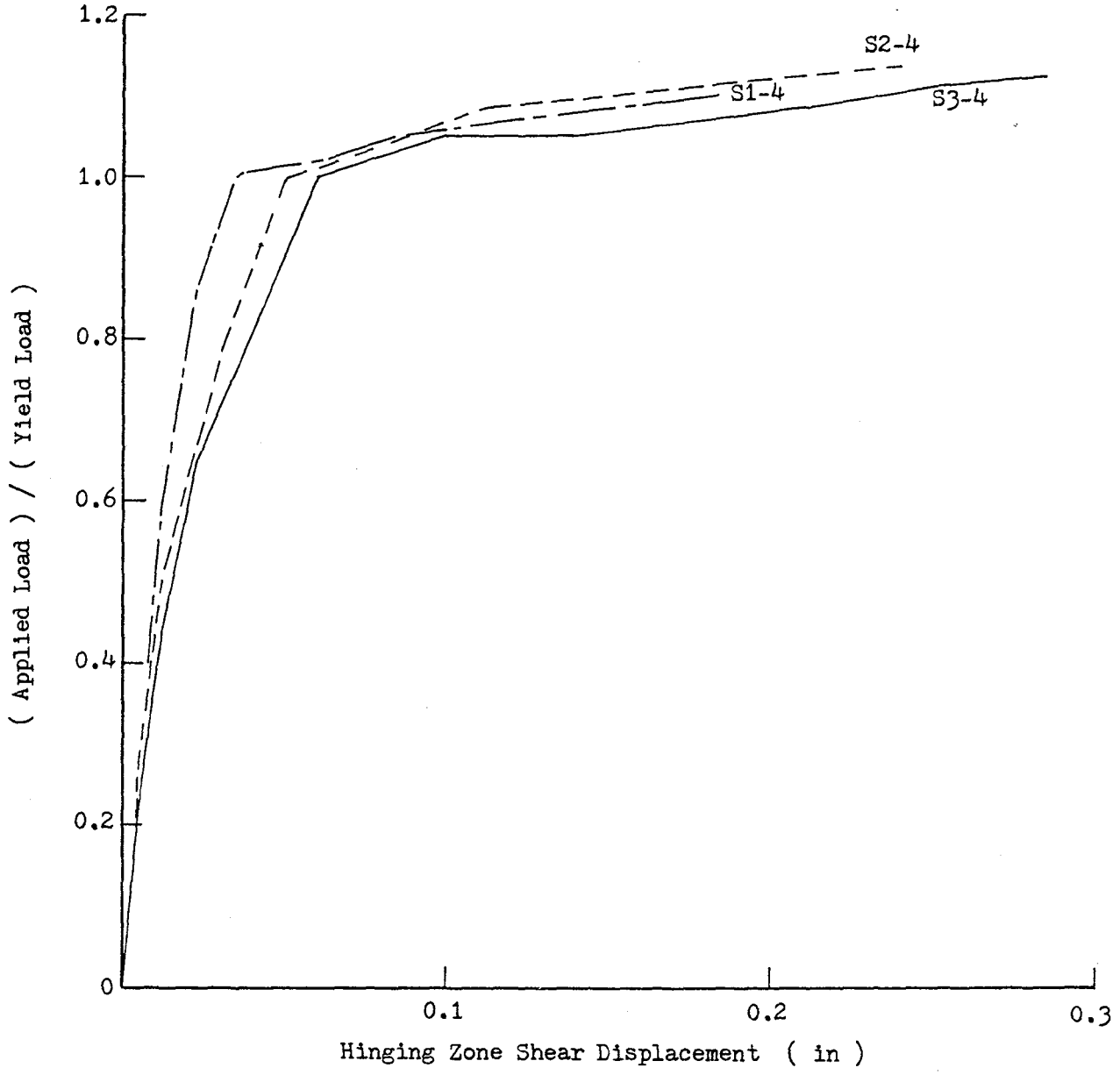

Fig. 4.11 Comparison of Hinging Zone Shear Displacement, Specimen S1-4, S2-4, S3-4

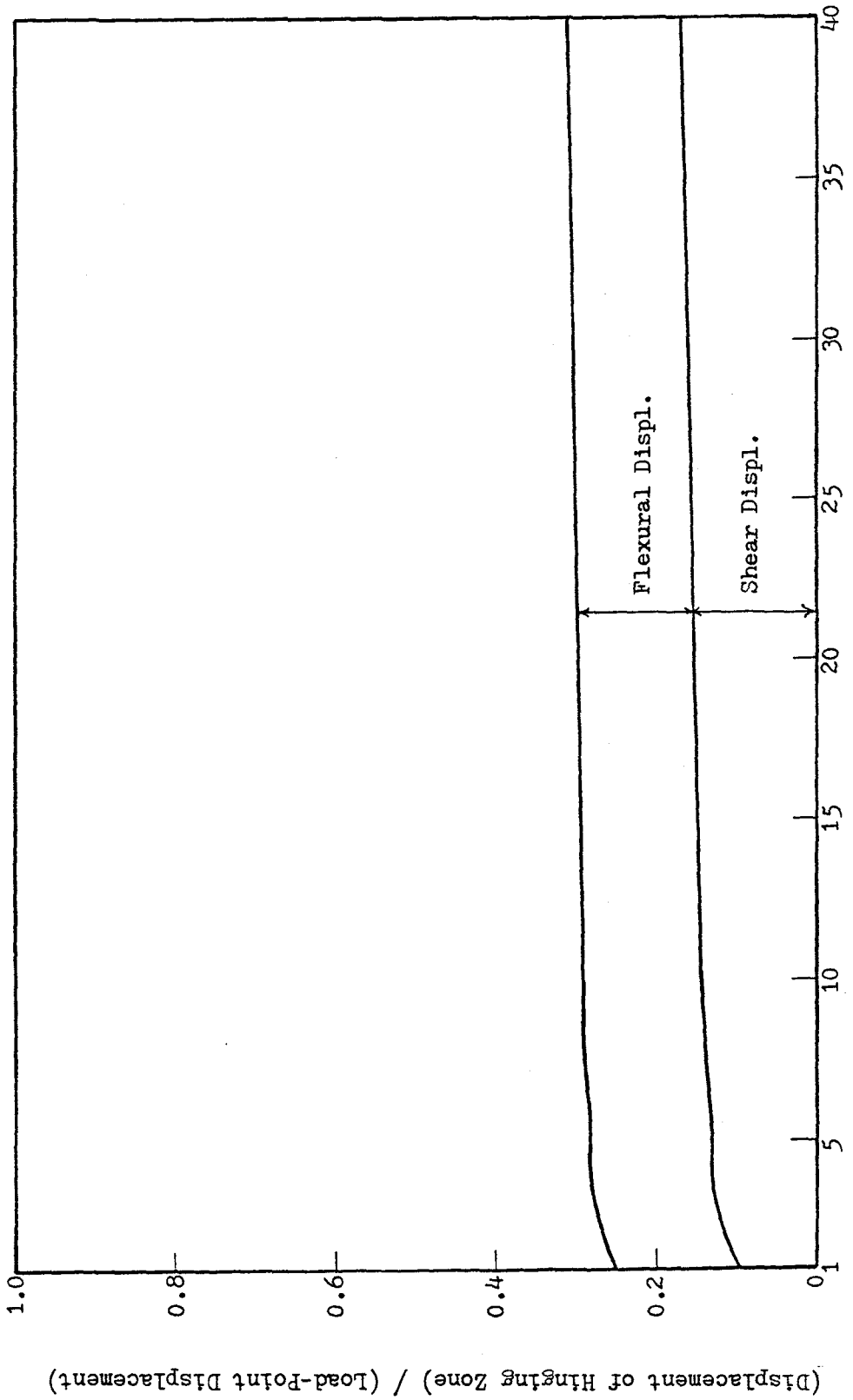

Fig. 4.12 Displacement Components vs. Number of Load Cycles, Specimen S1-1

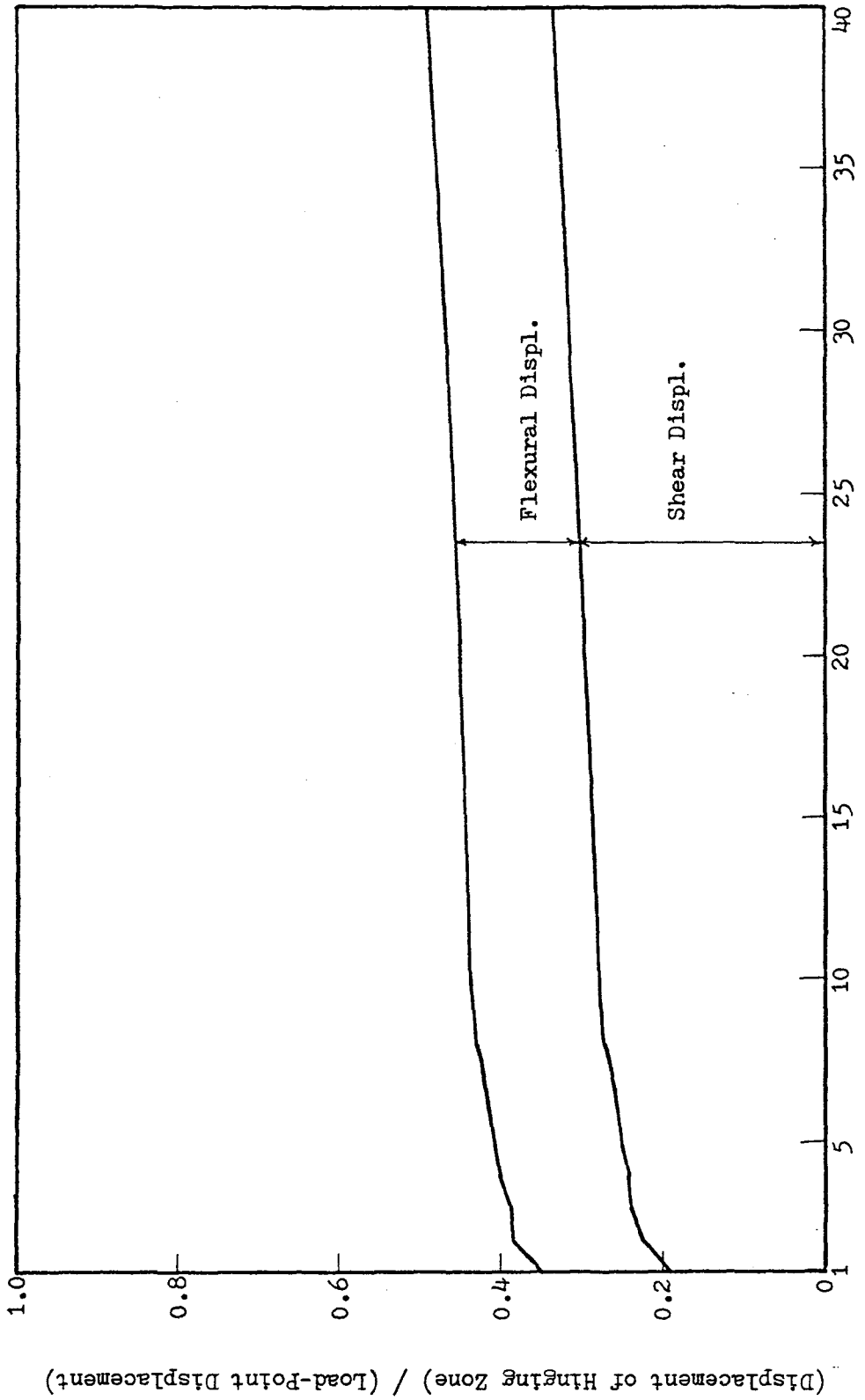

Fig. 4.13 Displacement Components vs. Number of Load Cycles, Specimen S2-1

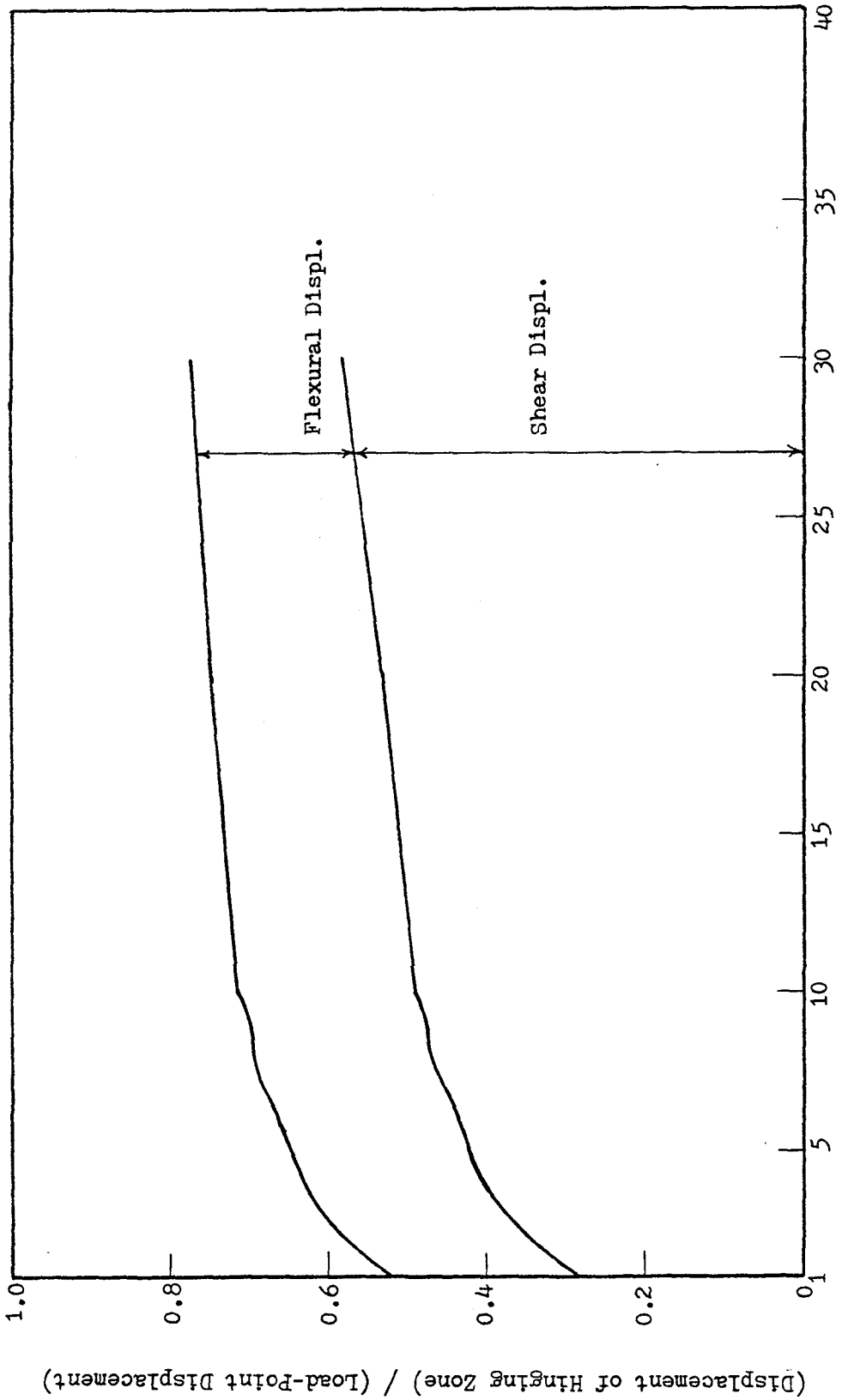

Fig. 4.14 Displacement Components vs. Number of Load Cycles, Specimen S3-1

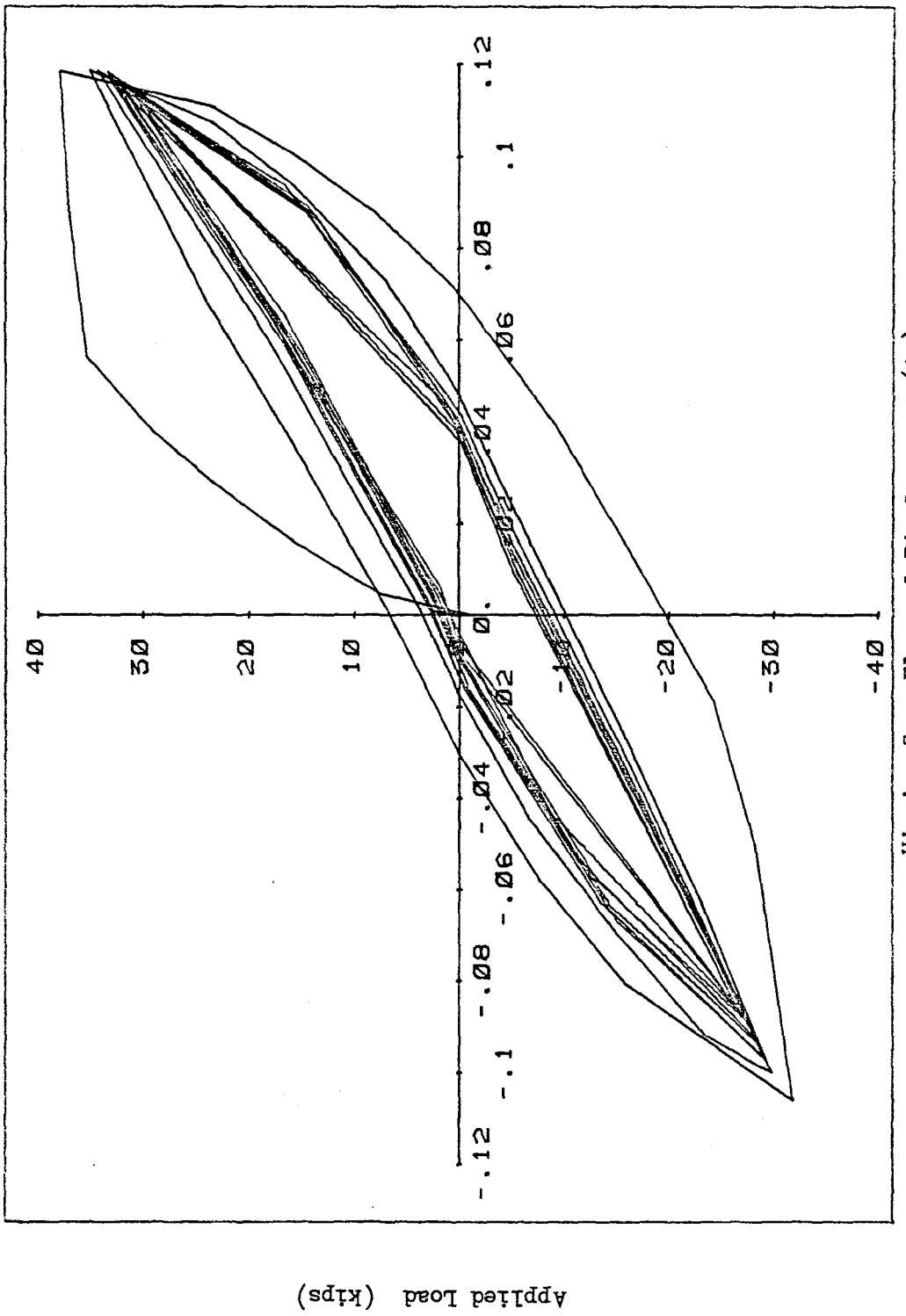

Fig. 4.15(a) Applied Load vs. Flexural Displacement of the Hinging Zone, Specimen S3-1

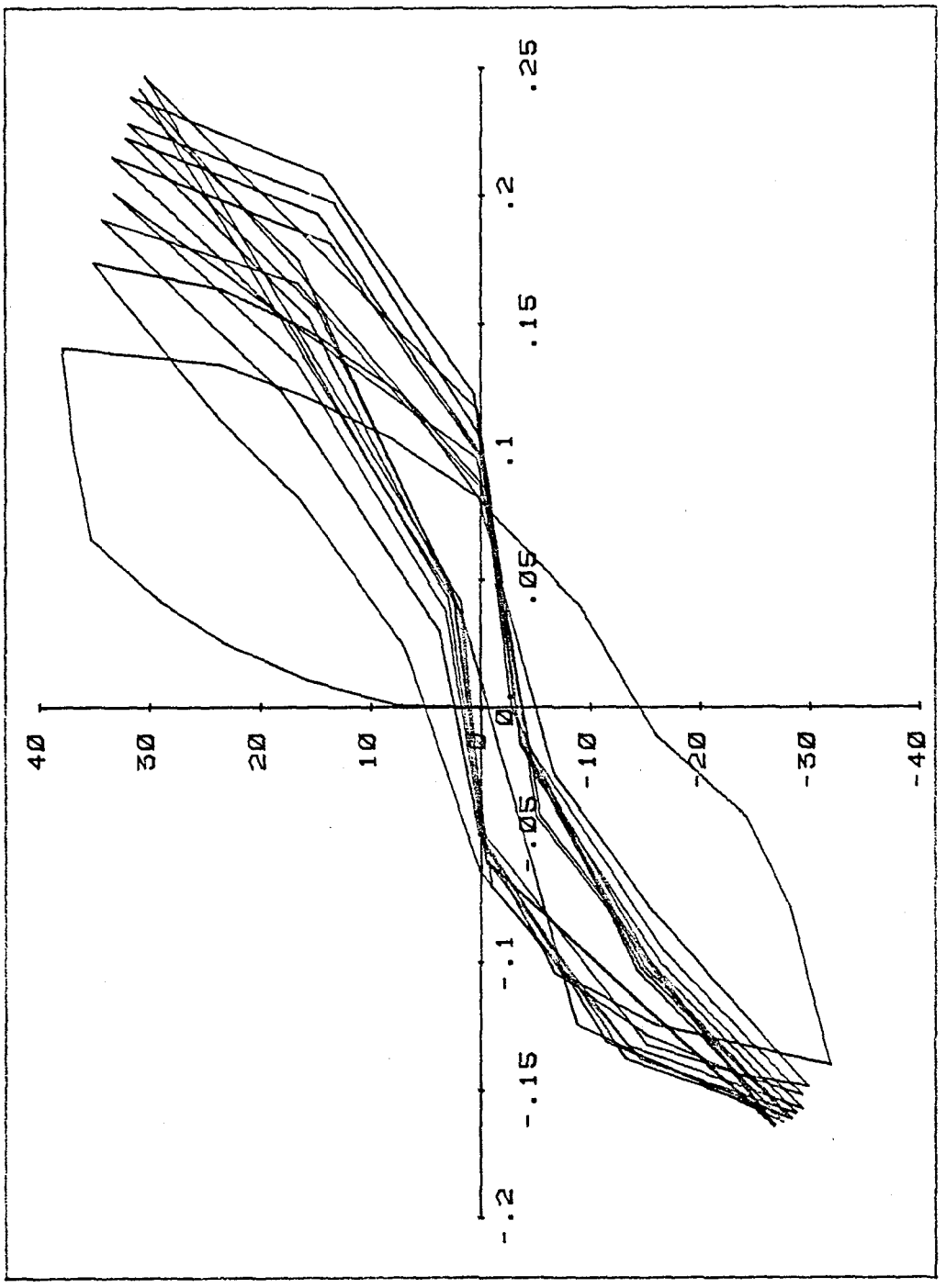

Fig. 4.15(b) Applied Load vs. Shear Displacement of the Hinging Zone, Specimen S3-1

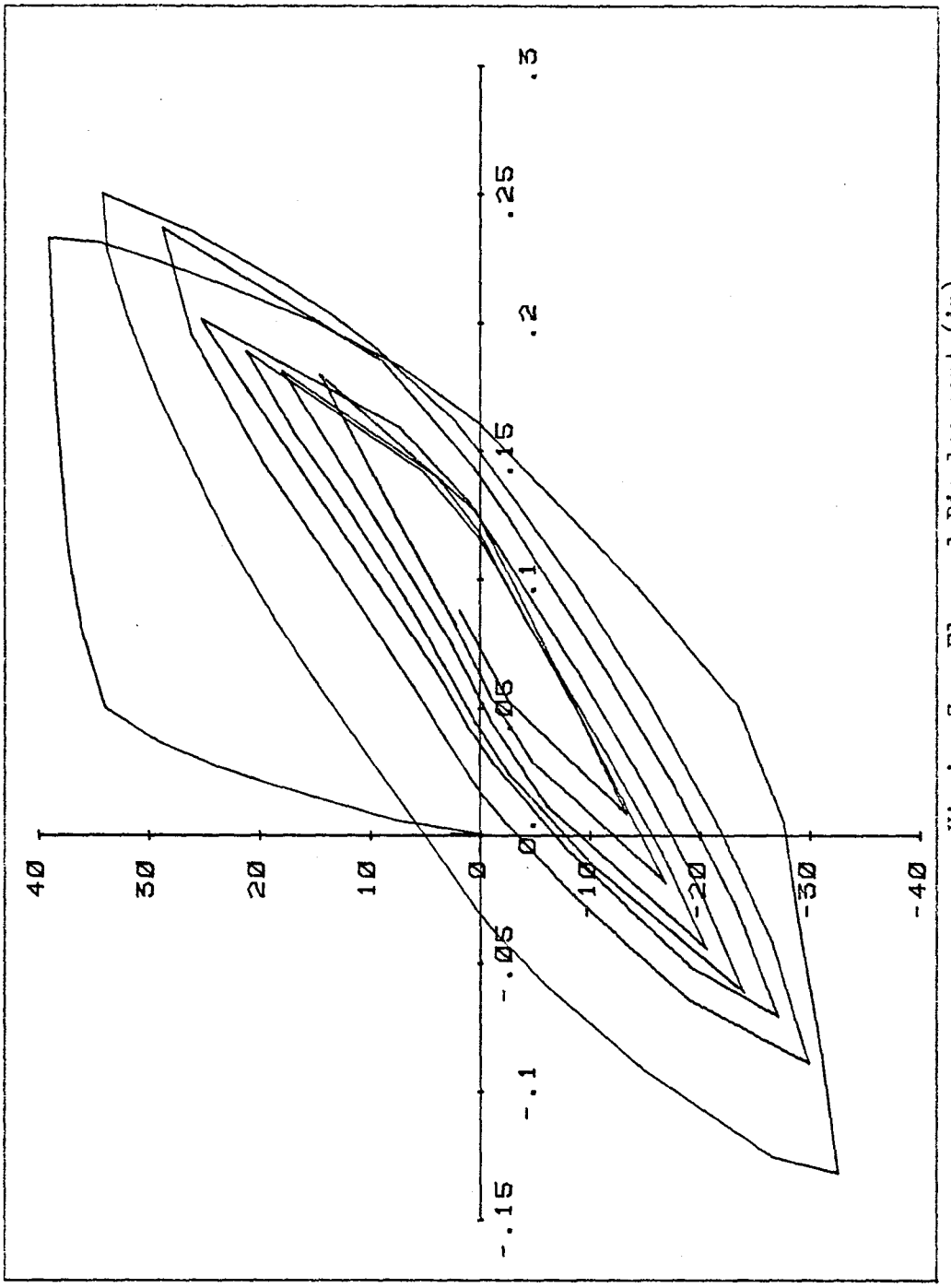

Fig. 4.16(a) Applied Load vs. Flexural Displacement of the Hinging Zone, Specimen S3-2

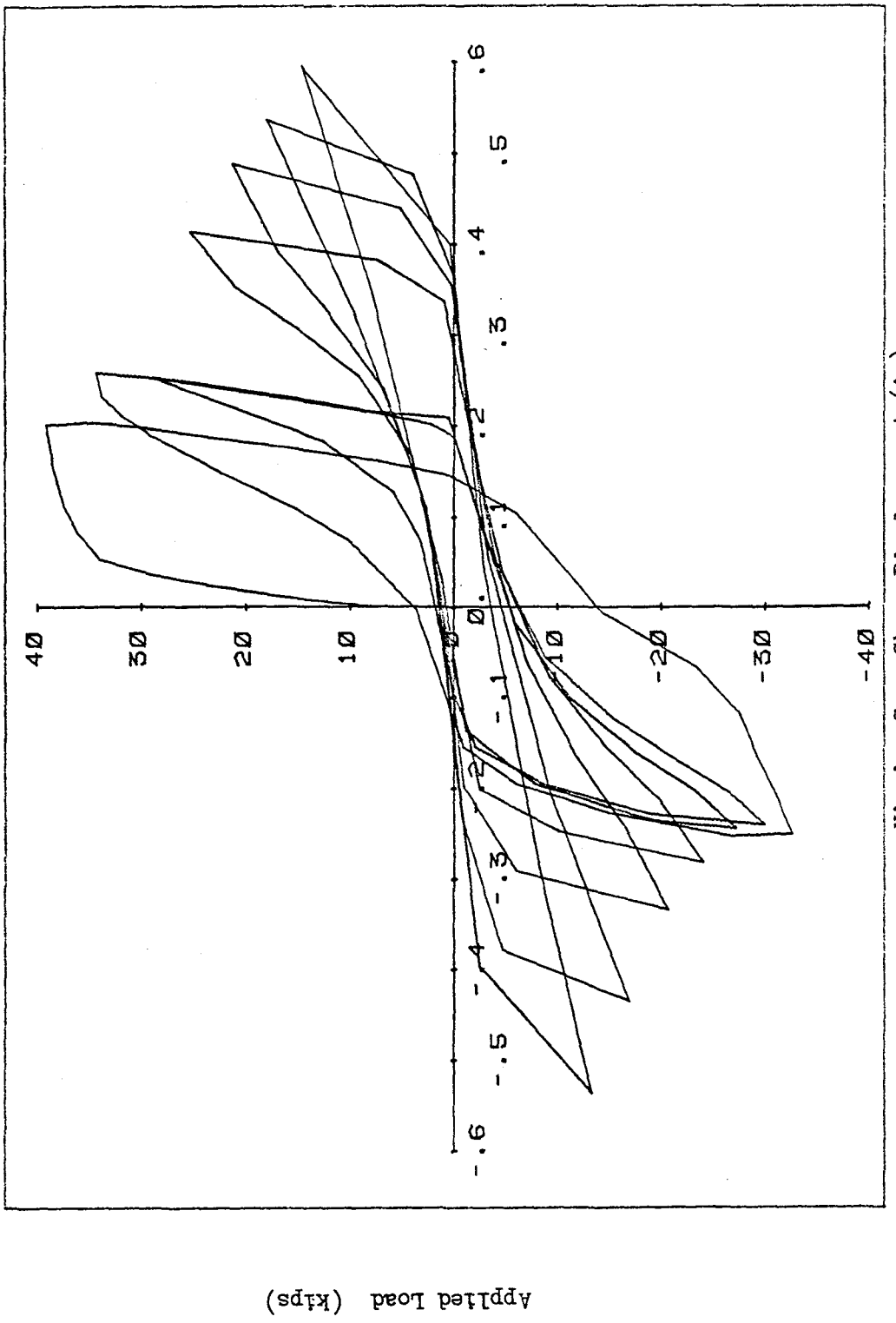

Fig. 4.16(b) Applied Load vs. Shear Displacement of the Hinging Zone, Specimen S3-2

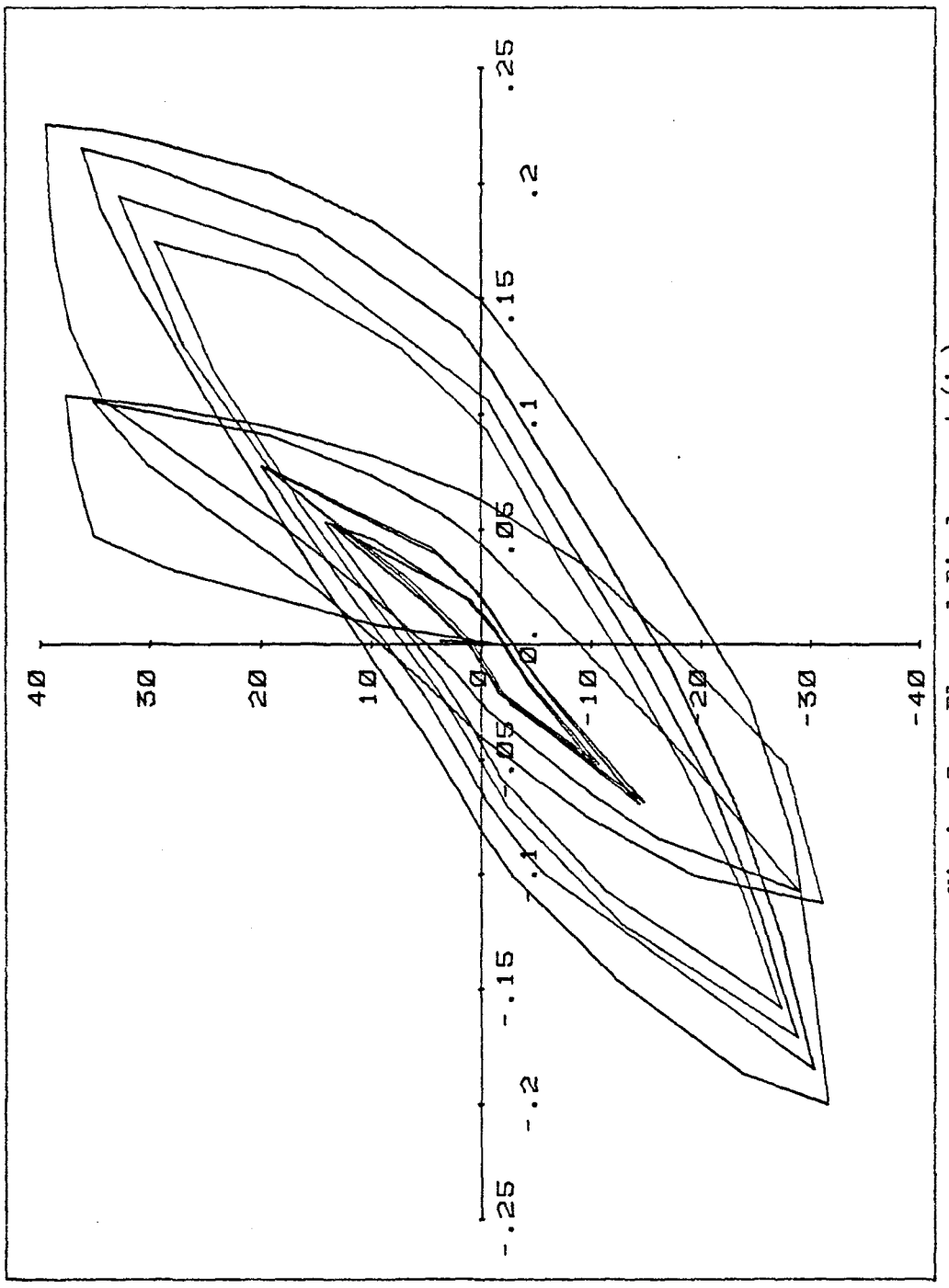

Fig. 4.17(a) Applied Load vs. Flexural Displacement of the Hinging Zone, Specimen S3-3

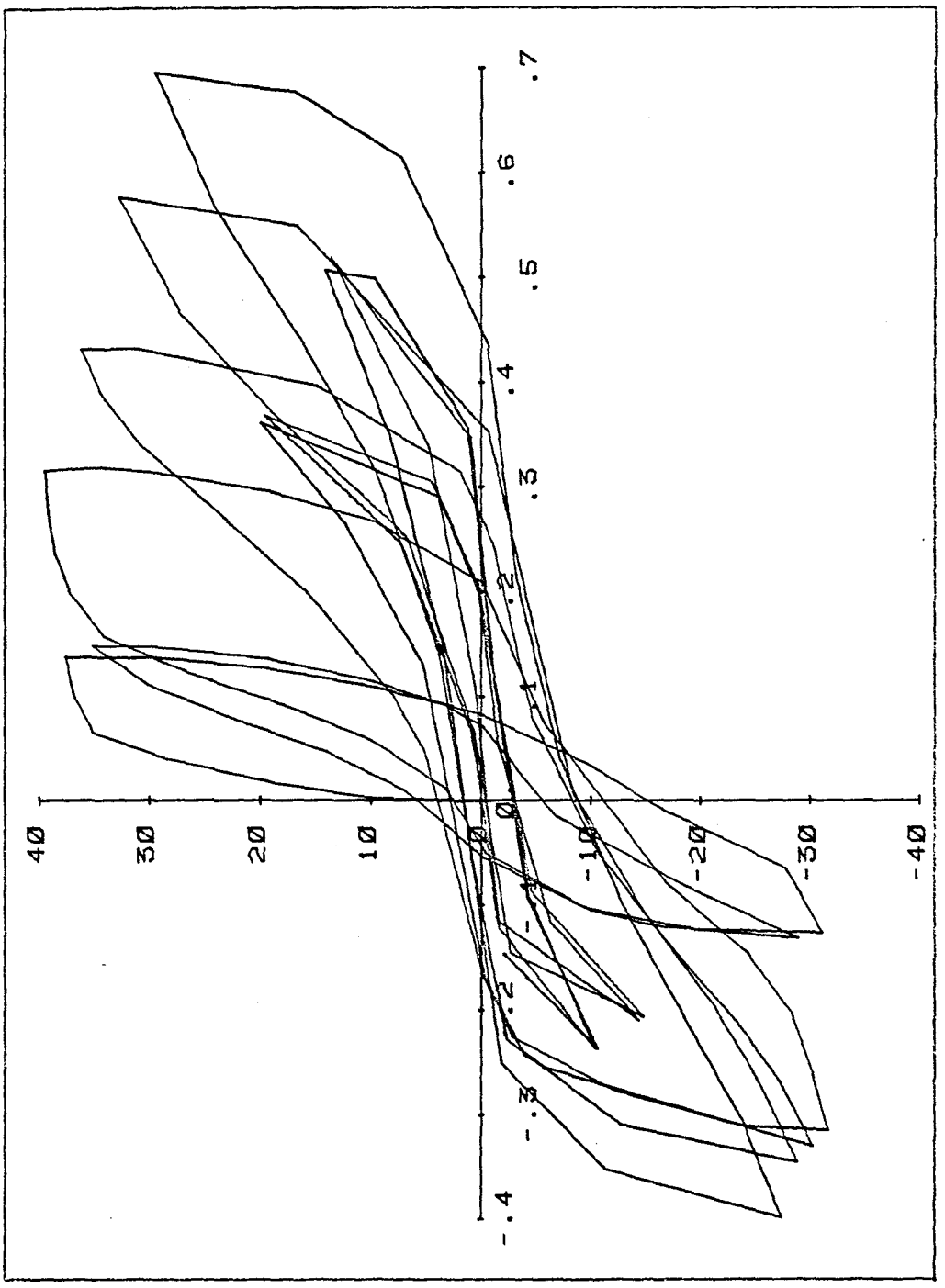

Fig. 4.17(b) Applied Load vs. Shear Displacement of the Hinging Zone, Specimen S3-3

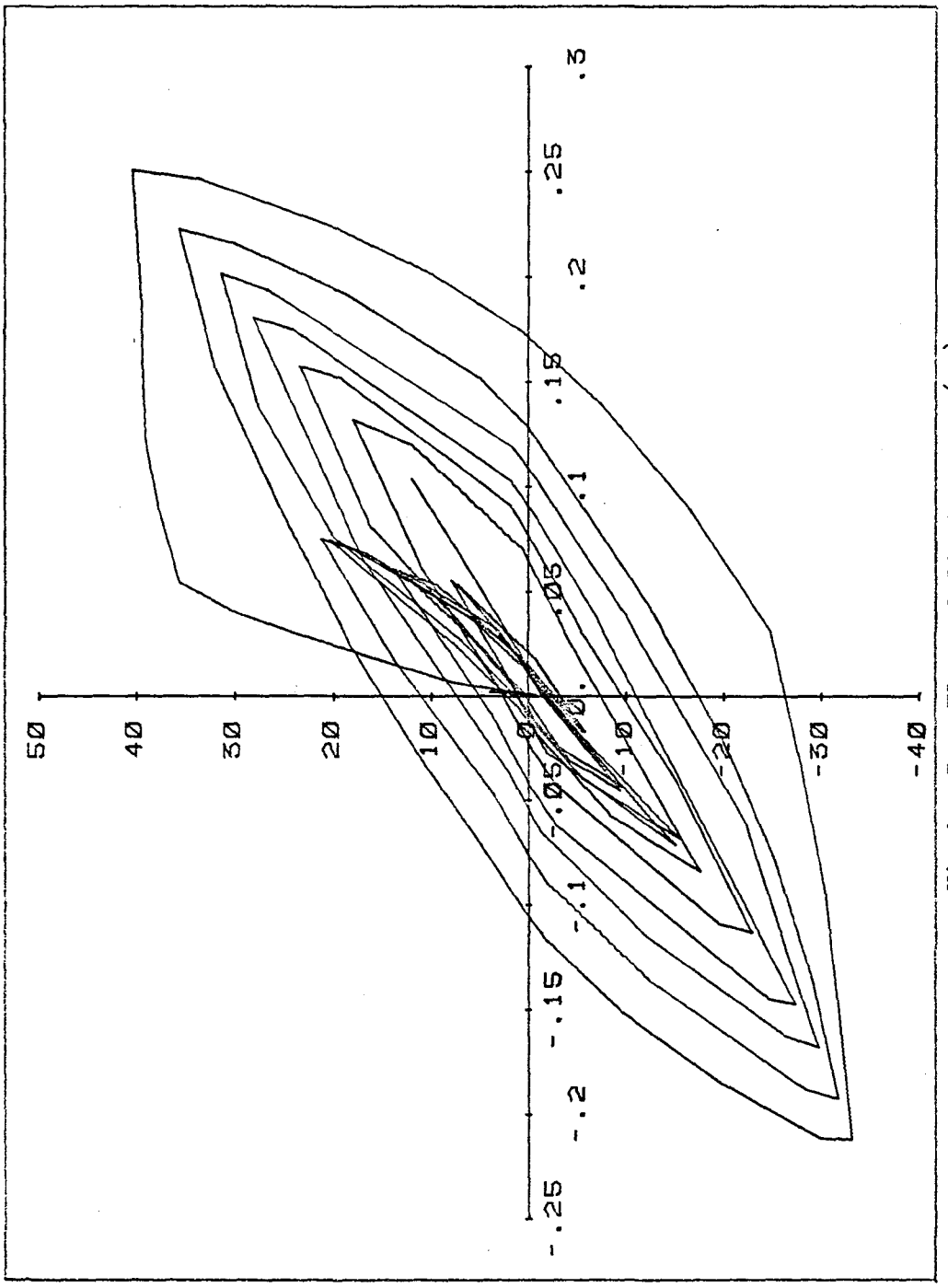

Fig. 4.18(a) Applied Load vs. Flexural Displacement of the Hinging Zone, Specimen S3-4

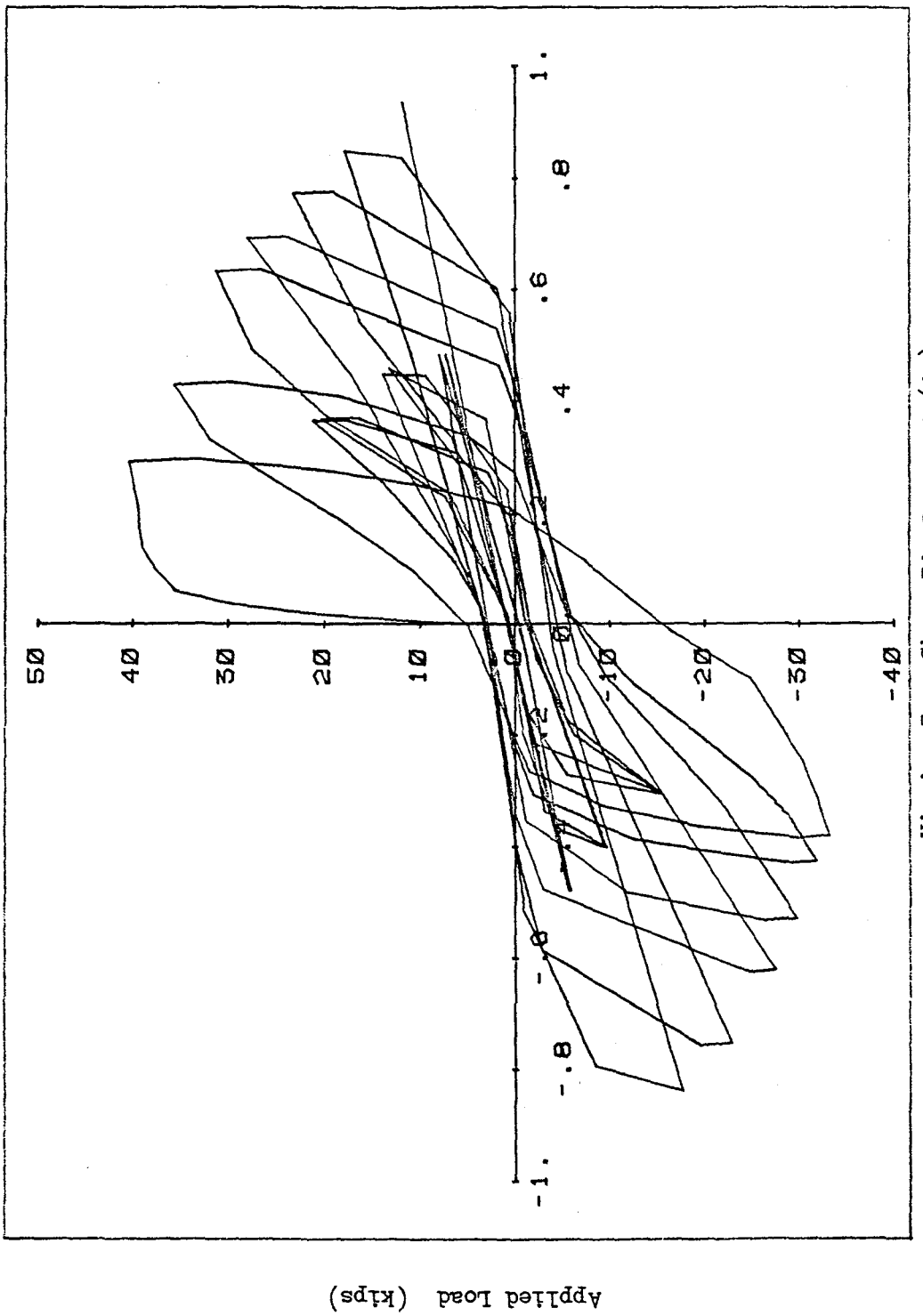

Fig. 4.18(b) Applied Load vs. Shear Displacement of the Hinging Zone, Specimen S3-4

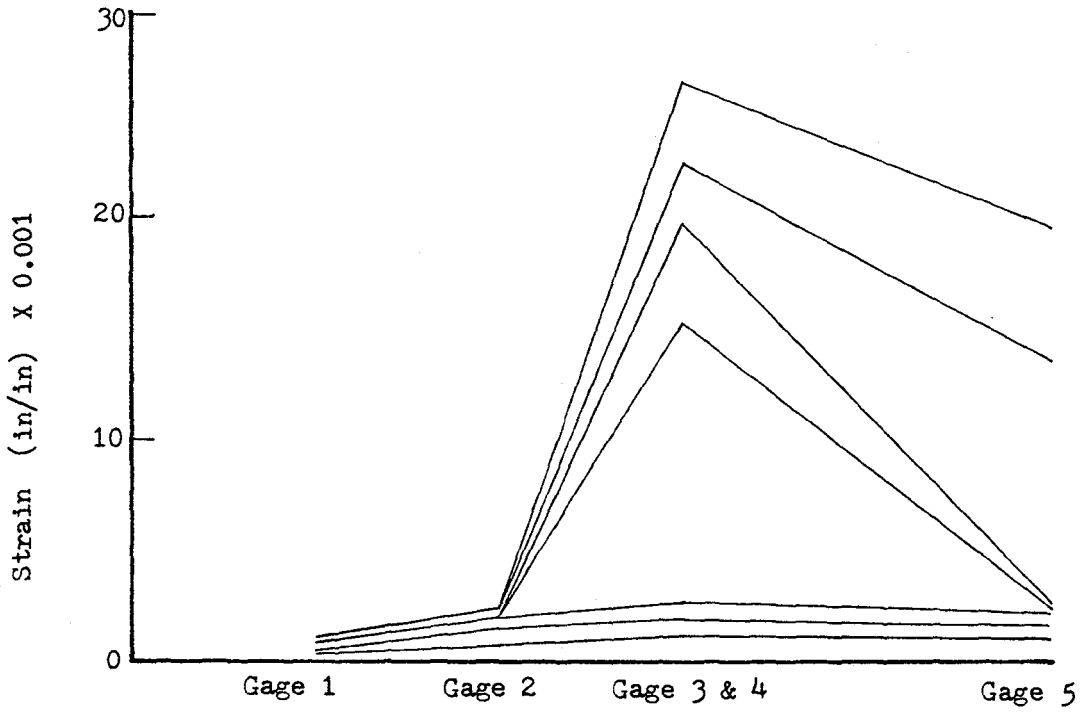

(a) Strain Variation

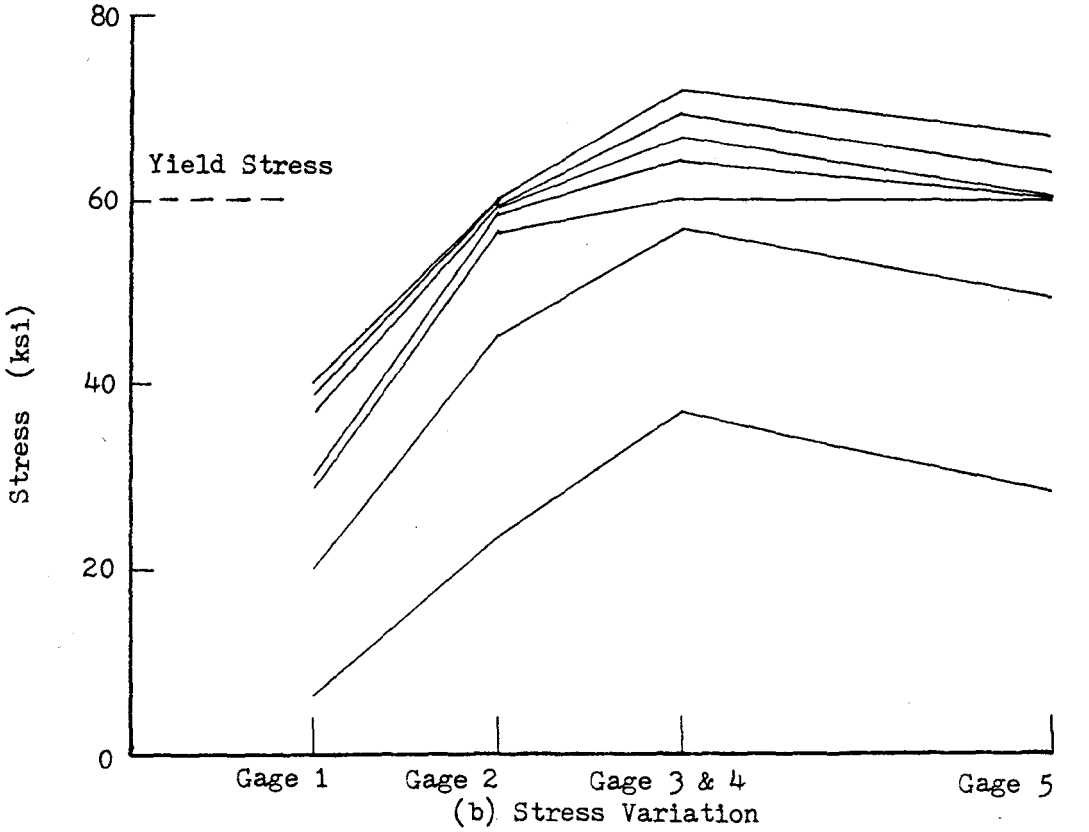

(b) Stress Variation

Fig. 5.1 Strain and Stress Variation Along Top Longitudinal Reinforcement in the Enlarged End Block, Specimen S1-4

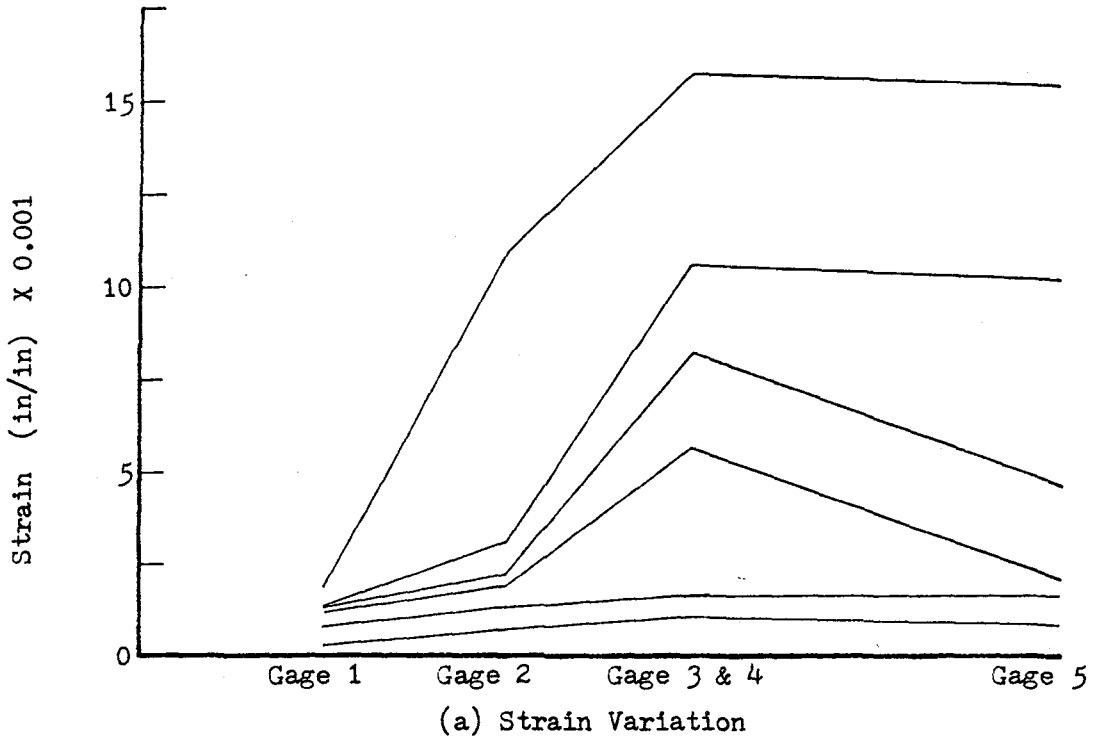

(a) Strain Variation

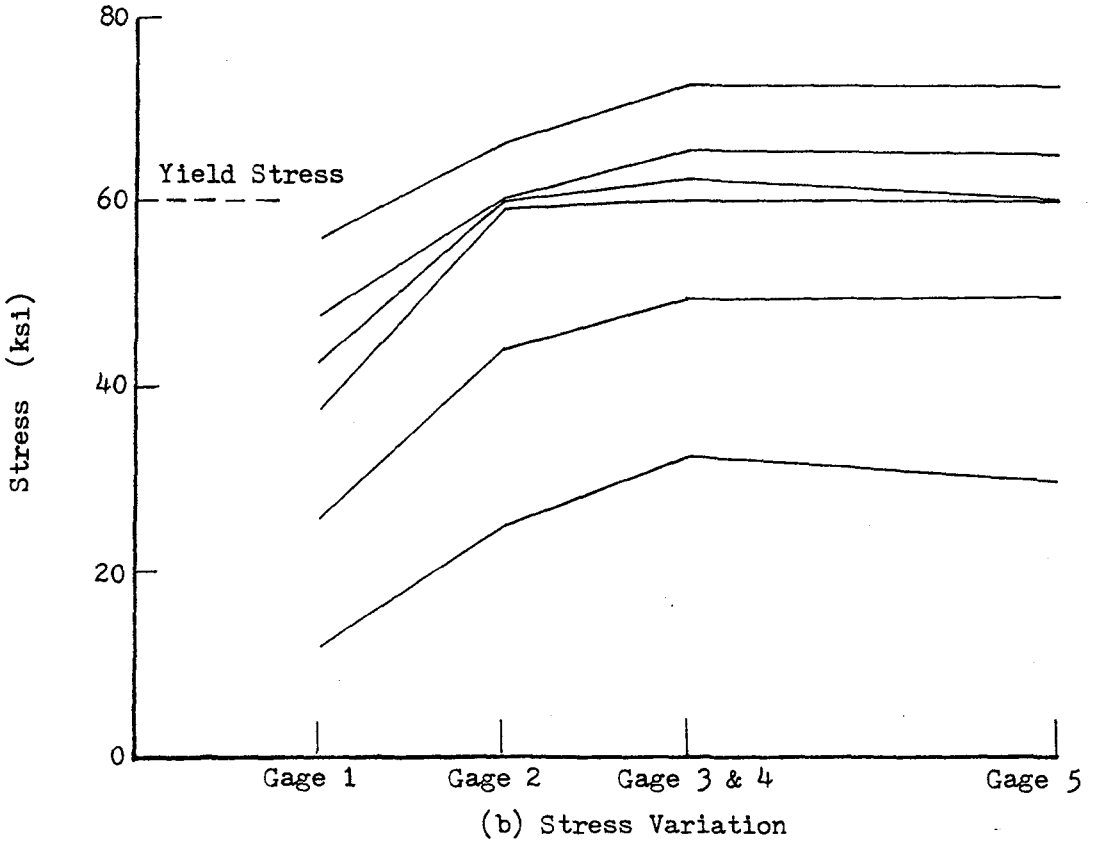

(b) Stress Variation

Fig. 5.2 Strain and Stress Variation Along Top Longitudinal Reinforcement in the Enlarged End Block, Specimen S2-2

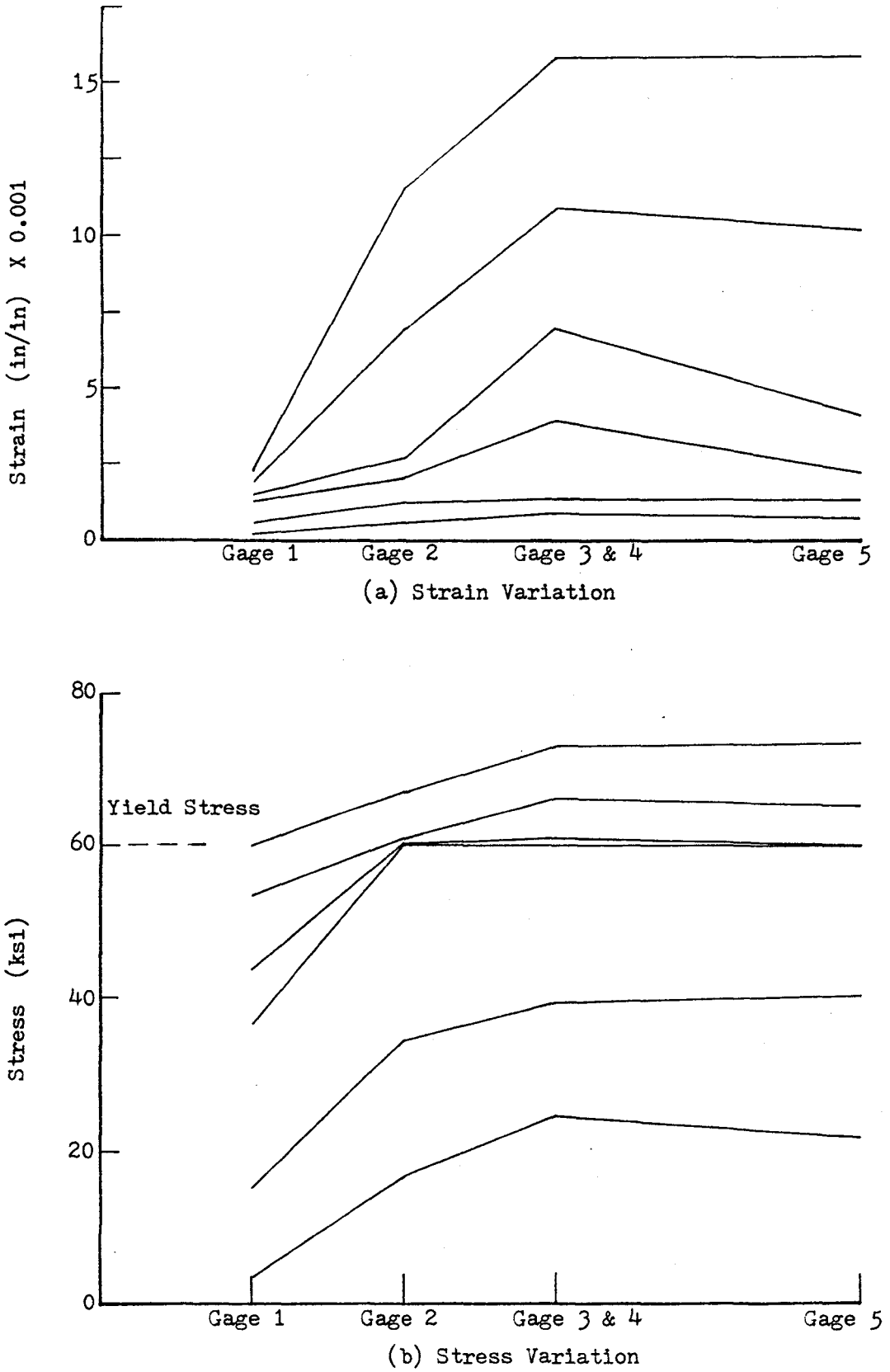

Fig. 5.3 Strain and Stress Variation Along Top Longitudinal Reinforcement in the Enlarged End Block, Specimen S3-2

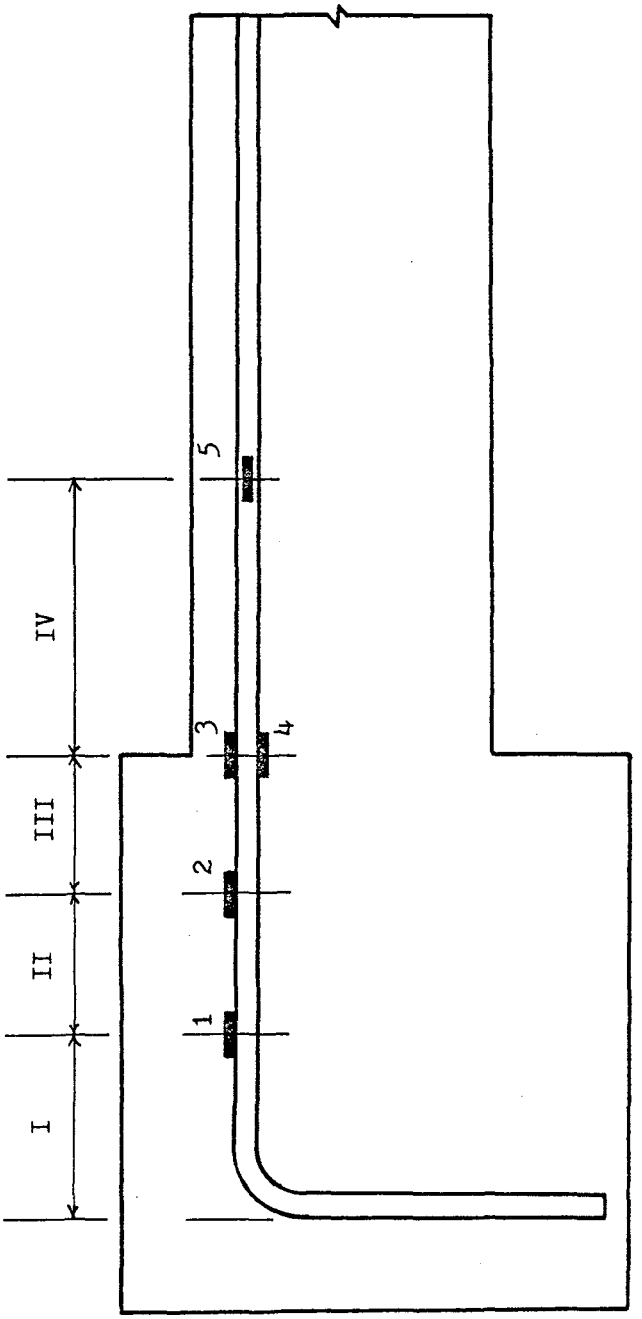

Fig. 5.4 Locations of Region I,II,III,IV

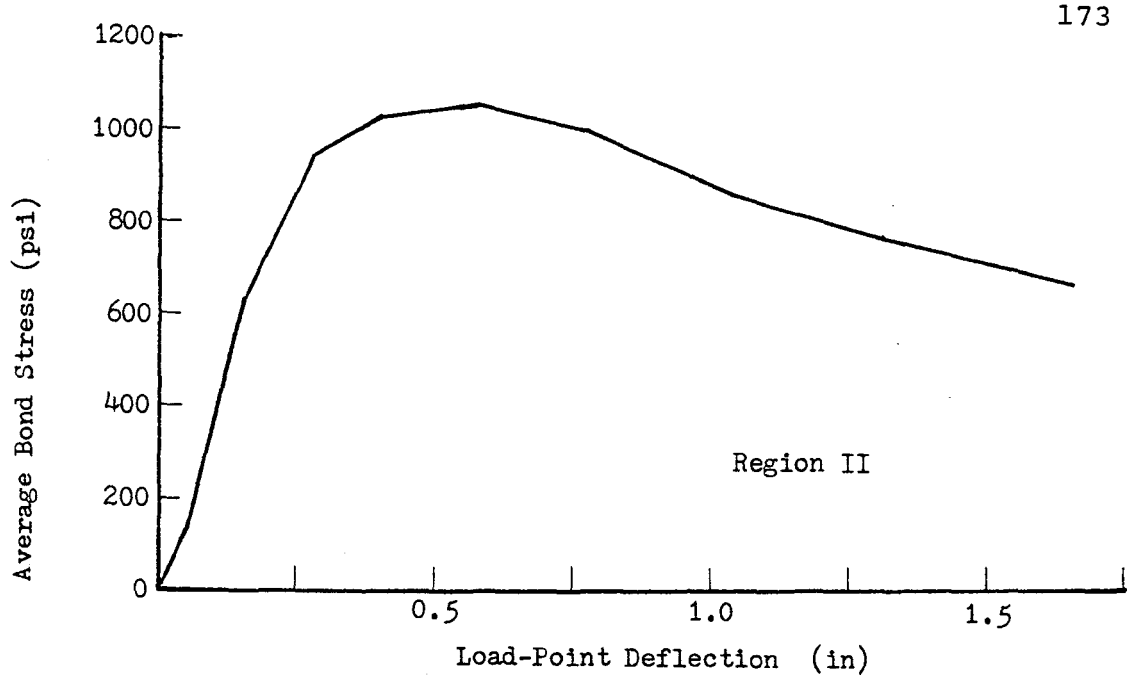

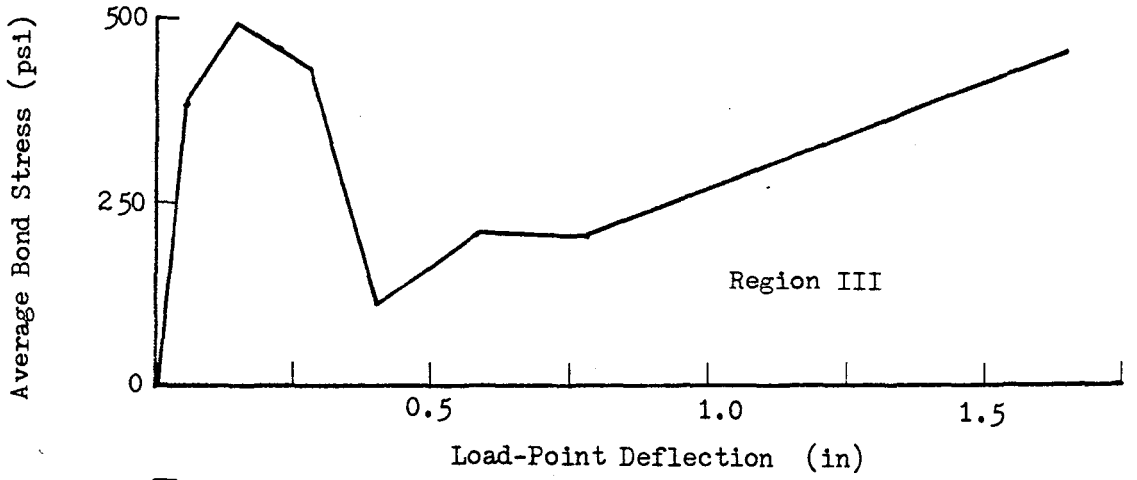

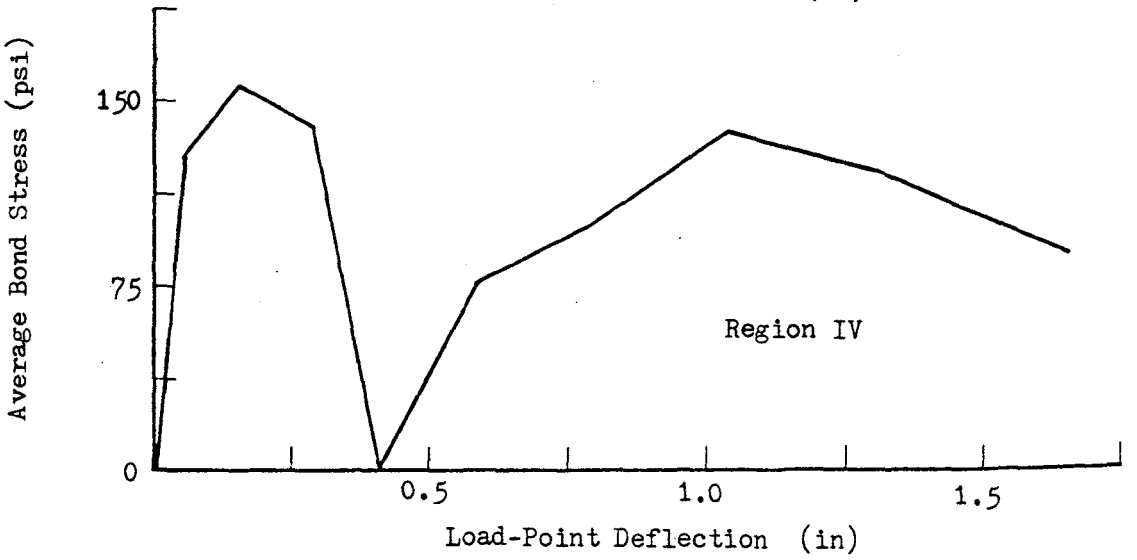

Fig. 5.5 Average Bond Stress vs. Load-Point Deflection, Specimen S1-4

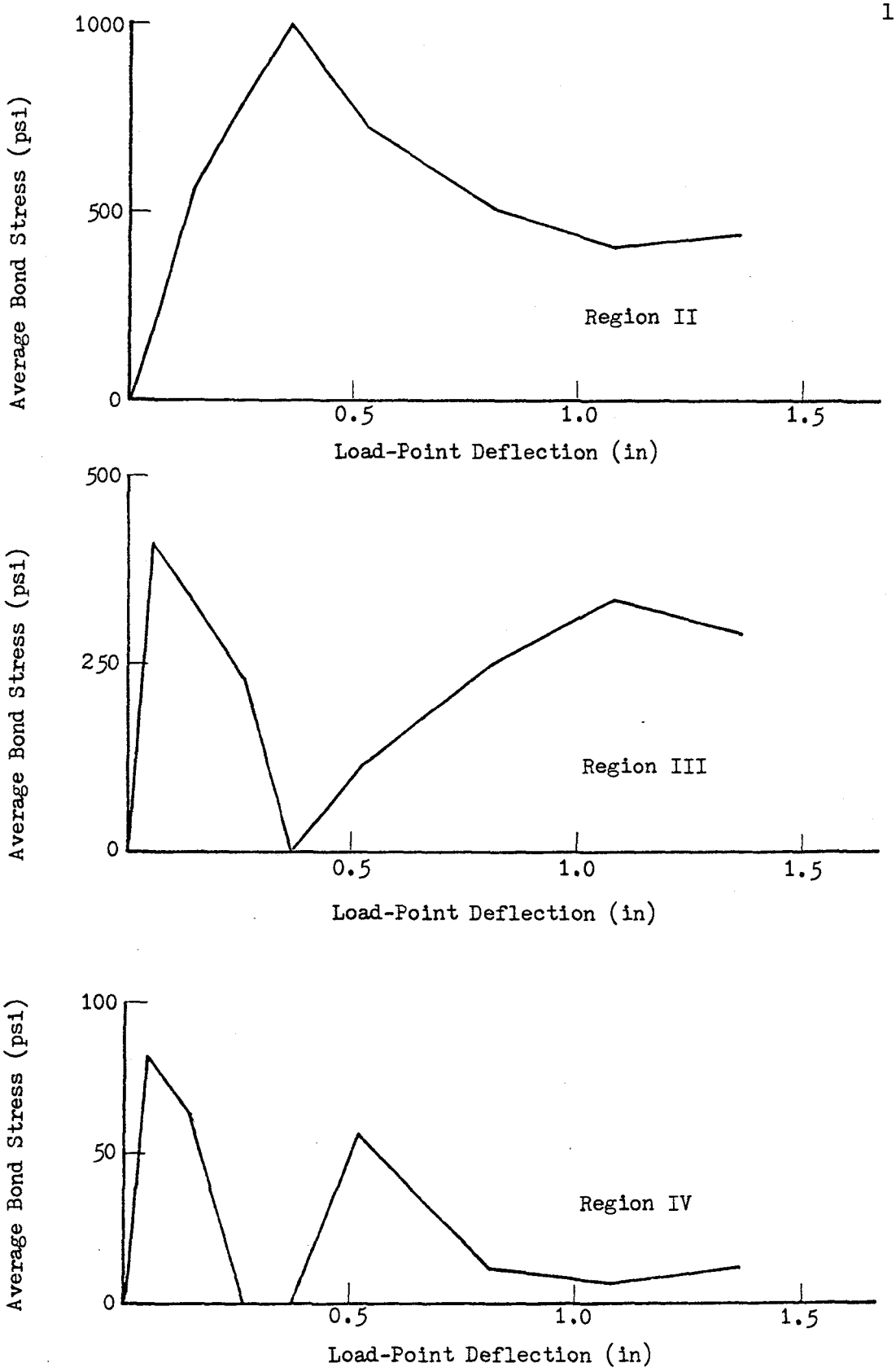

Fig. 5.6 Average Bond Stress vs. Load-Point Deflection, Specimen S2-2

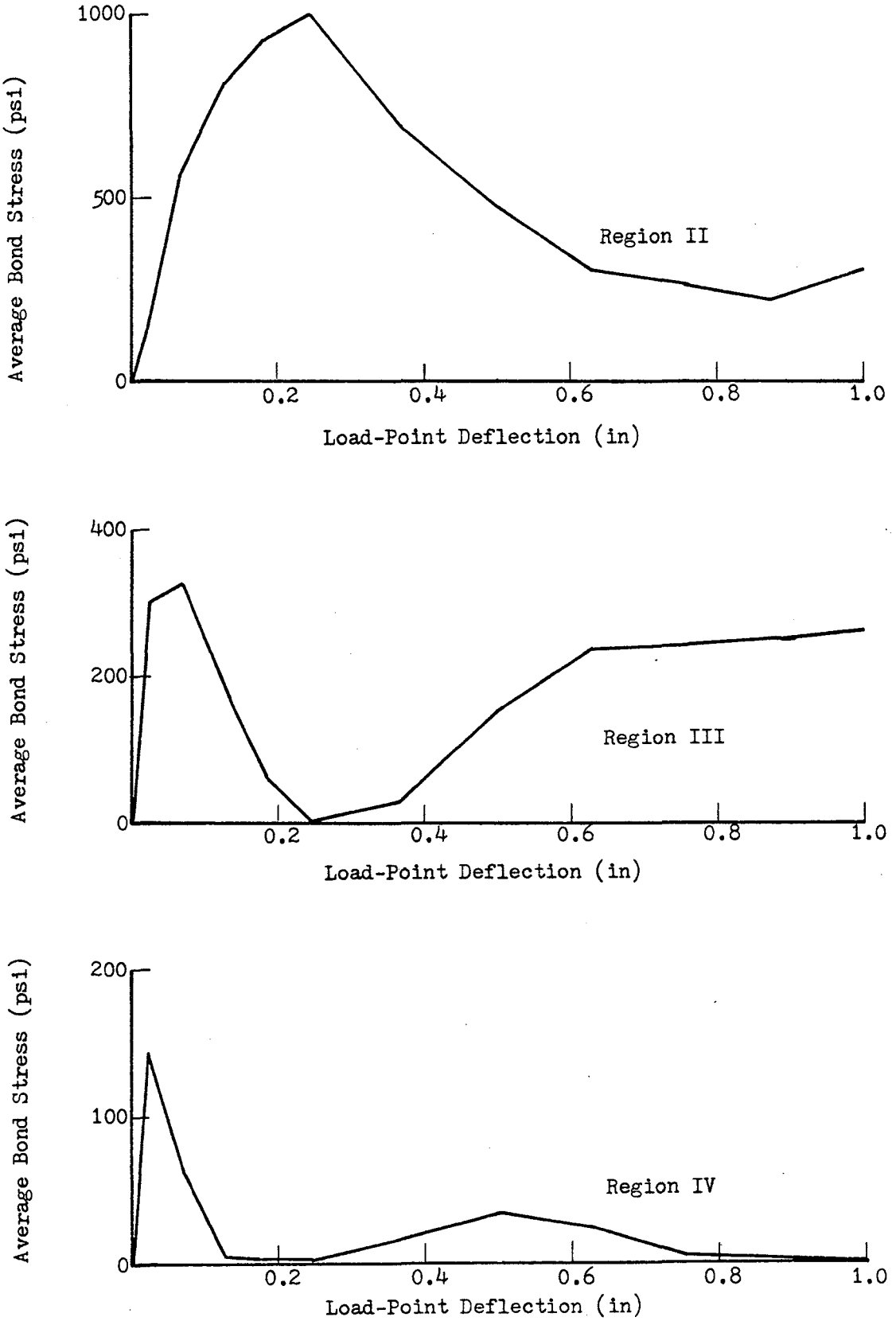

Fig. 5.7 Average Bond Stress vs. Load-Point Deflection, Specimen S3-2

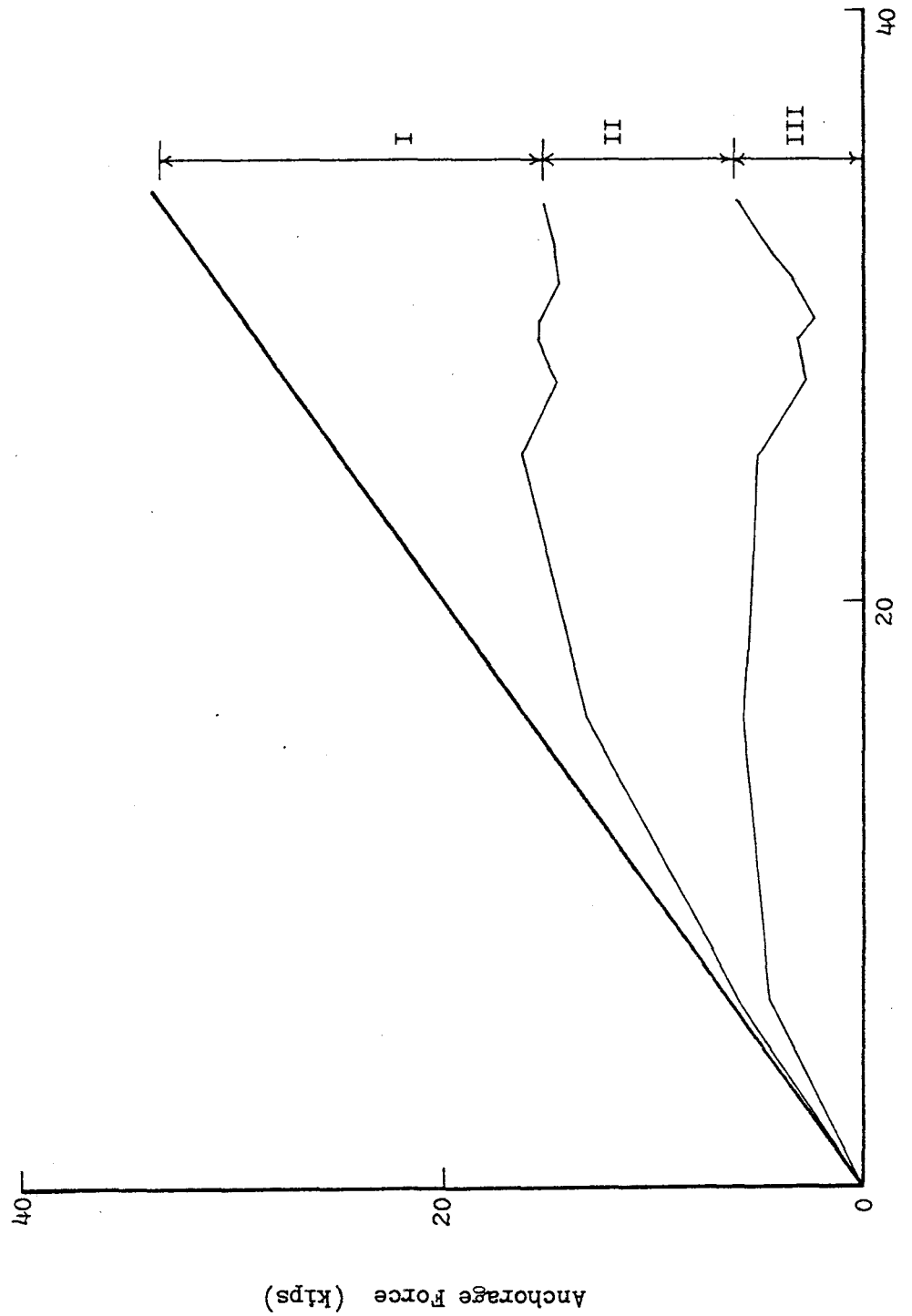

Fig. 5.8 Components of Anchorage Force During First Quarter-Cycle, Specimen S1-4

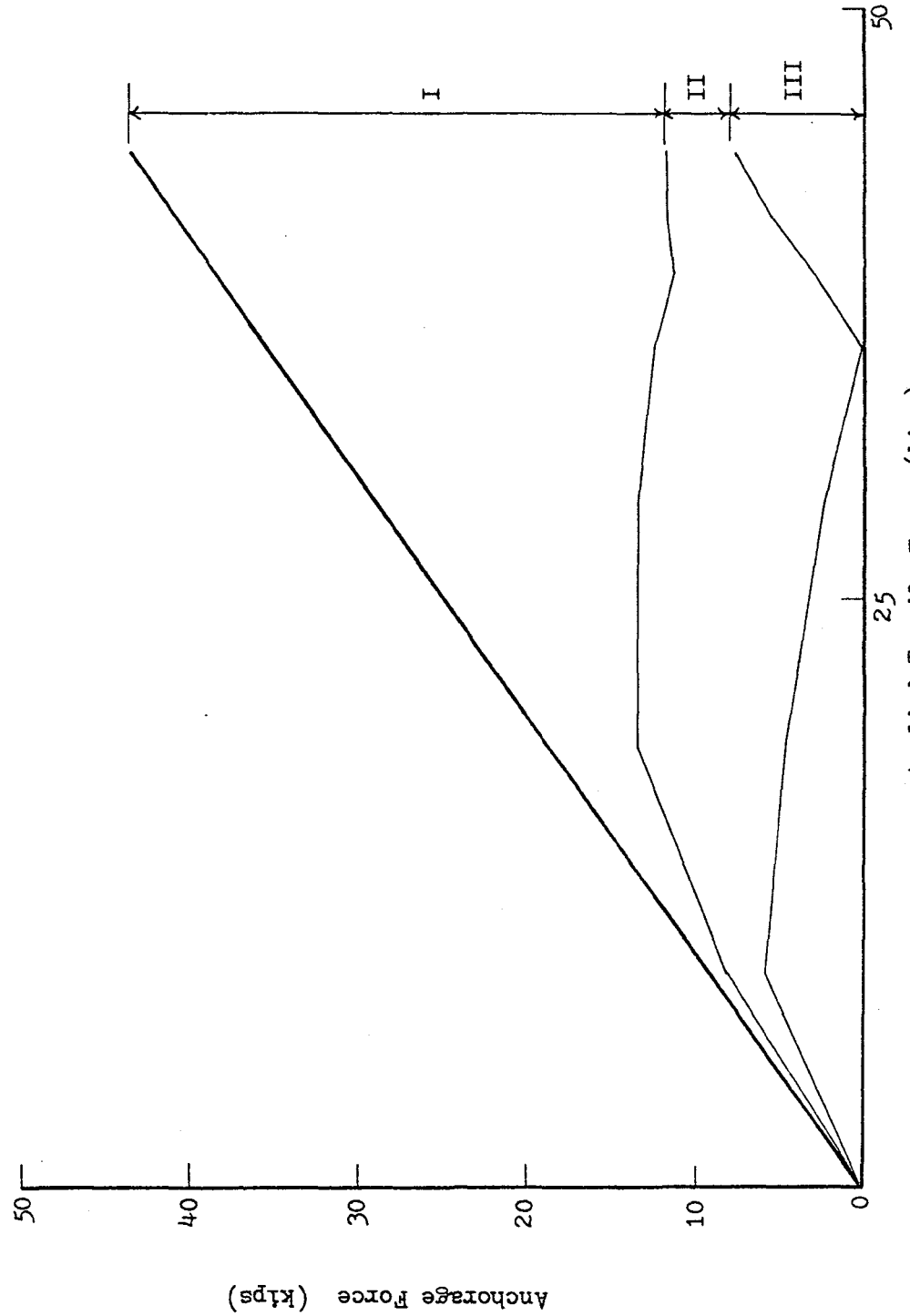

Fig. 5.9 Components of Anchorage Force During First Quarter-Cycle, Specimen S2-2

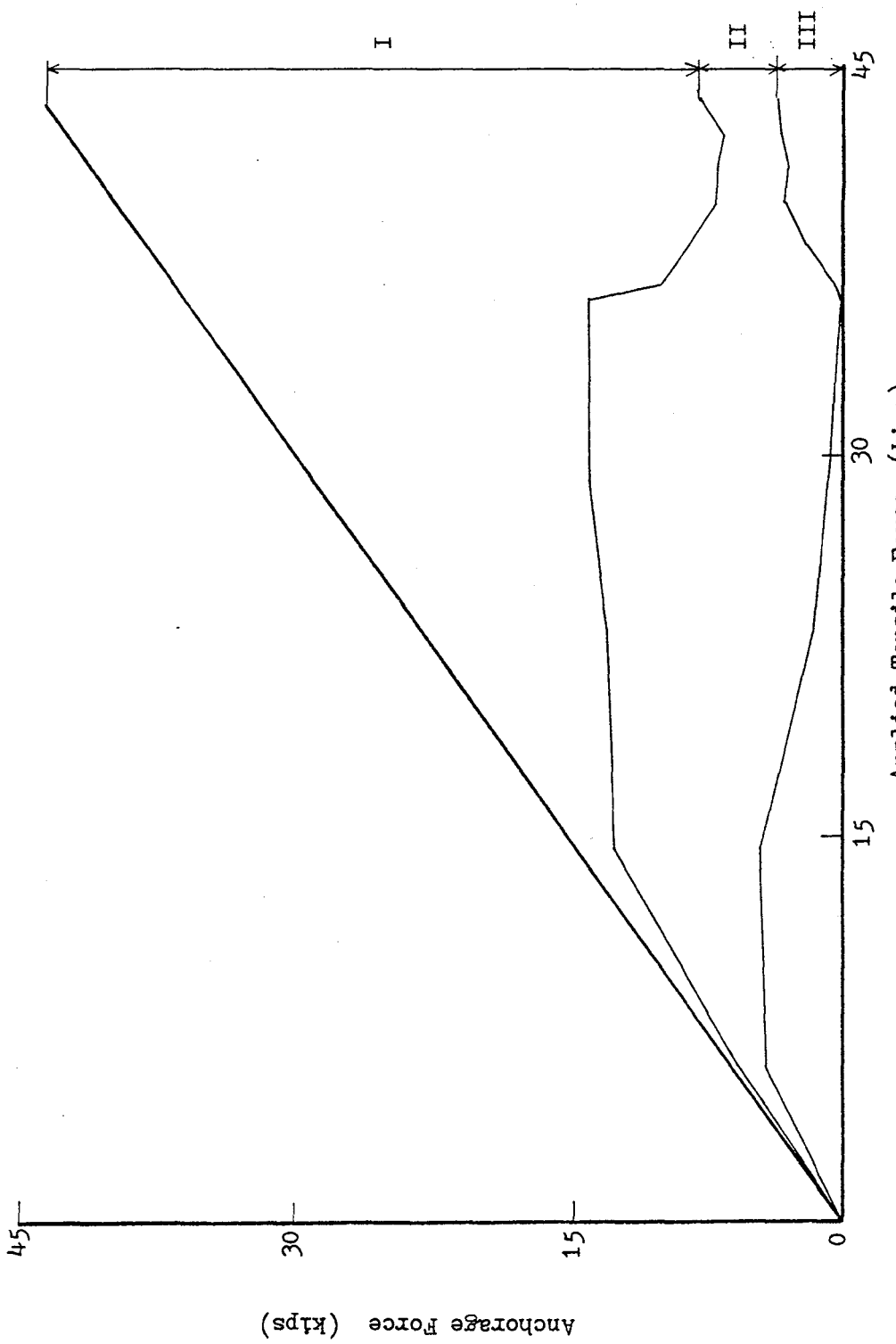

Fig. 5.10 Components of Anchorage Force During First Quarter-Cycle, Specimen S3-2

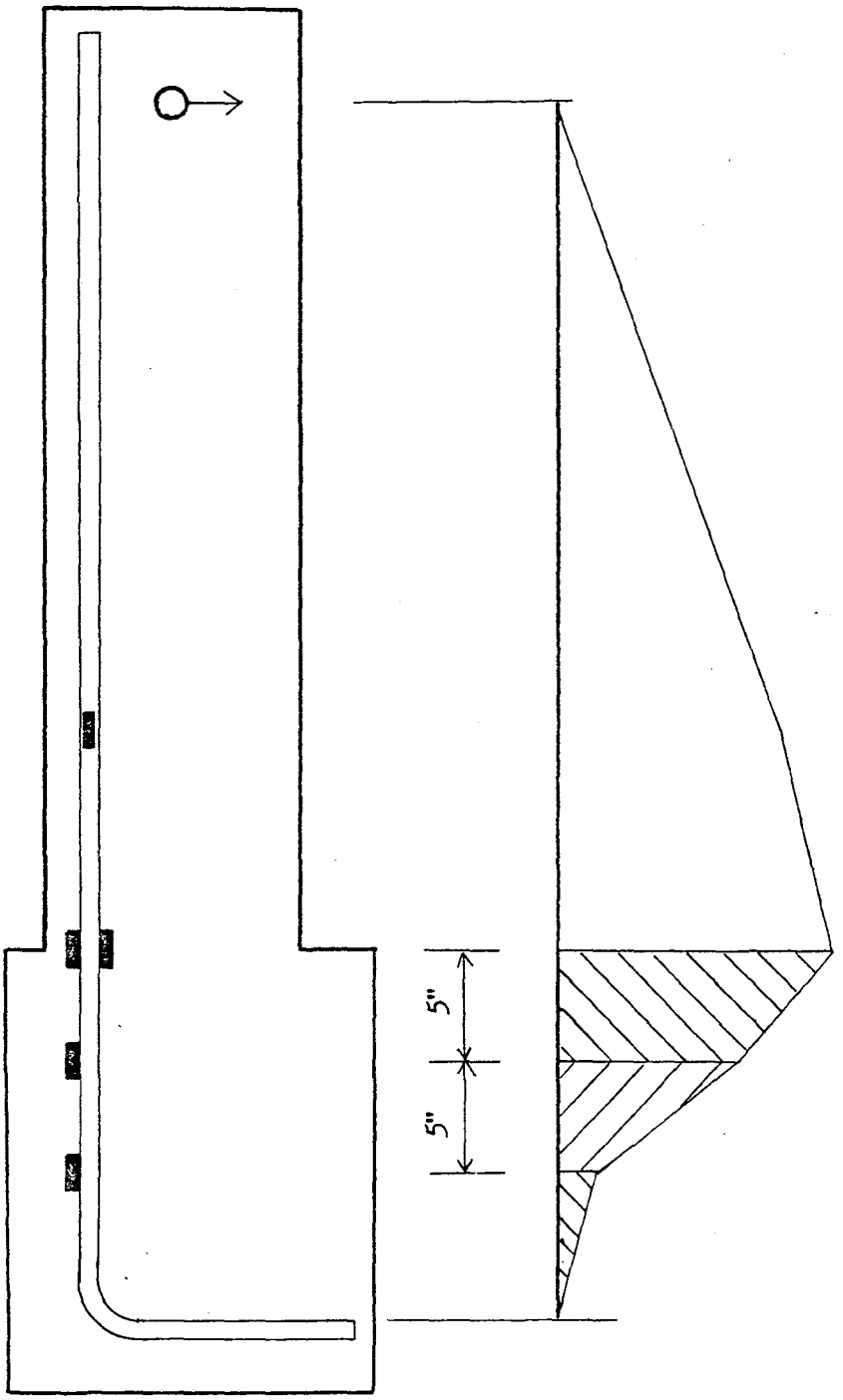

Fig. 5.11 Assumed Linear Strain Distribution for Determining Elongation of the Top Longitudinal Reinforcement

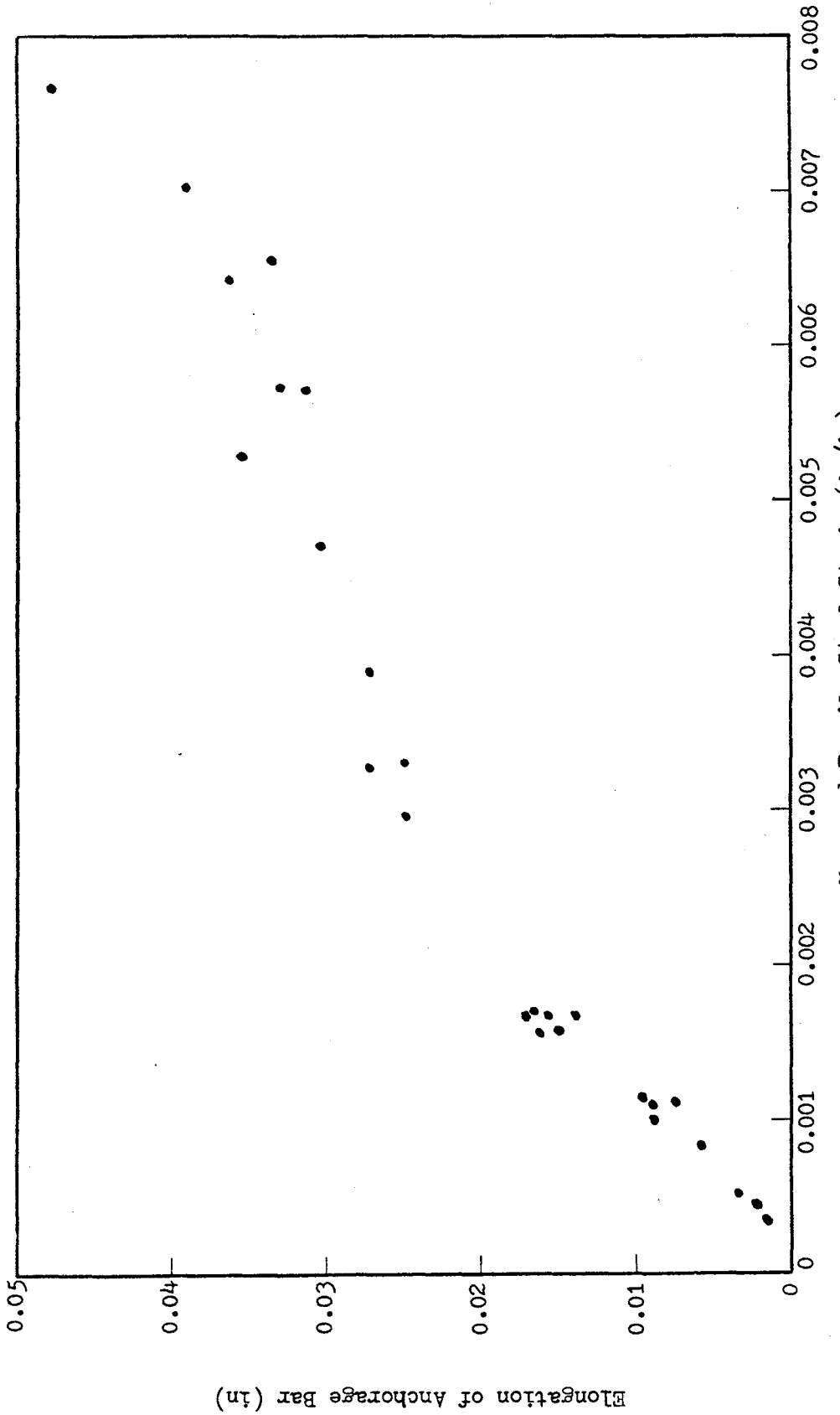

Fig. 5.12 Calculated Elongation of Top Longitudinal Reinforcement in the Enlarged End Block vs. Measured Steel Strain for No. 7 Bars

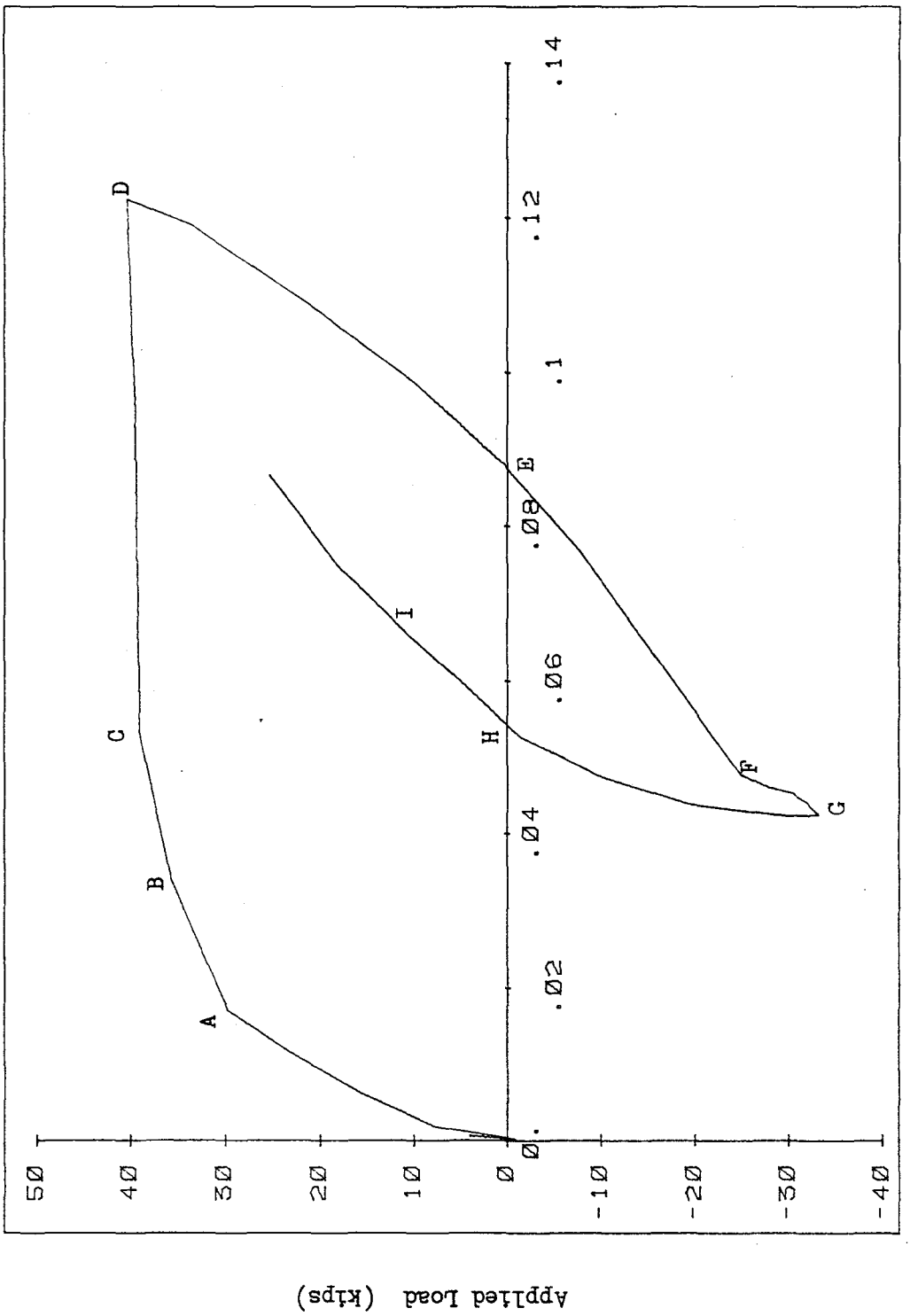

Fig. 5.13(a) Applied Load vs. Top Longitudinal Reinforcement Elongation During First Cycle, Specimen S3-4

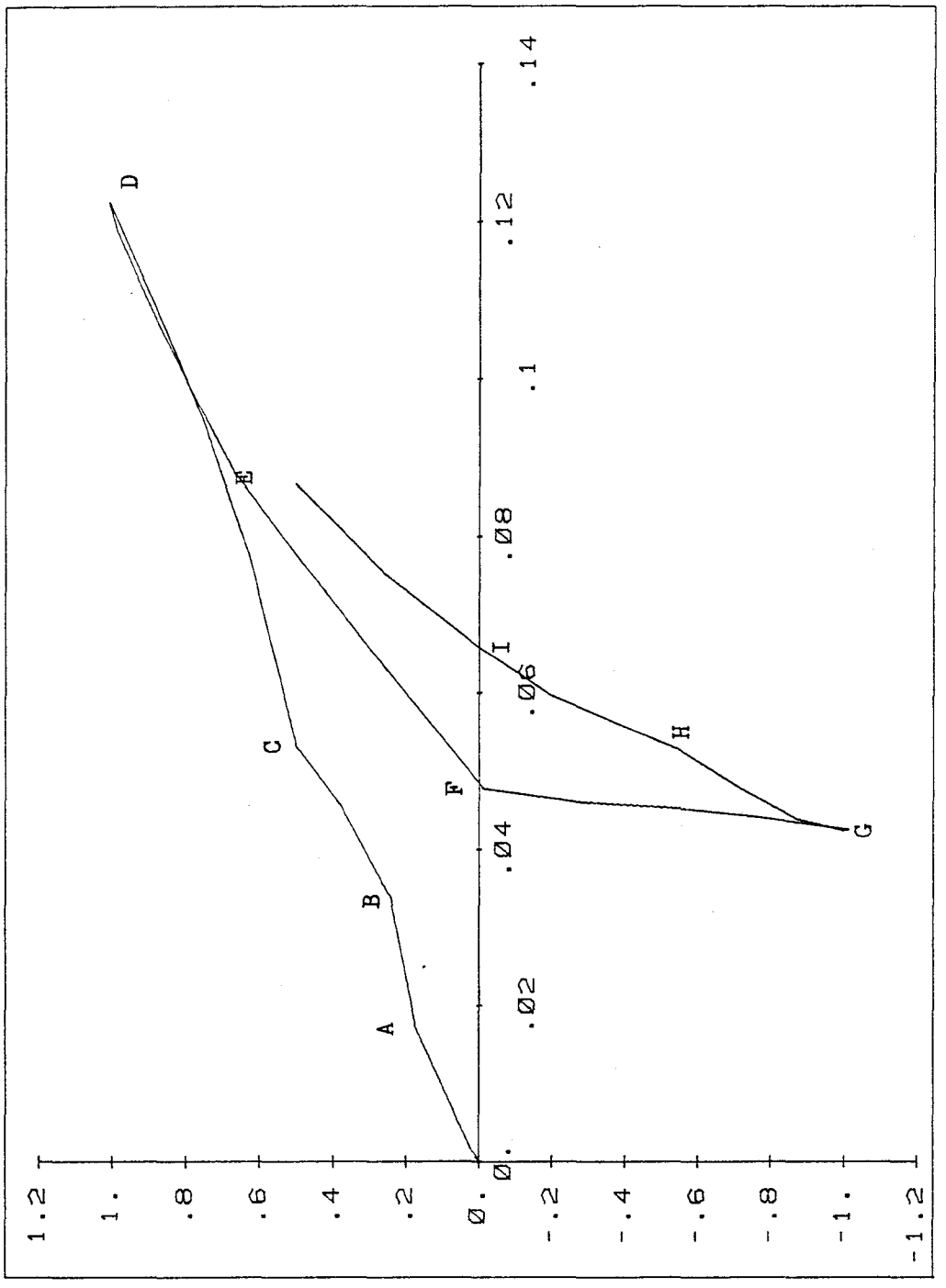

Fig. 5.13(b) Load-Point Deflection vs. Top Longitudinal Reinforcement Elongation During First Cycle, Specimen S3-4

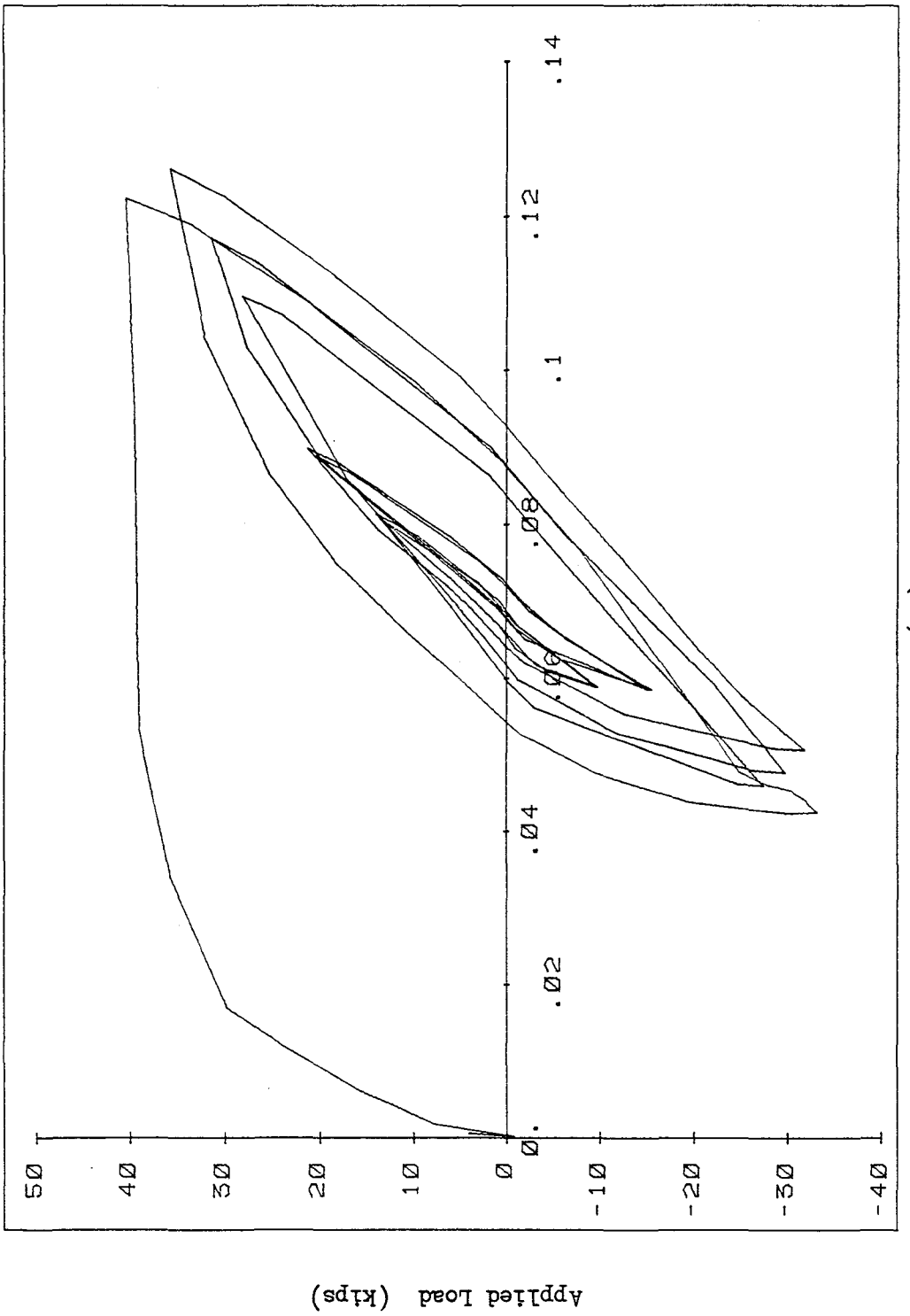

Fig. 5.14(a) Applied Load vs. Top Longitudinal Reinforcement Elongation, Specimen S3-4

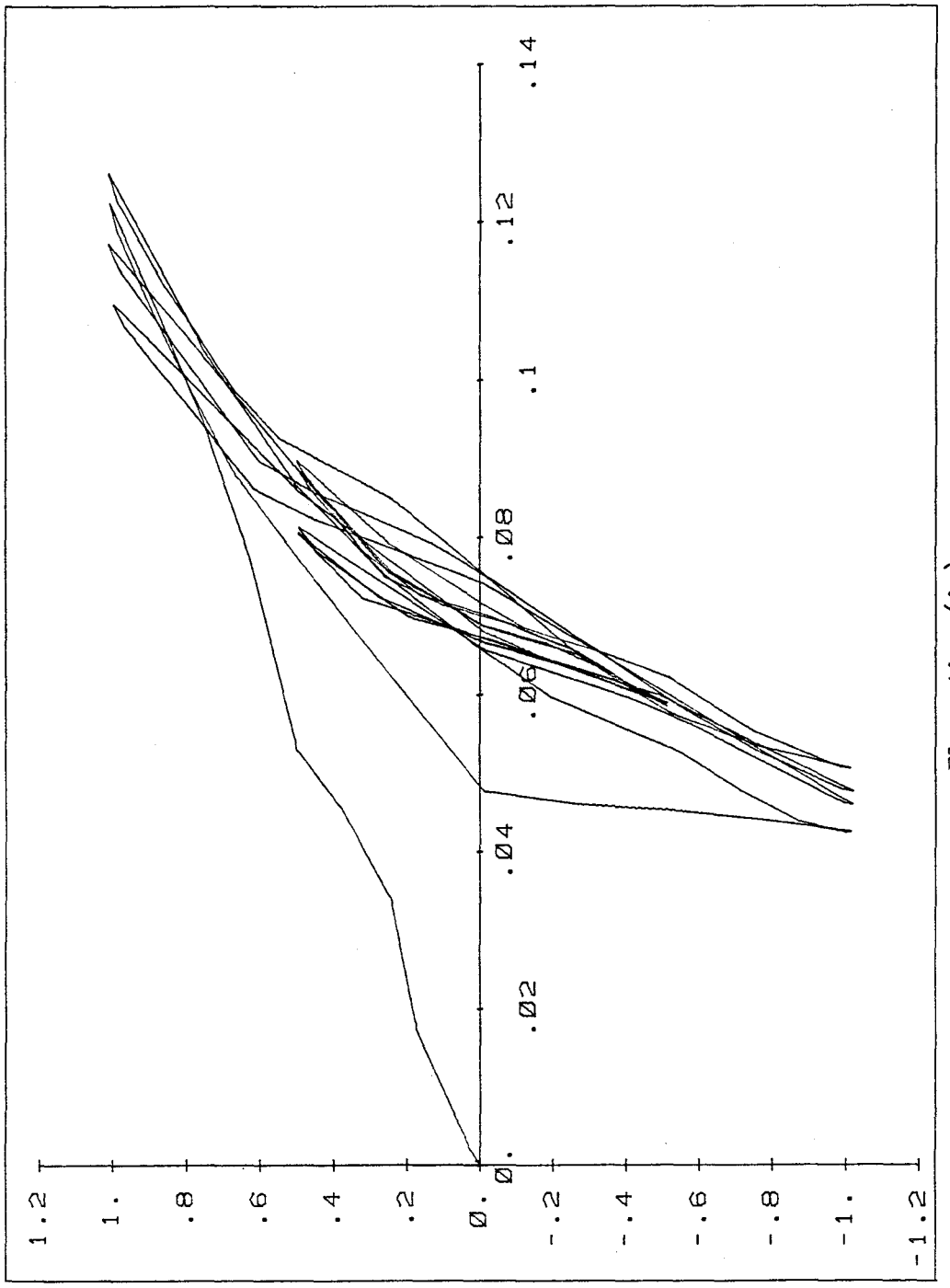

Fig. 5.14(b) Load-Point Deflection vs. Top Longitudinal Reinforcement Elongation, Specimen S3-4

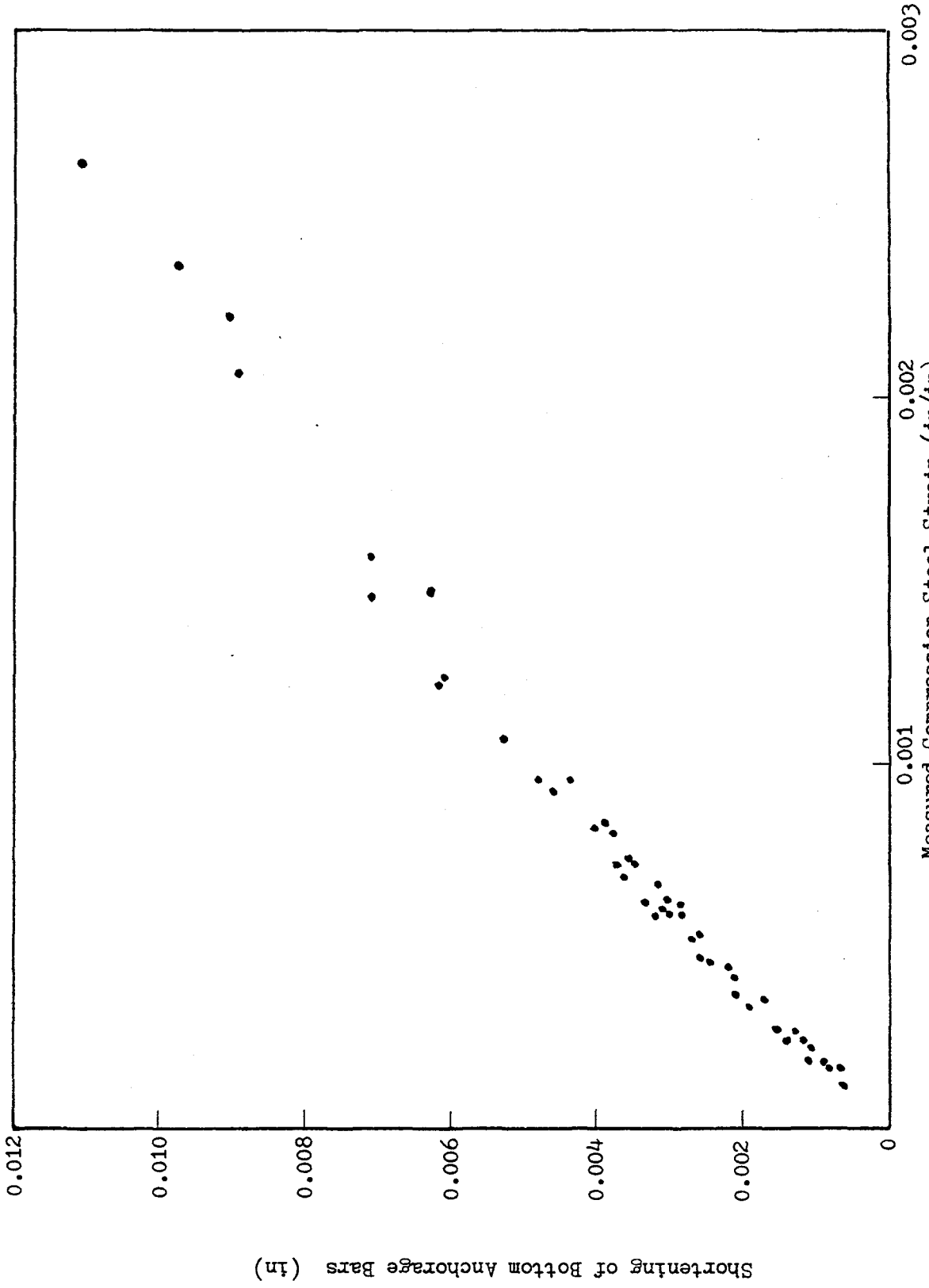

Fig. 5.15 Calculated Shortening of the Bottom Longitudinal Reinforcement in the Enlarged End Block vs. Measured Steel Strain for No. 6 Bars

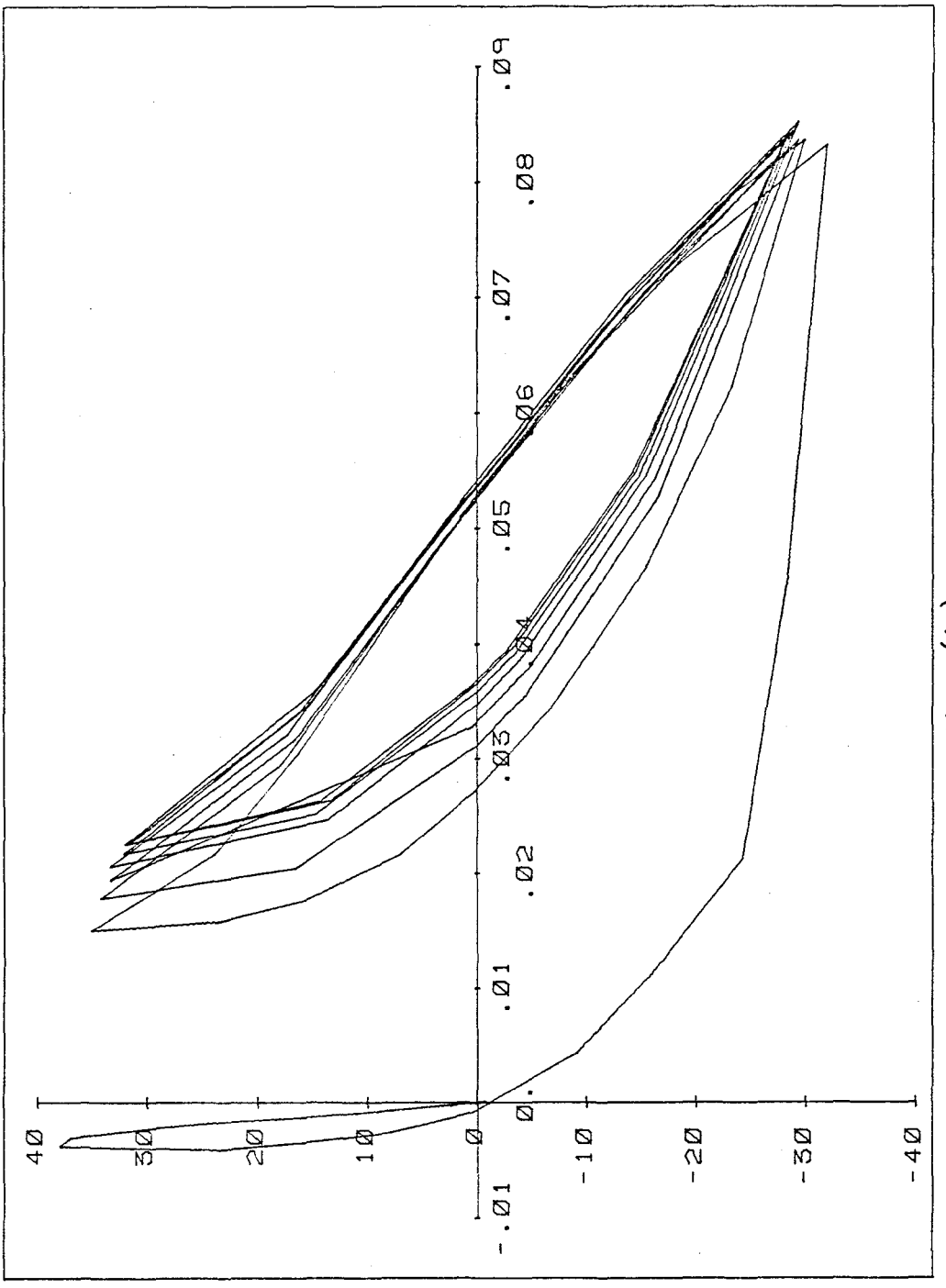

Fig. 5.16 Applied Load vs. Bottom Longitudinal Reinforcement Elongation, Specimen S3-1

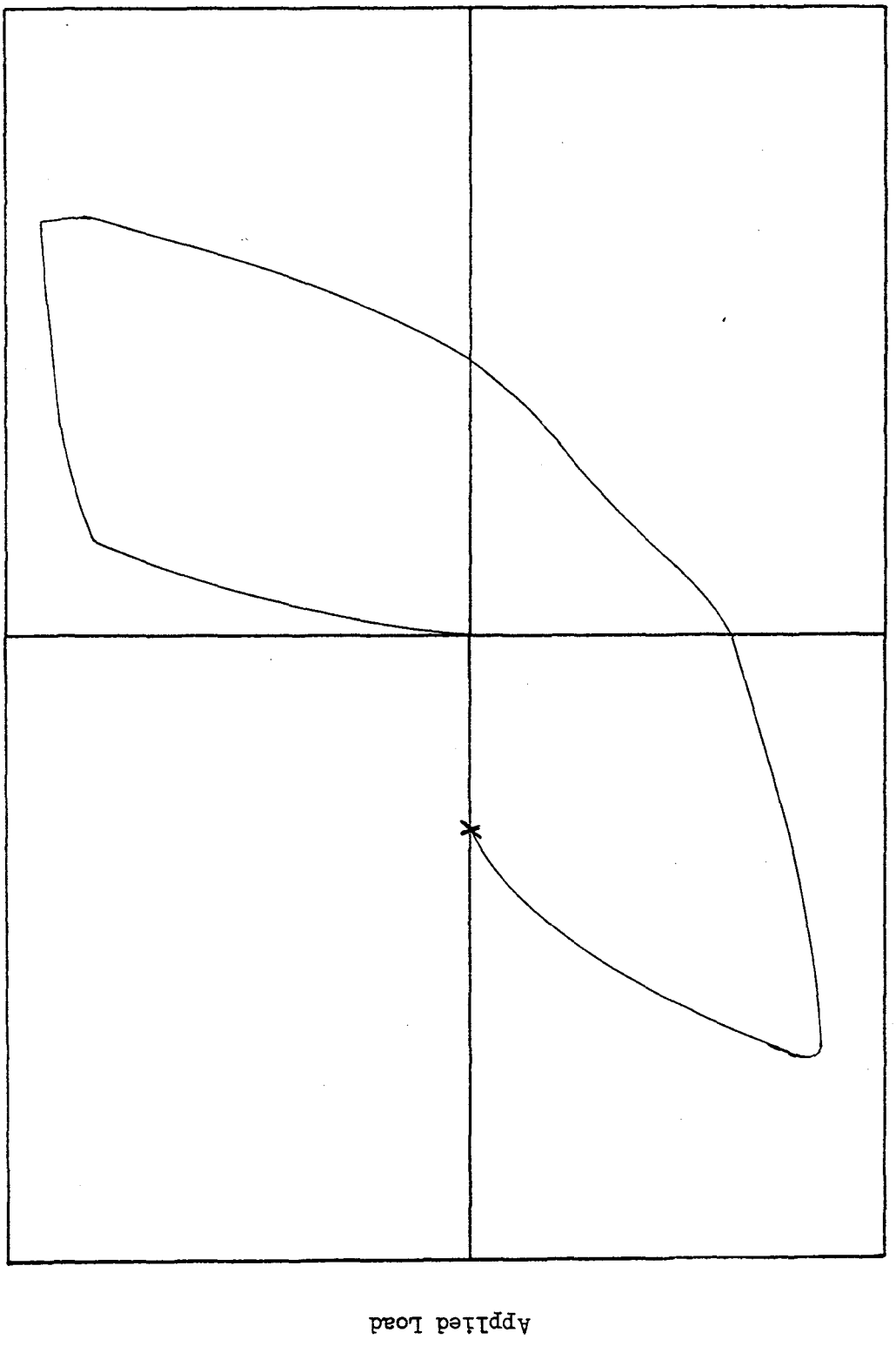

Fig. 5.17 Location in the Load-Deflection Curve Where Residual Steel Elongation is Taken During Each Cycle

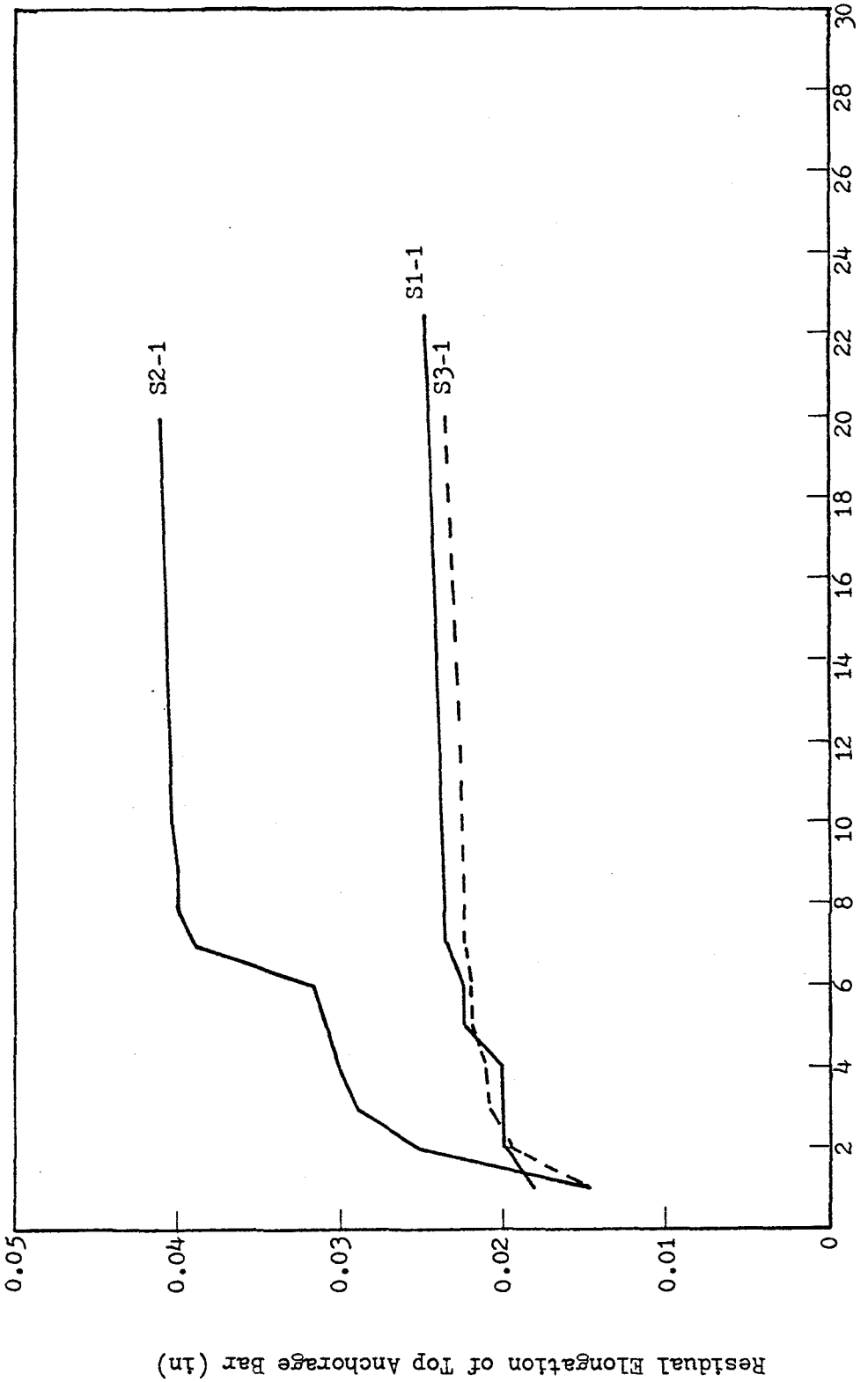

Fig. 5.18 Residual Elongation of the Top Longitudinal Reinforcement in the Enlarged End Block vs. Number of Cycles

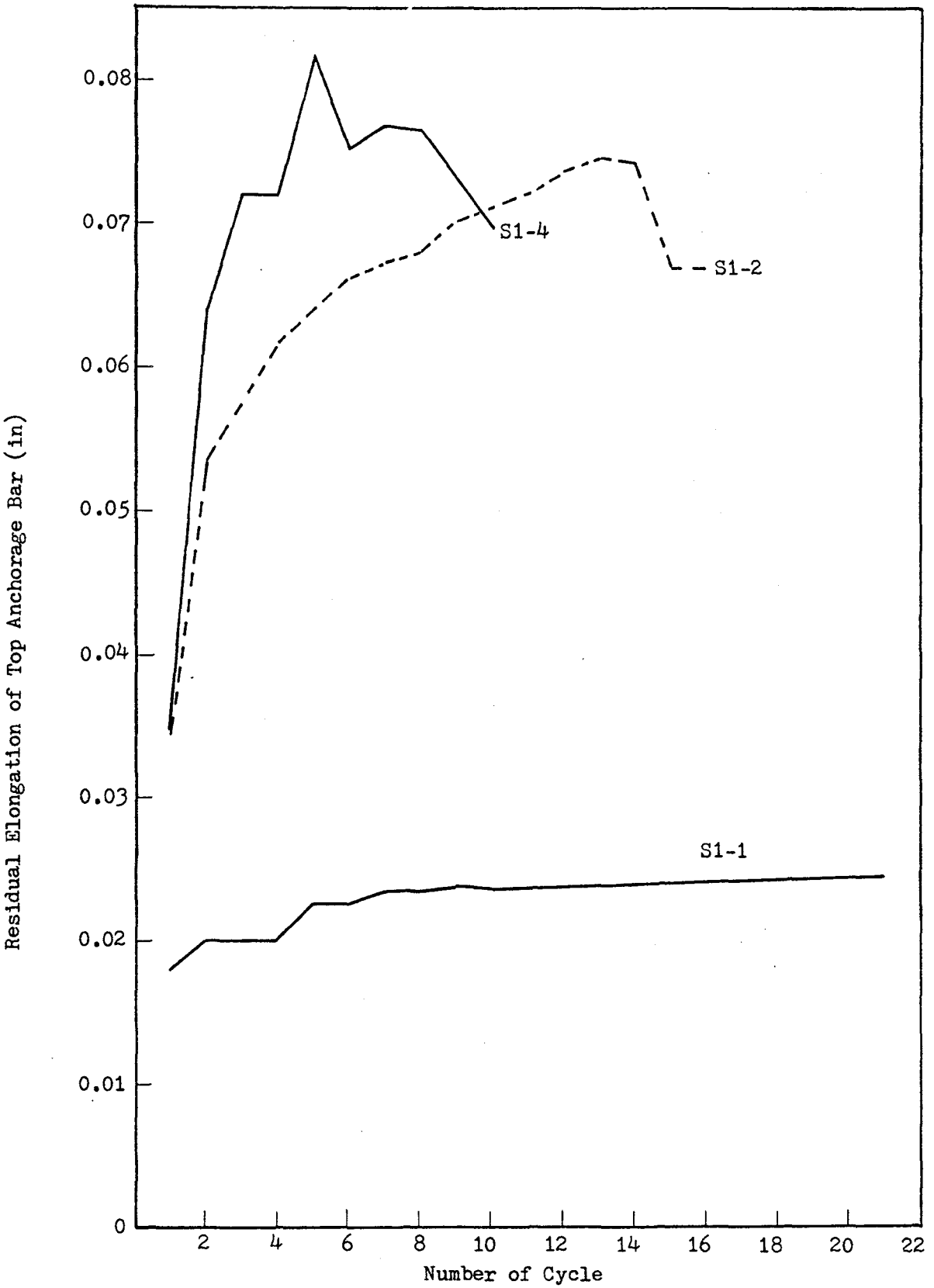

Fig. 5.19 Residual Elongation of the Top Longitudinal Reinforcement in the Enlarged End Block vs. Number of Cycles

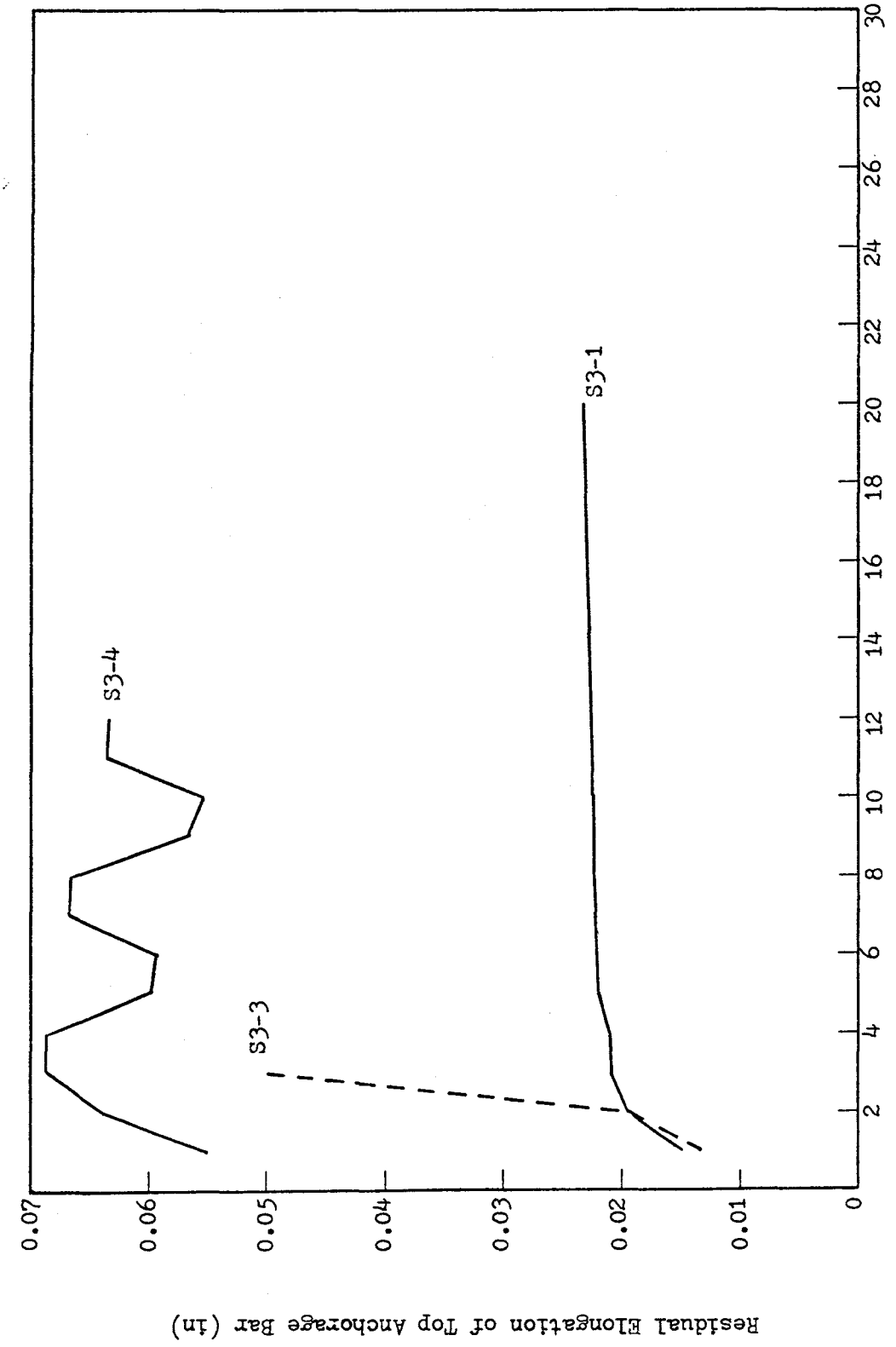

Fig. 5.20 Residual Elongation of the Top Longitudinal Reinforcement in the Enlarged End Block vs. Number of Cycles

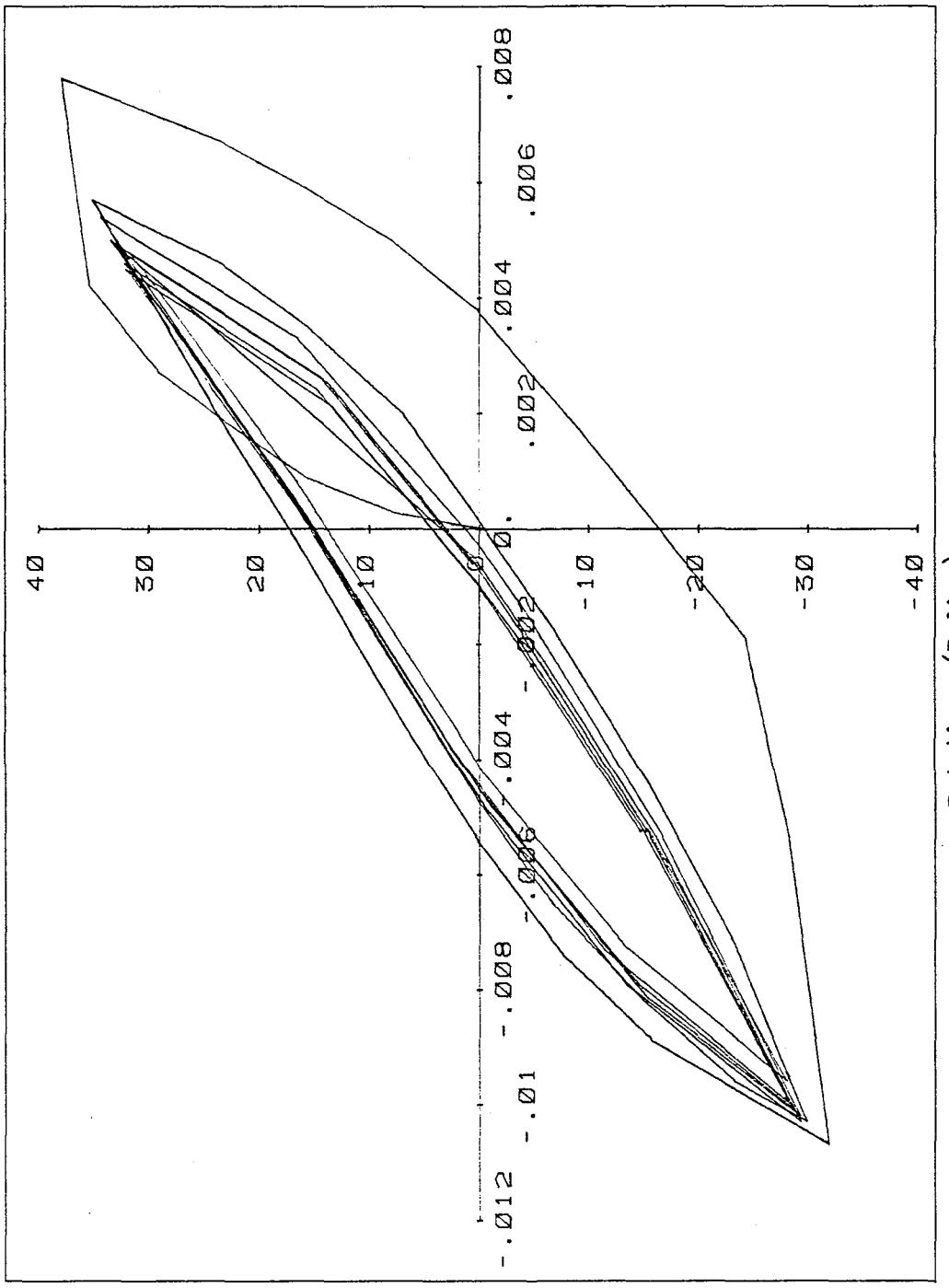

Fig. 5.21 Applied Load vs. Fixed End Rotation, Specimen S3-1

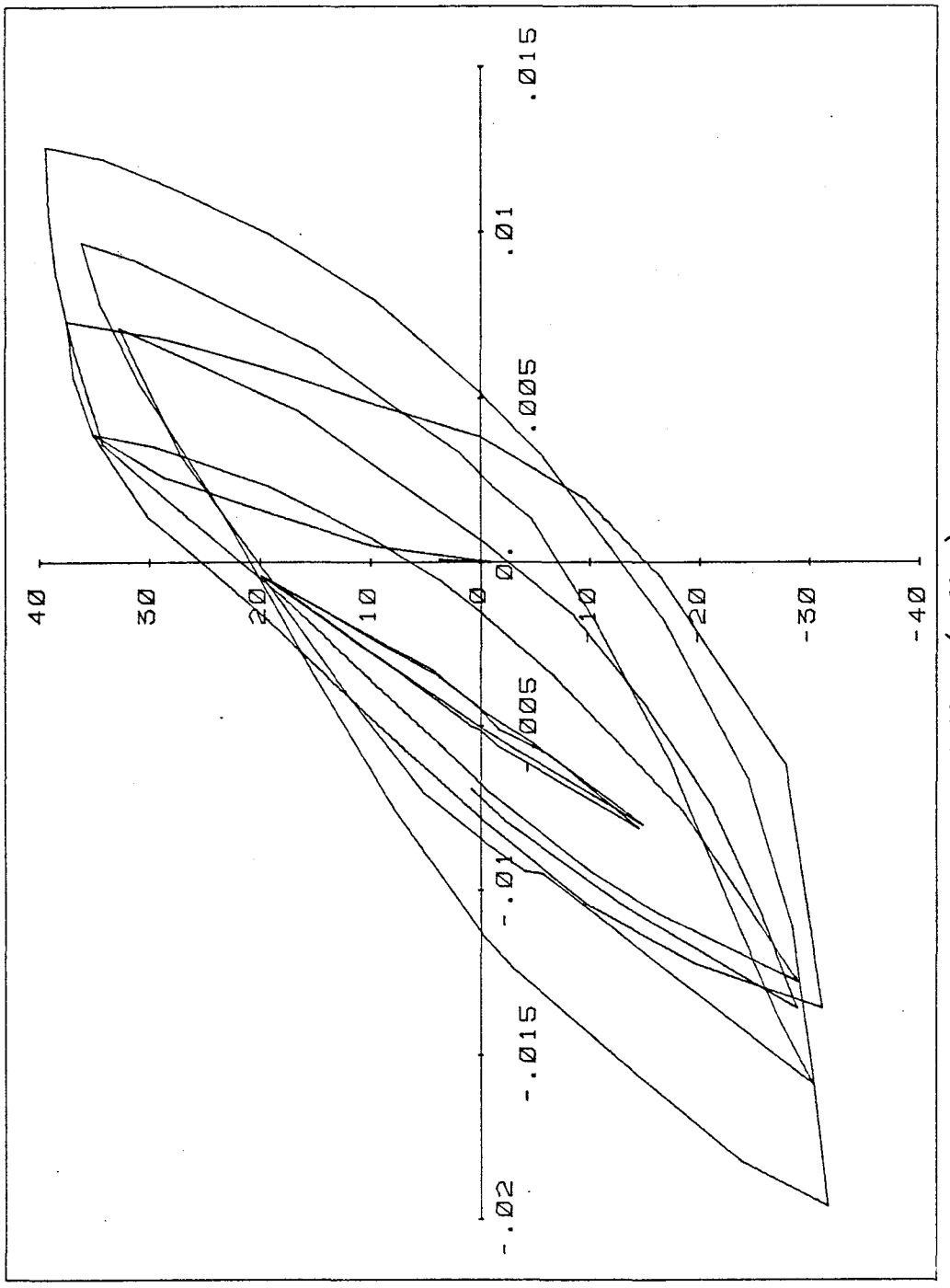

Fig. 5.22 Applied Load vs. Fixed End Rotation, Specimen S3-3

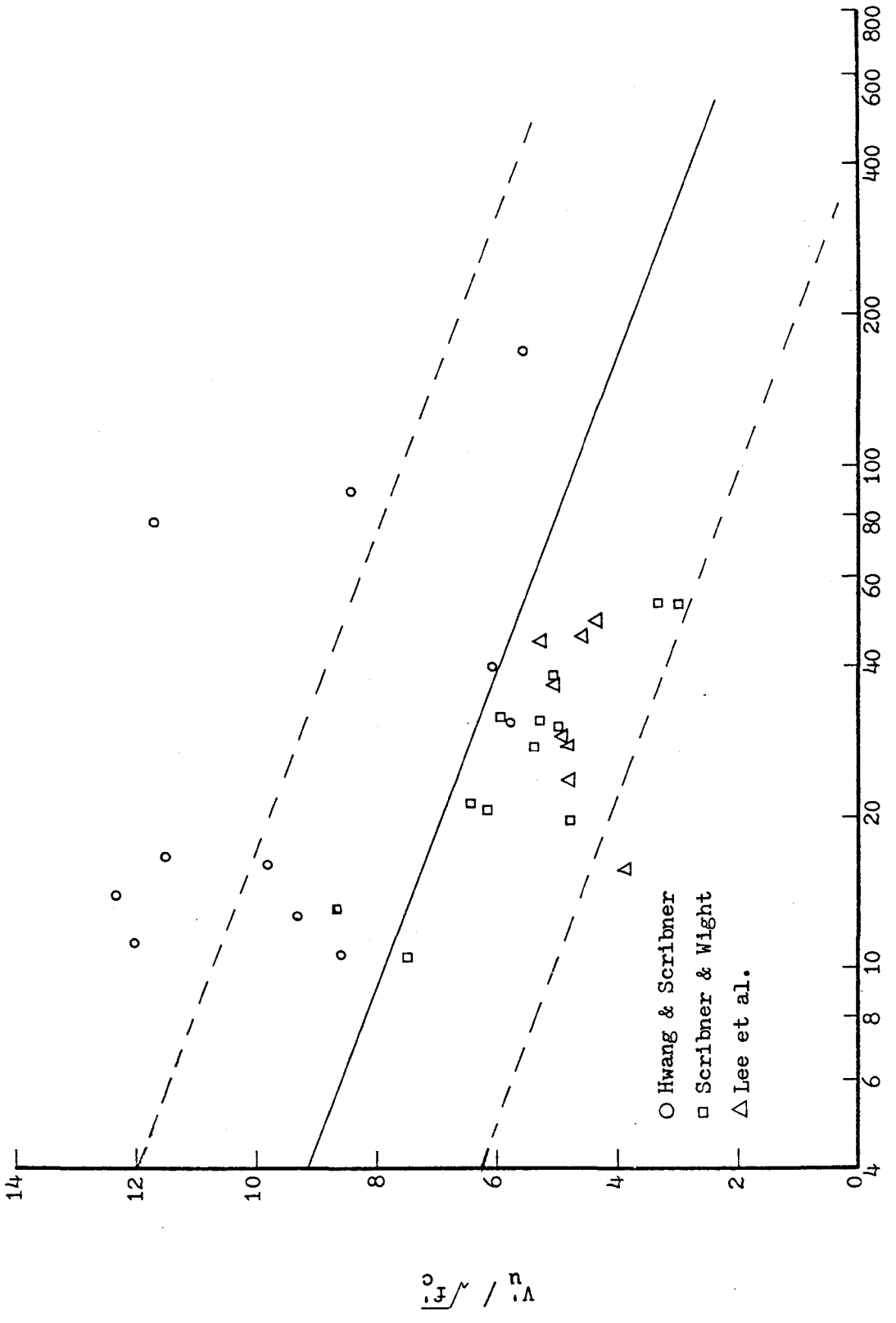

Fig. 6.1 Test Results Compared to Results Obtained by Six Other Researchers

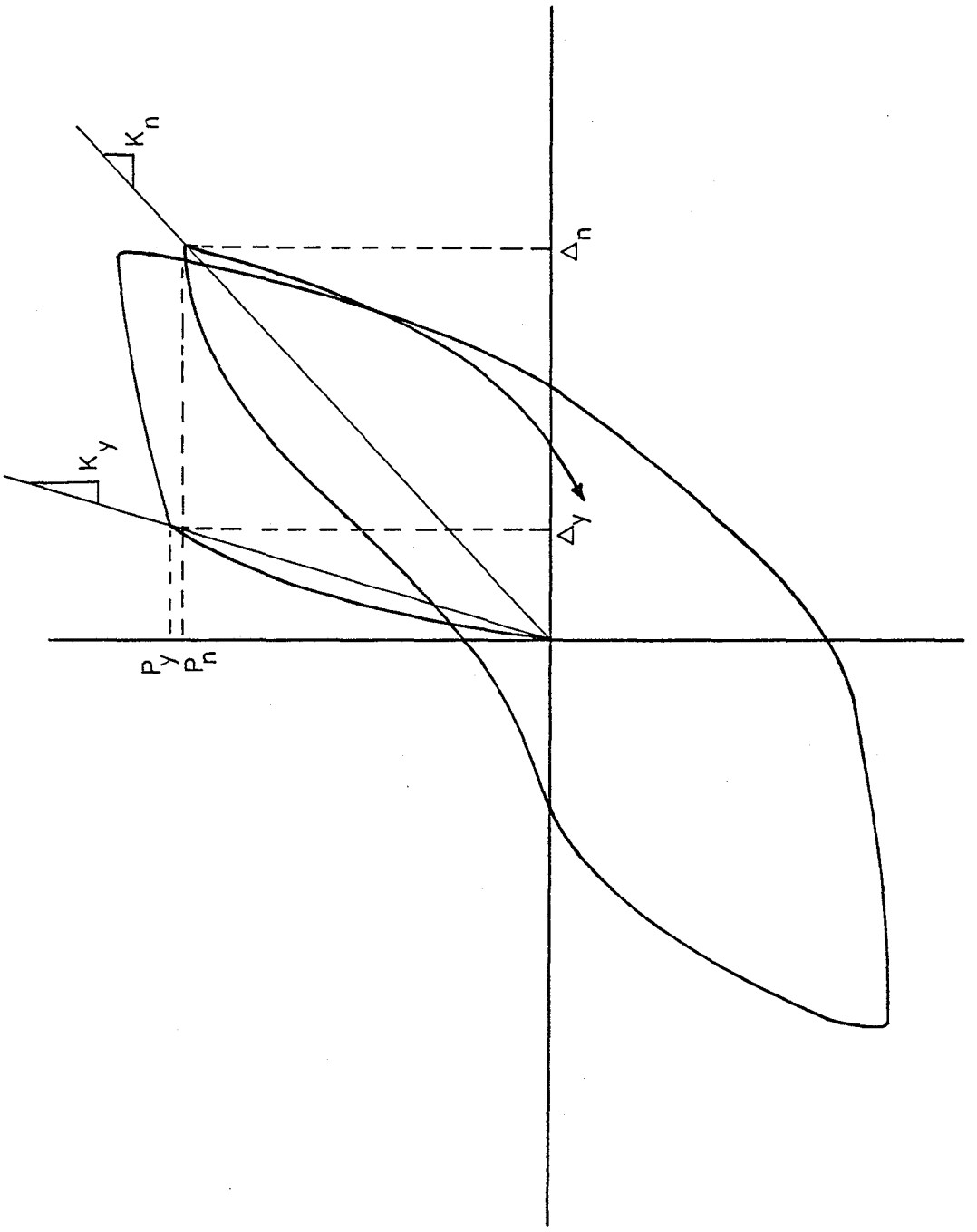

Fig. 6.2 Definitions for K_y, K_n, Δ_n, Δ_y

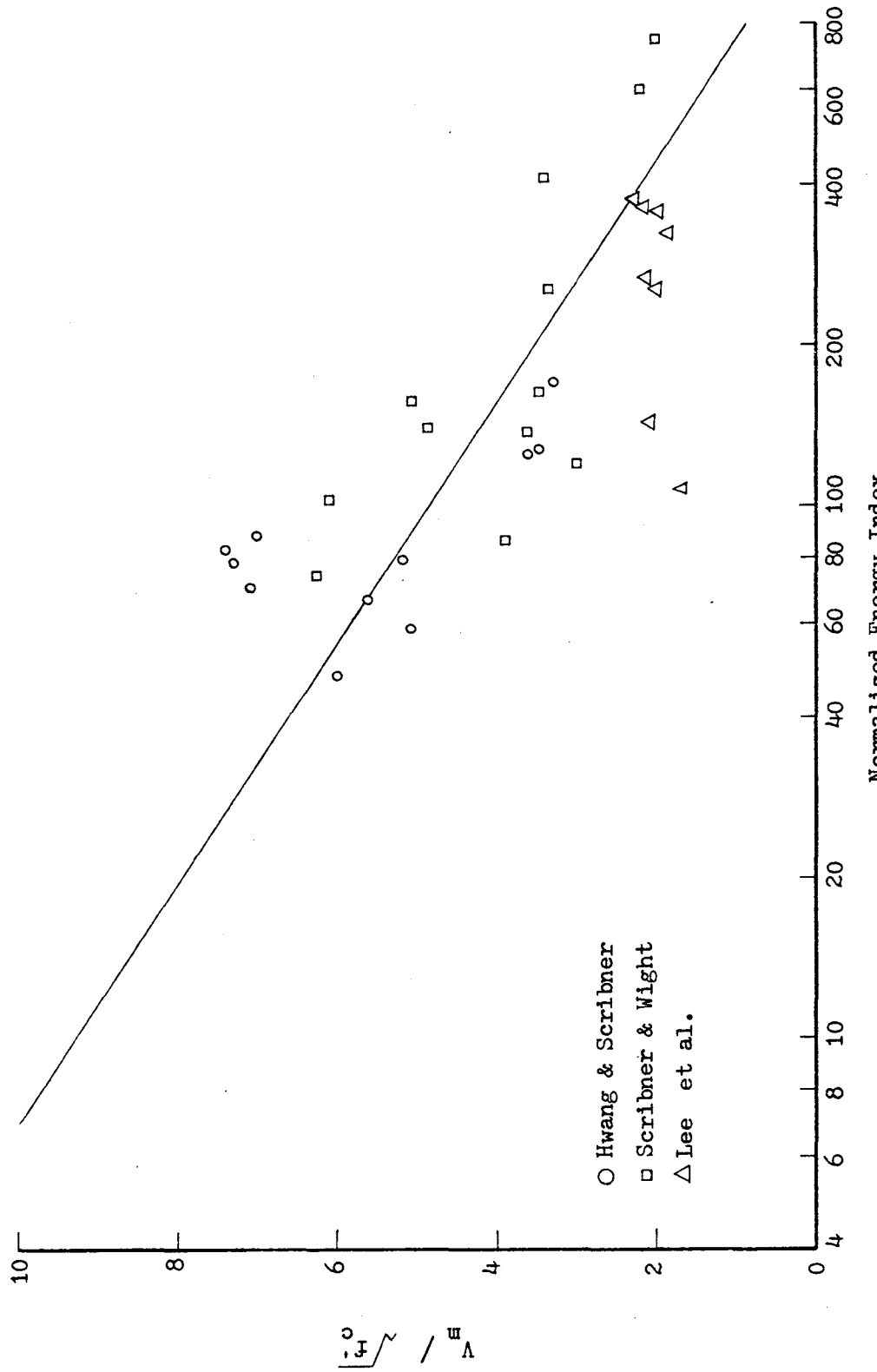

Fig. 6.3 Maximum Shear Stress vs. Normalized Energy Index

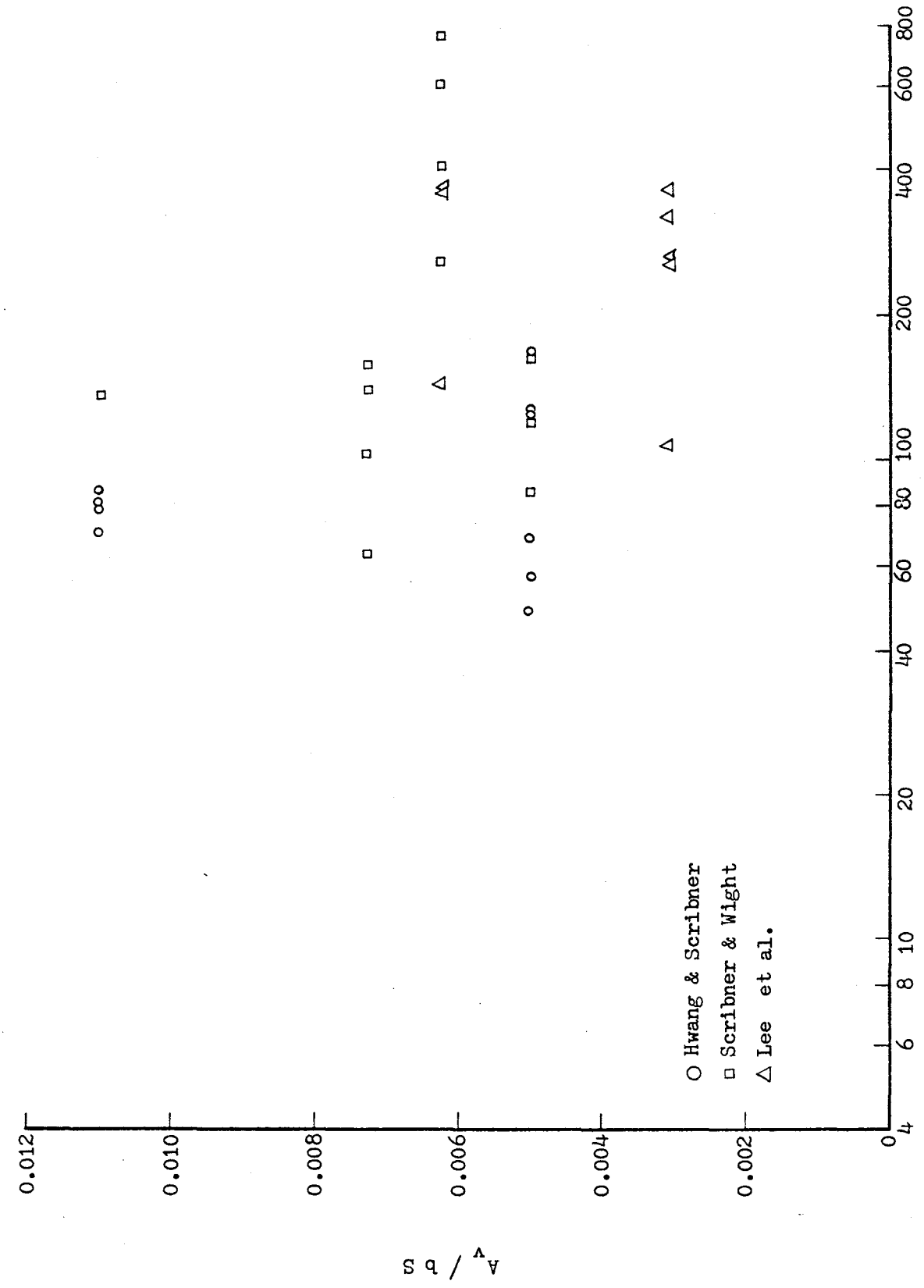

Fig. 6.4 Transverse Reinforcement Ratio vs. Normalized Energy Index

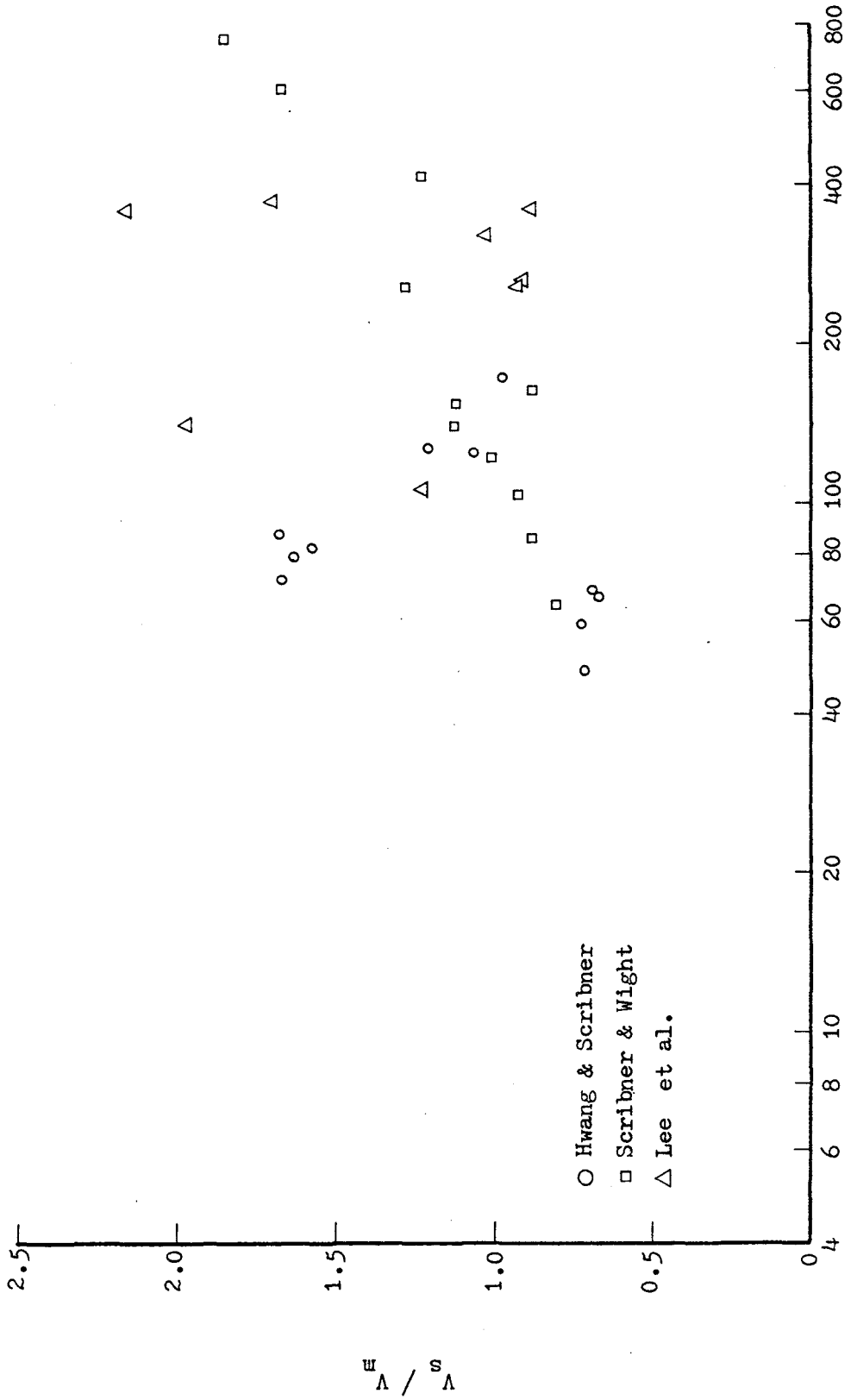

Fig. 6.5 V_s/V_m vs. Normalized Energy Index

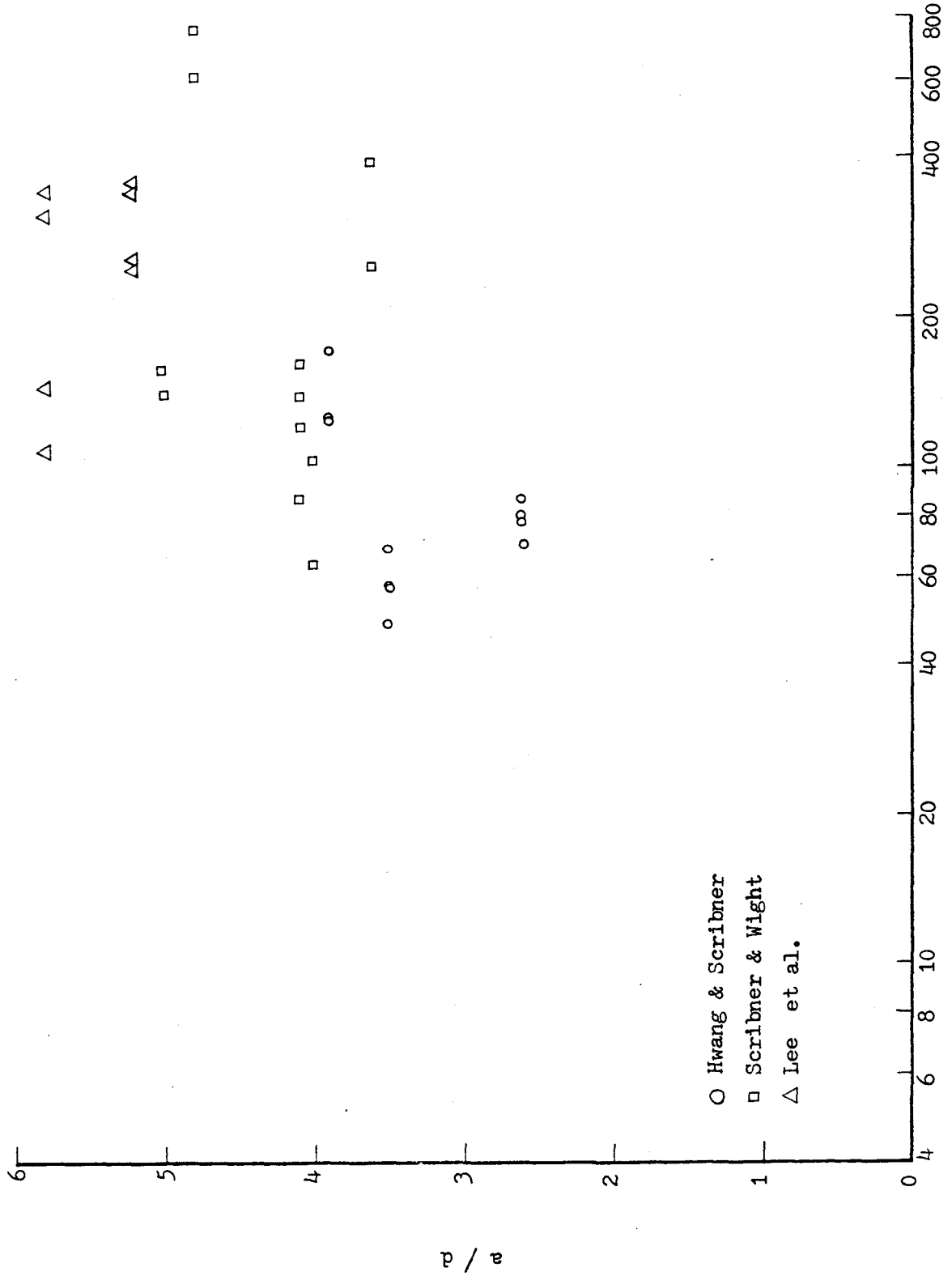

Fig. 6.6 Shear Span to Depth Ratio (a/d) vs. Normalized Energy Index

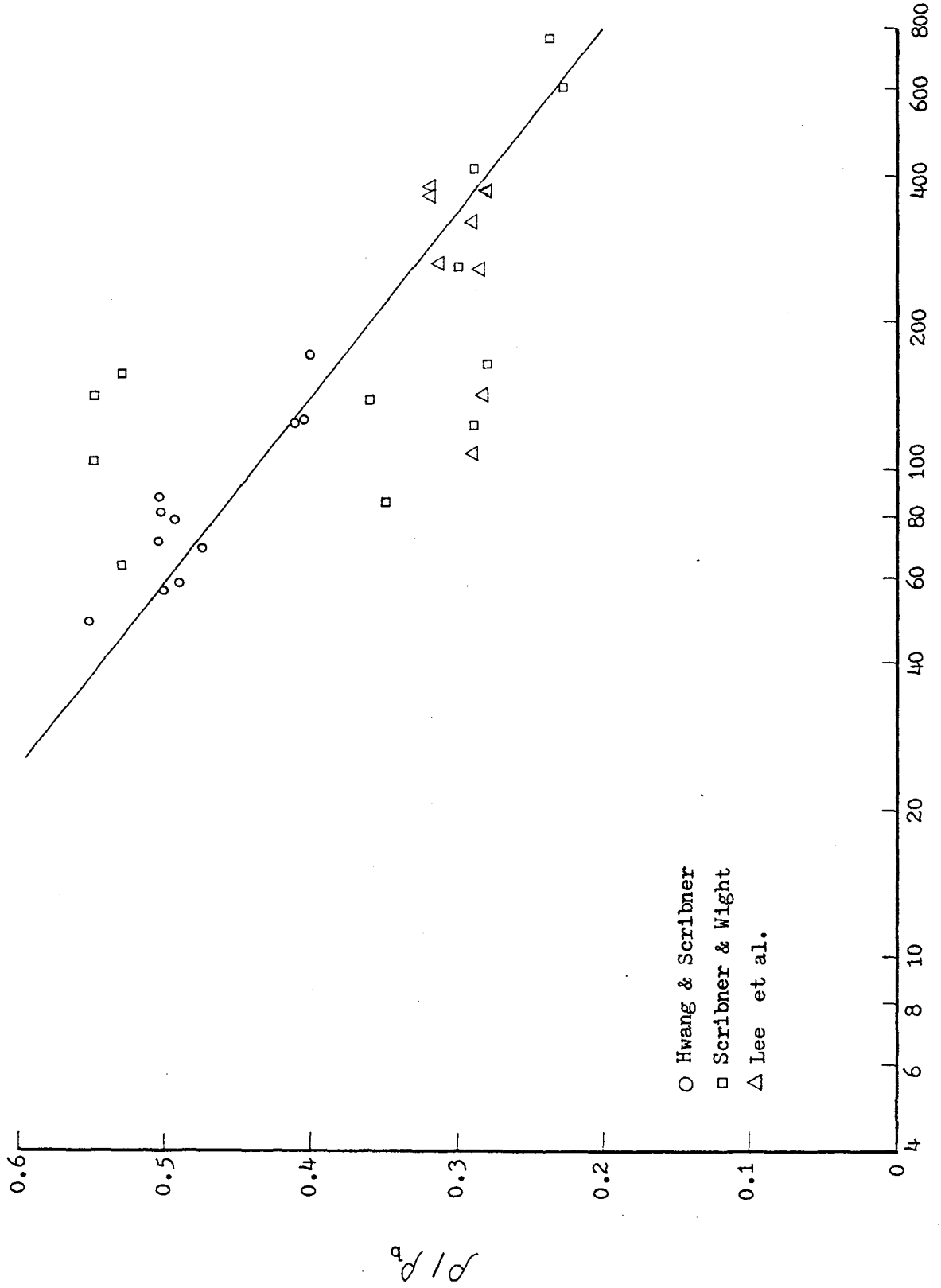

Fig. 6.7 ρ/ρ_b vs. Normalized Energy Index

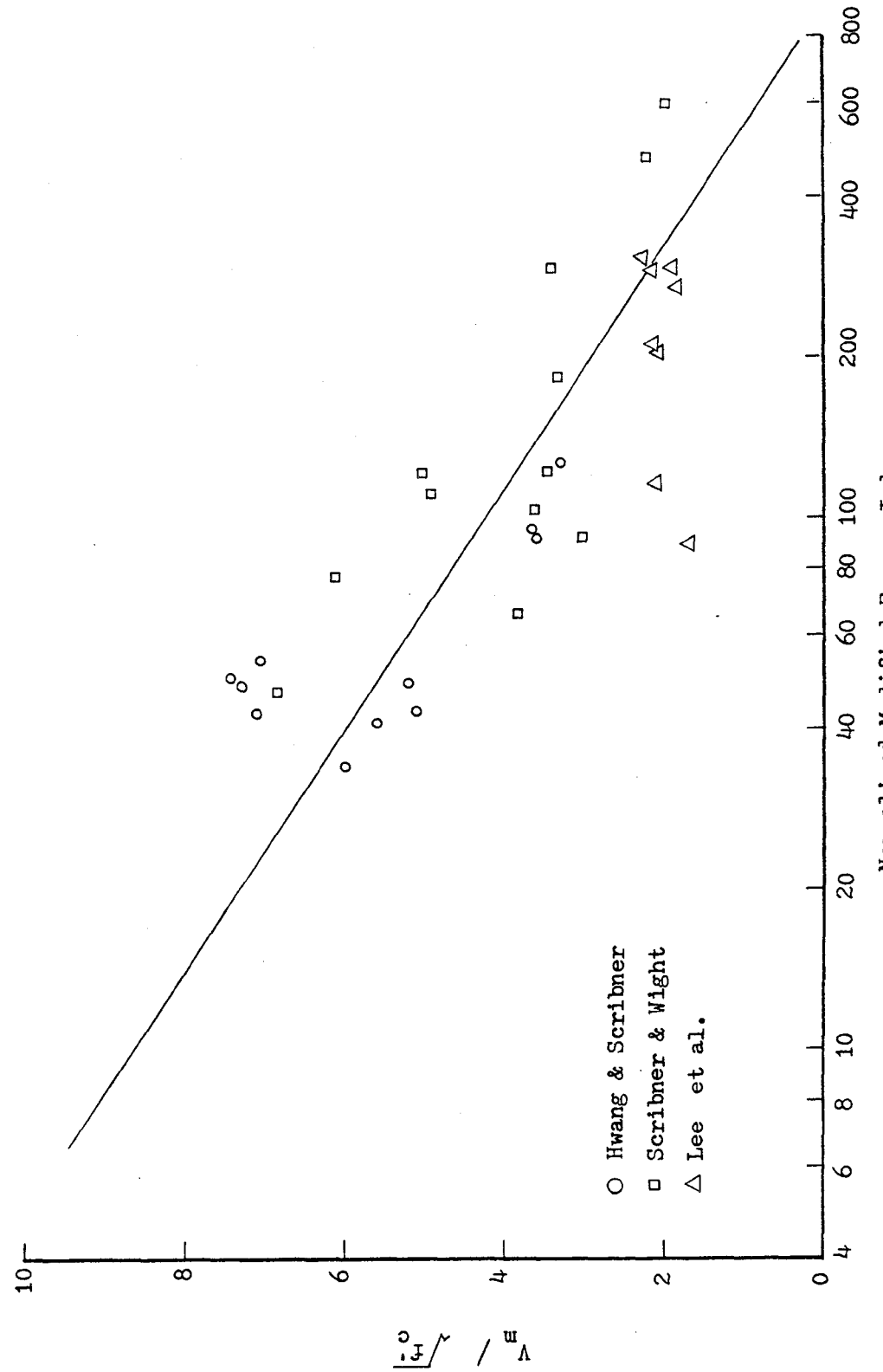

Fig. 6.8 Maximum Shear Stress vs. Normalized Modified Energy Index

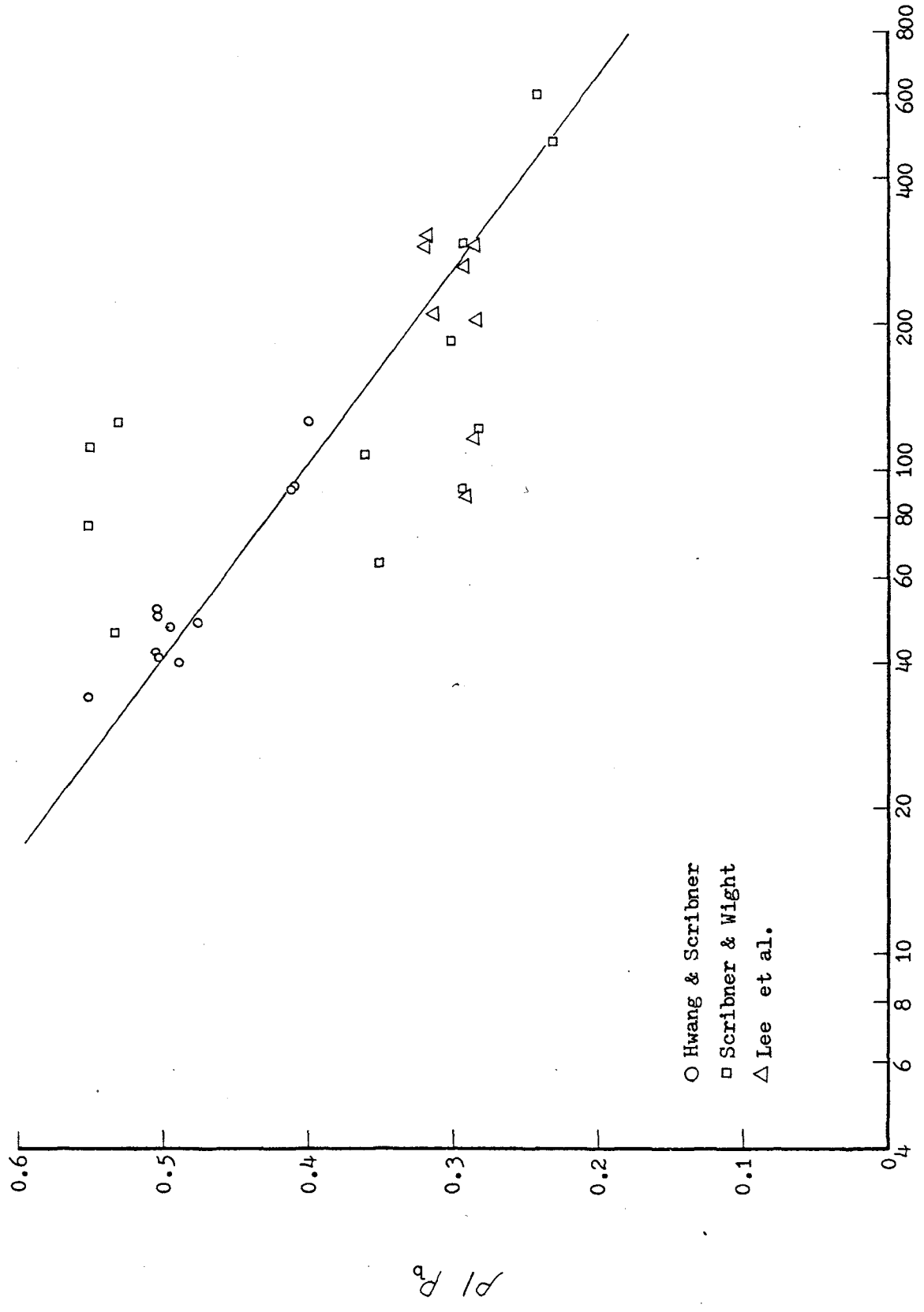

Fig. 6.9 ρ / ρ_b vs. Normalized Modified Energy Index

APPENDIX A

MATERIAL PROPERTIES

(A) REINFORCEMENT

Reinforcement used in this investigation was obtained from two sources. One ordered from a steel company was used in all specimens execpt specimens S1-4 and S2-3. Reinforcement used in specimen S1-4 and S2-3 was from the steel storage room in the University of Illinois. The coupon test of the reinforcement from each source showed that all bars of each size in either source had approximately the same stress-strain curves.

Three or more 13-inch long coupons were taken from each size bar to determine the properties of the reinforcement. Coupons were tested uniaxially in tension using an MTS universal testing machine. A one-inch extensometer was attached to the bar coupon to measure the strain. Both applied load and measured strain were plotted using an X-Y plotter during each test. Nominal bar area was assumed when converting the measure load-strain curve to a stress-strain curve for all reinforcement. A summary of the results of these coupon tests is given in Table A.1. A typical stress-strain curve for each size bar is shown in Fig.A.1(a) to A.1(g).

(B) CONCRETE

Normal strength (Type I) portland cement and limestone

with a maximum size of 3/4 inch were used for all specimens. The concrete mix design was chosen to provide approximately 4000 psi compressive strength at 28 days. Based on two trial mixes, the ratio of mix by weight was 1 : 3.67 : 3.83 : 0.80 (cement : sand : limestone : water).

Although the concrete mix used for all specimens was the same, the ultimate strength for each batch of concrete varied. It is believed that this difference was due to inescapable variations in water-cement ratios resulting from variations in material water content and concrete batching procedures.

Four 6x12 in. and two 6x6 in. cylinders were cast from each concrete batch, cured simultaneously with each specimen, and tested on the same day the cantilever beam specimen was tested. Stress-strain curves for the concrete were obtained from compression tests of 6x12 in. cylinders. A mechanical dial gage was used to measure cylinder longitudinal deformation over a six-inch gage length. The uniaxial compression load was read from the gage of the Riehle machine used to test the cylinders. A typical stress-strain curve for concrete is shown in Fig.A.2, and a summary of concrete strengths is given in Table A.2. The tensile strength of the concrete was obtained from splitting tests of 6x6 in. cylinders and the results are given in Table A.2.

Table A.1
Measured Properties from Steel Coupon

Bar size	Stress,ksi		Strain	
	Yield	Ultimate	Yield	Ultimate
2	53.4	72.7	0.0016	0.1635
2+	58.1	83.1	0.0020	0.1465
3	75.5	107.1	0.0050*	0.0985
5	72.4	106.9	0.0050*	0.0967
6	63.7	96.9	0.0022	0.1317
6+	62.1	92.8	0.0021	0.1500
7	59.3	101.3	0.0020	0.1350
7+	71.8	115.1	0.0050*	0.105

+ Reinforcement used in specimens S1-4 and S2-3

* No Well Defined Yield Point in Stress-Strain Curve

Table A.2
Measured Average Concrete Properties

Specimen	Slump (in)	Age (day)	Compressive Strength (psi)	Splitting Strength (psi)
S1-1	2.8	78	5900	592
S1-2	2.8	69	5880	584
S1-4	2.3	63	4980	435
S2-1	2.8	83	5100	392
S2-2	2.8	70	5390	468
S2-3	2.4	56	4710	376
S2-4	7.5	91	4780	425
S3-1	4.8	54	4910	403
S3-2	4.8	62	4970	442
S3-3	5.3	75	4980	455
S3-4	1.3	43	5060	440

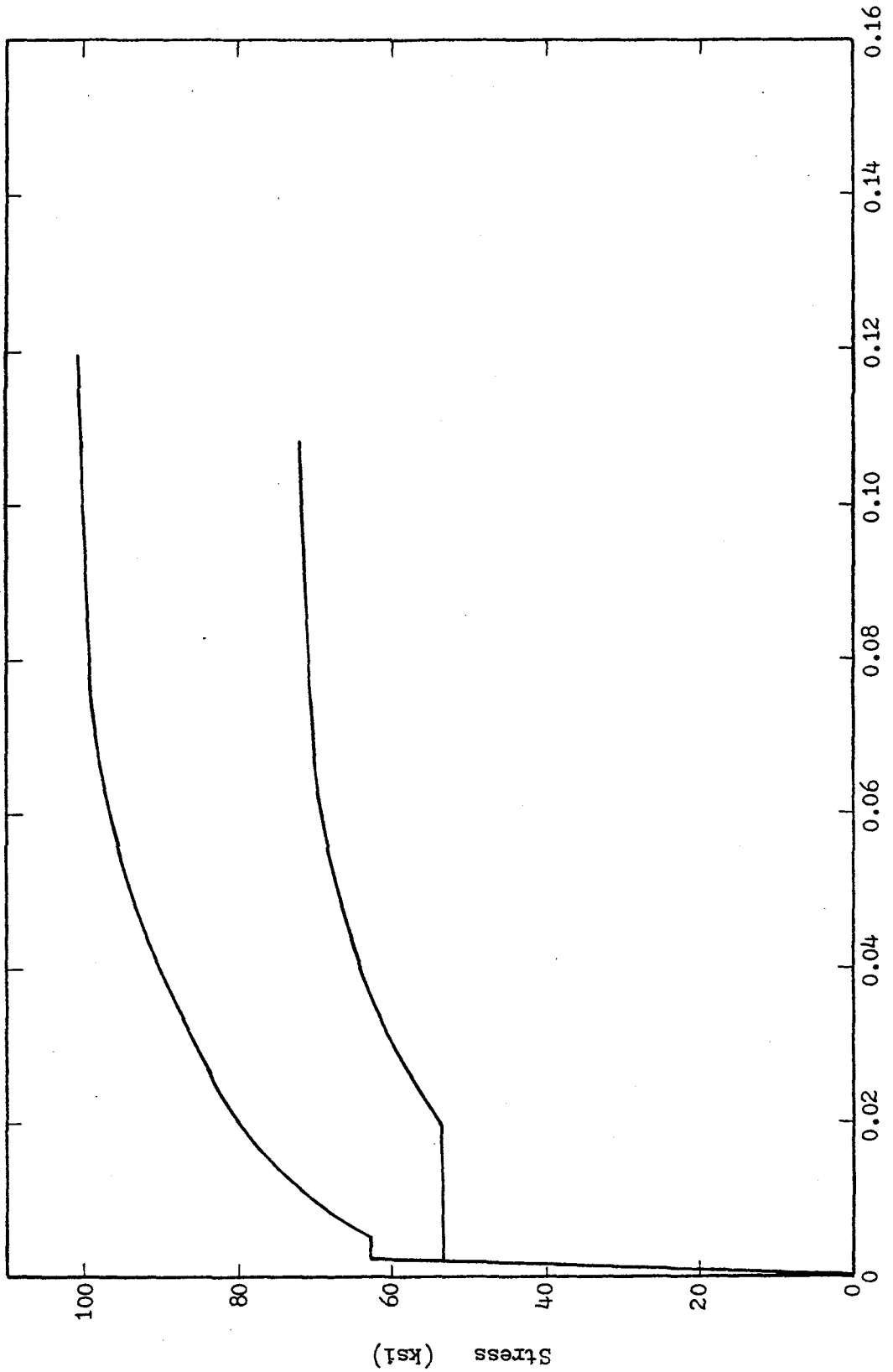

Fig. A.1(a) Typical Stress-Strain Curves for No. 2 and No. 6 Bars

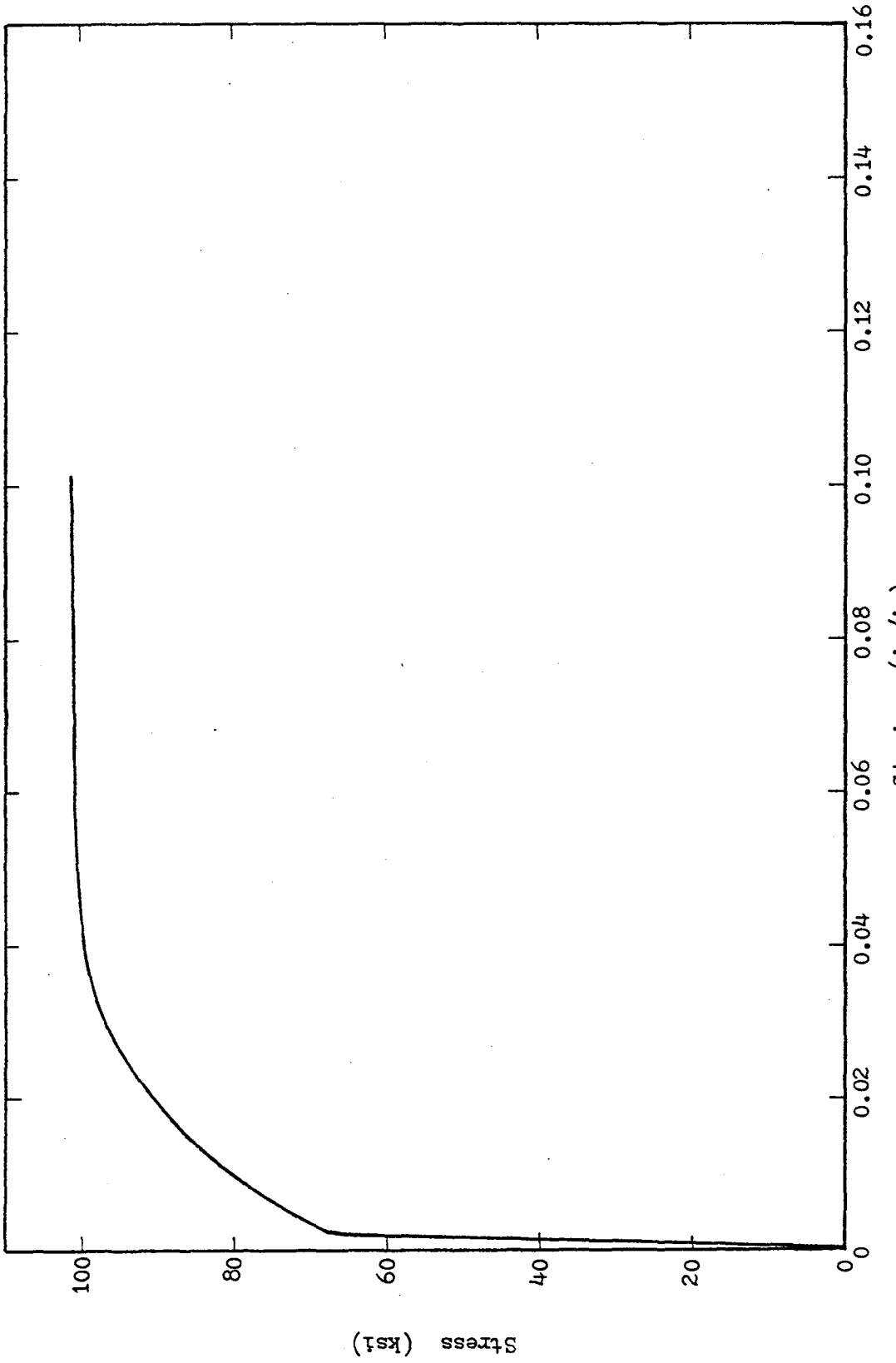

Fig. A.1(b) Typical Stress-Strain Curve for No. 3 Bars

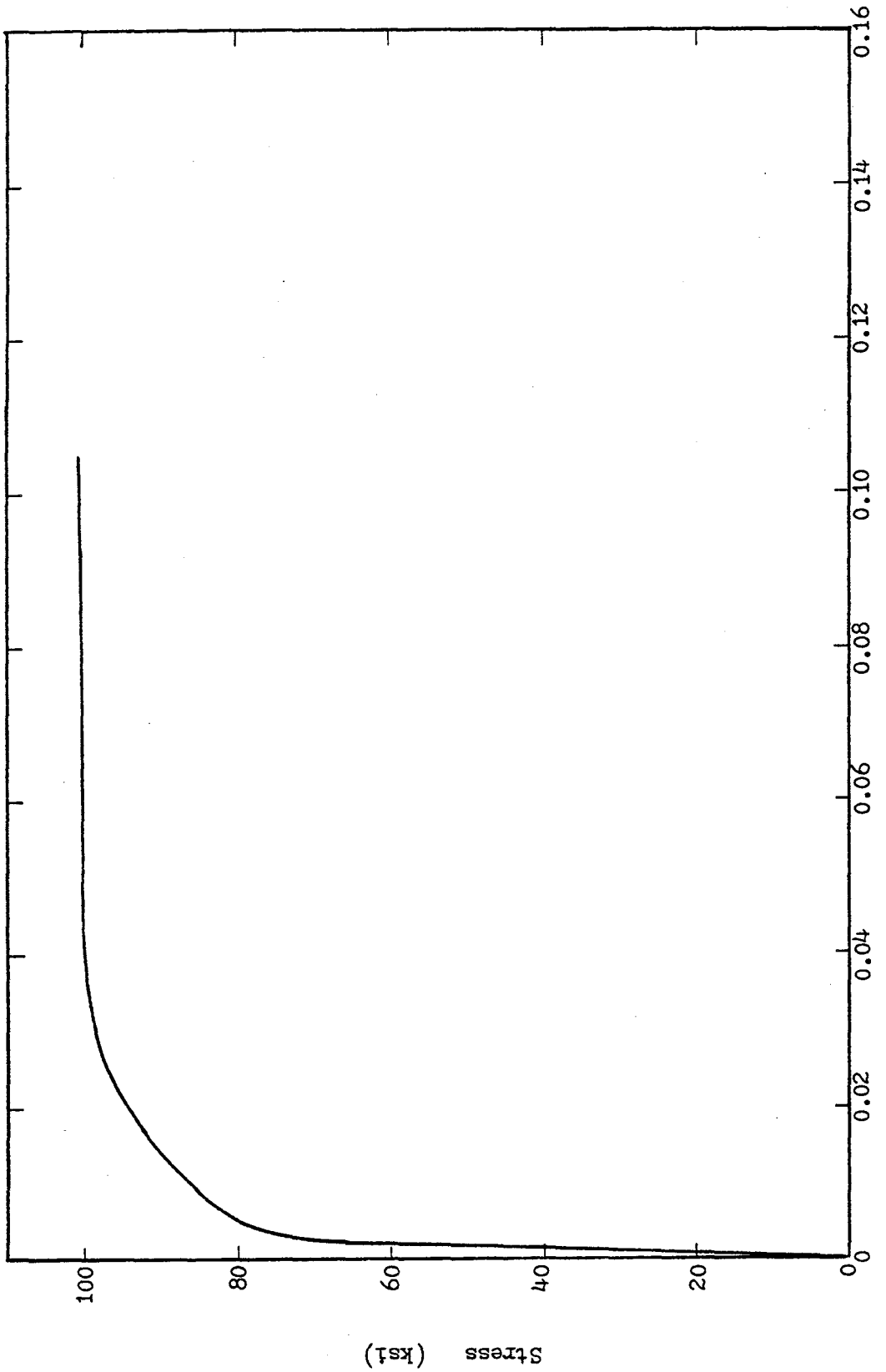

Fig. A.1(c) Typical Stress-Strain Curve for No. 5 Bars

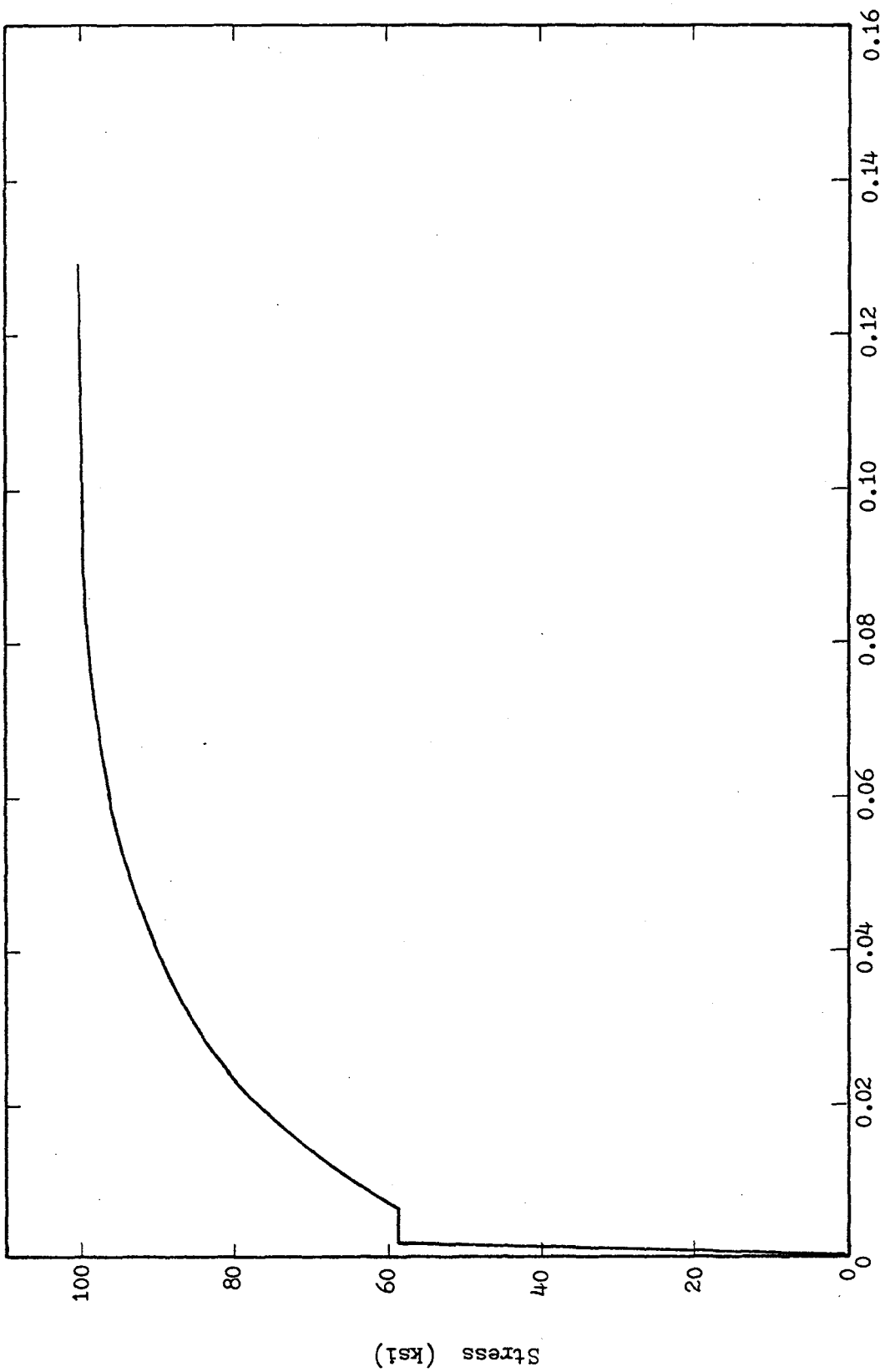

Fig. A.1(d) Typical Stress-Strain Curve for No. 7 Bars

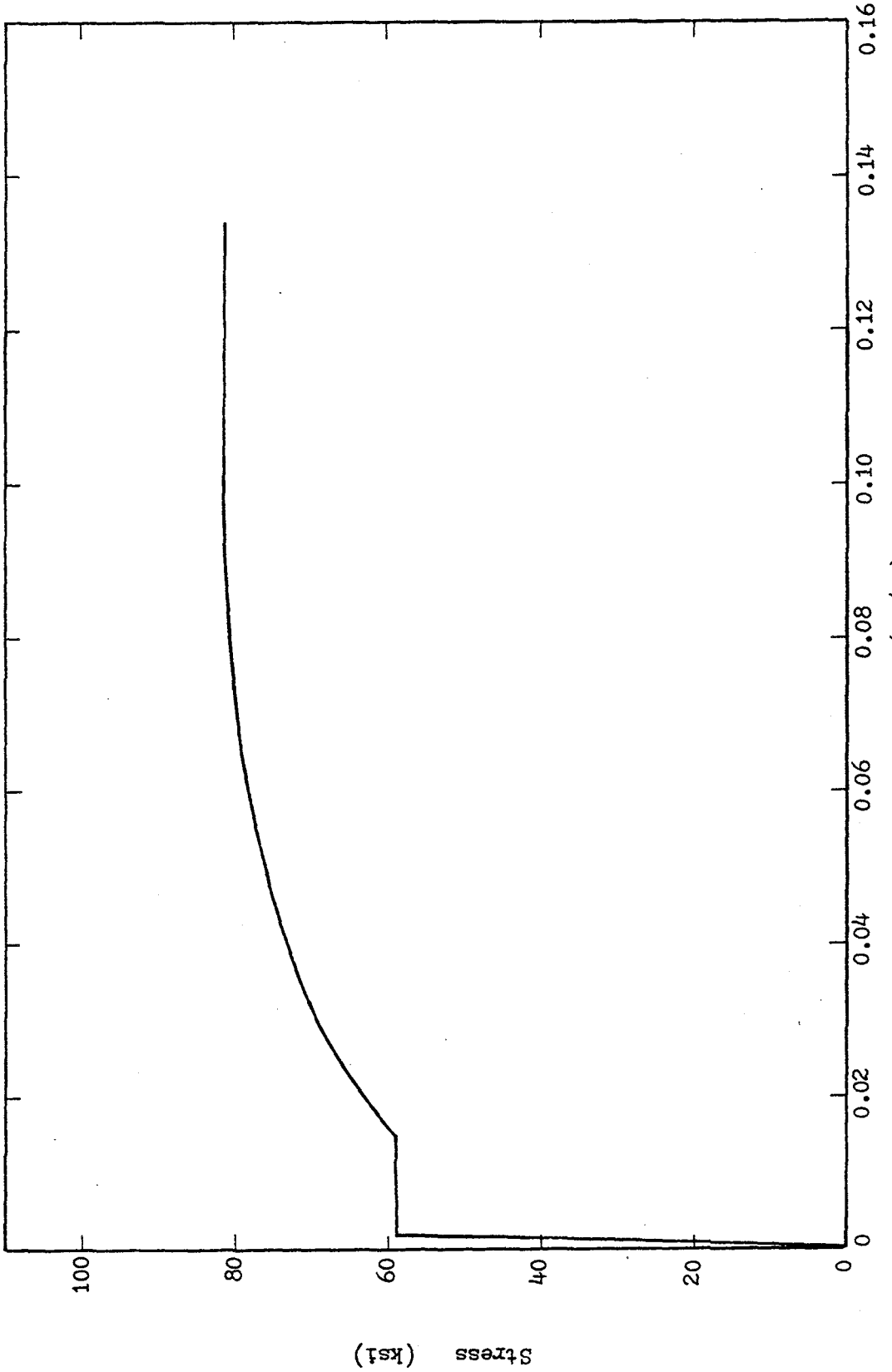

Fig. A.1(e) Typical Stress-Strain Curve For No. 2 Bars

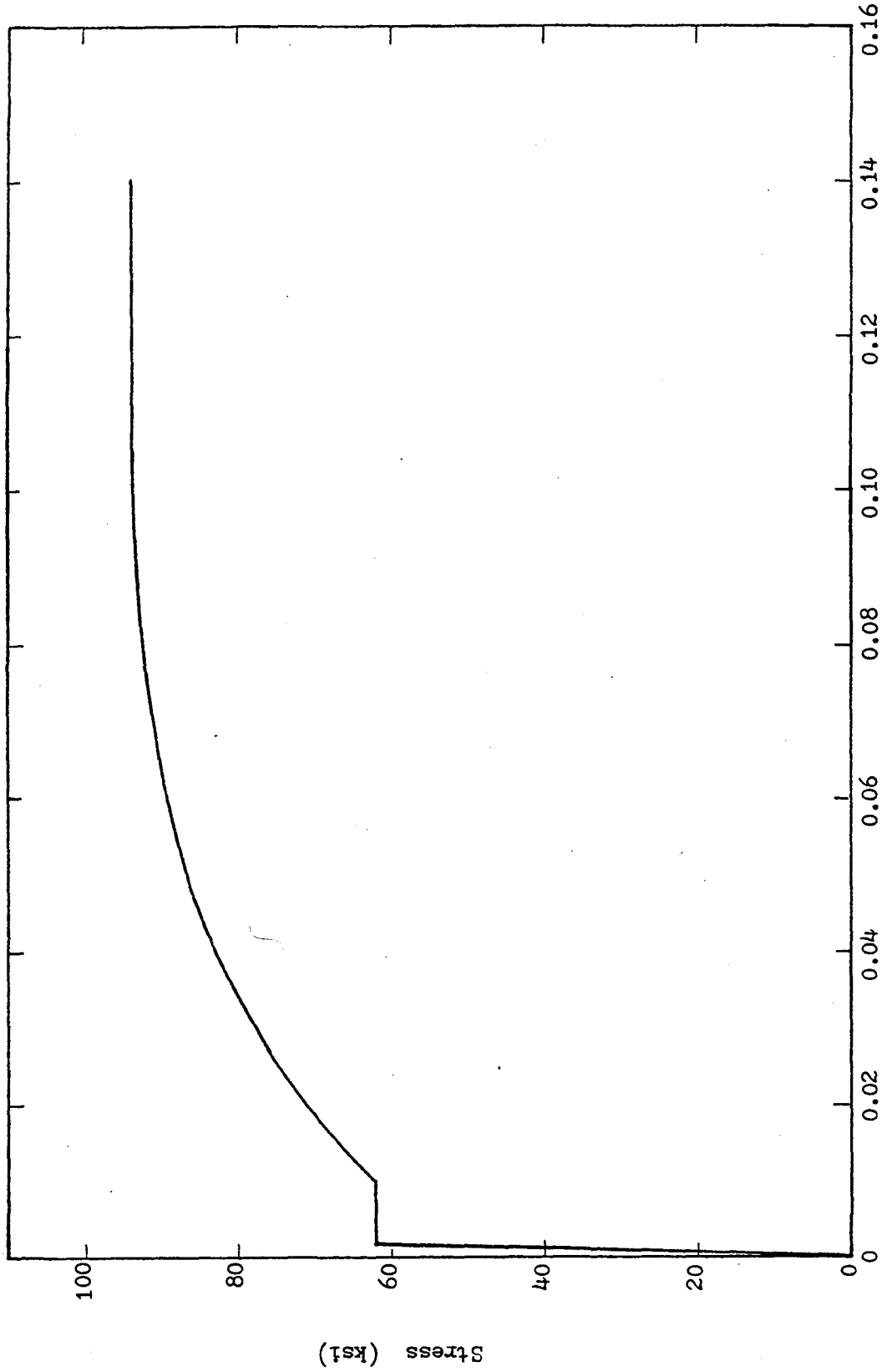

Fig. A.1(f) Typical Stress-Strain Curve for No. 6 Bars

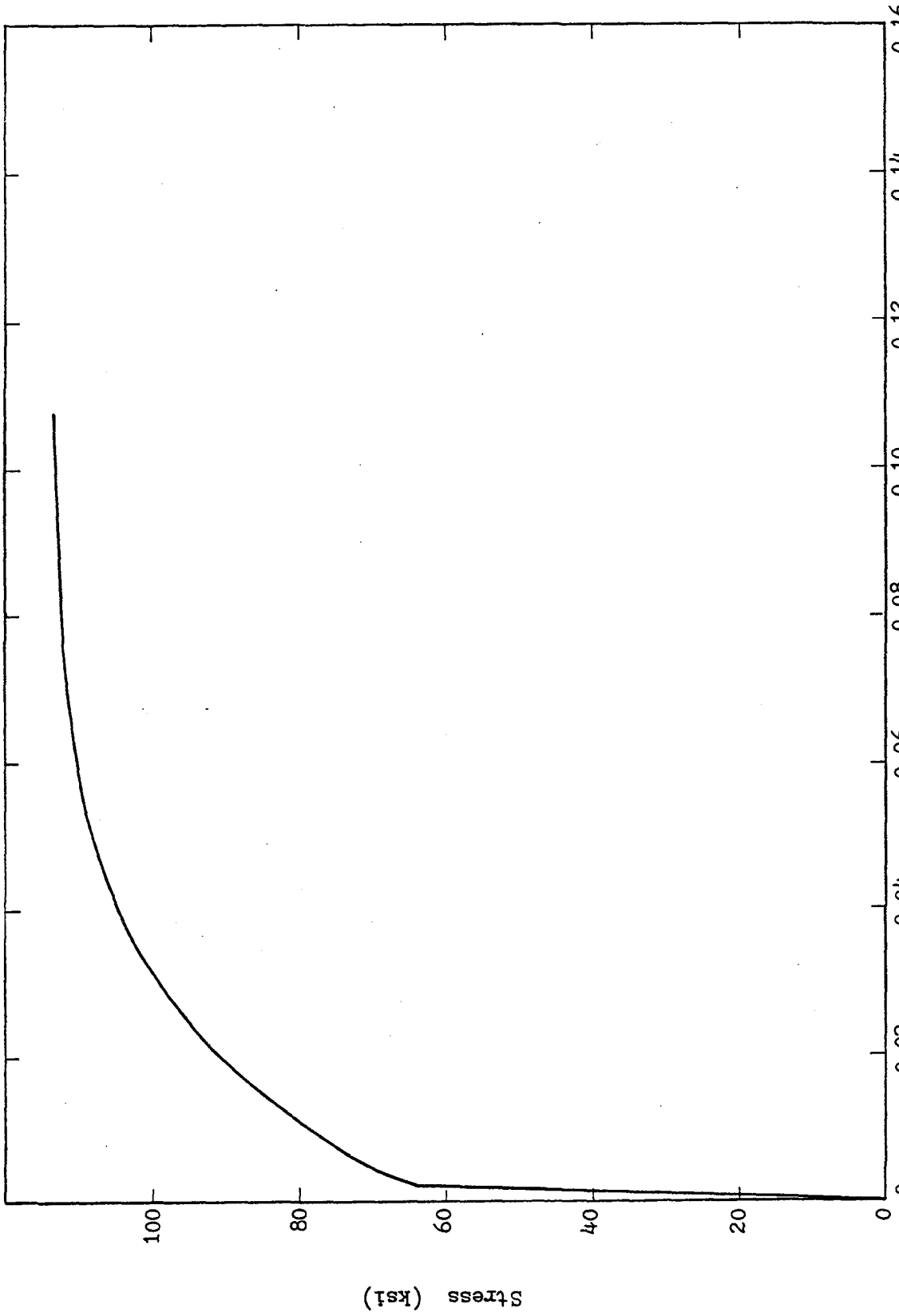

Fig. A.1(g) Typical Stress-Strain Curve for No. 7 Bars

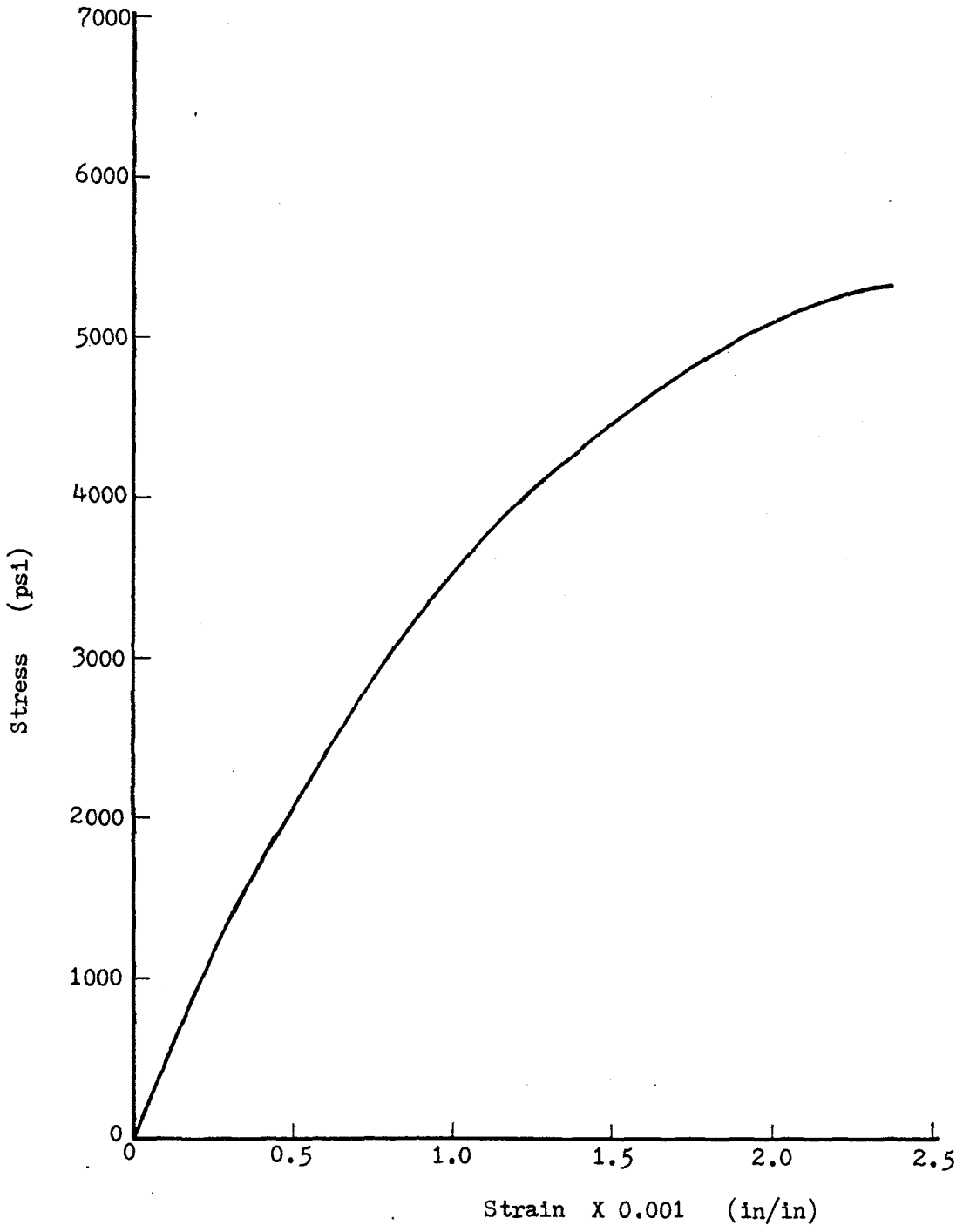

Fig. A.2 Typical Stress-Strain Curve for Concrete

APPENDIX B

SPECIMEN DESIGN

The ACI Building Code (318-77) and its Appendix A were used as a guide for specimen design. References given in parentheses in the following discussion of design procedures refer to the applicable paragraph in the ACI code.

The overall dimensions of the specimen were selected for compatibility with available testing equipment. Beam longitudinal reinforcement was chosen so that the maximum predicted moment would induce the desired maximum shear stress in the beam. Shear span to effective depth ratio was constrained to be greater than two. Specimens were designed to have maximum gross shear stresses of from 3 to 6 $\sqrt{f'_c}$.

Transverse reinforcement was designed to resist the expected maximum shear in each specimen at the ultimate design beam moment. The allowable shear stress for concrete was taken as 2 $\sqrt{f'_c}$, or 126 psi for the design concrete compressive strength of 4000 psi. Using Group III specimens as an example, beam shear stress was designed as 6 $\sqrt{f'_c}$, which required a force of:

$$6\sqrt{f'_c} * b * d = 29450 \text{ lb} = 29.5 \text{ kips}$$

Because the section nominal moment was calculated to be 833 in-kips, the selected shear span was (833x0.9)/29.5=25.4 inches. Required transverse reinforcement was calculated as

$$V_s = (A_v f_y d) / S \qquad (11.7)$$

$$A = \emptyset .15 A_s (S / d) \qquad (A.1)$$

Using a Grade 60, No. 3 deformed bar for stirrups and solving for required spacing:

$$S = \frac{A_v f_y d}{V - V_c} = \frac{(0.22)\ (60)\ (9.69)}{(29.5 - 9.8)} = 6.5 \text{ in.}$$

$$S = \frac{A_v\ d}{0.15\ A_s} = \frac{(0.22)\ (9.69)}{0.15\ (1.32)} = 10.8 \text{ in.}$$

Other provisions of the design code (A. 5.11) required a tie spacing in the beam no greater than d/4 within a distance of 4d from the enlarged block face, so the spacing for transverse reinforcement in the hinging zone in this and all other specimens was chosen as d/4.

Because the shear span length of this specimen was less than 4d, it was not necessary to place close stirrups at d/4 spacing beyond the load application point. Because the Uniform Building Code and SEAOC code require close spacing of ties in beams for a distance of only 2d from the face of the column, it was decided that d/4 spacing would be used for only a distance of 2d from the face of the enlarged end block. All lateral reinforcement consisted of closed, one-piece ties as required by ACI 318-77. Stirrups were placed at a distance of 1 in. from the face of the enlarged end block and thereafter at a spacing of 2.5 in. for a distance of 2d. In the enlarged end block, three stirrups were placed starting at a distance of 3 in. from the face of the enlarged end block at a spacing of 5 inches. To

insure that all inelastic deformation took place in the beam section of the specimen, three additional large stirrups were added in the enlarged end block adjacent to the stirrups mentioned above (Fig.C.1).

DEVELOPMENT OF LONGITUDINAL REINFORCEMENT

All longitudinal reinforcement was anchored in the enlarged end block by 90 degree standard hooks. The tensile stress which the hook would be expected to developed was calculated as (12.5.1)

$$f_h = \xi \sqrt{f'_c}$$

where

f_h = tensile stress developed by a standard hook, psi

ξ = constant for standard hook, $\xi = 360$ for #7 bars

$\xi = 450$ for #6 bars

The equivalent embedment length ℓ_e of the standard hook was calculated as (12.5.2)

$$\ell_e = 0.04 A_b f_y / \sqrt{f'_c}$$

where

ℓ_e = equivalent embedment length of a hook

A_s = area of an individual bar

The required development length specified by the code (A5.8) was 2/3 ℓ_e or 16 inches, where ℓ_e is calculated in accordance with section 12.2.2.

APPENDIX C

SPECIMEN FABRICATION & TEST SETUP

SPECIMEN FABRICATION

All test specimens were constructed in the Civil Engineering Structural laboratory of the University of Illinois. Fabrication sequence was the same for all specimens.

Reinforcing steel was first cut into pieces and bent in the laboratory using a DI-ACRO bender. Bending technique was supervised by a technician and the dimensions of the finished products conformed to applicable specifications of Chapter 7 of the ACI Building code. Beam main reinforcement was hung on two steel supports and then stirrups were fastened in position using eighteen gage annealed wire to complete fabrication of the steel cage. A complete steel cage is shown in Fig.C.1.

Specimens were cast in a horizontal position in plywood forms. Three forms were constructed to allow casting of three specimens simultaneously. Forms were constructed of 3/4 in. exterior grade plywood which was reinforced with 2x2 in. square fir wales and waterproofed with orange shellac. Form section were joined with 1/4 in. machine bolts. Before casting of specimen, forms were oiled to allow their easy removal from finished specimens.

Steel cages were placed in the forms and supported with

small concrete cubes. This insured proper concrete cover and held steel cages in position during casting. The assembled form with steel cage in place is shown in Fig.C.2. Concrete was mixed by a CYCLO-MIXER (Model 17Ø) according to the mix design specified in Appendix A. Concrete was placed in the forms and consolidated with a hand vibrator. Excess concrete was struct off with a wooden screed and smoothed with a metal float. The concrete attained its initial set in approximately five hours and it was then covered with wet burlap and plastic sheeting to retain moisture. Forms were removed on the day following the day of casting and specimens were maintained in a wet condition for at least seven days before the plastic sheeting and burlap was removed. Specimens were then allowed to cure uncovered until they were tested.

Standard 6 x 12 in. concrete test cylinders were cast at the same time each series of three specimens was cast. Cylinders were removed from the steel cylinder forms on the day following the day of casting and then moved to the site of the test beams where all were cured under like conditions until testing occurred.

TEST SET UP AND TEST PROCEDURES

(A) HOLDING FIXTURE

The enlarged end block of the specimen was clamped between two 1x16x2Ø in. steel plates with ten high strength steel rods.

The top plate was reinforced by four C-3x6 steel channels. The bottom plate was welded to a steel W-section which in turn was bolted to the laboratory floor. A concrete block was used to elevate the W-section to allow easy inspection of the specimen during the test.

(B) LOADING FIXTURE

A 100 kip capacity hydraulic ram was used to apply vertical load to the specimen. The ram was supported by an external frame, shown in Fig.C.3, and attached to the specimen by a greased spherical connection. A loading area of 8x8 in. was obtained by using 3/4 x 8 x 8 in. plates on top and bottom of the beam at the location of the loading point. The holding fixture is shown schematically in Fig.A.6.

TEST PROCEDURE

The specimen was held fixed at its enlarged block. Data acquistion equipment and loading fixture were in turn attached to the specimen. Before applying the designated load history, shown in Fig.2.3, a load of approximate 1/4 of the yield load was applied in the positive displacement direction and then removed to check the security of the attachments between the specimen and the testing frame. After the first cycle of load, bolts were checked and re-tightened if necessary. The recorded load deflection curves were used to monitor the progress of the test. Motion of the ram was stopped at various times to allow

readings from strain gages and LVDTs to be recorded. Test was terminated when the specimen had essentially lost its ability to resist displacement.

DATA ACQUISTION

The data acquisition equipment included: (1) an MTS ram and the control console (MTS Model 661.22), (2) Five LVDTs manufactured by Collins company, (3) a Hewlett Packard X-Y plotter, (4) thirteen strain gages manufactured by Micro-Measurement company (Type EA-Ø6-25ØBG-12Ø strain gages for longitudinal steel; Type EA-Ø6-125BG-12Ø strain gages for transverse steel), (5) an Endevco signal conditioning module (Model 447Ø), (6) a Vidar scanner (Model 61Ø), (7) a Vidar digital voltmeter (Model 521), and (8) a Teletype printer.

A steel frame made from 1 x 1 x 1/8 in. steel angles was attached to the enlarged end block to provide fixture for the LVDTs in the hinging zone and at the load application point. This device was used so that the displacement of the loading point was measured with respect to the enlarged end block, in other words, the rigid body motion of the whole specimen would not be included in the recorded loading point displacement.

The applied load was measured by a 1ØØ kip capacity load cell attached between the specimen and the MTS ram. Deflection of the ram end was measured by an LVDT built in the loading ram and by an independent LVDT attached underneath the beam at the

load application point. The readings from the LVDT in the loading ram were not used. Readings from the independent LVDT and load cell were continuously recorded by a Hewlett Packard X-Y plotter during the test. Four LVDTs were positioned over the beam hinging zone as shown in Fig.2.4. to measure the shearing and flexural deformation in this region. The hinging zone was assumed to extend into the beam a distance equal to the overall beam depth from the face of the enlarged end block. Thirteen electrical resistance strain gages were bonded to reinforcement at locations shown in Fig.2.5 in the specimen to record the strains in the reinforcing steel. Signals from LVDTs and strain gages were channeled through Endevco signal conditioning modules, a Vidar scanner, and a Vidar digital voltmeter. A Teletype printer printed the readings and punched them on a tape. The data from the paper tape was read into the Cyber computer in the University of Illinois, and a computer program was developed to convert the voltage signals into corresponding load, deflection and strain readings.

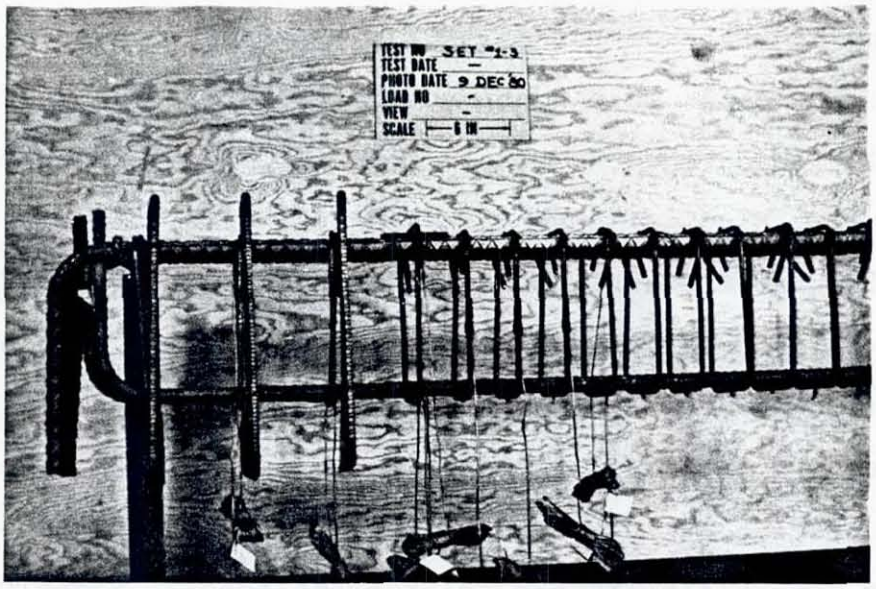

Fig. C.1 Completed Reinforcement Cage

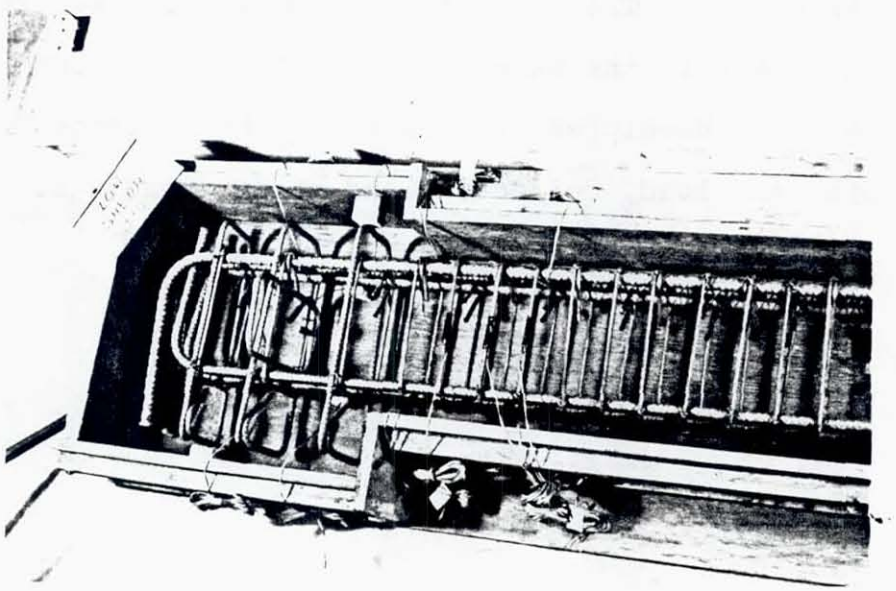

Fig. C.2 Reinforcement Cage in Plywood Form Ready for Casting

Fig. C.3 Test Setup and Loading Frame

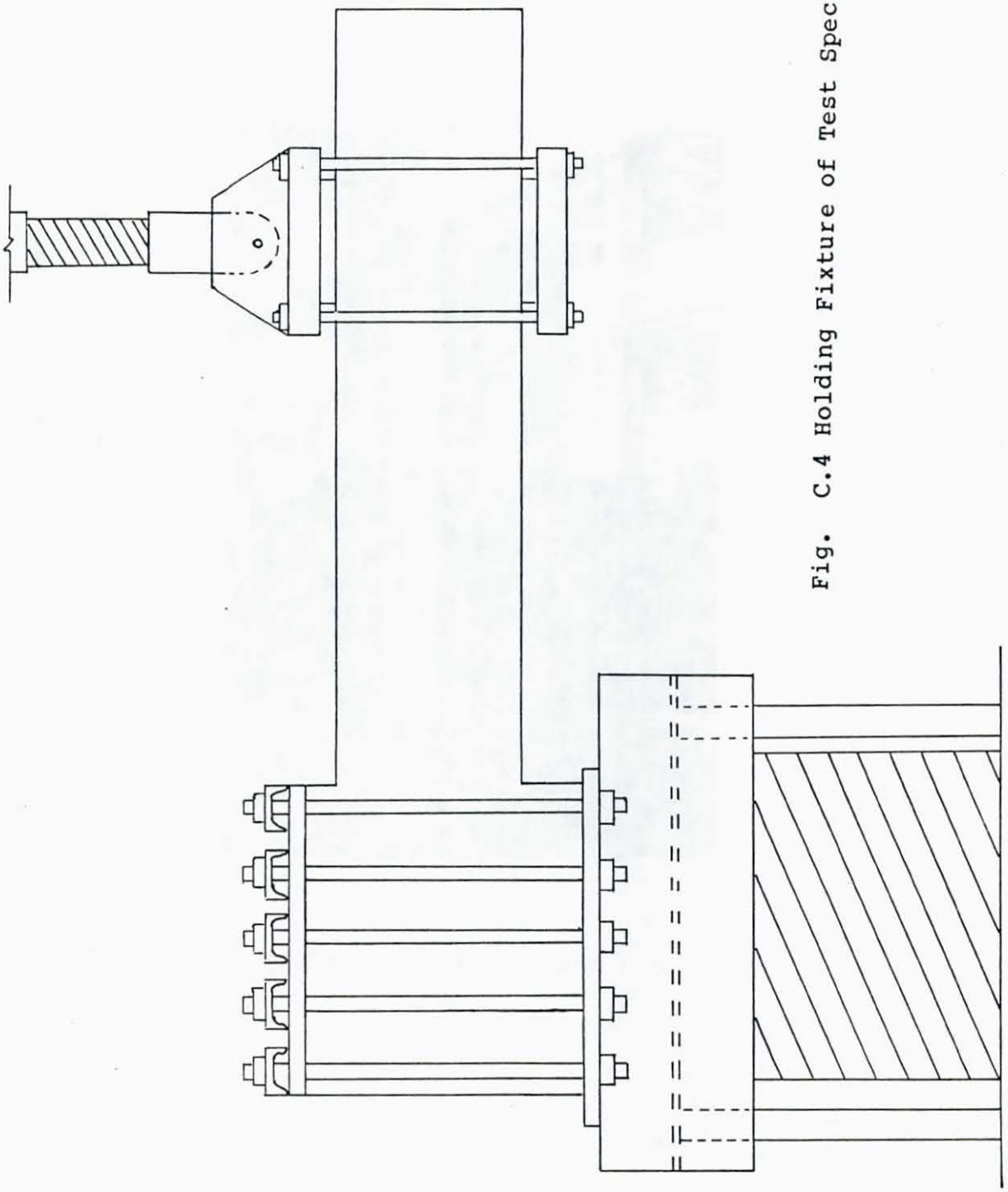

Fig. C.4 Holding Fixture of Test Specimen

APPENDIX D

CALCULATION OF FLEXURAL AND SHEAR DEFORMATION OF A HINGING ZONE

A deformed hinging zone of one of the specimen tested is shown in Fig D.1. Using the flexural and shear, and total displacement in the hinging zone defined in Chapter 4 and notation shown in Fig. D.1, let

L_1 = AB $\qquad$ θ_1 = BAC

L_2 = BC $\qquad$ θ_2 = ABD

L_3 = AD $\qquad$ θ_3 = BAF

L_4 = AF $\qquad$ θ_4 = FAE

L_5 = EF $\qquad$ θ_5 = AEF

$(H/2)$ = AE = EC = BF = FD, and $\pi/2$ = AEG = GEC.

Then from trigonometry

$$\theta_1 = \cos^{-1}\left(\frac{H^2 + L_1^2 - L_2^2}{2 H L_1}\right)$$

$$\theta_2 = \cos^{-1}\left(\frac{L_1^2 + H^2 - L_3^2}{2 H L_2}\right)$$

$$L_4 = \left(L_1^2 + (H/2)^2 - 2 L_1 (H/2) \cos \theta_2 \right)^{1/2}$$

$$\theta_4 = \theta_1 - \theta_3$$

$$L_5 = \left(L_4^2 + (H/2)^2 - 2 L_4 (H/2) \cos \theta_4 \right)^{1/2}$$

$$\theta_5 = \cos^{-1}\left(\frac{L_5^2 + (H/2)^2 - L_4^2}{2 L_5 (H/2)}\right)$$

$$\text{Flexural Rotation} = \frac{1}{2}\left(\pi - \theta_1 - \theta_2 \right)$$

$$\text{Shear Rotation} = \theta_5 - \pi/2 - (\text{Flexural Rotation})$$

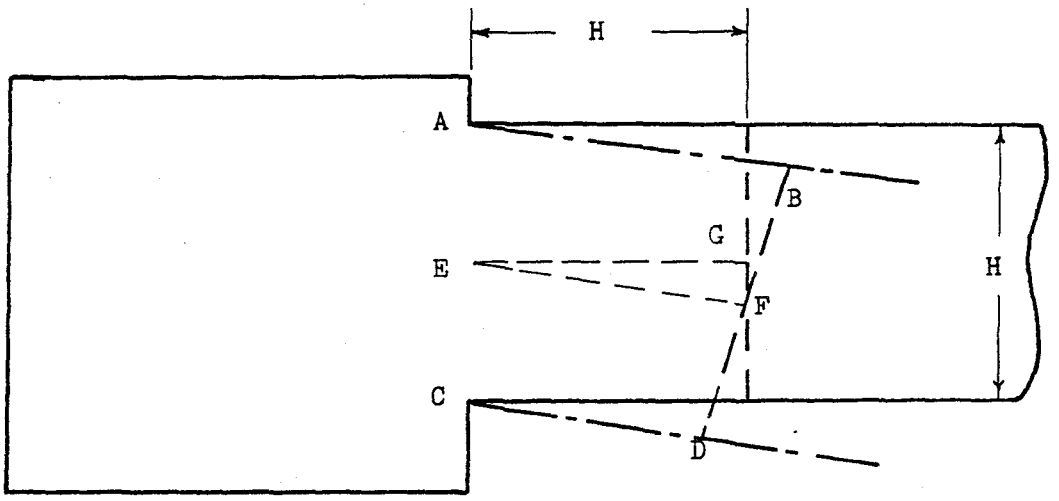

Fig. D.1 Deformation of Hinging Zone

REFERENCES

1. ACI 318-77, "Building Code Requirements for Reinforced Concrete," American Concrete Institute, Detroit, Michigan, 1977

2. ----------, "Commentary on Building Code Requirements for Reinforced Concrete," American Concrete Institute, Detroit, Michigan, 1977

3. ACI Committee 408, "Bond Stress- The State of the Art," Journal of the American Concrete Institute, Proceedings V.63, No. 11, November 1966, pp.1161-1188.

4. ACI-ASCE Committee 326, "Shear and Diagonal Tension," Journal of the American Concrete Institute, Proceedings V.59, No.1, January 1962, pp. 3-30.

5. ACI-ASCE Committee 426, "The Shear Strength of Reinforced Concrete Members," Journal of the Structural Division, ASCE, ST6, June 1973.

6. Aktan, A.E., Karlsson, B.I., and Sozen, M.A., "Stress-Strain Relationships of Reinforcing Bars Subjected to Large Strain Reversals," Civil Engineering Studies, Structural Research Series No. 397, University of Illinois, Urbana, June 1973.

7. Applied Technology Council, "Tentative Provisions for the Development of Seismic Regulations for Buildings," National Science Foundation, ATC 3-06, NSF 78-8

8. Banon, H., Biggs, J.M., and Irvine, H.M., "Prediction of Seismic Damage in Reinforced Concrete Frames," Seismic Behavior and Design of Buildings, Report No.3, MIT, MA., may 1980.

9. Bertero, V.V., and Popov, E.P., "Hysteretic Behavior of Ductile Moment-Resisting Reinforced Concrete Frame Components," Earthquake Engineering Research Center, Report No. EERC 75-16, University of California, Berkeley, CA., April 1975.

10. Bertero, V.V., Popov, E.P., and Wang, T.Y., "Hysteretic Behavior of Reinforced Concrete Flexural Members with Special Web Reinforcement," Earthquake Engineering Research Center, Report No. EERC 74-9, University of California, Berkeley, CA. August 1974.

11. Blume, J.A., Newmark, N.M., and Corning, L.H., "Design of Multistory Reinforced Concrete Buildings for Earthquake Motions," Published by Portland Cement Association, Skokie, IL., 1961.

12. Bresler, B., and Bertero, V., "Behavior of Reinforced Concrete under Repeated Load," Journal of the Structural Division, ASCE, Vol. 94, No. ST6, June 1968, PP.1567-1590.

13. Brown, R.H., and Jirsa, J.O., "Reinforced Concrete Beams under Load Reversals," Journal of the American Concrete Institute, Vol. 68, May 1971, pp380-390.

14. Burns, N.H., and Siess, C.P., "load-Deflection Characteristics of Beam-Column Connections in Reinforced Concrete," Civil Engineering Studies, Structural Research Series No.234, University of Illinois, Urbana, January 1962.

15. Clough, R.W., and Benuska, K.L., "Nonlinear Earthquake Behavior of Tall Buildings," Journal of the Engineering Mechanics Division, ASCE, Vol.93, No.EM3, June 1967, pp.129-146.

16. Derecho, A.T., Iqbal, M., Fintel, M., and Corley, W.G., "Loading History for Use in Quasi-Static Simulated Earthquake Loading Tests," American Concrete Institute Publication SP-63,Detroit, 1980, pp.329-356.

17. Emori, K., and Schnobrich, W.C., "Analysis of Reinforced Concrete Frame-Wall Structures for Strong Motion Earthquakes," Civil Engineering Studies, Structural Research Series No.457, University of Illinois, Urbana, December 1978.

18. Gavlin, N.L., "Bond Characteristics of Model Reinforcement," Civil Engineering Studies, Structural Reserach Series No. 427, University of Illinois, Urbana, April 1976.

19. Gosain, N.K., Brown, R.H., and Jirsa, J.O., "Shear Requirements for Load Reversals on RC Members," Journal of the Structural Division, ASCE, Vol. 103, No. ST7, July 1977, pp.1461-1476.

20. Gulkan, P., and Sozen, M.A., "Response and Energy-Dissipation of Reinforced Concrete Frames Subjected to Strong Base Motion," Civil Engineering Studies, Structural Research Series No. 377, University of Illinois, Urbana, May 1971.

21. Hanson, N.W., and Connor, H.W., "Seismic Resistance of Reinforced Concrete Beam-Column Joints," Journal of the

Structural Division, ASCE, Vol.93, No.ST5, October 1967, pp.533-560.

22. Iemura, H., "Earthquake Failure Criteria of Deteriorating Hysteretic Structures," Proceedings of the Seventh World Conference on Earthquake Engineering, Vol.5, pp.81-88 Istanbul, Turkey, September 1980.

23. Ismail, M.A.F., and Jirsa, J.O., "Bond Deterioration in Reinforced Concrete Subjected to Low Cycle Loads," Journal of the American Concrete Institute, Proceedings V.69, No.6, Title No. 69-34, June 1972, pp.334-343.

24. ----------, "Behavior of Anchored Bars under Low Cycle Overloads Producing Inelastic Strains," Journal of the American Concrete Institute, Proceedings V.69, No.7, Title No. 69-40, July 1972, pp.433-438.

25. Jirsa, J.O., "Factors Influencing the Hinging Behavior of Reinforced Concrete Members Under Cyclic Overloads," Paper No. 147, Session 3D, Fifth World Conference on Earthquake Engineering, Vol.1, Rome, 1973, pp.1198-1204

26. Kent, D.C., and Park, R., "Flexural Members with Confined Concrete," Journal of the Structural Division, ASCE, Vol. 97, No. ST7, July 1971, pp.1969-1990.

27. Krawinkler, H., and Popov, E. P., "Hysteretic Behavior of Reinforced Concrete Rectangular and T-Beams," Proceedings of Fifth World Conference on Earthquake Engineering, Vol 1, Rome 1973, pp. 249-258.

28. Lee, D.L.N., Hanson, R.D., and Wight, J.K., "Original and Repaired Reinforced Concrete Beam-Column Subassemblages Subjected to Earthquake Type Loading," UMEE 76R4, the University of Michigan, Ann Arbor, April 1976.

29. Lutz, L.A., and Gergely, P., "Mechanics of Bond and Slip of Deformed Bars in Concrete," Journal of the American Concrete Institute, Proceedings V.64, No. 11, Title No. 64-62, November 1967, pp711-721.

30. Ma, S.M., Bertero, V.V., and Popov, E.P., "Experimental and Analytical Studies on the Hysteretic Behavior of Reinforced Concrete Rectangular and T-Beams," Earthquake Engineering Research Center, Report No. EERC 76-2, University of California, Berkeley, CA., May 1976.

31. Marques, J.L.G., and Jirsa, J.O., "A Study of Hooked Bar Anchorages in Beam-Column Joints," Journal of the American Concrete Institute, Proceeding V. 72, No.5, Title No. 72-18, May 1975, pp.198-209.

32. Minor, J. and Jirsa, J.O., "Behavior of Bent Bar Anchorages," Journal of the American Concrete Institute, Proceedings V.72, No.4, Title No. 72-15, April 1975, pp.141-149.

33. Park, R., Kent, D.C., and Sampson, R.A., "Reinforced Concrete Members with Cyclic Loading," Journal of the Structural Division, ASCE, Vol. 98, No. ST7, July 1972, pp.1341-1360.

34. Park, R., and Paulay, T., "Reinforced Concrete Structures," a Wiley-Interscience Publication, John Wiley & Sons, New York,1975.

35. Saiidi, M. and Sozen, M.A., "Simple and Complex Models for Nonlinear Seismic Response of Reinforced Concrete Structures," Civil Engineering Studies, Structural Research Series No. 465, University of Illinois, Urbana, August 1979.

36. Scribner, C.F., and Wight, J.K., "Delaying Shear Strength Decay in Reinforced Concrete Flexural Member under Large Load Reversals," UMEE 78R2, the University of Michigan, Ann Arbor, May 1978.

37. Shimazu, T., and Hirai, M., "Strength Degradation of Reinforced Concrete Columns Subjected to Multi-Cycle Reversals of Lateral Load at Given Amplitudes of Post-Yielding Deformation," Fifth World Conference on Earthquake Engineering, Vol 1, Rome, 1973, pp.1139-1142.

38. Stanton, J.f., and McNiven, H.D., "The Development of a Mathematical Model to predict the Flexural Response of Reinforced Concrete Beams to Cyclic Loads, Using System Identification," Earthquake Engineering Research Center, Report No. UCB/EERC-79/02, University of California, Berkeley, CA., January 1979.

39. Takeda, T., Sozen, M.A., and Nielsen, N.N., "Reinforced Concrete Response to Simulated Earthquakes," Journal of the Structural Division, ASCE, Vol. 96, No. ST12, December 1970, pp.2557-2573.

40. Viwathanatepa, S., Popov, E.P., and Bertero, V.V., "Seismic Behavior of Reinforced Concrete Interior Beam-Column Subassemblages," Earthquake Engineering Research Center, Report No. UCB/EERC-79/14, University of California, Berkeley, CA., June 1979.

41. -------, "Effects of Generalized Loadings on Bond of Reinforcing Bars Embedded in Reinforced Concrete Blocks,"

Earthquake Engineering Research Center, Report No. UCB/EERC-79/22, University of California, Berkeley, CA., August 1979.

42. Wight, J.K., and Sozen, M.A., "Shear Strength Decay in Reinforced Concrete Columns Subjected to Large Deflection Reversals," Civil Engineering Studies, Structural Research Series No. 403, University of Illinois, Urbana, IL., August 1973.

43. Zagajeski, S.W., Bertero, V.V. and Bouwkamp, J.G., "Hysteretic Behavior of Reinforced Concrete Columns Subjected to High Axial and Cyclic Shear forces," Earthquake Engineering Research Center, Report No. UCB/EERC-78/05, University of California, Berkeley, CA., April 1978.